Satellite Orbit and Ephemeris Determination using Inter Satellite Links

by

Robert Wolf

Vollständiger Abdruck der an der Fakultät für Bauingenieur- und Vermessungswesen der Universität der Bundeswehr München zur Erlangung des akademischen Grades eines Doktors der Ingenieurswissenschaften (Dr.-Ing.) eingereichten Dissertation.

Abstract

Global navigation satellite systems like GPS, GLONASS or the future systems like Galileo require precise orbit and clock estimates in order to provide high positioning performance. Within the frame of this Ph. D. thesis, the theory of orbit determination and orbit computation is reviewed and a new approach for precise orbit and ephemeris determination using inter-satellite links is developed. To investigate the achievable accuracy, models of the various perturbing forces acting on a satellite have been elaborated and coded in a complex software package, allowing system level performance analysis as well as detailed evaluation of orbit prediction and orbit estimation algorithms. Several satellite constellations have been simulated, involving nearly all classes of orbit altitude and the results are compared.

The purpose of orbit determination in a satellite navigation system is the derivation of ephemeris parameters which can be broadcast to the user community (or the other satellites) and allow easy computation of the satellites position at the desired epoch. The broadcast ephemeris model of both today existing satellite navigation systems, GPS and GLONASS are investigated, as well as two new models developed within this thesis, which are derivates of the GLONASS model.

Furthermore, the topic of autonomous onboard processing is addressed. A conceptual design for an onboard orbit estimator is proposed and investigated with respect to the computational load. The algorithms have been implemented. The main benefits of ISL onboard processing, especially with respect to the great potential to ephemeris and clock state monitoring are investigated using complex simulations of failure scenarios. By simulating several types of non-integrity cases, it is showed that one single fault detection mechanism is likely to be insufficient. Within the algorithm design of the onboard processor, a reasonable combination of fault detection mechanisms is presented, covering different fault cases.

Zusammenfassung

Globale Navigationssysteme wie GPS, GLONASS oder zukünftige Systeme wie Galileo erfordern die hochpräzise Bestimmung der Orbital- und Uhrenparameter, um hohe Navigationsgenauigkeit bieten zu können. Im Rahmen dieser Dissertation wurde die Theorie der Orbitprädiktion und der Orbitbestimmung erörtert und ein neuer Ansatz für die präzisen Orbitbestimmung mit Hilfe von Intersatelliten-Messungen entwickelt. Um die erreichbare Genauigkeit und Präzision der Orbitbestimmung zu untersuchen, wurden mathematische Modelle der zahlreiche Orbitstörungen erarbeitet und in einem komplexen Software-Paket implemetiert. Dieses bietet die Möglichkeit für Systemstudien von Satellitennavigations-Systemen beliebiger Orbitklassen, sowie zur detaillierten Untersuchung spezieller Fragestellungen der Orbitprädiktion und -bestimmung. Eine Reihe von Simulationen mit existierenden sowie fiktiven Satelliten-Navigations-Systemen wurden durchgeführt, deren Ergebnisse in dieser Arbeit präsentiert werden.

Die präzise Orbitbestimmung in einem SatNav-System ist kein Selbstzweck, sondern dient lediglich der Bestimmung der Ephemeridenparameter, die - vom Satellite gesendet - es dem Nutzer-Empfänger erlauben, mit Hilfe einfacher Berechnungen die Position des Satelliten zu ermitteln. Die Ephemeridenformate beider existierender SatNav-Systeme - GPS und

GLONASS - wurden untersucht und mit zwei weiteren Formaten verglichen, die im Rahmen dieser Arbeit entwickelt wurden.

Desweiteren wurde das Thema der bordautonomen Verarbeitung von Messungen behandelt. Ein konzeptuelles Design für einen Onboard-Prozessor wurde vorgeschlagen und die Algorithmen implementiert. Dabei erfolgte eine Abschätzung der benötigten Prozessorleistung. Einer der Hauptvorteile der bordautonomen Verarbeitung von Intersatellitenmessungen, die Möglichkeit zur Überwachung der Integrität der Ephemeriden und Uhrenparameter, wurde in komplexen Simulationen untersucht. Durch die Simulation verschiedener Fehlerfälle wurde gezeigt, das kein Detektionsmechanismus allein, wohl aber eine sinnvolle Kombination solcher Mechanismen, zur bordautonomen Integritätsüberwachung geeignet sind. Die Ergebissen werden hier präsentiert.

Table of Contents

List of Figures

List of Tables

List of Acronyms

ABM	Adams-Bashford-Moulton
AUNAP	Autonavigationsprozessor
CAT I/II/II	Category (Precision Landings)
CDMA	Code Division Multiple Access
CPU	Central Processing Unit
DE200	Precise Planetary Ephemeris from Jet Propulsion Laboratory
DIODE	Détermination Immédiate d'Orbite par Doris Embarqué (Onboard Nav-Processor using Doris)
DLL	Delay Lock Loop
DOF	Degrees of Freedom
DORIS	Doppler Orbitography and Radiopositioning Integrated by Satellite
ECEF	Earth-Centred-Earth-Fixed (Reference Frame)
ECI-J2000	Earth Centred Inertial Reference Frame
EGM-96	Earth Gravity Model of 1996
EGNOS	European Geostationary Overlay System
ESA	Europen Space Agency
FD	Failure Detection (Algorithm)
FDI	Failure Detection and Isolation (Algorithm)
FDMA	Frequency Division Multiple Access
Galileo	Name of European Satellite Navigation System
GEM-T1/2/3	Goddard Earth Model
GEO	Geostationary Earth Orbit
GLONASS	Global Navigation Satellite System (Russia)
GNSS	Global Navigation Satellite System
GO	Integrity Flag State (= Healthy)
GPS	Global Positioning Service (also called Navstar GPS) (USA)
GRIM4-S4	Gravity Model from (Geoforschungzentrum Potsdam) based on Satellite Measurements only
ID	Identification (Number)
IERS	International Earth Rotation Service
IGSO	Inclicned Geosynchronous Orbit
ISL	Intersatellite Link

J2	Earths Oblateness Coefficient
JGM-2/3	Joint Gravity Model (Type 2 or 3)
JPL	Jet Propulsion Laboratory
LEO	Low Earth Orbit
LOS	Line of Sight
MEO	Medium Earth Orbit
MMH	Monometyl-Hydrazin
MOPS	Minimum Operational Performance Standards
MSAS	MSAT Space Augmentation System
NO GO	Integrity Flag State (= Unhealthy)
NTO	Nitro-Tetroxide
OCS	Operational Control System
PLL	Phase Lock Loop
PR	Pseudo Range
PRARE	Precise Range and Range-Rate Equipment
RAIM	Receiver Autonomous Integrity Monitoring
RK	Runge-Kutta
RMS	Root Mean Square
S/C	Spacecraft
S/V	Space Vehicle
SBAS	Space Based Augmentation System
SDMA	Space Division Multiple Access
TDMA	Time Division Multiple Access
TEC	Total Elctron Content (of the Ionosphere)
URE	User Range Error
UT	Universal Time
UT1	Universal Time 1(Siderial Time)
UTC	Universal Time Coordinated
WAAS	Wide Area Augmentation System
WGS-84	World Geodetic System of 1984
XIPS	Xenon Ion Propulsion System

1 INTRODUCTION

The conventional way of precise orbit determination is to take pseudorange, Doppler or angle measurements of a satellite with respect to a fixed point on the ground, and apply differential corrections to a (more or less accurate) predicted reference orbit.

A radio signal travelling from one satellite to another can also be used to derive the distance between these two space crafts. Although the distance is not measured between a satellite and a known point– like a ground station – but between two satellites, these measurements can be used to derive the satellite's state vectors, i.e. their position and velocity at a given time. Although these measurements can not be used solely, i.e. with out any ground reference, they provide additional information. The following picture shows two satellites, which are conducting inter satellite measurements. At the same time, ranging stations on the ground take measurements from both satellites.

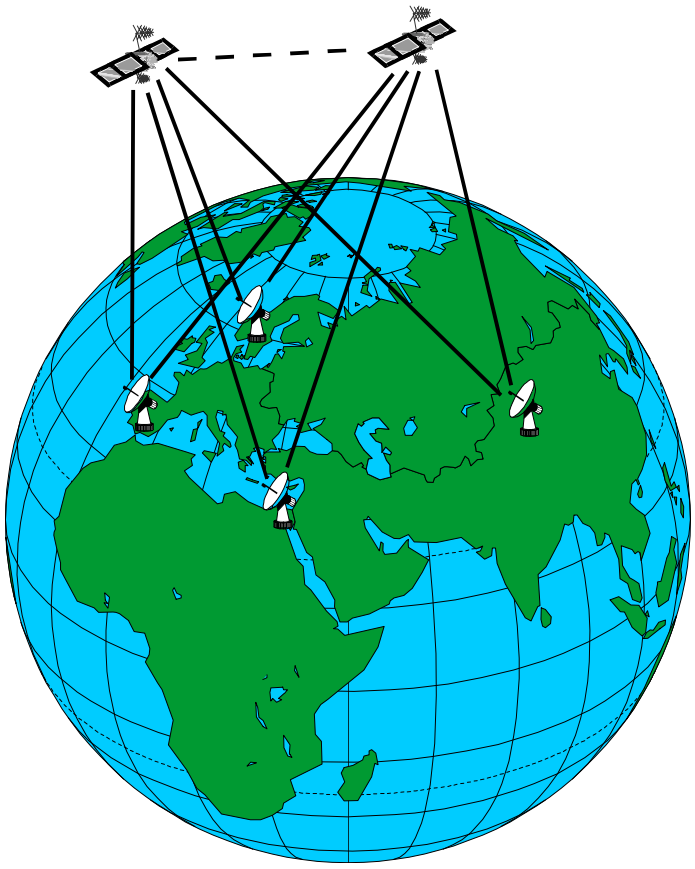

Figure 1-1Principle of Inter Satellite Measurements

The ISL (inter satellite links) provides an observation with a geometry completely different from those of the ground referenced links, as can be seen from the figure. This is an a advantage especially for satellites at higher orbits. From a satellite in geostationary orbit, the earth is seen under a small angle of approximately 17°, which implies also the limit for the

maximum possible separation angle between two ground referenced observations. This leads to a significant larger uncertainty in the off-radial components of the orbit, than in the radial component. In the following figure the distances between satellites and earth, as well as the earth's diameter are approximately drawn to scale.

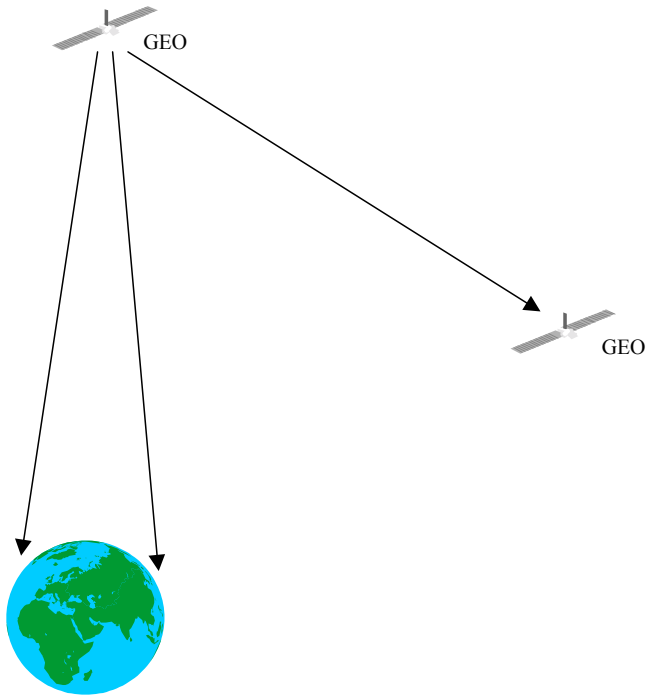

Figure 1-2 ISL Tracking Geometry for a GEO Satellite

An ISL to another GEO satellite results in a much better observability of the tangential orbit errors. As a result, the decorrelation of the clock error and the radial orbit error is enhanced and shortened. Another benefit from ISL's is the improvement in satellite tracking capability for satellites at low earth orbit (LEO). Usually a large scale ground network is required to provide reasonable coverage of the complete LEO satellite orbit. The ground network of the DORIS system, for instance, consist of 51 ground beacons distributed over the entire world. If for example a GEO would be used to establish an ISL, the LEO satellite would remain in view to that satellite for more than one third of its orbit. The next figure indicates the tracking geometry for a LEO / GEO inter satellite link.

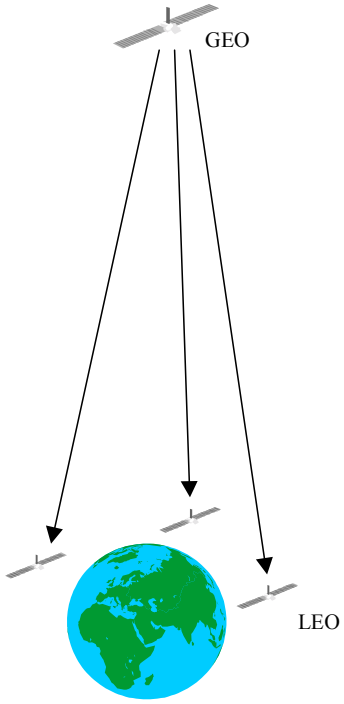

Figure 1-3 Tracking Geometry for LEO Satellite

On the other hand, its also clear that an ISL payload increases the complexity of the space craft (mass, power consumption) and therefore its cost. There is a trade off between the benefits with respect to accuracy / observability and overall system complexity, which has to be done.

This text deals with the mathematical methods to account for ISL's in the state estimation process. The majority of the equations and algorithms given in the next chapters have been implemented in a software package, thus also results from simulation runs will be given. At the end in this text, the topic of autonomous (onboard) state estimation will be investigated, which seems to be a perfect match for inter satellite links, at least on the first glance. The closing chapters contain recommendation concerning the possibilities of ISL's in the context of a future GNSS 2 as well as a conclusion.

2 ISL OBSERVATION MODEL

The majority of the observation used in the orbit determination of satellites orbiting the earth, are radio frequency (pseudo-) range and Doppler measurements. Angle measurements, i.e. azimuth and elevation provide insufficient accuracy for precise orbit determination. Laser ranging measurements, which are the most precise measurements available today, are strongly subjected to weather conditions. Thus, they are used mainly for calibration purposes. The observations considered in this text, are therefore only one and two-way range and range rate (Doppler) measurement.

2.1 Derivation of the Range Equation

The pseudo range between two points is the difference between two clock readings, the clock at the sender and the clock at the receiver. If the clocks are coarsely synchronized, the largest part of the measured clock difference will be due to the signal travelling at the speed of light, thus representing the geometric distance.

$$L = \left(T_{Sat} - T_{Ground/Sat2}\right) \cdot c = \qquad \text{Eq. 2.1-1}$$
$$= \rho_{Geometric} + c \cdot \left(\delta T_{Sat} - \delta T_{Ground/Sat2}\right) + \delta_{iono} + \delta_{Tropo} + \delta_{Multipath} + \varepsilon_{noise}$$

with

L Pseudo range

c Speed of light

δT_{Sat} Deviation of satellite clock from system time

δT_{Ground} Deviation of ground receiver clock from system time

δ_{Iono} Ionospheric delay

δ_{Tropo} Troposheric delay

$\delta_{Multipath}$ Multipath error

ε_{noise} Thermal noise

and

$$\rho_{Geometric} = \sqrt{\left(x_1 - x_2\right)^2 + \left(y_1 - y_2\right)^2 + \left(z_1 - z_2\right)^2} \qquad \text{Eq. 2.1-2}$$

being the geometric distance between the two points.

To obtain a linear measurement equation, the partials with respect to the unknown parameters have to be formed. Assuming that all other error contributions except the satellite clock can be measured or modelled, and therefore removed, we can write the linearized observation equation as a function of the three position errors and the satellite clock error. Remaining errors e.g. due to mismodelling are added to the measurement noise.

For a ground measurement, only the partials with respect to the satellites states are formed. The position of the ground station is assumed to be exact. The range equation for example would yield

$$L - L_0 = \frac{x_{Sat} - x_{GS}}{L_0} \cdot \Delta x + \frac{y_{Sat} - y_{GS}}{L_0} \cdot \Delta y + \frac{z_{Sat} - z_{GS}}{L_0} \cdot \Delta z + c \cdot \delta T_{Sat} \qquad \text{Eq. 2.1-3}$$

with

L_0 Predicted pseudo range computed from nominal trajectory

For inter satellite links, the partial of the range equation with respect to both satellites states would have to be formed. Above equation would transform to

$$L - L_0 = \qquad \text{Eq. 2.1-4}$$
$$= \frac{x_{Sat,1} - x_{Sat,2}}{L_0} \cdot \Delta x_1 + \frac{y_{Sat,1} - y_{Sat,2}}{L_0} \cdot \Delta y_1 + \frac{z_{Sat,1} - z_{Sat,2}}{L_0} \cdot \Delta z_1 + c \cdot \delta T_{Sat1}$$
$$- \frac{x_{Sat,1} - x_{Sat,2}}{L_0} \cdot \Delta x_2 - \frac{y_{Sat,1} - y_{Sat,2}}{L_0} \cdot \Delta y_2 - \frac{z_{Sat,1} - z_{Sat,2}}{L_0} \cdot \Delta z_2 - c \cdot \delta T_{Sat2}$$

As can be seen from the equation above, an ISL observation impacts the state variables of both, the measuring and the target satellite.

2.2 Derivation of the Range Rate Equation

A radio signal being emitted from a moving sender is subjected to shift in the received frequency, called the Doppler shift. This frequency shift is proportional to the velocity along the line of sight.

$$\frac{f_{\mathrm{Receive}}}{f_{Transmit}} = \left(1 - \frac{\dot{L}}{c}\right) \quad or \quad \Delta f = f_{\mathrm{Transmit}} \cdot \frac{\dot{L}}{c} \qquad \text{Eq. 2.2-1}$$

Normally, the frequency shift can not be directly measured, but has to be derived from the phase rate, (or the so called integrated Doppler count) instead. In the context of orbit determination, we are not interested in the frequency shift itself, but in the range rate which caused the shift. Fortunately, the phase rate can be directly scaled to a delta-range by multiplying with the carrier wave length. A division through the integration time yields the range rate, the value we are interested in. A drawback of a range rate derived from integrated Doppler counts is that it is an averaged instead of an instantaneous value. But for short integration times, this fact can be neglected.

From geometric considerations, or by forming the derivative of the range equation with respect to time, we obtain the measurement equation for a range rate observable.

The range rate, i.e. the velocity along the line of sight vector between two points can be written as:

$$\dot{L} = \frac{x_1 - x_2}{L} \cdot (\dot{x}_1 - \dot{x}_2) + \frac{y_1 - y_2}{L} \cdot (\dot{y}_1 - \dot{y}_2) + \frac{z_1 - z_2}{L} \cdot (\dot{z}_1 - \dot{z}_2) \qquad \text{Eq. 2.2-2}$$

with point index 1 being the (first) satellite and point two being either a known location on the earth's surface or a second satellite.

Forming the partials with respect to the satellites state yields

$$\frac{\partial \dot{L}}{\partial \dot{x}} = \frac{x_1 - x_2}{L} \qquad \text{Eq. 2.2-3}$$

$$\frac{\partial \dot{L}}{\partial x} = \frac{\dot{x}_1 - \dot{x}_2}{L} - \frac{\dot{L} \cdot (x_1 - x_2)}{L^2} = 0$$

The partial with respect to the position and velocity in y- and z-direction can be obtained in a similar manner. From the two equations above it can be see that the range rate equation is already linear. We can therefore write the linear measurement equation for a range rate observable in the case of an inter satellite link as

$$\dot{L} - \dot{L}_0 = \qquad \text{Eq. 2.2-4}$$

$$= \frac{x_{Sat,1} - x_{Sat,2}}{L_0} \cdot \Delta\dot{x}_1 + \frac{y_{Sat,1} - y_{Sat,2}}{L_0} \cdot \Delta\dot{y}_1 + \frac{z_{Sat,1} - z_{Sat,2}}{L_0} \cdot \Delta\dot{z}_1$$

$$- \frac{x_{Sat,1} - x_{Sat,2}}{L_0} \cdot \Delta\dot{x}_2 - \frac{y_{Sat,1} - y_{Sat,2}}{L_0} \cdot \Delta\dot{y}_2 - \frac{z_{Sat,1} - z_{Sat,2}}{L_0} \cdot \Delta\dot{z}_2$$

Note that the range rate measurement is independent of the clock state of the satellite.

3 STATE ESTIMATION

Generally spoken, the satellites orbit is determined by presuming an approximate trajectory and determining and applying differential corrections to that a-priori orbit. Basically, there are two concepts of ephemeris determination using differential corrections

- estimating the real time state using a Kalman filter
- estimating the initial conditions, i.e. position and velocity together with model parameters using a batch estimator. This can be done using the classical least squares adjustment or via Kalman filter.

The a-priori orbit, used for state prediction and linearization, can be generated using a geometric or dynamic model. The estimated orbit corrections can be fed back into the orbit propagator to obtain a better a priori orbit for successive epochs.

3.1 Linearization of Dynamic and Observation Model

Regardless of the estimator type, the observation equation as well as the dynamic equation have to be linear. The differential equations for the state dynamic have to be of the form

$$\dot{\bar{x}} = \mathbf{F} \cdot \bar{x} + \bar{n} \qquad \text{Eq. 3.1-1}$$

The systems state is observed by means of some measurements z, which are related to the systems state by the measurement matrix H, a system of linear observation equations

$$\bar{z} = \mathbf{H} \cdot \bar{x} + \bar{n} \qquad \text{Eq. 3.1-2}$$

where

$\bar{n}$ white noise

Unfortunately orbit propagation is a highly non-linear problem and the derivative of the systems state with respect to time is a system of non-linear functions of the systems state and of time.

$$\frac{d\bar{x}}{dt} = \mathbf{f}(\bar{x}(t), t) + \bar{n} \qquad \text{Eq. 3.1-3}$$

Measuring a slant range or a slant range rate also yields non-linear observation equations represented by

$$\bar{z} = \mathbf{h}\left(\bar{x}(t)\right) + \bar{n} \qquad \text{Eq. 3.1-4}$$

A solution is obtained by linearization of the dynamic functions and observation equations around a approximate system state, i.e. a precomputed trajectory.

$$\mathbf{f}\left(\vec{x}(t)\right) = \mathbf{f}\left(\hat{\vec{x}}(t)\right) + \left.\frac{\partial \mathbf{f}}{\partial \vec{x}}\right|_{\vec{x}=\hat{\vec{x}}} \left(\vec{x} - \hat{\vec{x}}\right) + \ldots \qquad \text{Eq. 3.1-5}$$

with

$$F = \left.\frac{\partial \mathbf{f}}{\partial \vec{x}}\right|_{\vec{x}=\hat{\vec{x}}}$$ Dynamic matrix of the residual or error state

and

$$\mathbf{h}(\vec{x}(t)) = \mathbf{h}\left(\hat{\vec{x}}(t)\right) + \left.\frac{\partial h}{\partial \vec{x}}\right|_{\vec{x}=\hat{\vec{x}}} \left(\vec{x} - \hat{\vec{x}}\right) + \ldots$$ Eq. 3.1-6

with

$$H = \left.\frac{\partial h}{\partial \vec{x}}\right|_{\vec{x}=\hat{\vec{x}}}$$ Measurement matrix of the residual or error state

The error state is the difference between thr real and the nominal system state

$$\Delta\bar{x}_k = \bar{x}_k\big|_{real} - \bar{x}_k\big|_{nominal}$$ Eq. 3.1-7

where the nominal state is obtained by integrating the nonlinear equations, i.e. numerically integrating the equations of motion.

$$\bar{x}_k\big|_{nominal} = \int_{t_{k-1}}^{t_k} \mathbf{f}(\bar{x}(t), t)dt$$ Eq. 3.1-8

In a similar manner, the residual observations can be derived

$$\Delta\bar{z}_k = \bar{z}_k\big|_{real} - \bar{z}_k\big|_{nominal}$$ Eq. 3.1-9

with

$$\bar{z}_k\big|_{nominal} = \mathbf{h}(\bar{x}(t)\big|_{nominal}, t)$$ Eq. 3.1-10

3.2 State Vector

The state vector at least contains the position errors, i.e. the difference between nominal and real position. If the clock offset can not be measured directly e.g. by two way measurements, it has to be estimated together with the orbit errors. This implies that for each epoch at least four measurement are available to estimate the instantaneous position. However, in orbit determination there are frequently less observations than states per measurement epoch. For example, a GPS satellite is (nearly) never tracked by more than two ground stations simultaneously. To allow the accumulation of measurements over a longer orbit arc, the velocity errors have to be estimated as well.

Thus, the minimum state vector consists of the following elements

$$\vec{X} = \begin{bmatrix} \Delta x \\ \Delta y \\ \Delta z \\ \Delta \dot{x} \\ \Delta \dot{y} \\ \Delta \dot{z} \\ \delta T \end{bmatrix}$$ Eq. 3.2-1

This state vector is normally sufficient for real time estimation, where the orbit integration time is relatively short. If a batch estimator is used, other states like dynamic model parameter errors and observation biases can be (and have to be!) included because integration times are typically several hours, up to days. The main accuracy driver of the orbit determination via batch estimation process is the prediction accuracy, because the state vector is estimate only at a certain epoch as a initial condition. Thus, if there is a weakness or imperfection in the physical modelling of the acting forces, the orbit determination accuracy will degrade with increasing integration time. The augmented state vector could therefore look like

$$\vec{X} = \begin{bmatrix} \Delta x \\ \Delta y \\ \Delta z \\ \Delta \dot{x} \\ \Delta \dot{y} \\ \Delta \dot{z} \\ \delta T \\ \delta \rho \\ \delta P_S \\ \text{etc.} \end{bmatrix}$$ Eq. 3.2-2

These force model imperfections may be for instance an inaccurate knowledge of the air density or the solar radiation flux. The estimator has to solve for these parameters additional to the satellites states. Thus, the solve-for parameter vector of a batch estimator normally has to be significantly larger than the state vector of a real time estimator.

If inter satellite links have to be considered, the state vector has to consist of the complete state vectors of all involved satellites.

$$\vec{X} = \begin{bmatrix} \vec{X}_1 \\ \vec{X}_2 \\ \dots \\ \vec{X}_n \end{bmatrix} \qquad \text{Eq. 3.2-3}$$

With at least 7 states, which have to be considered per satellite, it can easily be seen that the state of a complete constellation gets very large. This leads for instance to a state vector magnitude of 126 states for a constellation of 18 space vehicles. Although many small filters (one per each satellite) would result in a smaller computational burden, it is absolutely necessary to process all satellites in one large filter, because the state estimates of the satellites get correlated due to the inter satellite links.

3.3 State Transition and Transition Matrix

The system of linear differential equations

$$\dot{\bar{x}} = \mathbf{F} \cdot \bar{x} \qquad \text{Eq. 3.3-1}$$

is not very well suited for the implementation of a discrete estimation process in a digital computer. The discrete formulation of the Kalman filter for example requires the state transient to be expressed by a simple vector-matrix-operation

$$\bar{x}_k = \mathbf{\Phi}(t_k, t_{k-1}) \cdot \bar{x}_{k-1} \qquad \text{Eq. 3.3-2}$$

with $\Phi(t_k,t_{k-1})$ being the *transition matrix* from the epoch t_{k-1} to the epoch t_k. In a more general way, Eq. 3.3-2 can be expressed as

$$\vec{x}_k = \frac{\partial \vec{x}_k}{\partial \vec{x}_{k-1}} \cdot \vec{x}_{k-1} \qquad \text{Eq. 3.3-3}$$

with the transition matrix $\Phi(t_k,t_{k-1})$ being interpreted as the Jacobian

$$\frac{\partial \bar{x}_k}{\partial \bar{x}_{k-1}} = \begin{bmatrix} \frac{\partial x_k}{\partial x_{k-1}} & \frac{\partial x_k}{\partial y_{k-1}} & \frac{\partial x_k}{\partial z_{k-1}} & \dots \\ \frac{\partial y_k}{\partial x_{k-1}} & \frac{\partial y_k}{\partial y_{k-1}} & \frac{\partial y_k}{\partial z_{k-1}} & \dots \\ \frac{\partial z_k}{\partial x_{k-1}} & \frac{\partial z_k}{\partial y_{k-1}} & \frac{\partial z_k}{\partial z_{k-1}} & \dots \\ \dots & \dots & \dots & \dots \end{bmatrix} \qquad \text{Eq. 3.3-4}$$

The transition matrix is needed not only for the state transition and covariance propagation in the Kalman filter, but also for mapping observations from an arbitrary time to the initial epoch in a batch estimation process.

There are several ways to derive the transition matrix $\Phi(t_k,t_{k-1})$. If the dynamic matrix $\mathbf{F}$ is constant over the interval (t_k,t_{k-1}), the transition matrix $\Phi(t_k,t_{k-1})$ can be obtained by solving the differential equation using the so called matrix exponential.

$$\dot{\vec{x}} = \frac{d\vec{x}}{dt} = \mathbf{F}\cdot\vec{x} \qquad \text{Eq. 3.3-5}$$

$$\Rightarrow \frac{d\vec{x}}{\vec{x}} = \mathbf{F}\cdot dt$$

$$\Rightarrow \int_{k-1}^{k}\frac{d\vec{x}}{\vec{x}} = \int_{k-1}^{k}\mathbf{F}\cdot dt = \mathbf{F}\cdot\int_{k-1}^{k}dt$$

$$\Rightarrow \ln\vec{x}_k - \ln\vec{x}_{k-1} = \ln\frac{\vec{x}_k}{\vec{x}_{k-1}} = \mathbf{F}\cdot\left(t_k - t_{k-1}\right)$$

$$\Rightarrow \frac{\vec{x}_k}{\vec{x}_{k-1}} = e^{\mathbf{F}\cdot(t_k - t_{k-1})}$$

$$\Rightarrow \vec{x}_k = e^{\mathbf{F}\cdot(t_k - t_{k-1})}\cdot\vec{x}_{k-1}$$

By using the power expansion of the exponential function

$$e^{\mathbf{F}\cdot\Delta t} = \mathbf{I} + \mathbf{F}\cdot\Delta t + \tfrac{1}{2!}\cdot\mathbf{F}^2\cdot\Delta t^2 + \tfrac{1}{3!}\cdot\mathbf{F}^3\cdot\Delta t^3 + \ldots + \tfrac{1}{n!}\cdot\mathbf{F}^n\cdot\Delta t^n \qquad \text{Eq. 3.3-6}$$

and truncating after the linear term, we obtain the transition matrix by

$$\mathbf{\Phi} = \mathbf{I} + \mathbf{F}\cdot\Delta t \qquad \text{Eq. 3.3-7}$$

It has to be considered that the dynamic matrix has been obtained from linearization. Furthermore it can be considered as approximately constant only over relatively short period of time. Therefore, this way of obtaining the transition matrix is limited to short transition times.

Starting with the equations of motion and neglecting all influences but the point mass attraction of the Earth, we yield

$$\frac{dx}{dt} = \dot{x} \quad , \quad \frac{dy}{dt} = \dot{y} \quad , \quad \frac{dz}{dt} = \dot{z} \qquad \text{Eq. 3.3-8}$$

$$\frac{d\dot{x}}{dt} = \ddot{x} = -\frac{GM}{r^3}\cdot x$$

$$\frac{d\dot{y}}{dt} = \ddot{y} = -\frac{GM}{r^3}\cdot y$$

$$\frac{d\dot{z}}{dt} = \ddot{z} = -\frac{GM}{r^3}\cdot z$$

Calculating the partial with respect to position and velocity, the part of the a satellites dynamic matrix considering only position and velocity errors can therefore be expressed by

$$F_{Sat} = \begin{bmatrix} 0 & 0 & 0 & 1 & 0 & 0 \\ 0 & 0 & 0 & 0 & 1 & 0 \\ 0 & 0 & 0 & 0 & 0 & 1 \\ -(1-3\frac{x_k^2}{r_k^2})\frac{GM}{r_k^3} & 3\frac{x_k y_k}{r_k^5}GM & 3\frac{x_k z_k}{r_k^5}GM & 0 & 0 & 0 \\ 3\frac{x_k y_k}{r_k^5}GM & -(1-3\frac{y_k^2}{r_k^2})\frac{GM}{r_k^3} & 3\frac{y_k z_k}{r_k^5}GM & 0 & 0 & 0 \\ 3\frac{x_k z_k}{r_k^5}GM & 3\frac{y_k z_k}{r_k^5}GM & -(1-3\frac{z_k^2}{r_k^2})\frac{GM}{r_k^3} & 0 & 0 & 0 \end{bmatrix} \quad \text{Eq. 3.3-9}$$

An other way would be to compute the Jacobian directly, either analytically or by means of computing the partials numerically. The possible length of the transition interval (and therefore the orbit arc) is nearly unlimited, thus enabling long integration times. Unfortunately, the analytical solution is restrained to very simple orbit models. The numerical solution is the most accurate, because the state propagation is computed using the non linear force model. A drawback is the high computational burden, because for n states, the trajectory has to be propagated n+1 times. One trajectory is derived from the nominal state at epoch t_{k-1}, and n trajectories are computed by adding a small increment on each of the states, as indicated in Eq. 3.3-10.

$$\begin{aligned} \vec{X}_{0,k} &= f(x_{k-1}, y_{k-1}, z_{k-1}, \dot{x}_{k-1}, \dot{y}_{k-1}, \dot{z}_{k-1}, ...) \quad \text{Eq. 3.3-10} \\ \vec{X}_{x,k} &= f(x_{k-1} + \Delta x, y_{k-1}, z_{k-1}, \dot{x}_{k-1}, \dot{y}_{k-1}, \dot{z}_{k-1}, ...) \\ \vec{X}_{y,k} &= f(x_{k-1}, y_{k-1} + \Delta y, z_{k-1}, \dot{x}_{k-1}, \dot{y}_{k-1}, \dot{z}_{k-1}, ...) \\ \vec{X}_{z,k} &= f(x_{k-1}, y_{k-1}, z_{k-1} + \Delta z, \dot{x}_{k-1}, \dot{y}_{k-1}, \dot{z}_{k-1}, ...) \\ \vec{X}_{\dot{x},k} &= f(x_{k-1}, y_{k-1}, z_{k-1}, \dot{x}_{k-1} + \Delta \dot{x}, \dot{y}_{k-1}, \dot{z}_{k-1}, ...) \\ \vec{X}_{\dot{y},k} &= f(x_{k-1}, y_{k-1}, z_{k-1}, \dot{x}_{k-1}, \dot{y}_{k-1} + \Delta \dot{y}, \dot{z}_{k-1}, ...) \\ \vec{X}_{\dot{z},k} &= f(x_{k-1}, y_{k-1}, z_{k-1}, \dot{x}_{k-1}, \dot{y}_{k-1}, \dot{z}_{k-1} + \Delta \dot{z}, ...) \\ &... \end{aligned}$$

The transition matrix is then simply derived by subtracting the appropriate state at t_k, resulting from the modified state at epoch t_{k-1} and the nominal state and dividing by the increment.

$$\boldsymbol{\Phi}(t_k, t_{k-1}) = \begin{bmatrix} \frac{x_{x,k} - x_{0,k}}{\Delta x} & \frac{y_{x,k} - y_{0,k}}{\Delta x} & \frac{z_{x,k} - z_{0,k}}{\Delta x} & \frac{\dot{x}_{x,k} - \dot{x}_{0,k}}{\Delta x} & \cdots \\ \frac{x_{y,k} - x_{0,k}}{\Delta y} & \frac{y_{y,k} - y_{0,k}}{\Delta y} & \frac{z_{y,k} - z_{0,k}}{\Delta y} & \frac{\dot{x}_{y,k} - \dot{x}_{0,k}}{\Delta y} & \cdots \\ \frac{x_{z,k} - x_{0,k}}{\Delta z} & \frac{y_{z,k} - y_{0,k}}{\Delta z} & \frac{z_{z,k} - z_{0,k}}{\Delta z} & \frac{\dot{x}_{z,k} - \dot{x}_{0,k}}{\Delta z} & \cdots \\ \frac{x_{\dot{x},k} - x_{0,k}}{\Delta \dot{x}} & \frac{y_{\dot{x},k} - y_{0,k}}{\Delta \dot{x}} & \frac{z_{\dot{x},k} - z_{0,k}}{\Delta \dot{x}} & \frac{\dot{x}_{\dot{x},k} - \dot{x}_{0,k}}{\Delta \dot{x}} & \cdots \\ \frac{x_{\dot{y},k} - x_{0,k}}{\Delta \dot{y}} & \frac{y_{\dot{y},k} - y_{0,k}}{\Delta \dot{y}} & \frac{z_{\dot{y},k} - z_{0,k}}{\Delta \dot{y}} & \frac{\dot{x}_{\dot{y},k} - \dot{x}_{0,k}}{\Delta \dot{y}} & \cdots \\ \cdots & \cdots & \cdots & \cdots & \cdots \quad \cdots \end{bmatrix} \qquad \text{Eq. 3.3-11}$$

In the case of using inter satellite links, a transition matrix for the complete constellation is obtained simply arranging the individual transition matrices as indicated in Eq. 3.3-12.

$$\Phi_{Total} = \begin{bmatrix} \Phi_{Sat,1} & \overline{0} & \cdots & \overline{0} \\ \overline{0} & \Phi_{Sat,2} & \cdots & \overline{0} \\ \cdots & \cdots & \cdots & \cdots \\ \overline{0} & \overline{0} & \cdots & \Phi_{Sat,n} \end{bmatrix} \qquad \text{Eq. 3.3-12}$$

3.4 Least Squares Batch Estimation

Using a linear or linearized relationship between measurement z and state vector x

$$\overline{z} = \mathbf{H} \cdot \overline{x} \qquad \text{Eq. 3.4-1}$$

the sum of squares of the residual error gets minimised by

$$\overline{x} = \left(\mathbf{H}^T \mathbf{H}\right)^{-1} \cdot \mathbf{H}^T \cdot \overline{z} \qquad \text{Eq. 3.4-2}$$

The Matrix **H** contains the partial derivatives of the measurements with respect to the instantaneous state. For orbit determination, the measurements of a longer orbit arc have to be considered to estimate the state at a certain epoch, so the equation has to be rewritten

$$\overline{z} = \mathbf{H}' \cdot \overline{x}_0 \qquad \text{Eq. 3.4-3}$$

where the modified measurement matrix **H'** contains the partial derivatives of the measurements z with respect to the state vector at epoch x_0. This transforms Eq. 3.4-2 to

$$\overline{x}_0 = \left(\mathbf{H}'^T \mathbf{H}'\right)^{-1} \cdot \mathbf{H}'^T \cdot \overline{z} \qquad \text{Eq. 3.4-4}$$

The partials of the measurements with respect to the state at epoch are obtained by

$$\mathbf{H}'_k = \frac{\partial \bar{z}}{\partial \bar{x}_0} = \frac{\partial \bar{z}}{\partial \bar{x}} \cdot \frac{\partial \bar{x}}{\partial \bar{x}_0} = \mathbf{H} \cdot \frac{\partial \bar{x}}{\partial \bar{x}_0} \qquad \text{Eq. 3.4-5}$$

The partials of the actual state x with respect to the state at epoch x_0 are expressed by the Jacobian, and therefore the transition matrix $\mathbf{\Phi}$.

$$\bar{x} = \frac{\partial \bar{x}}{\partial \bar{x}_0} \cdot \bar{x}_0 = \mathbf{\Phi}(t, t_0) \cdot \bar{x}_0 \qquad \text{Eq. 3.4-6}$$

Thus we can write for an arbitrary instant of time t_k

$$\mathbf{H}'_k = \mathbf{H}_k \cdot \mathbf{\Phi}_k \qquad \text{Eq. 3.4-7}$$

The transition matrix from epoch to a time t_k can be computed successive from the preceding transition matrices, only the transient from the previous point to the instant has to be computed

$$\mathbf{\Phi}_k = \mathbf{\Phi}(t_k, t_0) = \mathbf{\Phi}(t_k, t_{k-1}) \cdot \mathbf{\Phi}(t_{k-1}, t_{k-2}) \cdot .... \cdot \mathbf{\Phi}(t_1, t_0) \qquad \text{Eq. 3.4-8}$$

If the transition matrix F is computed from a linearized dynamic matrix F, the time interval (t_k,t_0) has to be relatively short. For longer batch lengths one would use the numerically derived Jacobian (see Eq. 3.3-10, Eq. 3.3-11).

The measurement equation system containing measurements of a certain time interval is obtained by forming the appropriate observation matrices H'_k. For example, if the measurements of four observation times $t_0 - t_3$ are used to determine the state at t_0, the observation model would look the following way

$$\begin{bmatrix} \bar{z}_3 \\ \bar{z}_2 \\ \bar{z}_1 \\ \bar{z}_0 \end{bmatrix} = \begin{bmatrix} \mathbf{H}_3 \cdot \mathbf{\Phi}(t_3, t_0) \\ \mathbf{H}_2 \cdot \mathbf{\Phi}(t_2, t_0) \\ \mathbf{H}_1 \cdot \mathbf{\Phi}(t_1, t_0) \\ \mathbf{H}_0 \end{bmatrix} \cdot \bar{x}_0 \qquad \text{Eq. 3.4-9}$$

3.4.1 Weighted Least Squares

Usually, not all measurements z are made with the same accuracy. Thus, Eq. 3.4-2 has be rewritten as

$$\bar{x} = \left(\mathbf{H}^T \cdot \mathbf{W} \cdot \mathbf{H}\right)^{-1} \cdot \mathbf{H}^T \cdot \mathbf{W} \cdot \bar{z} \qquad \text{Eq. 3.4-10}$$

to account for the weights of the individual measurements. For uncorrelated measurements, the weighting matrix W is simply

$$\mathbf{W} = \begin{bmatrix} \frac{1}{\sigma_1^2} & 0 & 0 & \dots & 0 \\ 0 & \frac{1}{\sigma_{21}^2} & 0 & \dots & 0 \\ 0 & 0 & \frac{1}{\sigma_3^2} & \dots & 0 \\ \dots & \dots & \dots & \dots & 0 \\ 0 & 0 & 0 & 0 & \frac{1}{\sigma_{n1}^2} \end{bmatrix} \qquad \text{Eq. 3.4-11}$$

with σ_i^2 being the variance of the i-th measurement.

3.4.2 Introducing apriori Statistic Information

Sometimes, a good a-priori estimate of some states or the complete state vector, together with a related accuracy value (variance) is available. One way would be, to introduce the apriori knowledge of the known state variables as pseudo observations, and therefore to augment the measurement vector.

If an estimate of the complete state vector is available, typically from the last iteration in an iterative process, Eq. 3.4-2 can be, according to [BIR-77] rewritten to

$$\bar{x}_{LS} = \left(\mathbf{\Lambda} + \mathbf{H}^T\mathbf{H}\right)^{-1} \cdot \left(\mathbf{\Lambda} \cdot \vec{x}_0 + \mathbf{H}^T \cdot \bar{z}\right) \qquad \text{Eq. 3.4-12}$$

with Λ being the so called apriori information matrix. The information matrix is the inverse of the covariance matrix. Especially in the case of bad observation geometry together with good predictability (high orbit altitudes) this method can be used very successful.

3.5 Kalman Filtering

3.5.1 Real Time Estimation

If real time state estimation is desired, the state estimator can be implemented as a linearized or extended Kalman filter. In the following, only a brief overview of the Kalman filter algorithm is given. More detailed information can be found in literature, e.g. [GEL-88]. The Kalman filter estimates the state vector $\bar{x}$ of dynamic system, described by a system of first order linear differential equations contained in the transition matrix $\mathbf{\Phi}$.

With the linearized equations of motion, the transition or prediction of the error state can be written as

$$\tilde{\vec{x}}_k = \mathbf{\Phi}_{k-1} \cdot \hat{\vec{x}}_{k-1} \qquad \text{Eq. 3.5-1}$$

with

x state vector

Φ (linearized) transition matrix

The transition matrix can either be derived from the linearized dynamic matrix or by numerical derivation of the Jacobian (see chapter 3.3). The transition matrix is not only needed for state prediction, but also for propagation of the covariance matrix P. In fact, the "noise shaping" function of the transition matrix is essential, if states which can not be directly observed are included in the state vector, e.g. velocity is estimated from range measurements. According to [GEL-88], the covariance propagation can be written as

$$\tilde{P}_k = \Phi_{k-1} \cdot \hat{P}^T \cdot \Phi_{k-1}^T + \mathrm{diag}\left(Q_{k-1}\right) \qquad \text{Eq. 3.5-2}$$

with

P covariance matrix

Q process noise

If measurements are available, the predicted covariance matrix and state vector can be updated. The updated state is then obtained by

$$\hat{\vec{x}}_k = \tilde{\vec{x}}_k + K_k \cdot \left(\vec{z}_k - H_k \cdot \tilde{\vec{x}}_k\right) \qquad \text{Eq. 3.5-3}$$

with

z measurement

K Kalman gain matrix

and the updated covariance matrix by

$$\hat{P} = \left(I - K_k H_k\right)\tilde{P}_k \qquad \text{Eq. 3.5-4}$$

with

I Identity matrix

The Kalman gain matrix can be interpreted as a weighting matrix of the innovation introduced by the measurement z. It depends on the apriori covariance and the measurement noise and can be computed from the following equation.

$$K_k = \tilde{P}_k \cdot H_k^T \left(H_k \cdot \tilde{P} \cdot H_k^T + \mathrm{diag}\left(R_k\right)\right)^{-1} \qquad \text{Eq. 3.5-5}$$

with

R measurement noise

H (linearized) observation matrix

3.5.2 Filtering to Epoch

It is possible to operate the Kalman filter as a batch estimator. The filter algorithms are the same as for the real time filter, except there is no process noise, state transient or covariance propagation within the processed batch interval. Instead of the real time measurement matrix **H**, the measurement matrix

$$H'_k = \begin{bmatrix} H_k \cdot \Phi(t_k, t_0) \\ H_{k-1} \cdot \Phi(t_{k-1}, t_0) \\ \dots \\ H_1 \cdot \Phi(t_1, t_0) \\ H_0 \end{bmatrix} \qquad \text{Eq. 3.5-6}$$

which maps the measurements to an epoch, has to be applied. The remaining step from the Kalman filter algorithm have to be rewritten as follows:

$$K_k = \tilde{P}_k \cdot H'^T_k \left(H'_k \cdot \tilde{P} \cdot H'^T_k + \mathrm{diag}(R_k) \right)^{-1} \qquad \text{Eq. 3.5-7}$$

$$\hat{\tilde{x}}_k = \tilde{\tilde{x}}_k + K_k \cdot \left(\vec{z}_k - H'_k \cdot \tilde{\tilde{x}}_k \right) \qquad \text{Eq. 3.5-8}$$

$$\hat{P} = \left(I - K_k H'_k \right) \tilde{P}_k \qquad \text{Eq. 3.5-9}$$

The results obtained from a Kalman filter in batch mode are the same as obtained by the least squares adjustment.

3.5.3 Filter Structures

A Kalman filter can be implemented applying various structures. In a linearized Kalman filter the estimator would have an open loop structure, in which the filter observes the system state. In the context of orbit estimation this would mean, that the deviation from a pre-computed trajectory is estimated and corrections are only fed forward.

If the estimated deviations from the predicted orbit are fed back into the orbit propagator to obtain a better prediction for the next time, one has an extended Kalman filter utilising a closed loop structure.

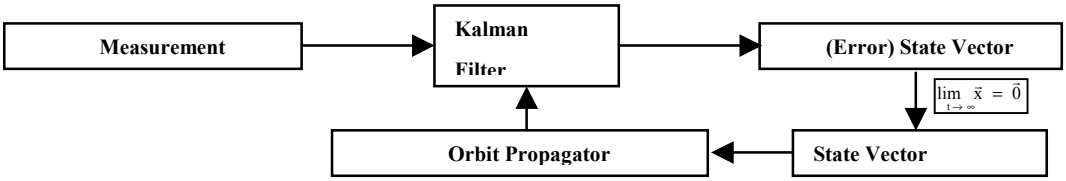

The greater flexibility of the extended filter if compared to the linearized filter is an advantage as well as a disadvantage. Good measurements presumed, the extended filter stays closer to the true state than the linearized, but it can be corrupted easily by biased measurements.

In practice, a mixed structure would be applied to the orbit estimation problem. The estimated errors are only fed back into the orbit propagator, if they are assumed to be known precise enough. The "feed back" criterion could be for example

$$\frac{|x|}{\sigma_x} > c_{Treshold}, \qquad \text{Eq. 3.5-10}$$

$$\text{with} \qquad 1 < c_{Treshold} < 10$$

where σ_x is the square root of the variance, obtain from the Kalman filter covariance matrix. In other words this would mean, the trajectory is corrected only if the uncertainty of the error is several times lower than the error itself.

4 ORBIT COMPUTATION

The computation of a satellite orbit can be done using different approaches:

- The analytical solution, where orbits are treated as conical sections (Kepler orbits)
- The numerical integration of the equations of motion, described by a (more or less) accurate force model.

Satellite orbiting in the relative vicinity of the earth are subject to a lot of disturbing forces, thus only the numeric integration approach leads to satisfactory result. An accurate orbit propagator is required not only for simulation purpose, but also for state prediction in the orbit estimation process, where differential corrections are applied to a reference trajectory. The longer the processed orbit arc, the more accurate the force model has to be.

4.1 Analytical Solution

The analytical solution is obtained by neglecting all acting forces but the central force. This is also known as the restricted two body problem, which has first been solved by Johannes Kepler. Starting with Newton's law of gravity about the attraction of two masses A and B

$$F_{AB}(\bar{x}) = G \cdot m_A m_B \cdot \frac{\bar{x}_A - \bar{x}_B}{(\bar{x}_A - \bar{x}_B)^3} \qquad \text{Eq. 4.1-1}$$

and assuming one mass to be negligible if compared to the other and building the sum of kinetic and potential energy leads to the Keplerian equations, where satellite orbits are treated as conical sections. Depending on whether the sum of kinetic and potential energy is positive, negative or zero determines the type of conical section.

$$\frac{v^2}{2} - \frac{GM}{r} = -\frac{GM}{2a} \quad \text{Ellipse} \qquad \text{Eq. 4.1-2}$$

$$\frac{v^2}{2} - \frac{GM}{r} = 0 \quad \text{Parabola} \qquad \text{Eq. 4.1-3}$$

$$\frac{v^2}{2} - \frac{GM}{r} = \frac{GM}{2a} \quad \text{Hyperbola} \qquad \text{Eq. 4.1-4}$$

withGM Gravitation constant times mass of central body

v Velocity of point mass

r Distance of point mass

a Major semiaxis of conical section

The negative sign of the total trajectory energy is related to a body which is never leaving the gravity influence of the earth as the central body. Therefore the orbits of earth orbiting satellites are represented by ellipses.

4.1.1 Kepler Orbits

The classical Kepler orbit is described by six parameters:

- a major semiaxis
- ε numerical eccentricity
- i inclination of the orbital plane
  - Ω right ascension of the ascending node
  - ω argument of perigee
  - T_0 time of perigee crossing

The three Keplerian law are associated with the following equations:

1. Keplerian law (orbit energy)

$$\frac{v^2}{2} - \frac{GM}{r} = -\frac{GM}{2a} \qquad \text{Eq. 4.1-5}$$

2. Keplerian law (rotational impact)

$$h = r \cdot v \cdot \cos\gamma \qquad \text{Eq. 4.1-6}$$

with γ angle between the normal on the radius vector and the velocity vector

3. Keplerian law (orbit period)

$$T^2 = \frac{4\pi^2}{GM} a^3 \qquad \text{Eq. 4.1-7}$$

Together with the geometrical equations for the ellipse, the movement of a satellite in his orbital plane can be described. In the following the equations are given only with a brief description.

Radius: $r = \frac{p}{1 + \varepsilon \cos\varphi}$ Eq. 4.1-8

Ellipse parameter: $p = a(1 - \varepsilon^2)$ Eq. 4.1-9

Time of flight: $t - T_0 = \frac{T}{2\pi} \cdot (M - \varepsilon \sin M)$ Eq. 4.1-10

Eccentric anomaly: $E = \arccos\left(\frac{\varepsilon + \cos\varphi}{1 + \varepsilon \cdot \cos\varphi}\right)$ Eq. 4.1-11

Mean anomaly: $M = E - \varepsilon \cdot \sin E$ Eq. 4.1-12

Mean Motion: $n = \frac{360}{T} = \frac{2\pi}{T}$ Eq. 4.1-13

Flight path angle: $\tan\gamma = \frac{\varepsilon \sin\varphi}{1 + \varepsilon \sin\varphi}$ Eq. 4.1-14

with φ true anomaly

M mean anomaly

T orbital period

To obtain three dimensional Cartesian co-ordinates, the ellipse parameters have to be transformed to Cartesian vector using the following expression:

$$\bar{x}_{OP} = \begin{Bmatrix} r\cos\varphi \\ r\sin\varphi \\ 0 \end{Bmatrix}$$ Eq. 4.1-15

The index OP indicates a reference frame lying in the orbital plane with the x-axis coinciding with the line of apsis, the z-axis normal to the orbit plane and the origin being the focus of the ellipse.

The transformation from the orbital plane frame to an inertial fixed frame (e.g. J2000) is done applying the following vector-matrix operation.

$$\bar{x}_I = \begin{bmatrix} \cos\Omega\cos\omega - \sin\Omega\sin\omega\cos i & -\cos\Omega\sin\omega - \sin\Omega\cos\omega\cos i & \sin\Omega\sin i \\ \sin\Omega\cos\omega + \cos\Omega\sin\omega\cos i & -\sin\Omega\sin\omega + \cos\Omega\cos\omega\cos i & -\cos\Omega\sin i \\ \sin\omega\sin i & \cos\omega\sin i & \cos i \end{bmatrix} \cdot \bar{x}_{OP} \qquad \text{Eq. 4.1-16}$$

Likewise, the transformation from the inertial to an earth centred earth fixed frame (e.g. WGS-84) is achieved by a similar operation.

$$\bar{x}_{ECEF} = \begin{bmatrix} \cos\Theta & \sin\Theta & 0 \\ -\sin\Theta & \cos\Theta & 0 \\ 0 & 0 & 1 \end{bmatrix} \cdot \bar{x}_I \qquad \text{Eq. 4.1-17}$$

with

Θ hour angle

4.1.2 Accounting for Secular Perturbations

A satellite trajectory computed using the Keplerian equations would diverge very soon from the actual one. Most of the acting forces cause periodically varying perturbations, although with increasing amplitude. The main secular perturbations are caused by the oblate shape of the earth's gravity field. The major deviation is due to the nodal regression caused by the oblateness. The following equation gives the derivative of the right ascension with respect to time.

$$\frac{d\Omega}{dt} = -n \cdot \frac{3}{2} \cdot J_2 \cdot \frac{R_E^2}{a^2 \cdot \sqrt{1-\varepsilon^2}} \cdot \cos i \qquad \text{Eq. 4.1-18}$$

with J_2 being the oblateness coefficient. The oblate gravity field has also an impact on the line of apsis

$$\frac{d\omega}{dt} = \frac{3}{4} \cdot n \cdot J_2 \frac{R_E^2 \left(4 - 5\sin^2 i\right)}{a^2 \sqrt{1-\varepsilon^2}} \qquad \text{Eq. 4.1-19}$$

and a minor impact on the mean motion

$$M = M_0 + n_{J2} \cdot t \qquad \text{Eq. 4.1-20}$$

$$n_{J2} = n_0 \left[1 + \frac{3}{4} \cdot J_2 \cdot \frac{R_E^2 \left(3\cos^2 i - 1\right)}{a^2 \cdot \sqrt{\left(1-\varepsilon^2\right)^3}} \cdot \cos i \right]$$

with

M mean anomaly at time t

M_0 mean anomaly at time T_0

Applying these equations, the Kepler orbits can be computed with Kepler parameters corrected for the influence of the oblate earth, thus leading to a somewhat more accurate orbit computation. Note, that the transformation into the earth fixed frame has to be conducted using the corrected values for Ω and ω.

4.2 Numerical Integration of the Equations of Motion

The equations of motion of a satellite are described by the following system of six ordinary linear differential equations, which has to be solved to obtain the satellites position and velocity vector in time.

$$\frac{dx}{dt} = \dot{x} \quad , \quad \frac{dy}{dt} = \dot{y} \quad , \quad \frac{dz}{dt} = \dot{z} \qquad \text{Eq. 4.2-1}$$

$$\frac{d\dot{x}}{dt} = \ddot{x} = \sum_k \frac{F_{x,k}}{m} = \sum_k a_{x,k} = f(x,y,z)$$

$$\frac{d\dot{y}}{dt} = \ddot{y} = \sum_k \frac{F_{y,k}}{m} = \sum_k a_{y,k} = f(x,y,z)$$

$$\frac{d\dot{z}}{dt} = \ddot{z} = \sum_k \frac{F_{z,k}}{m} = \sum_k a_{z,k} = f(x,y,z)$$

The integration of such a system of 1^{st} order linear differential equations can not be done analytically, but is a well known problem to numerical mathematics. There are several standard procedures to solve it, e.g. Runge-Kutta or Adams-Bashford-Moulton. These two shall be briefly outlined in this section.

One of the most versatile numerical integration algorithms is the Runge-Kutta procedure. It is a one-step algorithm, requiring only the preceding state vector to compute the actual one. It solves differential equations of the type

$$\dot{x}_i(t) = f_i(x,t) \qquad \text{Eq. 4.2-2}$$
$$x_i(t_0) = c_0$$

applying the following difference equation

$$x_{n+1} = x_n + \sum_{i=1}^{v} w_i k_j \qquad \text{Eq. 4.2-3}$$

$$k_i = h \cdot f(t_n + c_i h, x_n + \sum_{j=1}^{i-1} a_{ij} k_j)$$

with h step width (in time)

ci, ai coefficients, determined by the order and stage number of the algorithm

The classical Runge-Kutta algorithm is of 4th order and has 4 stages. The stage number indicates, how often the right hand function f(x, t) has to be evaluated. The four derivatives k_1 through k_4 are computed the following way:

$$\bar{k}_1 = f(\bar{x}_i)$$
$$\bar{k}_2 = f\left(\bar{x}_i + \frac{h}{2} \cdot \bar{k}_1\right)$$
$$\bar{k}_3 = f\left(\bar{x}_i + \frac{h}{2} \cdot \bar{k}_2\right)$$
$$\bar{k}_4 = f\left(\bar{x}_i + h \cdot \bar{k}_3\right)$$

Eq. 4.2-4

With these, the new state vector can be obtained by

$$\bar{x}_{i+1} = \bar{x}_i + \frac{h}{6} \cdot \left(\bar{k}_1 + 2 \cdot \bar{k}_2 + 2 \cdot \bar{k}_3 + \bar{k}_4\right)$$

Eq. 4.2-5

The step width h can be varied easily to minimise degradation due to round of errors. For an algorithm of order n, the error is of order n+1.

Multistep procedures use the last n state vectors to obtain the state at time k+1. The Adams-Bashford algorithm, indicated in Eq. 4.2-6 is called predictor, because it uses the past function evaluations to compute the present state. If the f_k's are stored, only one function evaluation per time interval h is required, regardless of the order.

$$x_{k+1} = x_k + h\sum_{i=0}^{n-1} \beta_i f_{k-i}$$

Eq. 4.2-6

The coefficients β_i are determined by the order of the algorithm, as indicated in Table 4-1. A drawback of the prediction algorithm are round off errors due to large coefficients at high orders. It is therefore often combined with a so called corrector algorithm (Adams-Moulton), using a predicted state at time k+1 to evaluate the right hand function.

$$x_{k+1} = x_k + h \cdot \beta_{-1} \cdot f_{k+1} + h\sum_{i=0}^{n-1} \beta_i^* f_{k-i}$$

Eq. 4.2-7

The coefficients β^* are determined by the order of the procedure and are indicated in Table 4-2.

The combined predictor-corrector-algorithm leads to satisfactory results, comparable with a Runge-Kutta procedure of the same order. It requires only 2 function evaluation per time interval h, regardless of the order. In practice, only the combined predictor-corrector algorithm is used.

The following equations describe explicitly the algorithm for a 4th order Adams-Bashford-Moulton numerical integration procedure.

$$\vec{p}_{k+1} = \vec{x}_k + \frac{h}{24}\cdot\left(55\cdot f(\vec{x}_k) - 59\cdot f(\vec{x}_{k-1}) + 37\cdot f(\vec{x}_{k-2}) - 9\cdot f(\vec{x}_{k-3})\right) \qquad \text{Eq. 4.2-8}$$

$$\vec{x}_{k+1} = \vec{x}_k + \frac{h}{24}\cdot\left(9\cdot f(\vec{p}_{k+1}) + 19\cdot f(\vec{x}_k) - 5\cdot f(\vec{x}_{k-1}) + f(\vec{x}_{k-2})\right)$$

The following tables summarise the coefficients for Adams-Bashford predictor and the corresponding Adams-Moulton corrector up to 8th order. Note, that the error of a nth order algorithm is also of (n+1)th order, similar to the Runge-Kutta type algorithms.

i →	0	1	2	3	4	5	6	7
β_{1i}	1							
β_{2i}	3/2	-1/2						
β_{3i}	23/12	-16/12	5/12					
β_{4i}	55/24	-59/24	37/24	-9/24				
β_{5i}	1901/720	-1387/360	109/30	-637/360	251/720			
β_{6i}	4277/1440	-2641/480	4991/720	-3649/720	959/480	-95/288		
β_{7i}	198721/60480	-18637/ 2520	235183/ 20160	-10754/ 945	135713/ 20160	-5603/2520	19087/ 60480	
β_{8i}	16083/4480	-1152169/ 120960	242653/ 13440	-296053/ 13440	2102243/ 120960	-115747/ 13440	32863/ 13440	-5257/ 17280

Table 4-1 Coefficients of the Adams-Bashford Algorithm

i →	-1	0	1	2	3	4	5	6
β^*_{1i}	1/2	1/2						
β^*_{2i}	5/12	2/3	-1/12					
β^*_{3i}	9/24	19/24	-5/24	1/24				
β^*_{4i}	251/720	323/360	-11/30	53/360	-19/720			
β^*_{5i}	95/288	1427/1440	-133/240	241/720	-173/1440	3/160		
β^*_{6i}	19087/ 60480	2713/2520	-15487/ 20160	586/945	-6737/ 20160	263/2520	-863/60480	
β^*_{7i}	5257/17280	139849/ 120960	-4511/4480	123133/ 120960	-88547/ 120960	1537/4480	-11351/ 120960	275/24192

Table 4-2 Coefficients of the Adams-Moulton Algorithm

A draw back of all multistep procedures is the necessity of n-1 preceding state vector. This means, multistep procedures require a "starter", usually a Runge-Kutta procedure. Another draw back is the inflexibility in adapting integration step width h to the required accuracy demands. Fortunately, nearly circular orbit can be computed using a fixed step width. This allows, after a starting phase with a low order Runge-Kutta type, the usage of higher order Adams-Bashford-Moulton type of numerical integrator.

Necessary for all numerical integration algorithms are starting values $\vec{x}_0, \dot{\vec{x}}_0$ as well as the explicit calculation of the sum of all acting forces or accelerations at each instant of time.

$$\sum_k \vec{a} = \vec{a}_G + \vec{a}_L + \vec{a}_S + \vec{a}_{SP} + \vec{a}_D + \vec{a}_T + \vec{a}_{SET} + \vec{a}_{OT} + \vec{a}_A + \vec{a}_{Minor} + \ldots \qquad \text{Eq. 4.2-9}$$

with the indices

- G Gravity
- L Lunar attraction
- S Solar attraction
- SP Solar Pressure
- D Aerodynamic drag forces
- T Thrust (vehicles propulsion system)
- SET Solid earth tides
- OT Ocean tides
- A Earth Albedo

The following chapters deal with the computation of these contributors to the sum of accelerations.

4.2.1 Earth's Gravity

The major part of the earth's gravity field is the spherical term, expressed by

$$g = -\frac{GM}{r^2} \qquad \text{Eq. 4.2-10}$$

is already taken into account in Kepler's formulation of the orbital movement. The largest orbit error, if compared to an unperturbed Keplerian orbit is the non-spherical part of the earth's gravity field. The gravity potential of the Earth can be described analytically in terms of spherical harmonics using the following expression:

$$U = \frac{GM}{r} + GM\sum_{n=2}^{N}\sum_{m=0}^{n}\frac{a_e^n}{r^{n+1}}P_{nm}(\sin\varphi)(C_{nm}\cos m\lambda + S_{nm}\sin m\lambda) \qquad \text{Eq. 4.2-11}$$

with

U Gravity potential

GM Earth's gravity constant

r magnitude of radius vector (of an arbitrary point)

a Earth's equatorial radius

n,m Degree and order of spherical harmonics

P_{nm} Legendre functions

C_{nm},S_{nm} Coefficients of spherical harmonics

φ Latitude

λ Longitude

The Legendre polynomials P_n and associated functions P_{nm} are defined as

$$P_n(x) = \frac{1}{2^n n!}\frac{d^n}{dx^n}(x^2-1)^n \qquad \text{Eq. 4.2-12}$$

and

$$P_{nm}(x) = (1-x^2)^{m/2}\frac{d^m P_n(x)}{dx^m} \qquad \text{Eq. 4.2-13}$$

The force acting on a point in the gravitation field is obtained by computing the gradient of the potential.

$$\vec{g} = \text{grad}(U) = \left(\frac{\partial U}{\partial x}, \frac{\partial U}{\partial y}, \frac{\partial U}{\partial z}\right) \qquad \text{Eq. 4.2-14}$$

This analytical expression is not very well suited for implementation. Soop (1994) indicates a recursive method for computing the Legendre polynomials and functions, as well as the partial derivatives required to compute the gravity force.

4.2.1.1 Computation of Legendre Polynomials and Functions

The Legendre polynomials can be computed recursively using starting values for the first two terms:

$$P_0(x) = 1; \quad P_1(x) = x \qquad \text{Eq. 4.2-15}$$

$$p_n(x) = \frac{2n-1}{n}\cdot xP_{n-1}(x) - \frac{n-1}{n}\cdot P_{n-2}(x) \quad \text{if } n \geq 2$$

The associated Legendre functions are obtained in two steps. First, the m-fold derivative of each polynomial $P_n(x)$ is computed

$$P_n^{(m)}(x) = \frac{d^m P_n(x)}{dx^m} \qquad \text{Eq. 4.2-16}$$

A direct derivation of the polynomials is, although straight forward, only applicable for lower degree and order of Legendre functions. Higher derivatives have to be computed recursively using the following algorithm:

$$P_n^{(m)}(x) = 0 \quad \text{if } n < m$$
$$P_n^{(m)}(x) = 1 \cdot 3 \cdot \ldots \cdot (2m-1) \quad \text{if} \quad n = m$$
$$P_n^{(m)}(x) = \frac{2n-1}{n-m} \cdot x \cdot P_{n-1}^{(m)}(x) - \frac{n+m-1}{n-m} \cdot P_{n-2}^{(m)}(x) \quad \text{if} \quad n > m \qquad \text{Eq. 4.2-17}$$

with the starting values:

$$P_0^{(1)}(x) = 0$$
$$P_1^{(1)}(x) = 1 \qquad \text{Eq. 4.2-18}$$
$$P_1^{(2)}(x) = 0$$

and afterwards multiplied by the factor

$$(1-x^2)^{m/2} \qquad \text{Eq. 4.2-19}$$

4.2.1.2 Normalisation

Usually, the coefficients C_{nm} and S_{nm} are given in fully normalised form. With this, the integral over the complete sphere equals 4π. To de-normalise the coefficients, they would have to be multiplied by the following factors:

$$\sqrt{(2n+1)} \quad \text{für } m=0; \qquad \sqrt{2(2n+1)\frac{(n-m)!}{(n+m)!}} \quad \text{für } m \geq 1 \qquad \text{Eq. 4.2-20}$$

This is not always desirable, because the reason for normalisation is the greater numerical stability of the normalised form. Non-normalised Legendre polynomials P_n and functions P_{nm} reach very high values for increasing degree and order, while the coefficients C_{nm} and S_{nm} get very small.

For example, the maximum range of a 64-bit double precision variable is exceeded for n,m > 150, while numerical errors become significant much earlier, at about degree and order 20. One has to keep in mind that for the computation of the geoid undulation the spherical harmonics up to degree and order 360 are computed. Recursive computation of normalised Legendre functions and polynomials is possible, although a bit tricky. Each function has to be multiplied by a normalisation factor and divided by the factors of the preceding functions. Eq. 4.2-15 to Eq. 4.2-19 therefore have to be rewritten. For the polynomials, the recursive normalisation factors can directly be applied.

$$\overline{P}_0(x) = 1; \qquad \overline{P}_1(x) = x \cdot \sqrt{3}$$
$$\overline{P}_n(x) = \frac{2n-1}{n} \cdot x \cdot \overline{P}_{n-1}(x) \cdot \sqrt{\frac{2n+1}{2n-1}}$$
$$-\frac{n-1}{n} \cdot \overline{P}_{n-2}(x) \cdot \sqrt{\frac{2n+1}{2n-3}} \quad \text{if } n \geq 2 \qquad \text{Eq. 4.2-21}$$

The normalisation factors of the associated Legendre functions contains faculties, which should not be computed explicitly.

$$\overline{P}_n^{(m)}(x) = \frac{d^m P_n(x)}{dx^m} \cdot \sqrt{2(2n+1)\frac{(n-m)!}{(n+m)!}} \qquad \text{Eq. 4.2-22}$$

Fortunately, they can be reduced in the resulting recursive normalisation factors. The recursive algorithm for fully normalised Legendre functions is given as

$$\overline{P}_n^{(m)}(x) = 0 \quad \text{if } n < m$$
$$\overline{P}_n^{(m)}(x) = 1 \cdot 3 \cdot \ldots \cdot (2m-1) \cdot \sqrt{\frac{2n+1}{(2n-1)(n+m)(n+m-1)}} \quad \text{if} \quad n = m$$
$$\overline{P}_n^{(m)}(x) = \frac{2n-1}{n-m} \cdot x \cdot \overline{P}_{n-1}^{(m)}(x) \cdot \sqrt{\frac{(2n+1)(n-m)}{(2n-1)(n+m)}}$$
$$-\frac{n+m-1}{n-m} \cdot \overline{P}_{n-2}^{(m)}(x) \cdot \sqrt{\frac{(2n+1)(n-m)(n-m-1)}{(2n-3)(n+m)(n+m-1)}} \quad \text{if} \quad n > m \qquad \text{Eq. 4.2-23}$$

with the normalized starting values:

$$\overline{P}_0^{(1)}(x) = 0$$
$$\overline{P}_1^{(1)}(x) = \sqrt{3} \qquad \text{Eq. 4.2-24}$$
$$\overline{P}_1^{(2)}(x) = 0$$

The method described above is numerically very stable and has been successfully used to compute Legendre functions up to degree and order 700. A drawback of this method is that the computational burden is about twice as high as for non-normalised Legendre functions. Thus, for a spherical harmonics expansion up to degree and order of say 15 –20 the de-normalisation of the coefficients would be favourable.

4.2.1.3 Computation of Gravity

The expression of the gravity potential in terms of a spherical harmonics expansion

$$U = \frac{GM}{r} + GM\sum_{n=2}^{N}\sum_{m=0}^{n}\frac{a_e^n}{r^{n+1}} P_{nm}(\sin\varphi)(C_{nm}\cos m\lambda + S_{nm}\sin m\lambda) \qquad \text{Eq. 4.2-25}$$

can be rearranged the following way (Colombo 1981)

$$U = \frac{GM}{r} + GM\sum_{n=2}^{N}\sum_{m=0}^{n}\frac{a_e^n}{r^{n+1}}\cos^m\varphi\cdot P_n^{(m)}(\sin\varphi)(C_{nm}\cos m\lambda + S_{nm}\sin m\lambda) \qquad \text{Eq. 4.2-26}$$

$$U = \frac{GM}{r} + GM\sum_{n=2}^{N}\sum_{m=0}^{n}\frac{a_e^n}{r^{n+m+1}}P_n^{(m)}(\sin\varphi)(C_{nm}r^m\cos^m\varphi\cdot\cos m\lambda + S_{nm}r^m\cos^m\varphi\cdot\sin m\lambda)$$

with

$$x = r\cos\varphi\cos\lambda \qquad \text{Eq. 4.2-27}$$
$$y = r\cos\varphi\sin\lambda$$
$$z = r\sin\varphi$$

Introducing the following abbreviations

$$\xi_m = r^m\cos^m\varphi\cos m\lambda \qquad \text{Eq. 4.2-28}$$
$$\eta_m = r_m\cos^m\varphi\sin m\lambda$$

yields for the gradient of the gravity potential

$$grad(U) = (\frac{\partial U}{\partial x},\frac{\partial U}{\partial y},\frac{\partial U}{\partial z}) = grad(\frac{GM}{r}) + GM\sum_{n=2}^{N}\sum_{m=0}^{n}grad\{\frac{a_e^n}{r^{n+m+1}}P_n^{(m)}(\sin\varphi)(C_{nm}\xi_m + S_{nm}\eta_m)\} \qquad \text{Eq. 4.2-29}$$

ξ_m, η_m can be computed recursively using the following simple expressions

$$\xi_0 = 1 \qquad \text{Eq. 4.2-30}$$
$$\eta_0 = 0$$
$$\xi_m = \xi_{m-1}x - \eta_{m-1}y$$
$$\eta_m = \xi_{m-1}y + \eta_{m-1}x$$

In the following the partials of the above expression are given

$$\frac{\partial}{\partial x}\{\frac{a_e^n}{r^{n+m+1}}\} = -(n+m+1)\frac{a_e^n}{r^{n+m+3}}x \qquad \text{Eq. 4.2-31}$$

$$\frac{\partial}{\partial y}\{\frac{a_e^n}{r^{n+m+1}}\} = -(n+m+1)\frac{a_e^n}{r^{n+m+3}}y \qquad \text{Eq. 4.2-32}$$

$$\frac{\partial}{\partial z}\{\frac{a_e^n}{r^{n+m+1}}\} = -(n+m+1)\frac{a_e^n}{r^{n+m+3}}z \qquad \text{Eq. 4.2-33}$$

$$\frac{\partial}{\partial x}[P_n^{(m)}(\sin\varphi)] = -\frac{zx}{r^3}P_n^{(m+1)}(\sin\varphi) \qquad \text{Eq. 4.2-34}$$

$$\frac{\partial}{\partial y}[P_n^{(m)}(\sin\varphi)] = -\frac{zy}{r^3}P_n^{(m+1)}(\sin\varphi) \qquad \text{Eq. 4.2-35}$$

$$\frac{\partial}{\partial z}[P_n^{(m)}(\sin\varphi)] = \frac{1}{r} - \frac{z^2}{r^3} P_n^{(m+1)}(\sin\varphi)$$ Eq. 4.2-36

$$\frac{\partial \xi_m}{\partial x} = \frac{m}{r}[\frac{x}{r}\xi_m + \tan\varphi\cos\lambda\sin\varphi\xi_m + \eta_m\frac{\sin\lambda}{\cos\varphi}] = m\xi_{m-1}$$ Eq. 4.2-37

$$\frac{\partial \xi_m}{\partial y} = \frac{m}{r}[\frac{y}{r}\xi_m + \tan\varphi\sin\lambda\sin\varphi\xi_m - \eta_m\frac{\cos\lambda}{\cos\varphi}] = -m\eta_{m-1}$$ Eq. 4.2-38

$$\frac{\partial \xi_m}{\partial z} = \frac{m}{r}[\frac{z}{r}\xi_m - \tan\varphi\cos\varphi\xi_m] = 0$$ Eq. 4.2-39

$$\frac{\partial \eta_m}{\partial x} = \frac{m}{r}[\frac{x}{r}\eta_m + \tan\varphi\cos\lambda\sin\varphi\eta_m - \xi_m\frac{\sin\lambda}{\cos\varphi}] = m\eta_{m-1}$$ Eq. 4.2-40

$$\frac{\partial \eta_m}{\partial y} = \frac{m}{r}[\frac{y}{r}\eta_m + \tan\varphi\sin\lambda\sin\varphi\eta_m + \xi_m\frac{\cos\lambda}{\cos\varphi}] = m\xi_{m-1}$$ Eq. 4.2-41

$$\frac{\partial \eta_m}{\partial z} = \frac{m}{r}[\frac{z}{r}\eta_m - \tan\varphi\cos\varphi\eta_m] = 0$$ Eq. 4.2-42

Especially the computation of the η and ξ is subject to numerical problems because they are in the order of magnitude of r^m. For a high order spherical expansion it is advantageous to compute

$$\overline{\eta} = \frac{\eta}{r^m}$$
$$\overline{\xi} = \frac{\xi}{r^m}$$ Eq. 4.2-43

which is dimensionless and restricted to the range between 0 and 1. The remaining factor r^m can be multiplied with the terms

$$\frac{a_e^n}{r^{n+m+1}} \quad \text{and} \quad \frac{a_e^n}{r^{n+m+3}}$$ Eq. 4.2-44

This has the additional advantage of bringing them into a numerical stable form

$$\frac{a_e^n}{r^{n+m+1}} \cdot \frac{1}{r^m} = \frac{\left(\frac{a_e}{r}\right)^n}{r} \qquad \text{Eq. 4.2-45}$$

$$\frac{a_e^n}{r^{n+m+3}} \cdot \frac{1}{r^m} = \frac{\left(\frac{a_e}{r}\right)^n}{r^3}$$

which is desirable even for lower degrees of spherical harmonics. The ratio of earth's equatorial radius and satellite orbit radius is always between 0 and 1, enhancing numerical stability. However, using the dimensionless values $\bar{\eta}$ and $\bar{\xi}$ doesn't increase computational load.

4.2.2 Third Body Attraction

The attraction acting on an orbiting satellite due to the other celestial bodies in the solar system, mainly Sun and Moon, could basically be computed like the acceleration from the earth's gravity field. However, due to the usually large distances it is sufficient to neglect all higher order terms, and regard the gravity field of celestial bodies as perfect spheres. The resulting acceleration, with respect to an earth centred inertial fixed reference frame, can be obtained from the following equation.

$$\left.\frac{d^2\vec{r}}{dt^2}\right|_{Sun,Moon} = GM_{S,M}\left[\frac{\vec{r}_{S,M} - \vec{r}}{|\vec{r}_{S,M} - \vec{r}|^3} - \frac{\vec{r}_{S,M}}{r_{S,M}^3}\right] \qquad \text{Eq. 4.2-46}$$

with

r Radius vector, S,M being indices for Sun and Moon. Without index means satellites radius vector.

GM Gravity constant of perturbing body (Sun, Moon)

This equation holds also for the major planets, although the influence even from Jupiter is several orders of magnitude lower than lunisolar perturbations. It is also referred to as the direct tidal effect.

4.2.3 Solar Pressure

The acceleration acting on an orbiting body due Solar radiation pressure can be obtained from the following expression, which simply characterises the satellite by it's cross section and mass.

$$\vec{a}_d = \mu \cdot P_s \cdot \frac{c_R \cdot A}{m} \cdot a_s^2 \cdot \frac{\vec{r} - \vec{r}_s}{|\vec{r} - \vec{r}_s|^3} \qquad \text{Eq. 4.2-47}$$

where

P_S =E/c

E Solar constant (nominal 1358 W/m²)

c vacuum speed of light

c_R reflectivity coefficient

a_S astronomical unit

A area / cross section

m mass

r , r_S radius vectors of Satellite and Sun respectively

μ eclipse factor

Normally, the "sensitivity" of the satellite to solar radiation, in Eq. 4.2-47 simplified as

$$\frac{c_R \cdot A}{m} \qquad \text{Eq. 4.2-48}$$

is a complicated function of the satellites shape, used materials and attitude with respect to the sun. But for generic system level studies, this simplification is absolutely sufficient.

The eclipse factor μ determines the amount of solar radiation acting on the satellite, being defined as

$\mu = 1$ for complete sun light

$\mu = 0$ for umbra phase

$0 < \mu < 1$ for penumbra phase

Occultation of the Sun can arise from Earth or Moon. It depends on the model, whether the penumbra phase is taken into account or not. Simpler models treat the earth's shadow as a cylinder or a cone, more sophisticated models computes the eclipse factor for the penumbra phase from the percentage of the visible sun "disc".

4.2.4 Air Drag

Satellites below 1000 km orbit height are strongly affected by drag forces. Although the air density is extremely low at such altitudes, the high velocity of a satellite leads to significant acceleration (or better deceleration), obtained by the following equation:

$$\vec{a}_D = \frac{c_D \cdot A}{m} \cdot \frac{\rho}{2} \cdot \left|\dot{\vec{r}}\right| \cdot \dot{\vec{r}} \qquad \text{Eq. 4.2-49}$$

where

a_D Acceleration due to air drag

c_D Drag coefficient

A area

m mass

ρ air density

$\dot{\vec{r}}$ velocity vector with respect to earth centred earth fixed coordinates

Again, shape and attitude of the satellite are simplified for the sake of generality, by characterising the satellite using the so called ballistic coefficient

$$\frac{c_D \cdot A}{m} \qquad \text{Eq. 4.2-50}$$

Determination of the air density is the most critical part in Eq. 4.2-49. It is subject to variation in solar flux and very difficult to model. Normally, the air density is modelled as a exponential function over a certain altitude range $h_L < h < h_U$.

$$\rho(h) = \rho_L \cdot e^{\frac{h-h_L}{H_0}} \qquad \text{Eq. 4.2-51}$$

with the so called scale height

$$H_0 = \frac{R \cdot T}{g} \qquad \text{Eq. 4.2-52}$$

and

ρ(h) air density at altitude h

ρL air density an lower bound of altitude range

R special gas constant (for air: 287 J / (kg * K))

T Thermodynamic temperature in Kelvin

g Gravity

The following table, found in [WEZ-91], indicates the parameters for an atmospheric model:

Altitude [km] h	Atmospheric Density ρ [kg/m³]				Scale Height H_0 [km]			
	Solar Min		Solar Max		Solar Min		Solar Max	
	Night	Day	Night	Day	Night	Day	Night	Day
100	9.8e-9	9.8e-9	9.8e-9	9.8e-9	6.0	5.9	5.9	5.9
200	1.8e-10	2.1e-10	3.2e-10	3.7e-10	33.4	37.9	43.2	49.4
300	5.0e-12	1.1e-11	2.6e-11	4.7e-11	44.5	53.2	57.0	67.9
400	4.8e-13	1.6e-12	5.0e-12	1.2e-11	52.8	60.5	69.5	79.8
500	4.1e-14	2.0e-13	8.5e-13	3.1e-12	60.4	67.4	74.6	88.7
600	1.0e-14	3.9e-14	2.0e-13	1.0e-12	76.1	76.4	81.8	96.1
700	4.1e-15	1.0e-14	4.8e-14	3.1e-13	133.7	95.6	92.8	105.0
800	2.4e-15	4.3e-15	1.7e-14	1.1e-13	213.4	138.7	113.5	115.8
900	1.6e-15	2.4e-15	7.3e-15	4.3e-14	324.8	215.4	153.2	134.2
1000	9.6e-16	1.7e-15	4.2e-15	2.0e-14	418.2	308.9	217.1	164.9

Table 4-3 Atmospheric Density and Scale Height

4.2.5 Solid Earth Tides

The solid earth tides result as a indirect effect from the attraction of Moon and Sun. They cause a deformation of the earth figure and the therefore of the earth's gravity field, which can be expressed as a deviation of the harmonic coefficients. The deviations of the earth's harmonic coefficients of 2nd and 3rd order due to solid tides can be expressed by following equation found in [ITN-96]:

$$\Delta C_{nm} + i\Delta S_{nm} = \frac{k_{nm}}{2n+1} \sum_{j=2}^{3} \frac{GM_j}{GM_E} \left(\frac{R_E}{r_j} \right)^{n+1} P_{nm}(\sin \Phi_j) e^{-im\lambda_j} \qquad \text{Eq. 4.2-53}$$

with

k_{nm} Nominal degree Love number for degree n and order m

R_E Equatorial radius of the Earth

GM_j Gravitational parameters for Earth (E), Moon (j = 2) and Sun (j = 3)

r_j Distance from geocenter to Moon (j = 2) and Sun (j = 3)

F_j Earth fixed geocentric latitude of Moon and Sun

l_j Earth fixed geocentric longitude of Moon and Sun

P_{nm} Legendre function of degree n and order m

The Love numbers are a measure for the elasticity of the earth body. A somewhat more simple expression for the acceleration due to the solid earth tides can be found in [RIZ-85]. The force acting on a satellite due to solid earth tides is given as

$$\ddot{\bar{r}}_{Sat} = \frac{k_2}{2} \cdot \frac{GM_{S,M}}{\bar{r}_{S,M}^3} \cdot \frac{a_E^5}{\bar{r}_{Sat}^4} \cdot \left[\left(3 - 15 \cdot \cos^2\theta\right) \cdot \frac{\bar{r}_{Sat}}{|\bar{r}_{Sat}|} + 6 \cdot \cos\theta \cdot \frac{\bar{r}_{S,M}}{|\bar{r}_{S,M}|} \right] \qquad \text{Eq. 4.2-54}$$

with

r Radius vector of satellite (Sat), Sun (S) and Moon (M)

θ Angle between radius vectors of satellite and tide causing body.

a_E Equatorial radius of Earth.

GM Gravitational constant of Sun (S) and Moon (M).

k_2 Love Number

In this model, only the dominating deformation effect on the earth's dynamic oblateness, represented by the 2nd zonal harmonic coefficient is considered. Despite being a simple earth tide model, it is sufficient for basic evaluations. It can be seen from Eq. 4.2-54 that the influence decreases with fourth power of the satellites radius vector.

4.2.6 Ocean Tides

The deformation of the earth's gravity field caused by ocean loading tides, can also be accounted for as a deviations of the harmonic coefficients. In [ITN-96], following expression can be found

$$\Delta C_{nm} - i\Delta S_{nm} = F_{nm} \sum_{s(n,m)} \sum_{+}^{-} \left(C_{snm}^{\pm} \mp S_{snm}^{\pm}\right) e^{\pm i\theta_f}, \qquad \text{Eq. 4.2-55}$$

where

$$F_{nm} = \frac{4\pi G\rho_w}{g} \sqrt{\frac{(n+m)!}{(n-m)! \cdot (2n+1) \cdot (2-\delta_{om})}} \left(\frac{1+k'_n}{2n+1}\right)$$

with

g mean equatorial gravity

G Gravity constant

k'_n load deformation coefficients

C_{snm} , S_{snm} Ocean tide coefficients for the tide constituent s

θ Argument of tide constitudent s

For a more detailed description see [ITN-96]. The computed deviations are used to correct the rigid earth gravity model coefficients. These modified coefficients are then used to compute the gravity acceleration, corrected for ocean tides.

4.2.7 Earth Albedo

The reflection of sun light from the earth's surface produces a force, similar to solar radiation pressure but smaller, acting on the satellite. Unfortunately, the reflected solar flux is subject to the density of clouds, the angle between satellite, earth and sun etc. A very rough estimate can be given using the following formula:

$$\vec{a}_{Albedo} = \Psi \cdot \frac{c_R \cdot A}{m} \cdot \frac{\vec{r}}{|\vec{r}|^3} \qquad \text{Eq. 4.2-56}$$

with

Ψ Radiation pressure from earth

r satellites position vector

c_R reflectivity coefficient

A area / cross section

m mass

where

$$\Psi = f\left(c_{R,Earth}, \alpha, ...\right) \qquad \text{Eq. 4.2-57}$$

is still a function of at least the earth's reflectivity, subject to cloud density and the angle between sun earth and satellite. Especially for LEO satellites, earth albedo is hard to model. For higher satellite orbits, earth albedo can usually be neglected.

4.2.8 Vehicle Thrust

When orbit corrections become necessary, an additional force resulting from the vehicles propulsion system has to taken into account.

$$\vec{a}_{Thrust} = \frac{T}{m(t)} \cdot \vec{b}(t) \qquad \text{Eq. 4.2-58}$$

with

T Thrust

b Vehicles thrust vector

m(t) Mass being a function of time

where the mass decrease while fuel is burned and exhausted is described by

$$m(t) = m_0 - \dot{m} \cdot t \qquad \text{Eq. 4.2-59}$$

The mass flow can be also be a (commanded) function of time. However, most of the chemical propulsion systems have a fixed mass flow.

4.3 Force Model Errors

A given force model will only be accurate to a certain degree. This lead to a divergence of the predicted trajectory, and the actual one. On the other hand, if computational recourses are rare, the orbit arc is short or the required accuracy is not that demanding, it is necessary to assess the impact of simplifying the force model. This section deals with the impact of these force model simplifications, as well as force model errors on the orbit prediction error.

4.3.1 Earth's Gravity

As shown in chapter 4.2.1, the impact of the higher order spherical harmonics of the earth's gravity field decreases with orbit altitude. Neglecting higher order terms will therefore lead to prediction errors, but depending on orbit altitude. Another error source is the imperfection of the harmonic coefficients. To assess the impact of neglecting higher order terms, as well as an imperfect gravity model, a reference trajectory has been computed using the full JGM-3, being a state of the art gravity model. Degree and order of the model has been decreased successively and the resulting trajectory has been compared to the reference orbit. Furthermore the reference trajectory has been compared to orbits computed with other full gravity models. The following gravity models have been compared:

Gravity Model	Maximum Degree x Order
JGM-3 (Reference Model)	70 x 70
JGM-2	70 x 70
GEM-T3	50 x 50
GRIM4-S4	66 x 66

Table 4-4 Assessed Gravity Models

All these models have been derived by satellite measurements. To show the impact of the orbit altitude, different reference orbit have been computed:

- a low earth orbit (LEO) with 1250 km orbit altitude
- a GPS like orbit (MEO) with 20200 km orbit altitude
- a geostationary orbit (GEO) with approximately 36 000 km orbit altitude

The following figure indicates the prediction errors if a 1250 km LEO is predicted using only a 15 x 15 gravity model. The errors shows a periodic behaviour reflecting the orbital period of

the satellite, as can be seen from the figure. Although the along track error seems to have a secular trend, the approximately quadratic trend is only the ascending branch of a sine wave, with the major semi axis being the amplitude. This isn't very surprising due to the fact that the equations of motion are described by a second order differential equation.

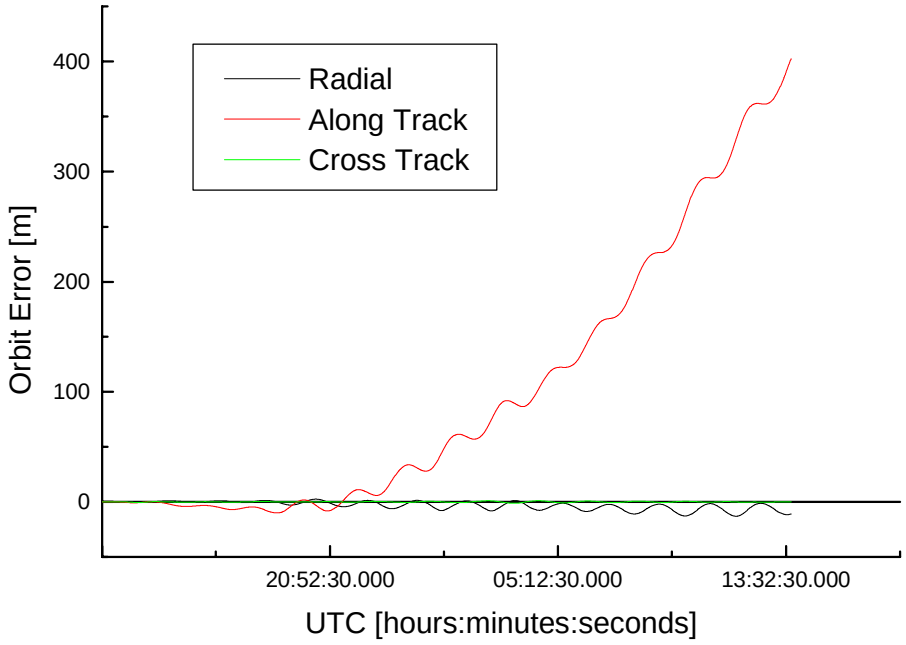

Figure 4-1 Prediction Error of LEO 1250 km with 15 x 15 Geopotential

The following tables show the evaluations of the orbit errors induced by successively neglecting more higher order harmonics down to a pure spherical gravity field, as well as a comparison to other gravity models. The gravity model "deviated JGM-3" has been obtained by adding to a coefficient the one sigma value of that coefficients uncertainty times a normal distributed random number with zero mean and variance one.

Table 4-5 shows the orbit error after one day for the LEO satellite. The neglecting of harmonics above 30 causes an error of the same order of magnitude as the uncertainties of the gravity model, represented by "deviated JGM-3". The differences to other gravity models (besides GEM-T3) are higher, but JGM-3 can be regarded as the state of the art gravity model. Comparison to the Kepler orbit shows a large error. For precise orbit determination, even for short time prediction with frequent measurement updates, a model considering less than degree and order 30 x 30 is not acceptable.

Table 4-6 shows the orbit error after shorter prediction period of 6 hours. Here, neglecting harmonics above 50's degree and order causes only small but noticeable orbit errors. But they are far below the model uncertainties.

	Radial [m]	**Along Track [m]**	**Cross Track [m]**
50 x 50	0	0.11	0
30 x 30	0.18	4.21	0.02
15 x 15	4.94	158.5	0.41
10 x 10	12.34	196.5	5.25
5 x 5	42.5	2.33 km	18.1
2 x 2	387	4.5 km	50.7
J2-Propagator (2 x 0)	1.1 km	79.4 km	42 km
Kepler (0 x 0)	18.4 km	404 km	90.4 km
JGM-2 (70 x 70)	0.36	24.4	0.1
GEM-T3 (50 x 50)	0.24	0.87	0.02
GRIM4-S4 (66 x 66)	0.37	24.6	0.03
Deviated JGM-3	0.18	2.94	0.03

Table 4-5 1250 km LEO 1 day

	Radial [m]	Along Track [m]	Cross Track [m]
50 x 50	0	0.01	0
30 x 30	0.04	0.34	0.01
15 x 15	0.91	4.53	0.19
10 x 10	4.2	67.6	2.8
5 x 5	43.7	762	7.6
2 x 2	330	1.4 km	62.1
J2-Propagator (2 x 0)	1.1 km	33 km	21 km
Kepler (0 x 0)	7.8 km	175 km	49.3 km
JGM-2 (70 x 70)	0.30	4.26	0.06
GEM-T3 (50 x 50)	0.11	0.48	0.02
GRIM4-S4 (66 x 66)	0.29	4.35	0.02
Deviated JGM-3	0.05	0.23	0.02

Table 4-6 1250 km LEO 6 hours

The next figure show the results obtained for a medium earth orbit (MEO). The chosen orbit of approximately 20200 km orbit altitude with 55° inclination represents a generic GPS orbit, which is the most appropriate for navigation satellites. It has been propagated using a 5 x 5 gravity model, and compared to the reference orbit using the full 70 x 70 model.

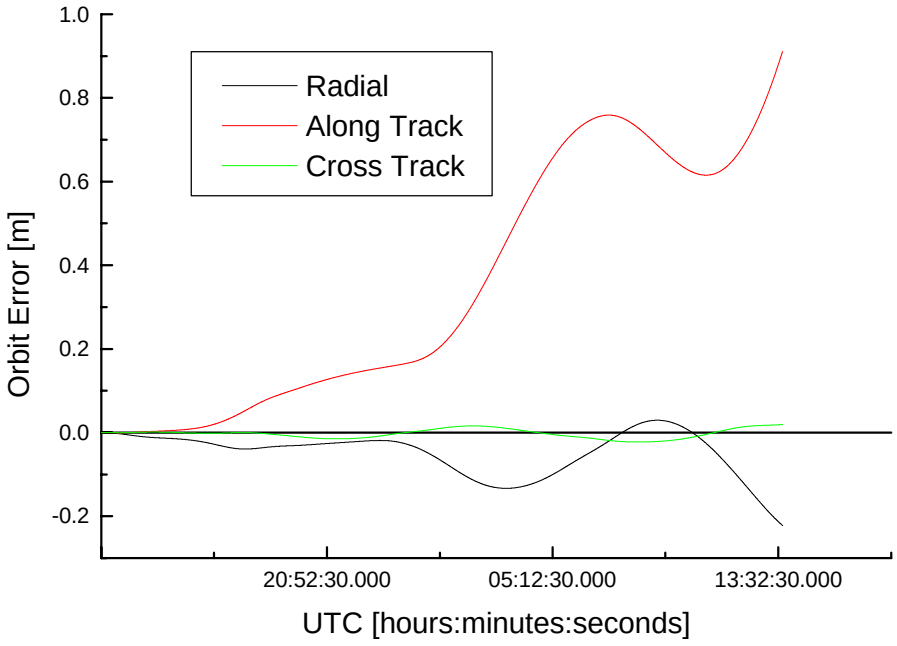

Figure 4-2 Orbit Error of MEO with 5 x 5 gravity model after 1 day

Here also the orbital period can also be seen in the error behaviour. The following tables indicates the 1σ error after one day and after six hours of prediction, for different gravity models.

	Radial [m]	Along Track [m]	Cross Track [m]
7 x 7	0	0.01	0
5 x 5	0.07	0.46	0.01
2 x 2	13.1	84.6	3.2
J2-Propagator (2 x 0)	378	3.3 km	2 km
Kepler (0 x 0)	1.5 km	16.8 m	4.7 km
JGM-2 (70 x 70)	0.02	0.13	0
GEM-T3 (50 x 50)	0.44	5.4	0
GRIM4-S4 (66 x 66)	0.32	3.96	0
Deviated JGM-3	0	0.01	0

Table 4-7 20200 km MEO 1 day

	Radial [m]	Along Track [m]	Cross Track [m]
7 x 7	0	0	0
5 x 5	0.02	0.07	0
2 x 2	8.2	10.7	2.9
J2-Propagator (2 x 0)	374	409	600
Kepler (0 x 0)	1.6 km	3.2 km	1.5 km
JGM-2 (70 x 70)	0.01	0.01	0
GEM-T3 (50 x 50)	0.48	1.22	0
GRIM4-S4 (66 x 66)	0.33	0.81	0
Deviated JGM-3	0	0	0

Table 4-8 20200 km MEO 6 hours

It can be seen that a satellite in that orbit altitude is fairly good predicted if a gravity model of 7 degree and order is used. Even for long term prediction (< 1 week) a 15 x 15 model is suffcient.

The next two tables shows the orbit errors for the GEO. It is obvious that the GEO is affected only by the lower harmonics. For a short prediction period a spherical harmonic expansion up to degree and order 5 is sufficient. For longer prediction periods, a gravity model up to 9 degree and order is sufficient.

	Radial [m]	**Along Track [m]**	**Cross Track [m]**
7 x 7	0	0	0
5 x 5	0	0.03	0.01
2 x 2	6.23	36.41	0.76
J2-Propagator (2 x 0)	71	187	0.8
Kepler (0 x 0)	1.8 km	13.1 km	0.97
JGM-2 (70 x 70)	0	0.01	0
GEM-T3 (50 x 50)	0.7	4.6	0
GRIM4-S4 (66 x 66)	0.5	3.4	0
Deviated JGM-3	0	0	0

Table 4-9 GEO 1 day

	Radial [m]	Along Track [m]	Cross Track [m]
7 x 7	0	0	0
5 x 5	0	0.01	0
2 x 2	6.2	14.8	0.8
J2-Propagator (2 x 0)	4.4	18.5	0.7
Kepler (0 x 0)	786	763	0.3
JGM-2 (70 x 70)	0	0	0
GEM-T3 (50 x 50)	0.44	0.58	0
GRIM4-S4 (66 x 66)	0.26	0.3	0
Deviated JGM-3	0	0	0

Table 4-10 GEO 6 hours

Another interesting fact is that the model uncertainties are negligible, especially if compared to the LEO orbit. This is due to the fact that the uncertainties of the lower order harmonics compared to their magnitude are far smaller than those of the higher order harmonics.

It is clear that the GEO orbit, due to the fact the it has a non inclined orbit and see's always the same part of the gravity field is subjected to extreme low perturbation from the higher order harmonics. A more general class of orbits, the inclined geosynchronous orbit (IGSO) has the same revolution period (and therefore orbit altitude) as the GEO. The error introduced to an IGSO orbit by neglecting higher order harmonics shows similar tendencies as for the GEO orbit. The IGSO is slightly more affected by tesseral and sectorial harmonics than the GEO, due to its inclined orbit. But also for this orbit class a 9 x 9 gravity model is sufficient.

4.3.2 Third Body Attraction (Direct Tidal Effects)

Figure 4-3 and Figure 4-4 show the orbit errors arising from neglecting the lunar attraction. All orbit errors show a oscillating characteristic with the along track error being superimposed by a linear trend.

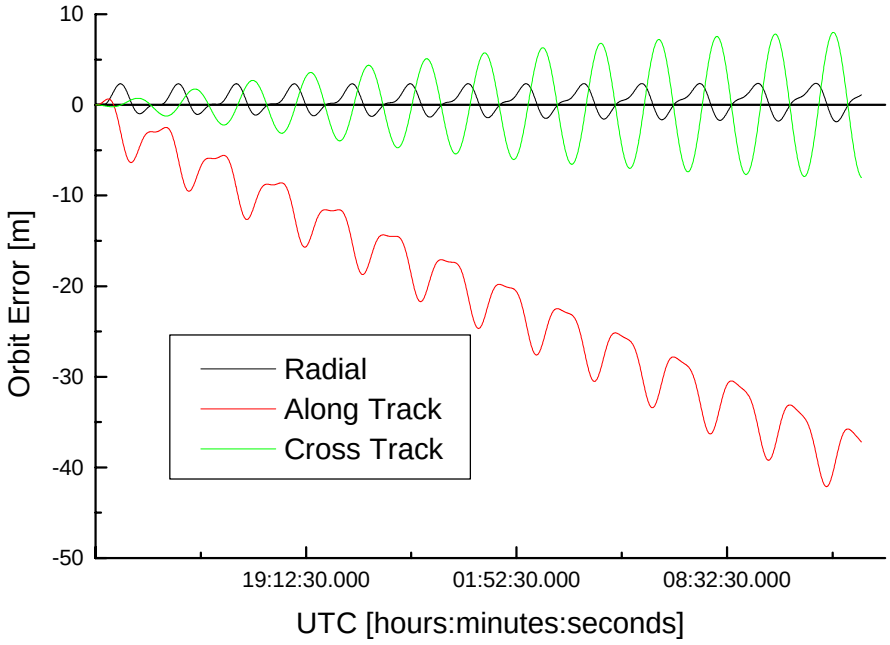

Figure 4-3 Orbit Error of LEO 1250 km neglecting Lunar Attraction

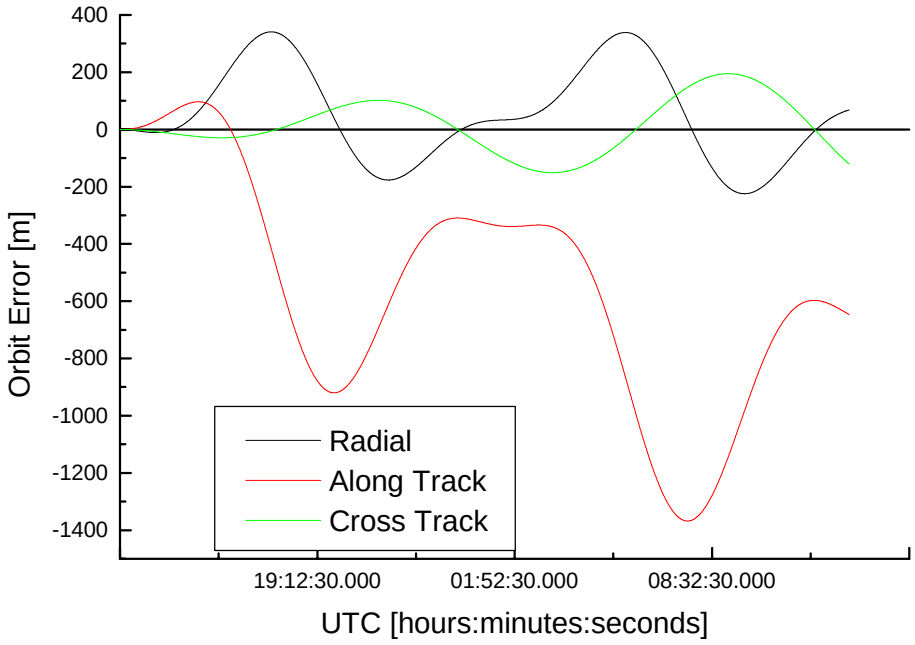

Figure 4-4 Orbit Error of MEO neglecting Lunar Attraction

Obviously the LEO satellite is less affected by third body attractions than satellites in MEO (or GEO and IGSO) orbits. It is a general tendency that the direct tidal effect increases with orbit height. This can easily be verified by setting the satellites radius in Eq. 4.2-46 to zero which causes the third body attraction to vanish.

The following table show the orbit errors due to neglecting lunar attraction for prediction periods of one day and six hours.

	Radial [m]	Along Track [m]	Cross Track [m]
LEO 1 day	1.24	23.5	4.0
LEO 6 hours	1.1	7.0	1.4
MEO 1 day	167	687	101
MEO 6 hours	201	288	19
GEO 1 day	1 km	2.9 km	370
GEO 6 hours	219	385	96
IGSO 1 day	1 km	3.1 km	446
IGSO 6 hours	464	410	175

Table 4-11 Lunar Tide Perturbation

The solar attraction, although being slightly lower in magnitude shows in principle the same error characteristic. Thus only the summary table or the root mean square error is given below.

	Radial [m]	Along Track [m]	Cross Track [m]
LEO 1 day	0.47	4.12	4.99
LEO 6 hours	0.46	1.05	1.3
MEO 1 day	69	144	119
MEO 6 hours	55	177	37
GEO 1 day	429	1 km	309
GEO 6 hours	308	240	94
IGSO 1 day	423	1 km	525
IGSO 6 hours	259	420	226

Table 4-12 Solar Tide Perturbation

Third body attraction has to be modelled, regardless of the application (but especially for navigation satellites). The errors introduced by neglecting these contributing forces are far from being negligible.

4.3.3 Solar Radiation Pressure

The following figures shows the orbit error due to direct solar radiation pressure for the investigated orbits. Obviously the LEO is affected less by (neglecting) solar radiation, due to the fact that the exciting force (=solar radiation pressure) has a slowly varying geometry.

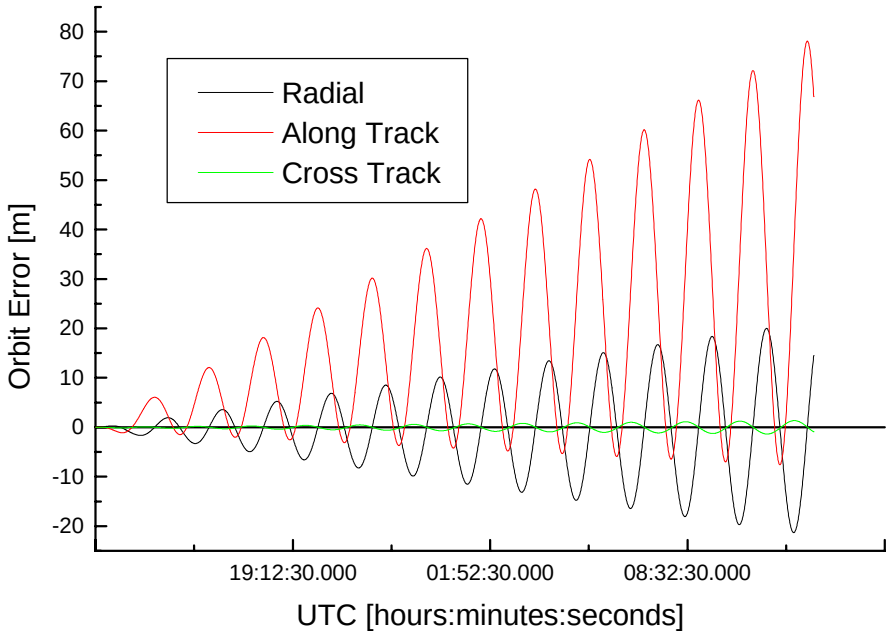

Figure 4-5 Orbit Error of 1250km LEO neglecting Solar Radiation Pressure

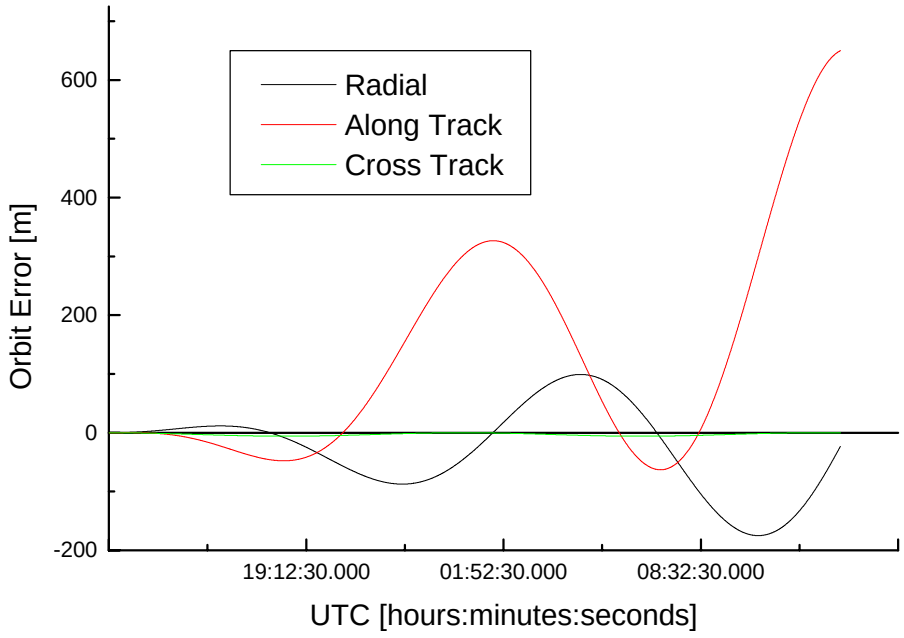

Figure 4-6 4-7Orbit Error of MEO neglecting Solar Radiation Pressure

The shorter revolution time is an important factor. The orbit error due to solar radiation shows also the characteristic of a sine wave with increasing amplitude, with the orbital period as natural frequency. Compared to the LEO orbit, the perturbation of the MEO orbit has a lower frequency, but is faster increasing in amplitude, as can be seen in the figures. Table 4-13 indicates the RMS error for different prediction periods and satellite orbits.

	Radial [m]	Along Track [m]	Cross Track [m]
LEO 1 day	8.8	27.6	0.57
LEO 6 hours	2.3	7.2	0.17
MEO 1 day	78.6	211	3.6
MEO 6 hour	7.2	35.5	3.6
GEO 1 day	182	589	10.3
GEO 6 hours	21.6	18.6	4.4
IGSO 1 day	175	511	19
IGSO 6 hours	23	26	12

Table 4-13 Solar Radiation Perturbation

It can be seen that for all orbits, even for short term prediction, this perturbation has to be considered.

4.3.4 Air Drag

The following tables shows the orbit error due to neglecting air drag. Satellites in orbits above 1000 km are hardly or not at all affected by air drag, thus being indicated in this table only for completeness. Unlike the other perturbations, the air drag error is not given as RMS value, but the instantaneous value at the end of the indicated period. This is due to the secular nature of air drag perturbation.

	Radial [m]	Along Track [m]	Cross Track [m]
500 km LEO	70	6.4 km	2.5
800 km LEO	1.96	199	0.1
1250 km LEO	0.09	6.2	0
MEO	0	0	0
GEO	0	0	0
IGSO	0	0	0

Table 4-14 Air Drag Perturbation after 1 Day

	Radial [m]	Along Track [m]	Cross Track [m]
500 km LEO	14	322	0.19
800 km LEO	0.65	9.83	0
1250 km LEO	0.01	0.18	0
MEO	0	0	0
GEO	0	0	0
IGSO	0	0	0

Table 4-15 Air Drag Perturbation after 6 Hours

The following figures indicates the orbit error of a 800 km LEO neglecting air drag, over a prediction period of one day.

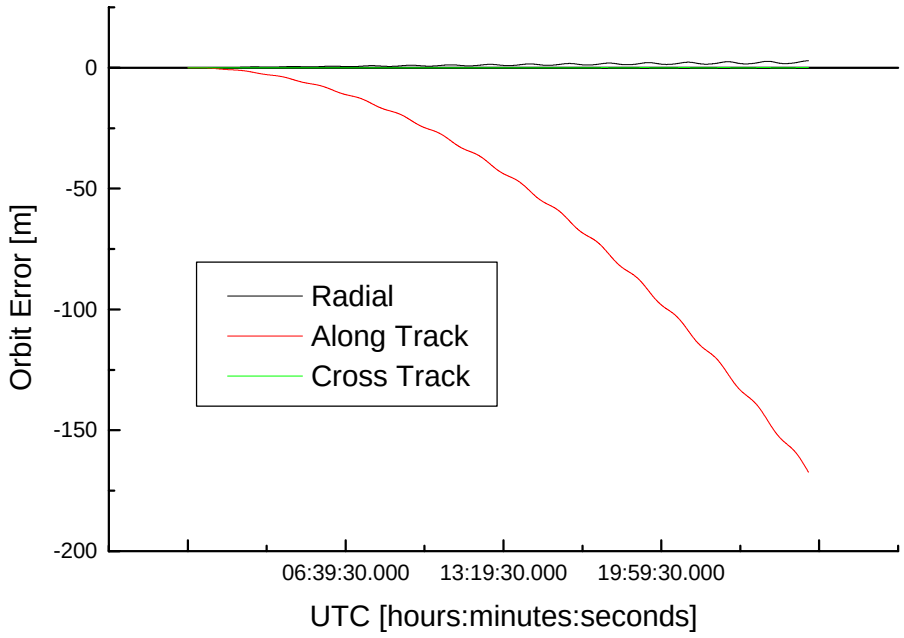

Figure 4-8 Orbit Error of 800 km LEO neglecting Air Drag

Air drag forces act in direction of the flight path, i.e. the along track error is affected most. As a secondary effect, the orbit altitude decreases due to the dissipation of kinetic energy. The

cross track however error shows a periodic error characteristic, with the orbital period as a natural frequency and increasing amplitude. This characteristic also superimposed to the (linear) secular tendency in the radial error.

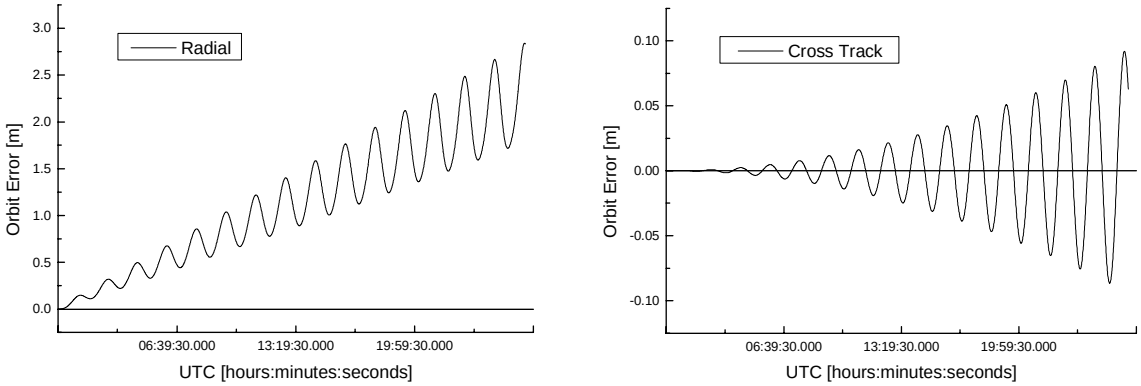

Figure 4-9 Radial / Cross Track Error of 800 km LEO neglecting Air Drag

Thus, for satellite orbits below 1000 km, air drag has to be modelled.

4.3.5 Other Perturbations

Other forces which contribute to the orbit perturbations are

- Solid earth tides
- Ocean tides
- Albedo (reflection from earth)
- Third body attraction due to major planets

In this section, only a few of them will be considered. LEO satellites are subject to perturbations from earth albedo, solid earth tides and ocean loading tides. These perturbations can be of non negligible magnitude in orbits below 800 km. Here, the major focus is on satellite orbits suited for navigation applications. A constellation consisting of LEO satellites requires a high number of space craft to make sure that always a minimum of four space vehicles are visible from any location on earth. The required number increases with decreasing orbit height, thus a navigation constellation would have an orbit altitude above 1000 km. Therefore, only two of the minor perturbation are shown in this section.

Figure 4-10 and Figure 4-11 show the prediction error due to neglecting solid earth tides. For the 800 km LEO, the error is quite noticeable after one day, but for the MEO it is almost negligible.

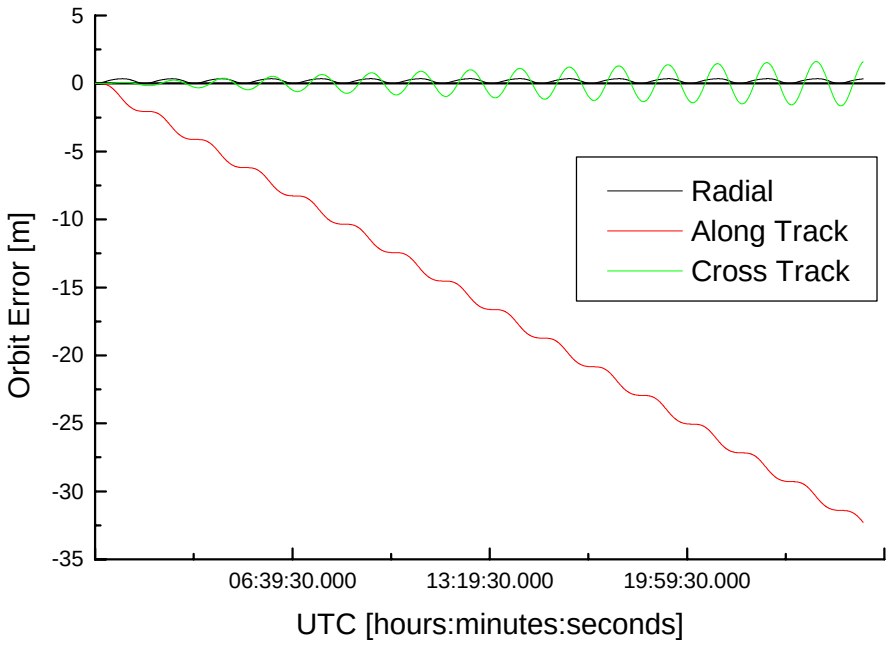

Figure 4-10 Orbit Error of 800 km LEO neglecting Solid Earth Tides

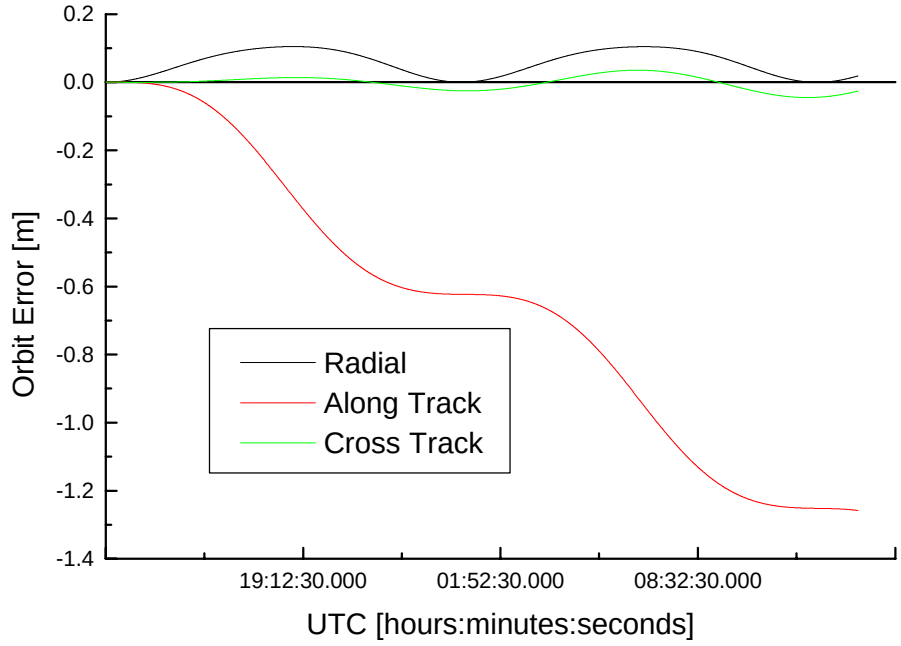

Figure 4-11 Orbit Error of MEO neglecting Solid Earth Tides

The following table indicates the resulting orbit errors (RMS), depending on the orbit type and prediction interval.

	Radial [m]	**Along Track [m]**	**Cross Track [m]**
500 km LEO	0.24	22	0.9
800 km LEO	0.23	20.5	0.82
1250 km LEO	0.24	16.3	0.47
MEO	0.07	0.75	0.02
GEO	0.04	0.27	0.01
IGSO	0.04	0.25	0.01

Table 4-16 Solid Earth Tide Perturbation after 1 day

As can be seen from the table above, the error contribution is negligible for MEO, GEO and IGSO orbits, but not for LEO orbits. In fact, for precise orbit prediction of LEO satellites even the ocean tides will have to be evaluated.

The attraction of the major planets in our solar system also cause a tidal effect like sun and moon, but orders of magnitude lower. Figure 4-12 shows the prediction error for an IGSO neglecting the attraction of the major planets over one week.

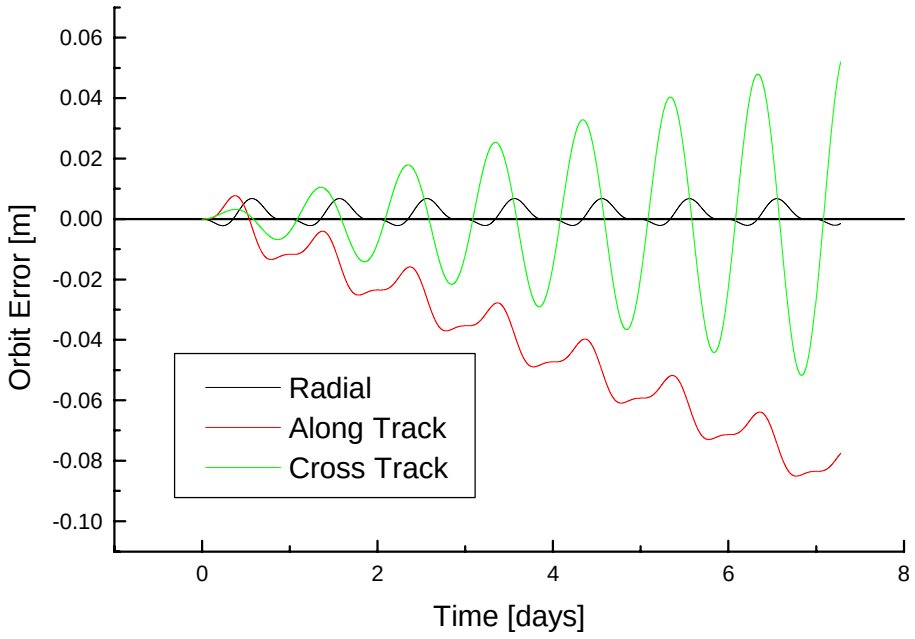

Figure 4-12 Prediction Error of IGSO neglecting Major Planets Attraction

Table 4-17 summarises the effect on different orbits after one week of prediction. It is clear that this perturbation can be neglected for earth orbiting satellites. They become more essential if interplanetary trajectories are to be considered. But this is far from the scope of this text focussing on (earth) navigation satellites.

	Radial [m]	Along Track [m]	Cross Track [m]
500 km LEO	0	0	0
800 km LEO	0	0	0
1250 km LEO	0.001	0	0
MEO	0	0.005	0.005
GEO	0.002	0.005	0.012
IGSO	0.003	0.047	0.022

Table 4-17 Attraction from Major planets Perturbation after 1 Week

4.3.6 Numerical Errors

Numerical integration algorithms have the possibility to estimate the so called local error by halving or doubling the step width and comparing the results. Unfortunately, the global error due to round off introduced by numerical integration can not be estimated that way. To assess the global error following calculation have been conducted:

Neglecting all accelerations except the central force, exact one revolution of a satellite orbit has been propagated. The resulting end state vector has been compared to the initial state vector, which would have to be identical presuming a perfect integration procedure. Three different integration algorithms have been evaluated:

- 4^{th} order Runge-Kutta
- 4^{th} order Adams-Bashford-Moulton
- 8^{th} order Adams-Bashford-Moulton

The step width has been varied to keep the local error below 1 cm.

Figure 4-13 shows the necessary step width for each integration method. It can be generally said, if the orbit altitude is low the step width has to be small due to the strong acceleration.

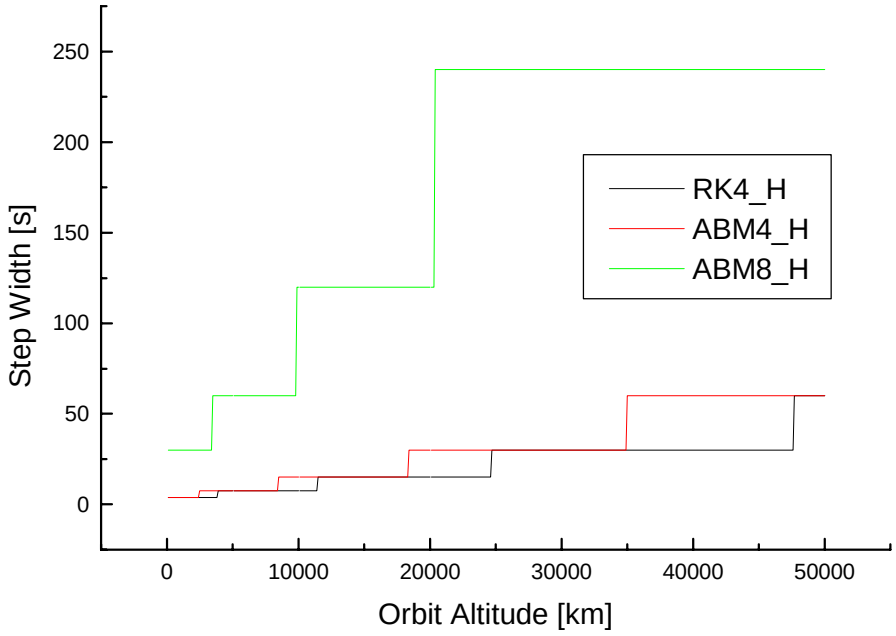

Figure 4-13 Integration Step Width vs. Orbit Altitude

It ca be seen that the Adams-Bashford-Moulton method of 4th order achieves the same local error as the 4th order Runge-Kutta using a slightly higher step width. The step width has a linear impact on the number of function evaluations which have to be performed. The 8th order A-B-M method achieves much higher step widths which is not surprising regarding the higher order. The next figure shows the number of necessary function evaluations, corresponding to the method and step width.

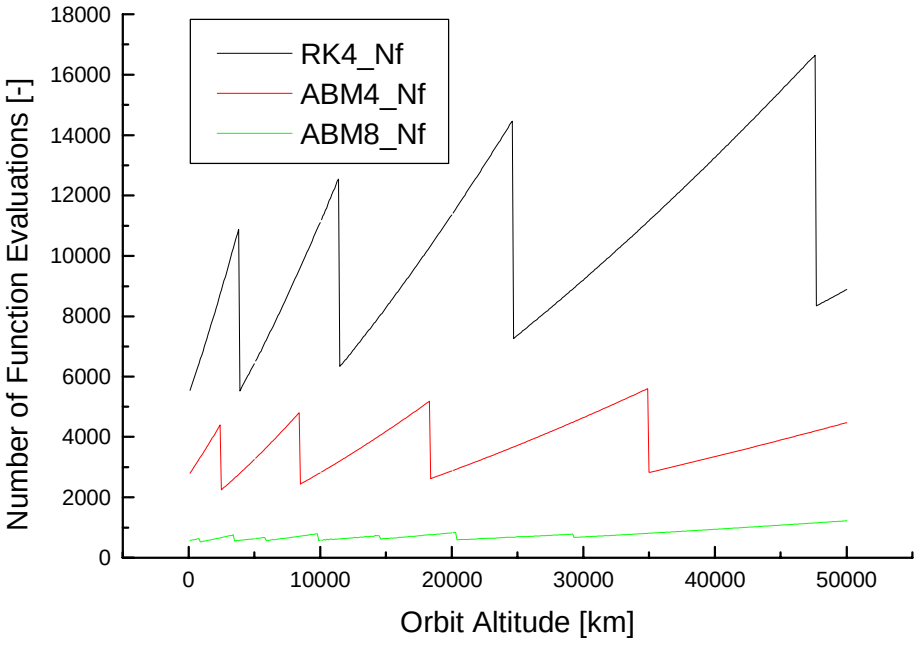

Figure 4-14 Number of Function Evaluations vs. Orbit Altitude

The "sawtooth" figure results from the fact that the number of function evaluations is halved when the step width is doubled. It can be seen that the 4th order Runge-Kutta method requires about double the number function evaluations than the 4th order Adams-Bashford-Moulton method. This is also not surprising, due to the fact that The Runge-Kutta requires for each step 4 function evaluations, and the Adams-Bashford-Moulton only two, regardless of the order.

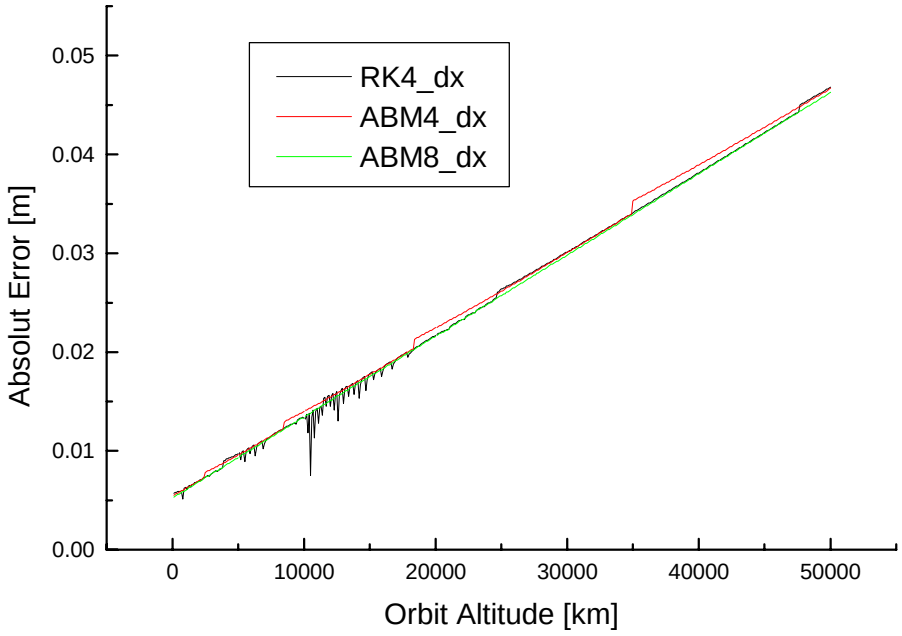

Figure 4-15 Absolute Error vs. Orbit Altitude

Figure 4-15 Absolute Error vs. Orbit Altitude shows the absolute position error after one revolution. A surprising result is that the position error is nearly independent from the method used but depends linear on orbit altitude. However, this is only true if the optimum step width has been applied.

Another intresting fact is that the absolute error is not bounded by the local error, which is kept constant at 1 cm. Thus, it can be said that the numerical accuracy is not the primary driver for the choice of the integration method. If long arcs have to be integrated without a discontinuing change in acceleration (e.g. thruster firing), one would choose a high order multistep method to save computation time. If only short arcs are processed, e.g. because the ephemeris data is needed every 10, 30 or 60 seconds, lower order algorithms are sufficient. Furthermore one has to keep in mind that mulistep methods need a starter calculation from a one-step method. When the orbit integration has to be reinitiated frequently, e.g. because of orbit manoeuvres (discontinuity in acceleration) or trajectory corrections from the state estimation process, the Runge-Kutta method will be in operation most of the time.

4.4 Precise Short Term Orbit Representation

In satellite navigation, the position of a satellite is required with a certain accuracy ranging from a few meters down to decimeter level. To achieve such an accuracy over a long time, a sophisticated orbit model is required, as has been shown in the preceding sections. Unfortunately, a user receiver is not equipped with a super computing facility, thus a simpler orbit representation is required.

The so called broadcast ephemeris message contain the actual parameters of an orbit model, which is accurate enough over a short period of validity. The parameter model is designed in a way that it represents only the desired orbit class with a sufficient accuracy over the period of validity, using only modest computation power. There are various possible models suited for the broadcast ephemeris message, but they all share some common characteristics:

- The state prediction requires no other information than included in the navigation message, or constants which are permanently stored in the receiver and need not to be updated.
- The user-receiver has to compute the positions of maybe up to 12 satellites. It is obvious that this should require only modest computational effort. That means, the state calculation has to be done using a geometric model(like the GPS broadcast ephemeris) or the numerical integration of a state vector (like the GLONASS broadcast ephemeris) using a simple force model.
- The ephemeris are given in Earth centred Earth fixed co-ordinates. Otherwise the user would have to compute all the earth rotation parameters (precession, nutation, polar motion, sidereal time).

The broadcast ephemeris are not derived directly from measurements. From the orbit determination process, the satellites state as well as some physical parameters have been determined to a certain accuracy. This information is used to extrapolate the satellites state vector. The computed satellite positions have to be converted into the earth centred earth fixed coordinate frame. The parameters of that simple, earth fixed broadcast ephemeris model are adjusted using a least squares estimator so that the position difference between the precise ephemeris and the broadcast ephemeris becomes minimal over that fit interval. It is obvious that the derived broadcast ephemeris is only optimal and therefore valid for that specified fit interval.

Both navigation satellite systems (GPS and GLONASS) provide an additional format of orbit representation, the almanac. This is an even more simple orbit description, fit over a longer interval, typically a week. This orbit propagator is only for visibility evaluations, therefore accuracy lies in the range of several kilometers. Both almanac types consist of a Keplerian orbit including the secular perturbation due to earth's oblateness.

In the following section, an overview over a few broadcast models is given, to show the variety of orbit representation possibilities.

4.4.1 GLONASS Broadcast Ephemeris

The GLONASS navigation message consists, besides some other information, of 9 ephemeris states:

x_0, y_0, z_0	Position in Cartesian ECEF coordinates
$\dot{x}_0, \dot{y}_0, \dot{z}_0$	Velocity in Cartesian ECEF coordinates
$\ddot{x}_{Res}, \ddot{y}_{Res}, \ddot{z}_{Res}$	Residual acceleration over the fit interval, mainly due to lunisolar attraction, in Cartesian ECEF coordinates
t_0	Reference time of ephemeris

A broadcast message as described above, requires a very simple force model, referenced in the earth fixed frame, which accounts for the following components:

- central force of earth's gravity
- dynamic oblateness represented by the C_{20} coefficient
- centripetal acceleration introduced by the rotating reference frame
- Coriolis acceleration introduced by the rotating reference frame

The simplified equations of motion expressed by

Eq. 4.4-1

$$\frac{dx}{dt} = \dot{x}$$
$$\frac{dy}{dt} = \dot{y}$$
$$\frac{dz}{dt} = \dot{z}$$
$$\frac{d\dot{x}}{dt} = -\frac{\mu}{r^3}x + \frac{3}{2}C_{20}\frac{GMa_e^2}{r^5}x\left(1-5\frac{z^2}{r^2}\right) + \omega_e^2 x + 2\omega_e\dot{y} + \ddot{x}_{Res}$$
$$\frac{d\dot{y}}{dt} = -\frac{\mu}{r^3}y + \frac{3}{2}C_{20}\frac{GMa_e^2}{r^5}y\left(1-5\frac{z^2}{r^2}\right) + \omega_e^2 y - 2\omega_e\dot{x} + \ddot{y}_{Res}$$
$$\frac{d\dot{z}}{dt} = -\frac{\mu}{r^3}z + \frac{3}{2}C_{20}\frac{GMa_e^2}{r^5}z\left(3-5\frac{z^2}{r^2}\right) + \ddot{z}_{Res}$$

with

$\omega_e = 7.292115 \cdot 10^{-5}\ s^{-1}$ Angular velocity of Earth's rotation

are solved using a fourth order Runge-Kutta algorithm. Note that the integration is performed in the earth fixed frame, thus, it is not necessary for the user to compute earth rotation parameters.

The desired position at time t is obtained by integrating from the position at time t_0 which is given in the navigation message. The GLONASS navigation message valid for

$$\left|t - t_0\right| \le 15 \text{ minutes} \qquad \text{Eq. 4.4-2}$$

which means, the time of the reference state t_0 lies in the middle of the 30 minutes period of validity.

4.4.1.1 Extended GLONASS Format

It is easy to augment the GLONASS message to enhance accuracy or adapt the message for more perturbed orbits, simply by allowing the acceleration to vary over time. An extended GLONASS message using 12 Parameters could look like

$$\overline{X}_{\text{Broadcast}} = \left(x_0, y_0, z_0, \dot{x}_0, \dot{y}_0, \dot{z}_0, a_{x0}, a_{y0}, a_{z0}, a_{x1}, a_{y1}, a_{z1}, a_{x2}, a_{y2}, a_{z2}\right) \qquad \text{Eq. 4.4-3}$$

with the reference position and velocity being the same as in the GLONASS message, and the constant residual acceleration being replaced by

$$\begin{aligned} \ddot{x}_{Res} &= a_{x0} + a_{x1}\left(t - t_0\right) \\ \ddot{y}_{Res} &= a_{y0} + a_{y1}\left(t - t_0\right) \\ \ddot{z}_{Res} &= a_{z0} + a_{z1}\left(t - t_0\right) \end{aligned} \qquad \text{Eq. 4.4-4}$$

If even more adaptability to perturbations, or simply a longer period of validity is required, the navigation message could also be extended to 15 Parameters,

$$\overline{X}_{\text{Broadcast}} = \left(x_0, y_0, z_0, \dot{x}_0, \dot{y}_0, \dot{z}_0, a_{x0}, a_{y0}, a_{z0}, a_{x1}, a_{y1}, a_{z1}, a_{x2}, a_{y2}, a_{z2}\right) \qquad \text{Eq. 4.4-5}$$

with the residual acceleration being modelled as a quadratic term.

$$\begin{aligned} \ddot{x}_{Res} &= a_{x0} + a_{x1}\left(t - t_0\right) + a_{x2}\left(t - t_0\right)^2 \\ \ddot{y}_{Res} &= a_{y0} + a_{y1}\left(t - t_0\right) + a_{y2}\left(t - t_0\right)^2 \\ \ddot{z}_{Res} &= a_{z0} + a_{z1}\left(t - t_0\right) + a_{z2}\left(t - t_0\right)^2 \end{aligned} \qquad \text{Eq. 4.4-6}$$

In both cases, the same propagator is used as in the standard GLONASS message.

4.4.2 GPS Broadcast Ephemeris

In contrary to the integrating-a-force-model based GLONASS broadcast ephemeris, the GPS state propagator consists of a Keplerian orbit propagator accounting for secular and periodic

perturbations. The following 15 ephemeris related parameters are part of the GPS navigation message.

M_0	Mean anomaly at reference time
Δn	Mean motion difference from computed value
e	Eccentricity
$\sqrt{A}$	Square root of semi-major axis
Ω_0	Longitude of ascending node of orbital plane at weekly epoch
i_0	Inclination angle at reference time
ω	Argument of perigee
OMEGADOT (=$d\Omega/dt$)	Rate of right ascension
IDOT (=di/dt)	rate of inclination angle
Cuc	Amplitude of the cosine harmonic correction term to the argument of latitude
Cus	Amplitude of the sine harmonic correction term to the argument of latitude
Crc	Amplitude of the cosine harmonic correction term to the orbit radius
Crs	Amplitude of the sine harmonic correction term to the orbit radius
Cic	Amplitude of the cosine harmonic correction term to the angle of inclination
Cis	Amplitude of the sine harmonic correction term to the angle of inclination
t_{oe}	reference time of ephemeris

The following computations are necessary, to derive the satellites position in an earth centred earth fixed reference frame.

$A = \left(\sqrt{A}\right)^2$	Semi-major axis	Eq. 4.4-7
$n_0 = \sqrt{\frac{GM}{A^3}}$	Computed mean motion	Eq. 4.4-8

$t_k = t - t_{oe}$	Time from ephemeris reference epoch	Eq. 4.4-9
$n = n_0 + \Delta n$	Corrected mean motion	Eq. 4.4-10
$M_k = M_0 + n \cdot t_k$	Mean anomaly	Eq. 4.4-11
$M_k = E_k - e \cdot \sin E_k$	Kepler's equation for eccentric anomaly, solved by iteration	Eq. 4.4-12
$\nu_k = \arctan\left(\frac{\sqrt{1-e^2}\,\sin E_k}{\cos E_k - e}\right)$	True anomaly	Eq. 4.4-13
$E_k = \arccos\left(\frac{e + \cos \nu_k}{1 + e \cdot \cos \nu_k}\right)$	Eccentric anomaly	Eq. 4.4-14
$\Phi_k = \nu_k + \omega$	Argument of latitude	Eq. 4.4-15
$\delta u_k = C_{us} \cdot \sin 2\Phi_k + C_{uc} \cdot \cos 2\Phi_k$	Argument of latitude correction	Eq. 4.4-16
$\delta r_k = C_{rs} \cdot \sin 2\Phi_k + C_{rc} \cdot \cos 2\Phi_k$	Radius correction	Eq. 4.4-17
$\delta i_k = C_{is} \cdot \sin 2\Phi_k + C_{ic} \cdot \cos 2\Phi_k$	Correction to inclination	Eq. 4.4-18
$u_k = \Phi_k + \delta u_k$	Corrected argument of latitude	Eq. 4.4-19
$r_k = A \cdot (1 - e \cdot \cos E_k) + \delta r_k$	Corrected radius	Eq. 4.4-20
$i_k = i_0 + \delta i_k + IDOT \cdot t_k$	Corrected inclination	Eq. 4.4-21
$\Omega_k = \Omega_0 + (\dot{\Omega} - \dot{\Omega}_E) \cdot t_k - \dot{\Omega}_E \cdot t_{oe}$	Corrected longitude of ascending node	Eq. 4.4-22
$x'_k = r_k \cdot \cos u_k$ $y'_k = r_k \cdot \sin u_k$	Position in orbital plane	Eq. 4.4-23
$x_k = x'_k \cos \Omega_k - y'_k \cos i_k \sin \Omega_k$ $y_k = x'_k \sin \Omega_k + y'_k \cos i_k \cos \Omega_k$ $z_k = \sin i_k$	Position in Earth-Centered-Earth-Fixed coordinates	Eq. 4.4-24

This propagator accounts for secular as well periodic perturbations, as can be seen from the equation. Period of validity is 4 hours.

4.4.3 WAAS GEO Broadcast Ephemeris

The broadcast ephemeris proposed for the GEO's within a SBAS (Space Based Augmentation System) makes use of the fact that a geostationary satellite nominally is a fixed point in the sky, with respect to earth. The ephemeris parameters look similar to the GLONASS navigation message.

x_0, y_0, z_0 Position in Cartesian ECEF co-ordinates

$\dot{x}_0, \dot{y}_0, \dot{z}_0$ Velocity in Cartesian ECEF co-ordinates

$\ddot{x}_0, \ddot{y}_0, \ddot{z}_0$ Acceleration over the fit interval in Cartesian ECEF co-ordinates

t_0 Reference time of ephemeris

But unlike the GLONASS propagator, no "earth gravity model" is used to propagate the space craft position. Instead, a very simple polynomial of second degree is used to account for the perturbations, as indicated in Eq. 4.4-25.

$$x(t) = x_0 + \dot{x}_0 \cdot (t - t_0) + \tfrac{1}{2}\ddot{x} \cdot (t - t_0)^2$$
$$y(t) = y_0 + \dot{y}_0 \cdot (t - t_0) + \tfrac{1}{2}\ddot{y} \cdot (t - t_0)^2 \qquad \text{Eq. 4.4-25}$$
$$z(t) = z_0 + \dot{z}_0 \cdot (t - t_0) + \tfrac{1}{2}\ddot{z} \cdot (t - t_0)^2$$

This propagator is not suited to account for periodic perturbations, thus the period of validity is limited to a few minutes.

4.4.4 INTELSAT Ephemeris Format

Although the INTELSAT space crafts are communication and not navigation satellites, the ephemeris representation used is quite interesting. Like in the WAAS GEO ephemeris message, it makes also use of the unique property of the geostationary orbit. The space craft motion represented by the following 11 parameters.

LM0	Longitude at reference time
LM1	Rate of change of longitude angle
LM2	Rate of change of longitude drift
LonC	Amplitude of the cosine harmonic correction term to satellites longitude
LonC1	Rate of change of amplitude of the cosine harmonic correction term to satellites longitude
LonS	Amplitude of the sine harmonic correction term to satellites longitude
LonS1	Rate of change of amplitude of the sine harmonic correction term to satellites longitude
LatC	Amplitude of the cosine harmonic correction term to satellites latitude
LatC1	Amplitude of the cosine harmonic correction term to satellites latitude
LatS	Amplitude of the cosine harmonic correction term to satellites latitude
LatS1	Amplitude of the cosine harmonic correction term to satellites latitude
t_{oe}	reference time of ephemeris

This ephemeris model also uses no "orbit" model, but treats the GEO as a nominally fixed point, which is subject to secular and periodic perturbations. The following equations are used to determine the space crafts position.

$\mathrm{Lon}_M(t) = \mathrm{LM0} + \mathrm{LM1} \cdot (t - t_0) + \mathrm{LM2} \cdot (t - t_0)^2$	Longitude, corrected for secular perturbations	Eq. 4.4-26
$\mathrm{Lon}_C(t) = (\mathrm{LonC} + \mathrm{LonC1} \cdot (t - t_0)) \cdot \cos(\theta)$	Harmonic cosine correction term of longitude	Eq. 4.4-27
$\mathrm{Lon}_S(t) = (\mathrm{LonS} + \mathrm{LonS1} \cdot (t - t_0)) \cdot \sin(\theta)$	Harmonic sine correction term of longitude	Eq. 4.4-28
$\mathrm{Lat}_C(t) = (\mathrm{LatC} + \mathrm{LatC1} \cdot (t - t_0)) \cdot \cos(\theta)$	Harmonic cosine correction term of latitude	Eq. 4.4-29

$$Lat_S(t) = (LatS + LatSl \cdot (t - t_0)) \cdot \sin(\theta)$$ Harmonic sine correction term of latitude Eq. 4.4-30

with $\theta = \omega_E \cdot UTC$

being the hour angle. Both, latitude and longitude harmonic corrections, account for periodic errors with increasing amplitude (see section 4.3-Force Model Errors).

The resulting longitude and latitude of the space craft is obtained by adding all correction of secular and harmonic terms.

$$Lon = Lon_M + Lon_C + Lon_S$$ Eq. 4.4-31

$$Lat = Lat_C + Lat_S$$

Unfortunately, this ephemeris format is not intended to account for radial perturbations (However it could easily be modified to do so!). For communication purposes like television broadcast, only elevation and azimuth of the satellite are necessary to align the dish antenna. But for navigation, the radial component is the most important, due to its large impact on the ranging error.

Driven by the requirement for accurate pointing instead of accurate ranging, the period of validity is one week. Nevertheless, the transformation to Cartesian co-ordinates is given below.

$$x = R_{GEO} \cdot \cos Lon \cdot \cos Lat$$ Eq. 4.4-32

$$y = R_{GEO} \cdot \sin Lon \cdot \cos Lat$$

$$z = R_{GEO} \cdot \sin Lat$$

with $R_{GEO} = 42164537$ m

5 SOFTWARE DESCRIPTION

Based on the theory given in the preceding chapters, a software package has been implemented. The intention was to allow the analysis of arbitrary satellite constellations, ground networks, force models. The main features are given in Table 5-1.

Function / Module	Description
Orbit Simulation	Numerical force model integration
Force Model	• Earth's gravity as spherical harmonics expansion • Solar- Lunar- and major planets attraction • solid earth tides • air drag • solar radiation pressure • Vehicle Thrust (if commanded)
Gravity Models	• EGM-96 (360x360), WGS-84 (180x180) • JGM-1(70x70), JGM-2 (70x70), JGM-3(70x70) GEM-T1 (36x36), GEM-T2 (50x43), GEM-T3 (50x50) • GRIM4-S4 (66x66)
Planetary Ephemeris	JPL DE200 files
Integration	• 4^{th} order Runge-Kutta with automated step size control • 8^{th} order Adams-Bashford-Moulton using fixed step size
Number of Satellites	Not limited
Orbit types	Arbitrary
Main Output	Precise ephemeris represented by a time series of state vectors (position / velocity)
Orbit Estimation	The orbit estimation from simulated measurements using differential corrections applied to the predicted trajectory
Measurements	Generated using geometry to "true trajectory", modified by introducing measurement errors
Types	• Range • Range Rate
Link Types	• Ground links • Inter satellite links (ISL)
Errors Simulation	• Free space attenuation • Ionospheric refraction • Tropospheric refraction • Random clock offset

Function / Module	Description
	• Clock drift
Estimator	• Weighted least squares with a priori statistics • Real time Kalman filter • Batch mode Kalman filter
Predicted Trajectory	Force model integration, used to generate reference trajectory to allow linearization
"True Trajectory"	Force model integration, but using slightly different force model, used to derive measurements
Errors Simulation	• Random walk on solar constant • Random walk on air density • Deviated harmonic coefficients
Number of Ground stations	Not limited
Number of links	Not limited
Main Output	• Covariance of radial / along track / cross track error • Instantaneous radial / along track / cross track error
Force Model Errors	Impact analysis of contributing forces by comparing orbits generated using different force models
Main Output	• Root mean square of radial / along track / cross track error • Instantaneous radial / along track / cross track error
Broadcast Ephemeris	Least squares fit of a broadcast model over a time series of satellite positions in earth-centred-earth-fixed co-ordinates
Main Output	• Root mean square of radial / along track / cross track error • Instantaneous radial / along track / cross track error • User Range Error (URE)
Integrity Analysis	A RAIM algorithm is used to compute integrity of one selected satellite for a given misdetection probability and false alarm rate
Main Output	• Minimum detectable bias / protection level • Instantaneous radial / along track / cross track error • Error detection flag • Error isolation flag • Type of error identified

Table 5-1 Main Software Features

The following sections contain brief a description of the implementation and functionality of the main software components. Additionally, equations for some "remaining" topics like measurement errors and co-ordinate transformation are given.

5.1 Orbit Integration

The orbit integrator has to compute the forces acting on the satellites and conduct a numerical integration. The forces are fixed in different co-ordinate frames vary with time in an other. The main force, earth's gravity is fixed with respect to the terrestrial frame, whereas third body attraction and solar radiation depend on the ephemeris of celestial body which can be expressed easier in inertial co-ordinates.

The computations are therefore performed in the inertial frame ECI-J2000. The acceleration of the rotating earth gravity field has therefore to be converted into inertial referenced acceleration for each computation epoch. The transformation matrix from the terrestrial frame to the inertial frame consists of four elements, sidereal angle (hour angle), precession, nutation and polar motion. Only the first three can be computed, although with some computational effort, directly. Polar motion , as well as the true length of day, has a random component and is predicted by the IERS (Bulletin A) and updated from measurements. Normally these earth rotation parameters are estimated within the orbit determination process. The software however does not account for polar motion and true length of day up to now, but implementation is planned for the near future.

The following figure shows the flow chart of an orbit propagator. Starting from a satellite position and velocity at a given time, the contributing forces are computed sequentially and integrated numerically to derive the state at the next epoch. This process is repeated, thus a time series of satellite states is generated.

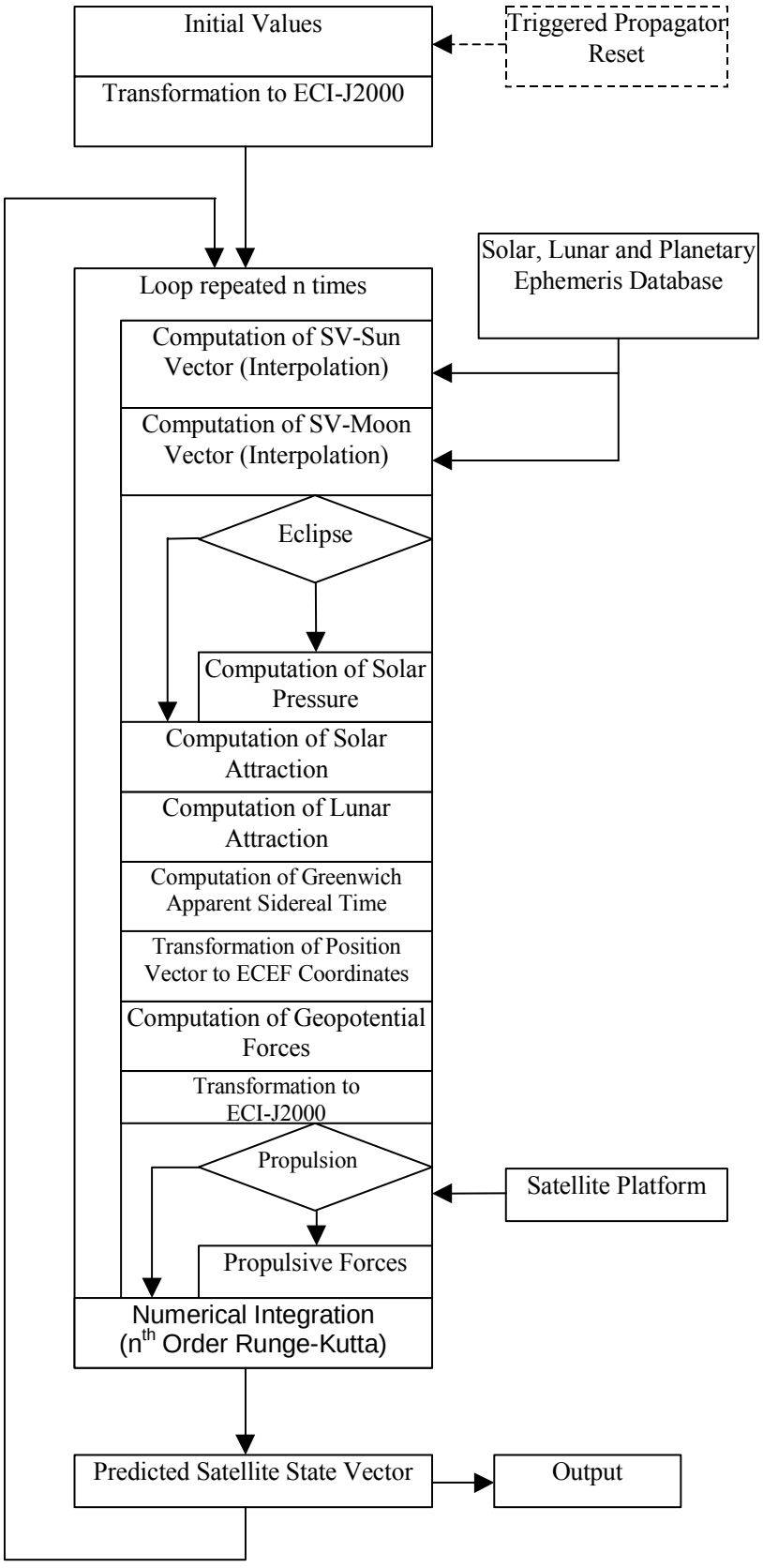

Figure 5-1 Orbit Integration Process

5.2 Real time State Estimation

The real time state estimator requires linearised equations for the state dynamics and the observations. Orbit propagation is a highly non linear process, as well as slant ranges are non linear observations. Thus, a non linear predictor is needed to derive approximate values for the state and the predicted measurements. This task is performed by the orbit propagator described above.

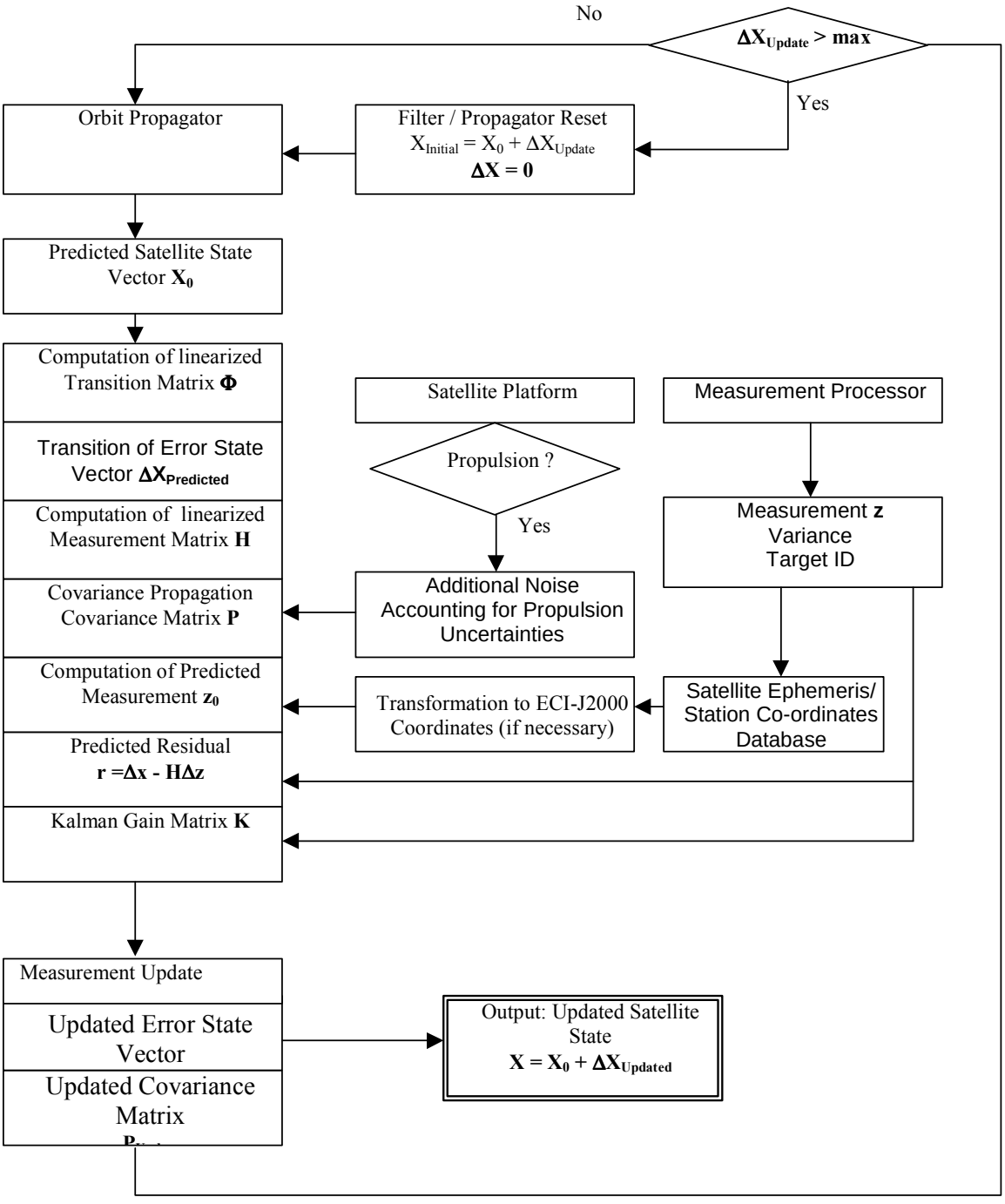

Figure 5-2 State Estimation Process

5.3 Measurement Simulation

Measurements are computed from the geometric range or range rate using the true satellite orbits and adding delays from the signal path, clock offsets and random errors. The computed range is also used to derive the free distance attenuation of the signals. The following measurement equation indicates the considered components of a pseudo range measurement.

$$PR_0 = \rho_{Geometric} + c \cdot \left(\delta T_{Sat} - \delta T_{Ground/Sat2} + \delta_{iono} + \delta_{Tropo} + \delta_{Multipath}\right) + \varepsilon_{noise} \qquad \text{Eq. 5.3-1}$$

The largest part is represented by the true geometric range. The delays, which are scaled with the speed of light to obtain a distance, are

- Satellite clock offset
- Ground station clock offset or 2nd satellite clock offset
- Ionospheric delay
- Tropospheric delay
- Multipath

The two clock offsets are generated by initialising the clock offset variable of each satellite and ground station using a random number with

- 3 milliseconds standard deviation for the satellite clocks.
- 100 nanoseconds standard deviation for the ground station clocks

The errors introduced by the signal propagation path are considered by computing tropospheric and ionospheric delays from models. The last error contributor is the thermal noise, which has been computed using the range dependent free distance attenuation.

Under the assumption, that tropospheric and ionospheric delays can be removed to a certain degree using models, only the residual errors of these contributor are considered in the measurement noise, as indicated in the following equation.

$$\sigma^2_{Range} = \sigma^2_{Thermal} + \left(0.2 \cdot \delta_{Tropo}\right)^2 + \left(0.5 \cdot \Delta_{Iono}\right)^2 + \delta^2_{Multipath} \qquad \text{Eq. 5.3-2}$$

The simulated range measurements is then obtained by

$$PR = PR_0 + RANDOM \cdot \sigma_{Range} \qquad \text{Eq. 5.3-3}$$

The error of a range rate measurement has been assumed to depend only on the thermal noise.

$$\sigma^2_{Range\,Rate} = \sigma^2_{Thermal} \qquad \text{Eq. 5.3-4}$$

The measurement errors had been obtained by

$$\dot{PR} = \dot{PR}_0 + RANDOM \cdot \sigma_{Range\,Rate} \qquad \text{Eq. 5.3-5}$$

where

PR	Range measurement
PR_0	Real range
$\dot{PR}$	Range rate measurement
$\dot{PR}_0$	Real range rate

and RANDOM is a function generating a normally distributed random number with zero mean and variance 1.

5.3.1 Thermal Noise

An important number in a link budget calculation is the signal to noise ratio expressed by

$$(\frac{C}{N_0})_{dB-Hz} = P_T + G_T + A_T + A_D + G_R + A_R + A_S - T_{sys/dB} - k_{/dB} \qquad \text{Eq. 5.3-6}$$

with

k	Boltzmann's constant k=1.38 × 10^{-23} [Ws / ^{0}K]
T_{SYS}	Equivalent noise temperature of the system
A_D	Free space attenuation
G_T	Transmit antenna gain in main direction; f(frequency, beamwidth)
G_R	Receiver antenna gain in main direction; f(frequency, beamwidth)
A_S	System losses (including cable losses, the A/D converter, signal processing losses)
A_T	Pointing loss of the transmit antenna
A_R	Pointing loss of the receive antenna
P_T	Antenna transmitted power

The equation above, as well as the following equation concerning link budget can be found for instance in the "Blue Books" [BLU-96] by Parkinson / Spilker. Most of the parameters in the equation above are a function of the link technology used, e.g. power, antenna pattern, frequency etc, and therefore not directly dependent of the link geometry, i.e. distance. The only directly geometry dependent component is the free space attenuation given by

$$(A_D)_{dB} = 20 \cdot \log_{10}(\frac{\lambda}{4\pi d}) \qquad \text{Eq. 5.3-7}$$

The carrier to noise ratio can therefore coarsely be regarded as a function of the inverse square of the geometric distance.

$$\frac{C}{N_0} \approx f\left(\frac{1}{d^2}\right) \qquad \text{Eq. 5.3-8}$$

Code range, phase and doppler measurements are strongly dependent of the carrier to noise ratio, as indicated in equation 5.3-9, 5.3-10 and 5.3-11.

Code Range measurement precision performance of a DLL:

$$\sigma_\tau = \pm D\sqrt{\frac{dB_L}{2C/N_0}\left(1+\frac{2}{(C/N_0)T_i}\right)} \qquad \text{Eq. 5.3-9}$$

Phase measurement precision performance of a PLL:

$$\sigma_\tau = \pm\left(\frac{\lambda}{2\pi}\right)\sqrt{\frac{B_{Lp}}{C/N_0}\left(1+\frac{1}{2(C/N_0)T_i}\right)} \qquad \text{Eq. 5.3-10}$$

Doppler measurement precision performance:

$$\theta_{Doppler} = \frac{\omega_L\sqrt{\omega_L}}{2\sqrt{2\xi}}\sqrt{\frac{N_o}{C}} \qquad \text{Eq. 5.3-11}$$

with

T_i Integration time

C/N_0 Carrier noise density

D Chip length

B_L B_{LP} Noise bandwidth of tracking loop

λ Wavelength of carrier

ω_L Natural angle frequency of a PLL

ζ Attenuation factor of a loop filter

d Early-late spacing of DLL (d=0.01 ... 1)

From the equations above, generally a quadratic relationship between the distance and the measurement noise can be derived for code and phase measurements. In the following it will be shown that for realistic values the relationship is nearly linear.

Let us assume some typical values for a GPS like scenario:

Chip length D	300 m
Carrier wave length λ	19 cm
Bandwidth of phase lock loop (PLL) B_{Lp}	20 Hz
Bandwidth of delay lock loop (DLL) B_L	1 Hz
Early late spacing of DLL d	0.1
Integration time T_I	20 ms

Assuming C /N_0 to be - for a given link technique - approximately a function of the inverse square of the geometric distance (equation 5.3-8), we obtain

$$\frac{C}{N_0} = \frac{K_{C/N_0}}{d^2} \qquad \text{Eq. 5.3-12}$$

Where the parameter $K_{C/N0}$ still has to be determined. By assuming a (rather pessimistic) C /N_0 of 30 dB_{Hz} for a GPS satellite close to the horizon (elevation ~ 0°) which would have a range of approximately 25 000 km, we obtain the link budget dependent factor $K_{C/N0}$ by

$$\left.\frac{C}{N_0}\right|_{dB,Hz} = 30dB_{Hz} = 10 \cdot \log_{10}\left(\frac{C}{N_0}\right) \qquad \text{Eq. 5.3-13}$$

$$\frac{C}{N_0} = 10^3 = \frac{K_{C/N_0}}{(25000km)^2}$$

$$K_{C/N_0} = 6.25 \cdot 10^{17}$$

5.3-9 and 5.3-10 have been evaluated using the parameter values indicated above, but with three different integration time constants T_I. The results has been plotted. Figure 5-3 and 5-4 show the results for the code range and carrier noise.

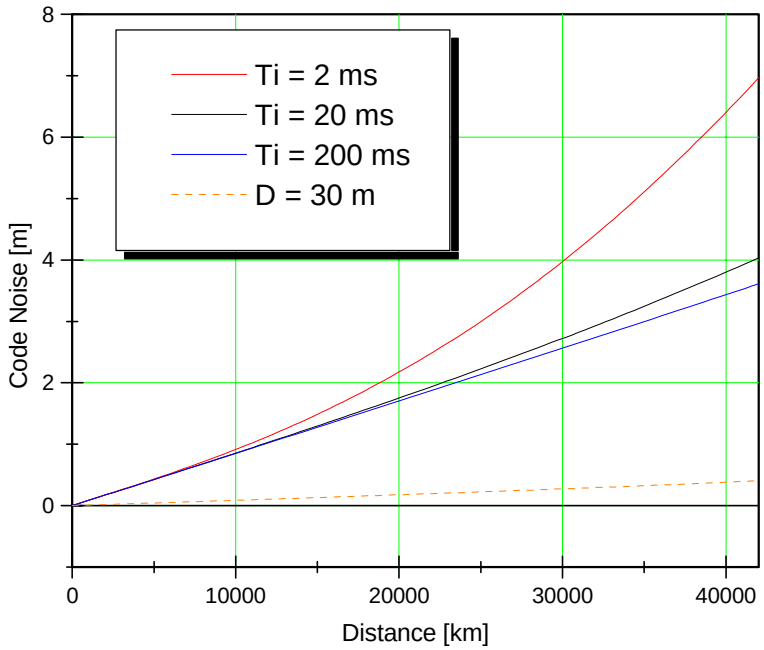

Figure 5-3 Code Noise vs. Range

The relationship between code noise and range is approximately, but not exactly linear, as can be seen in the figure above. The integration time of 20 ms has been chose as a typical value for a GPS user receiver. Using only ten times higher integration time for example would lead to an even more linear relationship between code noise and distance. The integration time of a DORIS receiver, for example is around 10 seconds. Presuming a sufficiently long integration time T_i, the receiver noise of a code range measurement, a phase measurement or a Doppler measurement is indirect proportional to the range. The same could be done by decreasing chip length, which would also directly enhance measurement precision.

The next figure shows the dependence of carrier noise and range. This can be regarded as a nearly linear function of the geometric distance.

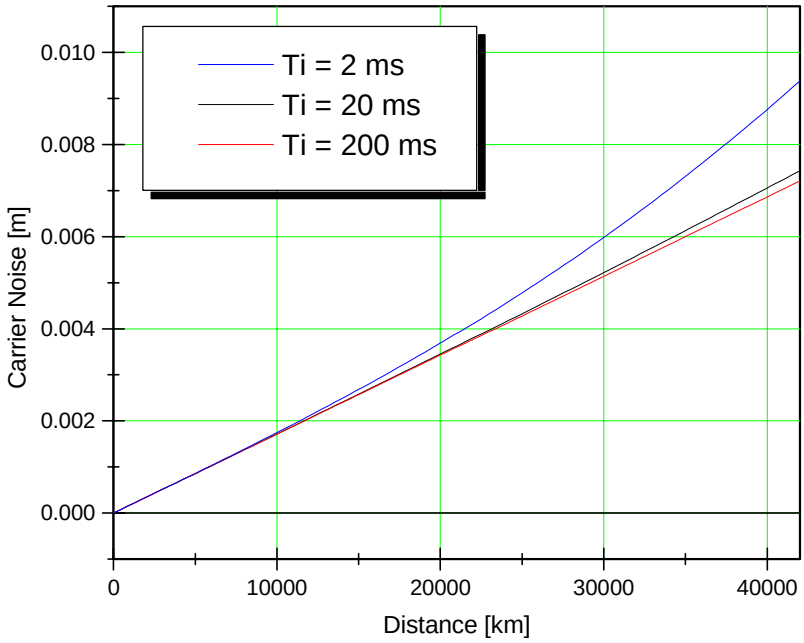

Figure 5-4 Carrier Noise vs. Range

For system level studies, it is therefore accurate enough to model the range measurement accuracy using linear relationship between distance and measurement precision due to thermal noise given by

$$\sigma_R \approx K_R \cdot d \qquad \text{Eq. 5.3-14}$$

with

d Distance, Range

K_R Link technology factor for ranging noise, can be obtained from

$$K_R = D\sqrt{\frac{d}{2}B_L \frac{k_{Boltz}N}{A_{Rx}A_{Tx}A_{Sys}G_{Rx}G_{Tx}P_T}} \frac{1}{4\pi fc} \qquad \text{Eq. 5.3-15}$$

The exact quantification of the link technology factor K_R is subject to link budget design, but in the frame of an inter satellite study conducted for ESA, it has been shown that

$K_R \sim 1 \times 10^{-9}$ m/m

can easily be achieved and has been found to be a reasonable value for the simulations in this thesis. This leads to a ranging precision of approximately 2.5 cm due to thermal noise for a 25000 km range. This can be regarded as a realistic value for a carrier smoothed code range.

To derive the precision of a range rate measurement, we start with the formulation of the Doppler shift and difference the range rate with respect to the Doppler shift.

$$f_{Rx} = f_{Tx} \cdot \left(1 + \frac{\dot{R}}{c}\right) \qquad \text{Eq. 5.3-16}$$

$$\Delta f = \left(f_{Rx} - f_{Tx}\right) = f_{Tx} \cdot \frac{\dot{R}}{c} = \theta$$

$$\dot{R} = \theta \cdot \frac{c}{f_{Tx}}$$

$$\frac{\partial \dot{R}}{\partial \theta} = \frac{c}{f_{Tx}}$$

We can therefore rewrite 5.3-11 to

$$\sigma_{RR} = \frac{\partial \dot{R}}{\partial \theta} \cdot \theta_{Doppler} = \frac{c}{f_{Tx}} \frac{\omega_L \sqrt{\omega_L}}{2\sqrt{2\xi}} \sqrt{\frac{N_o}{C}} \qquad \text{Eq. 5.3-17}$$

The precision of a Doppler measurement is strongly related to the phase measurement. Thus we assume also a linear relationship between distance and range rate accuracy.

$$\sigma_{RR} \approx K_{RR} \cdot d \qquad \text{Eq. 5.3-18}$$

From the DORIS system specification we obtain a value of 0.3 mm/s for low earth orbits. Thus we can find a scale factor of approximately

$K_{RR} = 2 \times 10^{-10}$ m/s

to be a representative. Figure 5-5 shows the range rate precision up to a distance of 42 000 km.

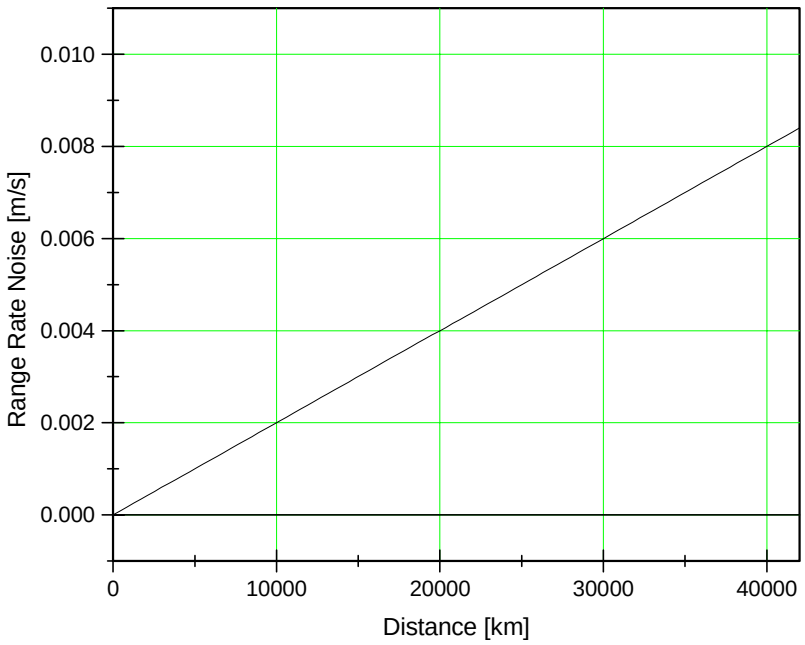

Figure 5-5 Range Rate Noise vs. Distance

5.3.2 Ionospheric Model

Radio signal travelling through the ionosphere are subject to refraction. The degree of refraction depends on the frequency, and due to a non uniform distribution of the electron density, also on the signal path. Ionospheric delay is obtained by integrating the Total Electron Content (TEC) along the signal path. A good approximation of the nominal TEC distribution is the Chapman profile shown below.

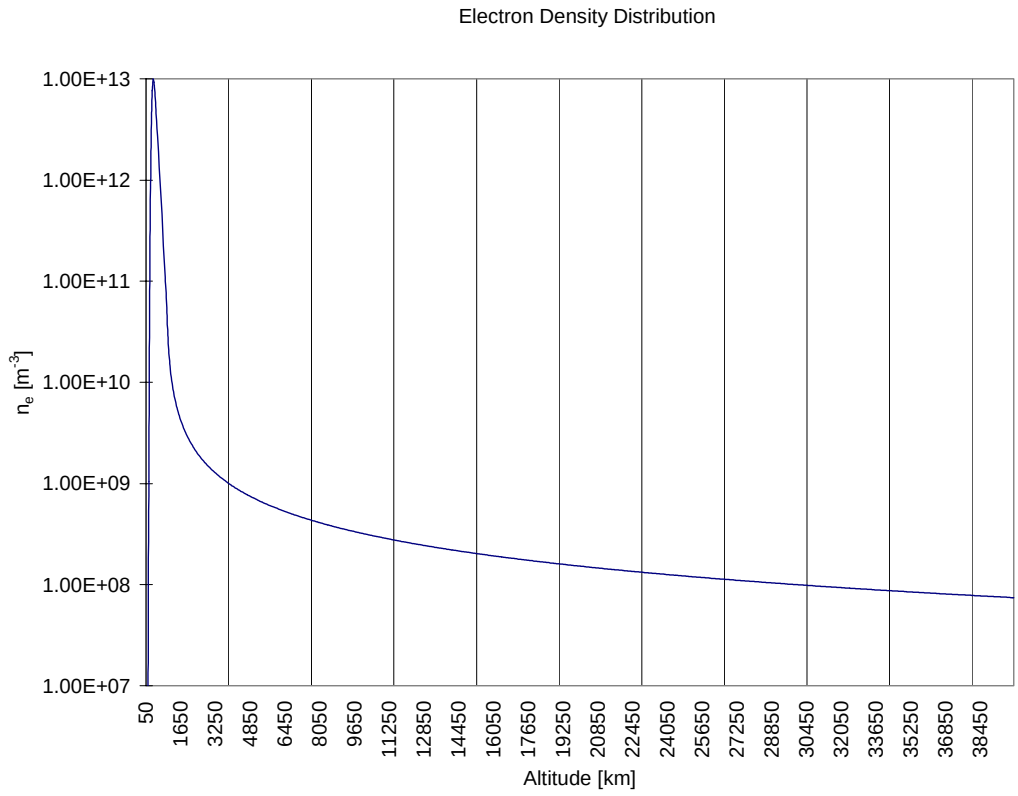

Figure 5-6 Chapman Profile of the Ionosphere

It shows that the ionospheric density has a large maximum at approximately 350 – 400 km. Additional to this nominal shape, the ionosphere is subject to the local time (i.e. the sun angle), disturbances, ionospheric storms and the solar cycle. For the simulations in this thesis, a simple model for the ionosphere had to be sufficient. To account for the nominal shape of the ionosphere, the Chapman profile has been approximated by three ionospheric "layers", with linear electron density distribution.

$$TEC_i = a_i \cdot r + b_i \qquad \text{Eq. 5.3-19}$$

with

i = 0 from 50 - 380 km altitude

i = 1 for altitudes between 380 and 1000 km

i = 2 for altitudes between 1000 and 30000 km

This linear approximation has the advantage that the electron content can be integrated piecewise analytically, only as a function of the known starting and end points of the signal path, thus increasing computation speed compared to a numerical integration of the curved profile.

The ionospheric delay is then obtained from

$$\Delta_{IO} = \frac{40.3}{f^2} \cdot TEC \qquad \text{Eq. 5.3-20}$$

whith

TEC Total Electron Content along the signal path

f Frequency

The error of the model has been assumed to be 50%. This value is added to the observation variance.

5.3.3 Tropospheric Model

A radio signal is also subject to tropospheric refraction, causing a delay in the signal reception time, similar to the ionospheric delay, but much less in magnitude. There are several tropospheric models in use. The one utilised in the simulations is the Saastamionen tropospheric model [HWL-94].

$$\Delta_{Tr} = \frac{0.002277}{\cos(\frac{\pi}{2} - \delta)} \cdot (p + (\frac{1255}{T} + 0.05) \cdot e - \tan(\frac{\pi}{2} - \delta)) \qquad \text{Eq. 5.3-21}$$

with

p atmospheric pressure

T Temperature

e Partial pressure of water vapour

δ Elevation

It can be assumed as sufficient to take average values for p and T and e. The residual error has been assumed as 20 % of the result from above equation.

5.3.4 Multipath Simulation

Multipath is not easy to model, but can be assumed as being a more or less slowly varying bias. It was simulated using the function

$$y = e^{A \cdot \sin \omega t} \qquad \text{Eq. 5.3-22}$$

which resembles a multipath figure with a slowly varying geometry. All delays and errors have been added to the measurements as biases.

5.4 Co-ordinate Transformation

In an orbit simulation / orbit determination process a lot of information will be needed in different reference frames. For example, the satellites equations of motion are described in an inertial frame, while the coordinates of a tracking station or user will be given in an earth-centred-earth-fixed frame. Therefore it will be necessary to transform force, velocity and position vectors from one frame to another.

This is done using rotation matrices. To perform a complete transformation from inertial (ECI J-2000) to earth-centred-earth-fixed (ECEF), one has to account for four different effects.

- Precession
- Nutation
- Polar Motion
- Sidereal Time

$$R_{ECI}^{ECEF} = R_{PM} \cdot R_S \cdot R_N \cdot R_{Pr} \qquad \text{Eq. 5.4-1}$$

Note that a matrix multiplication is non commutative, but orthogonal rotation matrices have the following property

$$R^{-1} = R^T \Rightarrow R_{ECEF}^{ECI} = R_{ECI}^{ECEF\,T} \qquad \text{Eq. 5.4-2}$$

i.e. transformation matrix for the backward transformation is simply obtained from the transponed. The following equations are found in [HWL-94] or in the Astronomical Almanac.

5.4.1 Precession

The transformation matrix accounting for precession is given by

$$R_P = \begin{bmatrix} \cos z \cos\vartheta \cos\zeta - \sin z \sin\zeta & -\cos z \cos\vartheta \sin\zeta - \sin z \cos\zeta & -\cos z \sin\vartheta \\ \sin z \cos\vartheta \cos\zeta + \cos z \sin\zeta & -\sin z \cos\vartheta \sin\zeta + \cos z \cos\zeta & -\sin z \sin\vartheta \\ \sin\vartheta \cos\zeta & -\sin\vartheta \sin\zeta & \cos\vartheta \end{bmatrix} \qquad \text{Eq. 5.4-3}$$

where the necessary Euler angles are derived from

$$\begin{aligned} \zeta &= 2306''.2181 \cdot T + 0''.30188 \cdot T^2 + 0''.017998 \cdot T^3 \\ z &= 2306''.2181 \cdot T + 1''.09468 \cdot T^2 + 0''.018203 \cdot T^3 \\ \vartheta &= 2004''.3109 \cdot T - 0''.42665 \cdot T^2 - 0''.041833 \cdot T^3 \end{aligned} \qquad \text{Eq. 5.4-4}$$

T is the time interval between the observation date and the J2000.0 standard epoch, expressed in Julian centuries. One Julian century has 36525 days. Note that the transformation angles ζ,ϑ,z are given in arc seconds. They have to be scaled radians prior to further use in equation 5.4-3.

5.4.2 Nutation

The nutation matrix is given by

$$R_N = \begin{bmatrix} 1 & -\Delta\psi\cos\varepsilon & -\Delta\psi\sin\varepsilon \\ \Delta\psi\cos\varepsilon & 1 & -\Delta\varepsilon \\ \Delta\psi\sin\varepsilon & \Delta\varepsilon & 1 \end{bmatrix} \qquad \text{Eq. 5.4-5}$$

with the mean obliquity of the rotation axis given by

$$\varepsilon = 23°26'21".448 - 46".8150 \cdot T - 0".00059 \cdot T^2 + 0".001813 \cdot T^3 \qquad \text{Eq. 5.4-6}$$

where

T Time interval between the observation epoch and the J2000.0 standard epoch

$\Delta\psi$ Nutation parameter in longitude

$\Delta\varepsilon$ Nutation parameter in obliquity

The nutation parameters $\Delta\psi$ and $\Delta\varepsilon$ can be obtained from a series expansion, which can be found in [ITN-96]. A drawback the series expansion method is that a lot of trigonometric functions have to be evaluated, causing a high computation load. Fortunately, the nutation parameters are available as pre-computed values in the JPL DE200 ephemeris files.

5.4.3 Polar Motion

The transformation matrix accounting for polar motion can be expressed by

$$R_N = \begin{bmatrix} 1 & 0 & x_P \\ 0 & 1 & -y_P \\ -x_P & y_P & 1 \end{bmatrix} \qquad \text{Eq. 5.4-7}$$

The values for co-ordinates of the earth pole are available from the IERS (International Earth Rotation Service), either as predicted values in the Bulletin A, or as post processed values in the Bulletin B. In precise orbit determination, these parameters are estimated, using IERS Bulletin A as predicted values.

5.4.4 Earth Rotation (Hour Angle)

While the time derived from earth's revolution is defined from one midday to the next and indicated as Universal Time (UT), earth's rotation with respect to an inertial frame is obtained from the sidereal time. The so called hour angle is related to UT1, that is UT corrected for polar motion, by

$$\Theta_0 = 1.0027379093 \cdot UT1 + \vartheta_0 + \Delta\psi\cos\varepsilon \qquad \text{Eq. 5.4-8}$$

The first term accounts for the scale factor between synodal and sidereal rotation period. The second term represents the actual sidereal time at the Greenwich meridian and is computed using the following formulation

$$\vartheta_0 = 24110.54841 + 8640184.812866 \cdot T_0 + 0.093104 \cdot T_0^2 - 6.2 \cdot 10^{-6} \cdot T_0^3 \qquad \text{Eq. 5.4-9}$$

where ϑ_0 is in seconds. T_0 is the interval between the standard epoch of J2000 and date of observation at 0^h UT.

The third term accounts for nutation. While UT1 is a continuos time scale, coupled with earth's rotation, Universal Time Coordinated (UTC) is a realisation of UT1 using atomic clocks. The relationship between UT1 and UTC is expressed by

$$UT1 = UTC + dUT1 \qquad \text{Eq. 5.4-10}$$

The quantity dUT1 has an absolute value of less than 1 second and is determined by the IERS. If dUT1 gets larger than 0.9 seconds, a leap second is added to UTC.

5.5 Broadcast Ephemeris

The broadcast ephemeris of a satellite is not obtained directly from the observations, but adjusted to the position vectors within a specified interval, i.e. the period of validity. The position vectors have been derived by propagating the satellites state from a known state forward. This "known state" can be a deterministic initial state, if it is derived from simulation, or the best estimate at a certain time, derived from measurements. The latter would be the case in an operational satellite navigation system.

5.5.1 Adjustment of the Broadcast Message

The broadcast message has to be adjusted to the precise ephemeris, determined and predicted by the orbit estimation process. The "observations" used to feed the adjustment process, are a time series of precise ephemeris position vectors. Figure 5-7 shows the basic adjustment process.

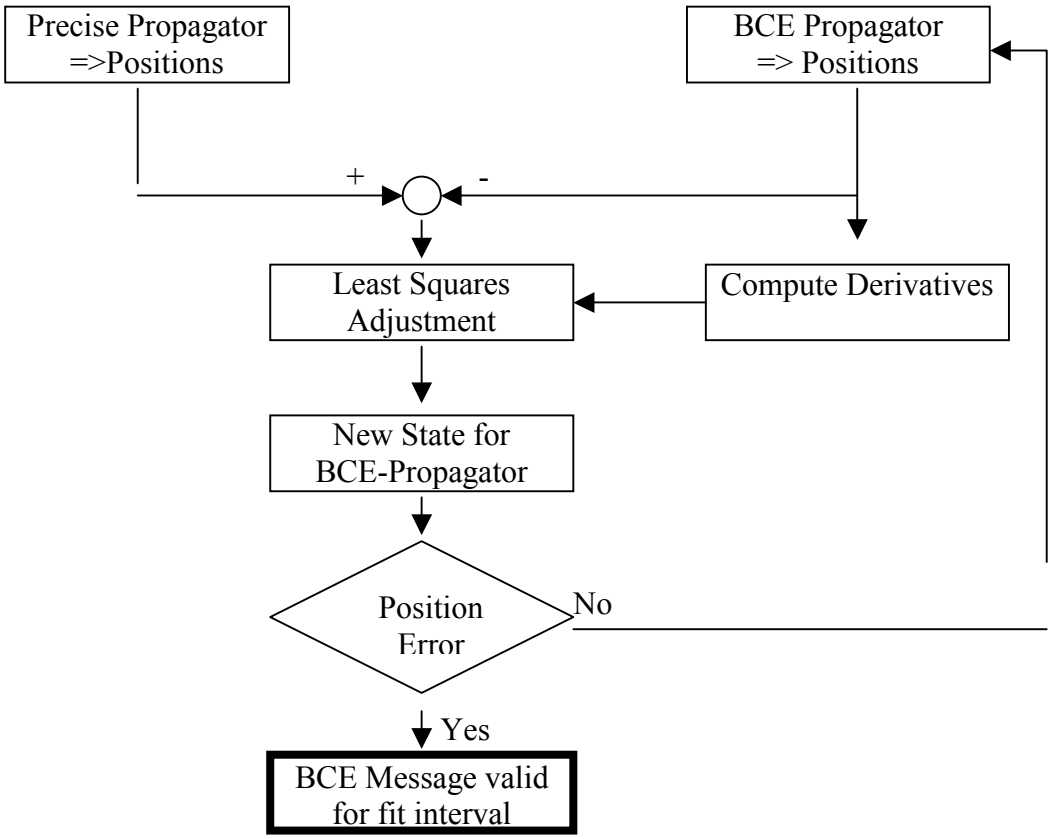

Figure 5-7 Broadcast Message Adjustment

5.5.2 Ephemeris Contribution to URE

In a satellite navigation application, an important quantity is the range error, which the user will experience. While the user range error (URE) is composed of many contributors, here only the ephemeris contribution will be addressed. The contribution of the (broadcast) ephemeris it self can be divided into three sub-contributors:

- orbit determination error
- orbit propagation error
- broadcast model fit error

The RMS error of the broadcast ephemeris is component-wise computed using the following equations.

$$\sigma_{radial} = \sqrt{\frac{\sum_{n} \left(\left(\overline{x}_{Broadcast} - \overline{x}_{True} \right) \cdot \overline{e}_{radial} \right)^2}{n}} \qquad \text{Eq. 5.5-1}$$

$$\sigma_{along} = \sqrt{\frac{\sum_{n} \left(\left(\overline{x}_{Broadcast} - \overline{x}_{True} \right) \cdot \overline{e}_{along} \right)^2}{n}}$$

$$\sigma_{cross} = \sqrt{\frac{\sum_{n} \left(\left(\overline{x}_{Broadcast} - \overline{x}_{True} \right) \cdot \overline{e}_{cross} \right)^2}{n}}$$

with

e_{radial} Unit vector in radial direction

e_{along} Unit vector in along track direction

e_{cross} Unit vector in cross track direction

Using these error components, the URE can be computed under the (justified) assumption that the worst URE is obtained from a satellite at nearly zero elevation.

$$URE = \sqrt{\sigma_{radial}^2 \cdot \cos\alpha + \left(\sigma_{along}^2 + \sigma_{cross}^2 \right) \cdot \sin\alpha} \qquad \text{Eq. 5.5-2}$$

where

α Angle between the satellites radius vector and the local horizontal plane of an observer, which is <u>not</u> the elevation.

5.6 Autonomous Integrity Monitoring

Another feature of the software package is the simulation of an onboard processor, using onboard measurements from ground links and inter satellite links to evaluate the integrity of its ephemeris and clock states. One investigated approach utilises a RAIM (Receiver Autonomous Integrity Monitoring) algorithm. RAIM algorithms are well known in the GPS user (receiver) domain. They basically work on the sample variance of the observation residuals, as well as on the observation matrix, containing the unit vectors of the line-of-sights and measurement variances. The following figure shows the flow chart of the integrity monitoring.

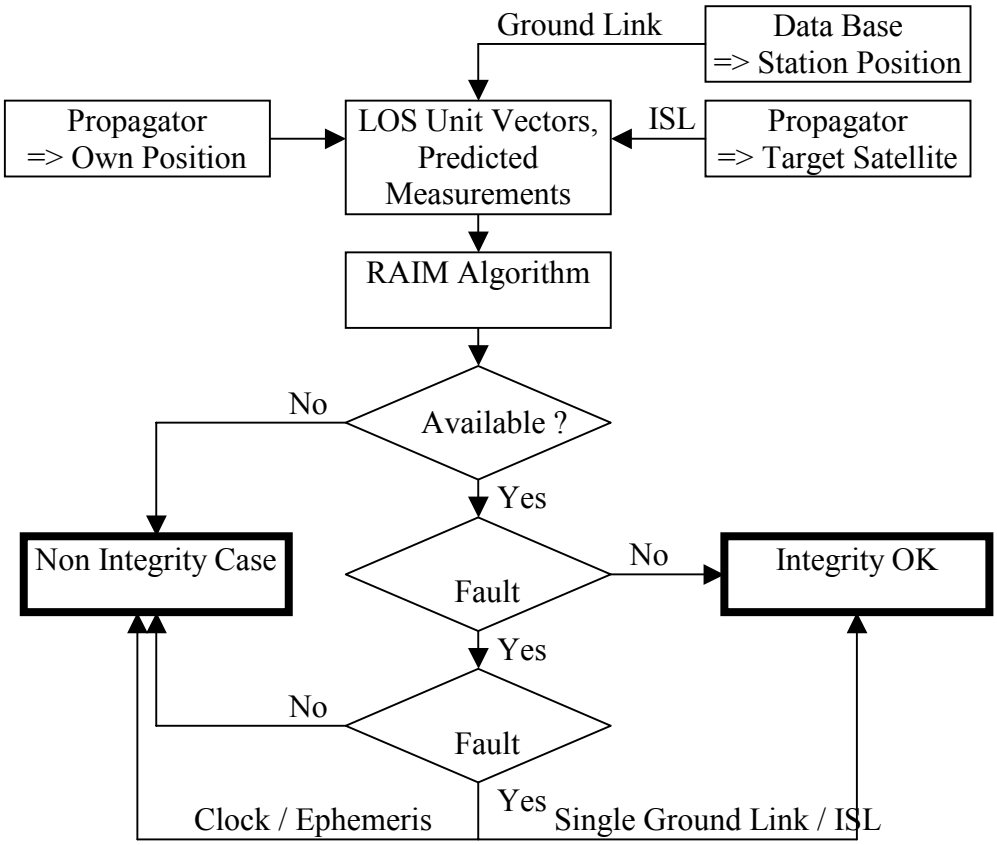

Figure 5-8 Integrity Processing Check

Most RAIM algorithms check the sample variance against a protection level, computed from the observation matrix. If the protection level is exceeded, one measurement after the other is removed, and the check is repeated with n-1 observations. Therefore a faulty measurement can be isolated, if there is enough redundancy in the measurements.

The mathematical formulation of the fault detection (FD) / and isolation (FDI) problem for satellite based integrity monitoring is generally given as follows. If it is assumed that no more

than one error has occurred and if at a given point of time *m* (*m* > 4 for FD and *m* > 5 for FDI) range type measurements are available, then linearization yields the linear model

$$\mathbf{y} = \mathbf{G}\mathbf{x} + \boldsymbol{\varepsilon} \qquad \text{Eq. 5.6-1}$$

But what, if no measurement is faulty but the ephemeris or clock state? To allow the isolation of the satellites own faulty clock or ephemeris, these parameters are introduced as pseudo observations and the above equation replaced by

$$\mathbf{y}^* = \mathbf{G}^* \cdot \mathbf{x} + \boldsymbol{\varepsilon}^* \qquad \text{Eq. 5.6-2}$$

with

$$\mathbf{y}^* = \begin{pmatrix} 0 \\ 0 \\ 0 \\ 0 \\ \mathbf{y}_M \end{pmatrix}, \ \mathbf{G}^* = \begin{pmatrix} \mathbf{e}_R^T & 0 \\ \mathbf{e}_{AT}^T & 0 \\ \mathbf{e}_{CT}^T & 0 \\ \mathbf{0}^T & 1 \\ \mathbf{G} & \mathbf{g} \end{pmatrix} \text{ and } \boldsymbol{\varepsilon}^* = \begin{pmatrix} \varepsilon_R \\ \varepsilon_{AT} \\ \varepsilon_{CT} \\ \varepsilon_C \\ \boldsymbol{\varepsilon}_M \end{pmatrix} \qquad \text{Eq. 5.6-3}$$

and

$\mathbf{e}_R^T, \mathbf{e}_{AT}^T, \mathbf{e}_{CT}^T$ unit vector in radial, along track and cross track direction

The residuals are given as zero, i.e. "no ephemeris fault" and "no clock fault". The RAIM algorithm is now capable of removing the bad assumption of "no radial error" for example, if the removal of this row in the system of observation equations minimises the sample variance of residuals.

A major draw back of that kind of snapshot algorithm based on the sample variance is the need for a sophisticated pre-processing of the raw data. The sample variance taken from the raw measurements is still too noisy, thus leading to lots of false alarms.

Another possible way of monitoring the integrity of a satellites position and clock is by separating satellite dynamics / errors / and observation noise by their dynamic behaviour. This can be achieved using the Kalman filter with the following state vector

$$\bar{x} = \begin{bmatrix} \Delta x \\ \Delta y \\ \Delta z \\ \Delta T \\ \Delta \dot{x} \\ \Delta \dot{y} \\ \Delta \dot{z} \\ \Delta \dot{T} \end{bmatrix} \qquad \text{Eq. 5.6-4}$$

which is kept very adaptive by adding high process noise. The Kalman filter is then inert with respect to noise, but reacts immediately on real errors. The dynamic model which has been

implemented and used successfully assumes the errors in x-y-z direction (ECEF reference frame) as well as the satellite clock to be composed of a step and a ramp, expressed by to the following transition matrix:

$$\Phi = \begin{bmatrix} 1 & 0 & 0 & 0 & 1 & 0 & 0 & 0 \\ 0 & 1 & 0 & 0 & 0 & 1 & 0 & 0 \\ 0 & 0 & 1 & 0 & 0 & 0 & 1 & 0 \\ 0 & 0 & 0 & 1 & 0 & 0 & 0 & 1 \\ 0 & 0 & 0 & 0 & 1 & 0 & 0 & 0 \\ 0 & 0 & 0 & 0 & 0 & 1 & 0 & 0 \\ 0 & 0 & 0 & 0 & 0 & 0 & 1 & 0 \\ 0 & 0 & 0 & 0 & 0 & 0 & 0 & 1 \end{bmatrix}$$

The observation matrix is given by

$$H = \begin{bmatrix} 1 & 0 & 0 & 0 & 0 & 0 & 0 & 0 \\ 0 & 1 & 0 & 0 & 0 & 0 & 0 & 0 \\ 0 & 0 & 1 & 0 & 0 & 0 & 0 & 0 \\ 0 & 0 & 0 & 1 & 0 & 0 & 0 & 0 \end{bmatrix}$$

Note that this dynamic system is very close to the one used to estimate the orbit corrections, but much less smoothing character. Moreover, the same filter tuning cannot be used for integrity monitoring and orbit estimation. This approach is more suited for onboard processing and therefore elaborated in more detail in chapter 7.

6 SIMULATION AND RESULTS

Several simulations have been performed to assess the achievable orbit determination accuracy, varying in

- Types of orbits and constellation
- Ground network
- Observation types, i.e. ground based only or ground and intersatellite links.

This chapter gives an overview of the analysed scenarios, as well as the results.

6.1 Constellations, Ground Networks and Simulation Scenarios

6.1.1 Constellations

Most of the constellation are so called Walker constellations, characterised by three numbers

T/P/F

where T Total number of satellites

P Number of orbit planes

F Factor of pattern unit (PU = 360°/T), to obtain phase difference between satellites on adjacent orbit planes

The following equations hold two obtain the orbital parameters for each satellite.

Satellite spacing: $\frac{360°}{T} \cdot P$

Orbit plane spacing: $\frac{360°}{P}$

Phase difference between adjacent planes: $\frac{360°}{T} \cdot F$

The phase difference has to be interpreted the following way: Assuming a phase difference of 30 ° and a satellite on one orbit plane is passing his ascending node (i.e. mean anomaly = 0°), the next satellite on the right hand adjacent plane is already ahead in mean anomaly by 30°.

Theses Walker constellations are a good starting point for constellation analysis, because they provide reasonable earth coverage with direct computable satellite orbit parameters. Note that these constellations are reasonable, but not optimal for satellite navigation systems. Walker constellation have one inherent draw back, due to their symmetry. An optimised constellation, like the today's GPS constellation has more or less evolved from a 24/6/1 Walker constellation, but the satellites and orbit planes are not evenly spaced anymore.

6.1.1.1 Optimized GPS Constellation

The GPS constellation as been analysed to obtain a reference for possible GNSS 2 constellations. The following picture shows the ground tracks, as well as the locations of the 5 monitoring stations of the OCS.

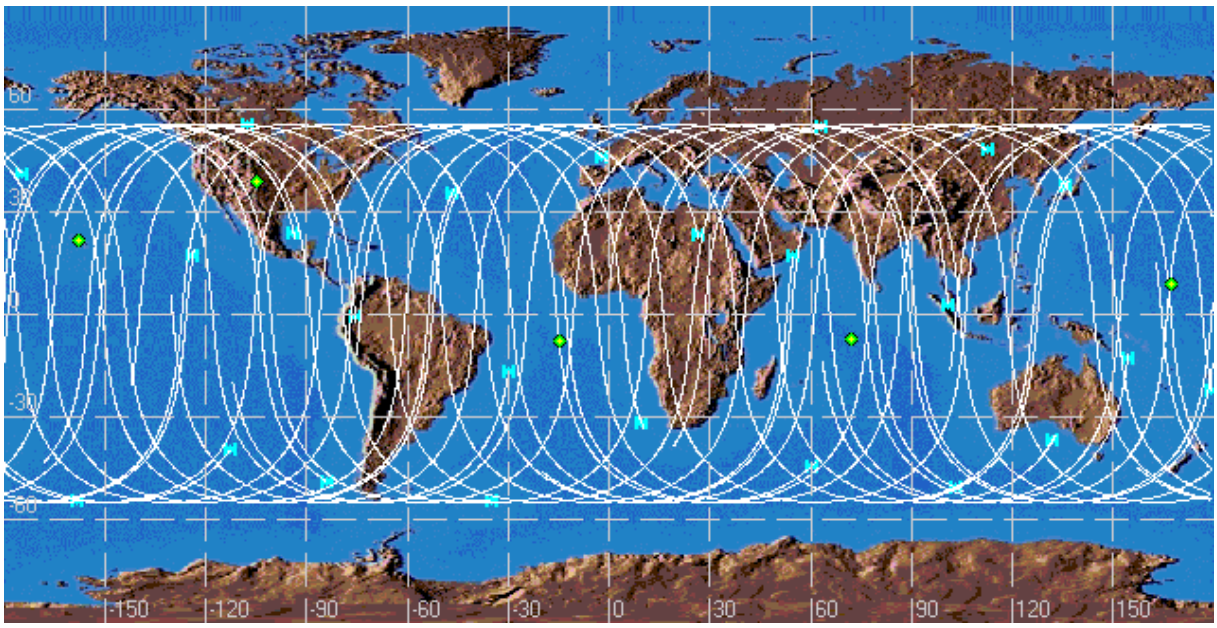

Figure 6-1 Ground Tracks of Optimized GPS constellation

The next picture shows the minimum visibility, i.e. number of simultaneous satellites over a period of 24 hours. It can be seen, that the minimum required number of 4 satellites is assured world wide. The following table shows the orbital parameters of the space vehicles. These have been take from [MOPS-98]. The satellite slots and the orbital planes are not evenly spaced, as would be in Walker constellation.

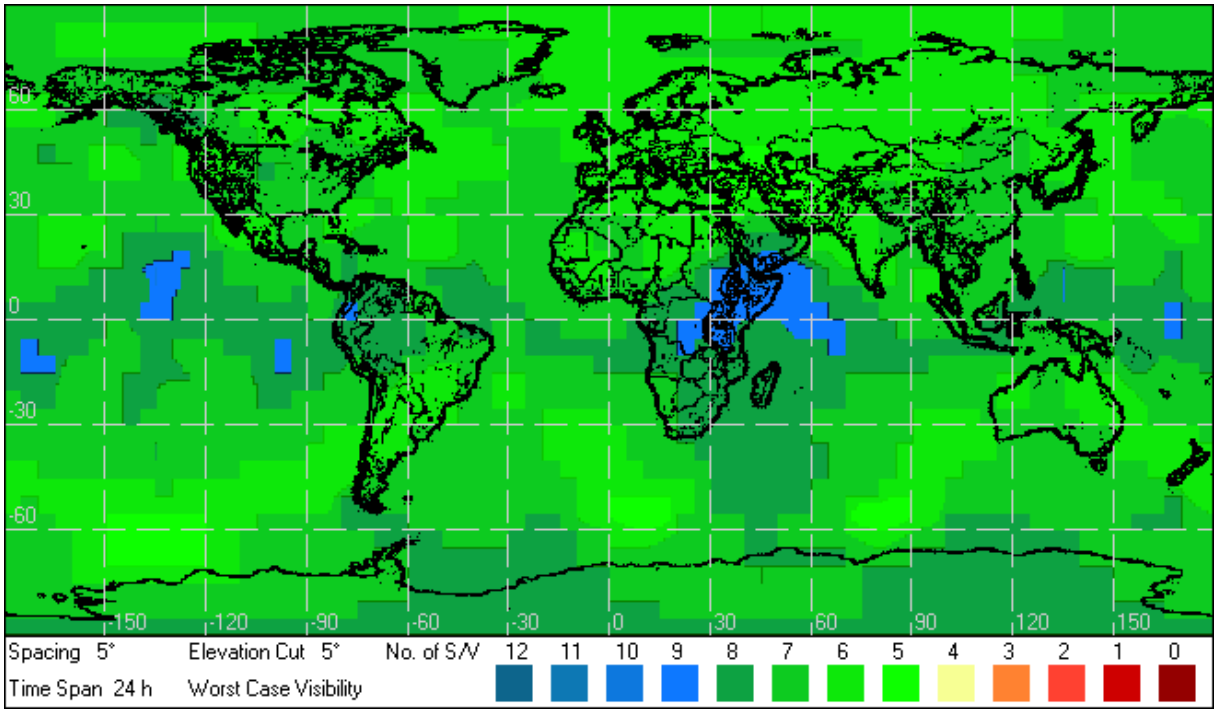

Figure 6-2 Visibility of Optimized GPS Constellation over 24 h

S/V	$T_{reference}$	a	ε	i	Ω	ω	φ
1	1. July 1993 00:00:00	26560 km	0	55	272.85	0	268.13
2	1. July 1993 00:00:00	26560 km	0	55	272.85	0	161.79
3	1. July 1993 00:00:00	26560 km	0	55	272.85	0	11.68
4	1. July 1993 00:00:00	26560 km	0	55	272.85	0	41.81
5	1. July 1993 00:00:00	26560 km	0	55	332.85	0	80.96
6	1. July 1993 00:00:00	26560 km	0	55	332.85	0	173.34
7	1. July 1993 00:00:00	26560 km	0	55	332.85	0	309.98
8	1. July 1993 00:00:00	26560 km	0	55	332.85	0	204.38
9	1. July 1993 00:00:00	26560 km	0	55	32.85	0	111.88
10	1. July 1993 00:00:00	26560 km	0	55	32.85	0	11.80
11	1. July 1993 00:00:00	26560 km	0	55	32.85	0	339.67
12	1. July 1993 00:00:00	26560 km	0	55	32.85	0	241.56
13	1. July 1993 00:00:00	26560 km	0	55	92.85	0	135.23
14	1. July 1993 00:00:00	26560 km	0	55	92.85	0	265.45
15	1. July 1993 00:00:00	26560 km	0	55	92.85	0	35.16
16	1. July 1993 00:00:00	26560 km	0	55	92.85	0	167.36
17	1. July 1993 00:00:00	26560 km	0	55	152.85	0	197.05
18	1. July 1993 00:00:00	26560 km	0	55	152.85	0	302.60
19	1. July 1993 00:00:00	26560 km	0	55	152.85	0	333.69
20	1. July 1993 00:00:00	26560 km	0	55	152.85	0	66.07
21	1. July 1993 00:00:00	26560 km	0	55	212.85	0	238.89
22	1. July 1993 00:00:00	26560 km	0	55	212.85	0	345.23
23	1. July 1993 00:00:00	26560 km	0	55	212.85	0	105.21
24	1. July 1993 00:00:00	26560 km	0	55	212.85	0	135.35

Table 6-1 Optimized GPS Constellation

6.1.1.2 IGSO Walker Constellation

The next analysed constellation is a 18 / 6 / 2 Walker constellation with 55 ° inclination. This means

- 18 satellites total in the constellation
- 6 orbital planes, with the ascending nodes spaced by 60°
- 3 satellites per plane, spaced in mean anomaly by 120°
- The phase difference adjacent planes is 40°

The orbit altitude is fixed by selecting the orbit class IGSO, which means Inclined Geo-Synchronous Orbit. Due to their orbital period of 23 hours 56 minutes (sidereal day), they are synchronised with earth's rotation rate. At their ascending node, they cross the equator at the same point every time, leading to the characteristic "8 shape" of the ground track.

A special case of this orbit class is the Geo Stationary Orbit (GEO) which remains as a fixed point with respect to an earth fixed reference frame. The following picture shows the ground tracks, as well as the ground station locations of a " custom global network" used in this scenario.

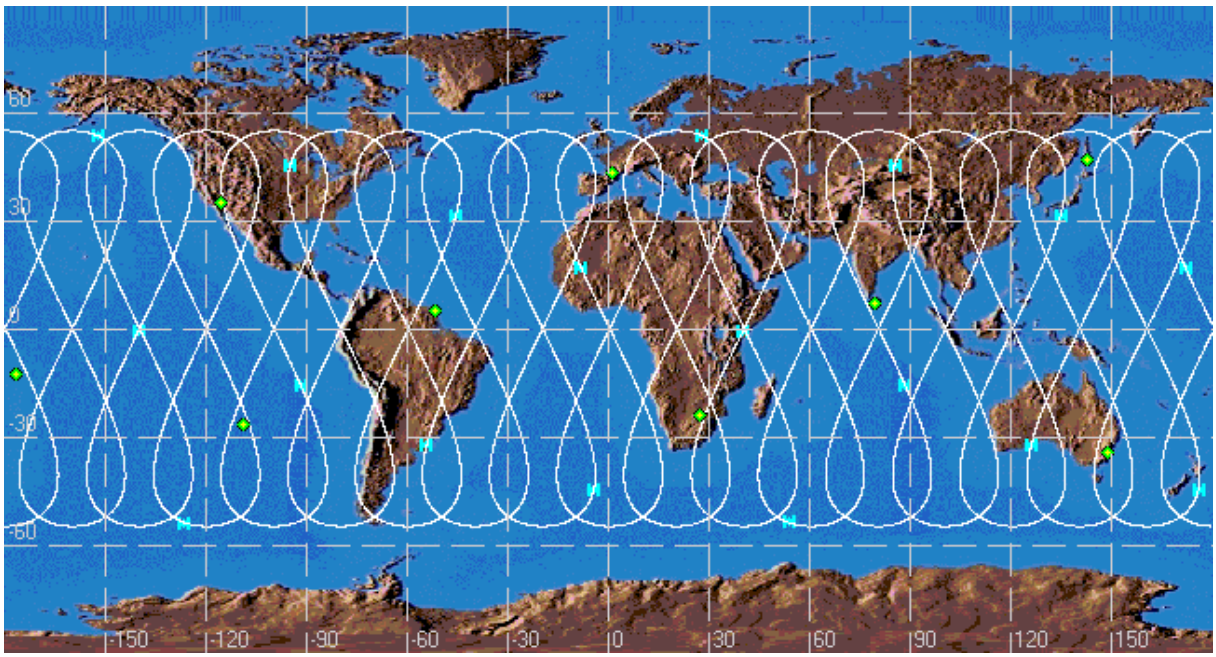

Figure 6-3 Ground Tracks of IGSO Walker Constellation

The following picture shows the minimum visibility of this constellation over a period of 24 hours. Although only 18 satellites are present in this constellation, it provides a good coverage. There are always more than 4 satellites visible.

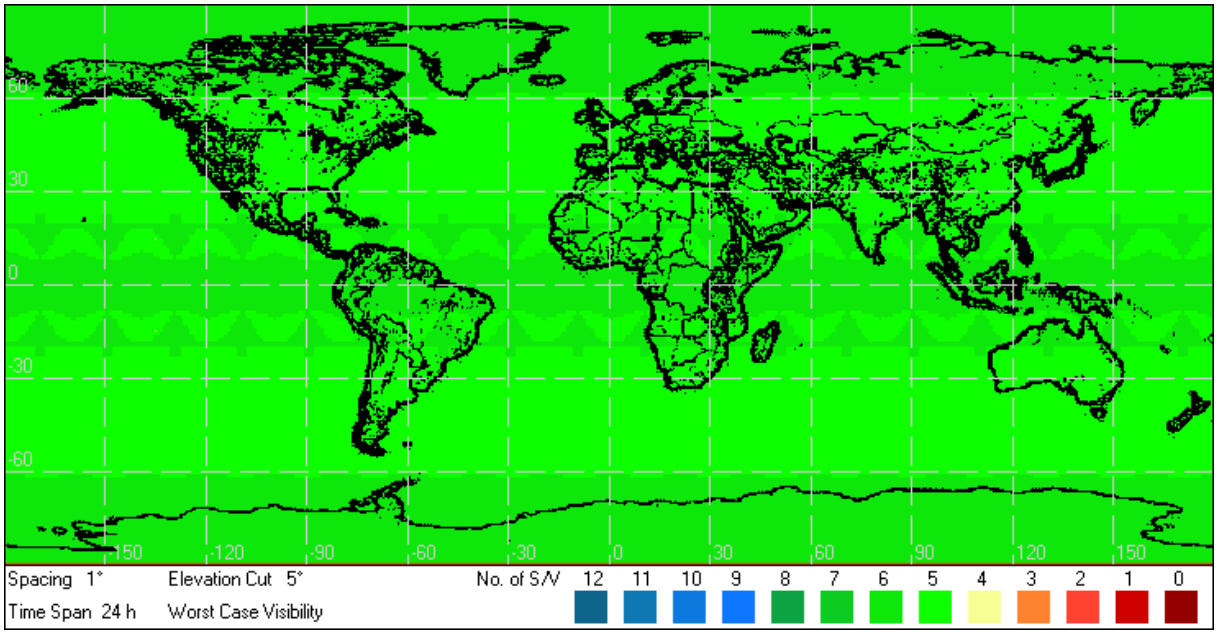

Figure 6-4 Visibility of IGSO Walker Constellation

6.1.1.3 IGSO on three Loops

Another constellation which ahs been favoured by the ESA as a possible constellation for GNSS 2 is the following one: 18 satellites are placed on orbital planes that way, that the longitude of their ascending nodes (not right ascension) are located at 10°E / 110°W / 130°E over the equator. IGSO's share the same ground tracks, is the spacing of their orbit planes is equal to their spacing in mean anomaly.

6 space crafts orbit on 3 loops over Japan, Europe / Africa and North America / South Pacific. The inclination is 70°. The following picture shows the satellites on their common ground tracks. The ground track locations shown are that of the custom global network.

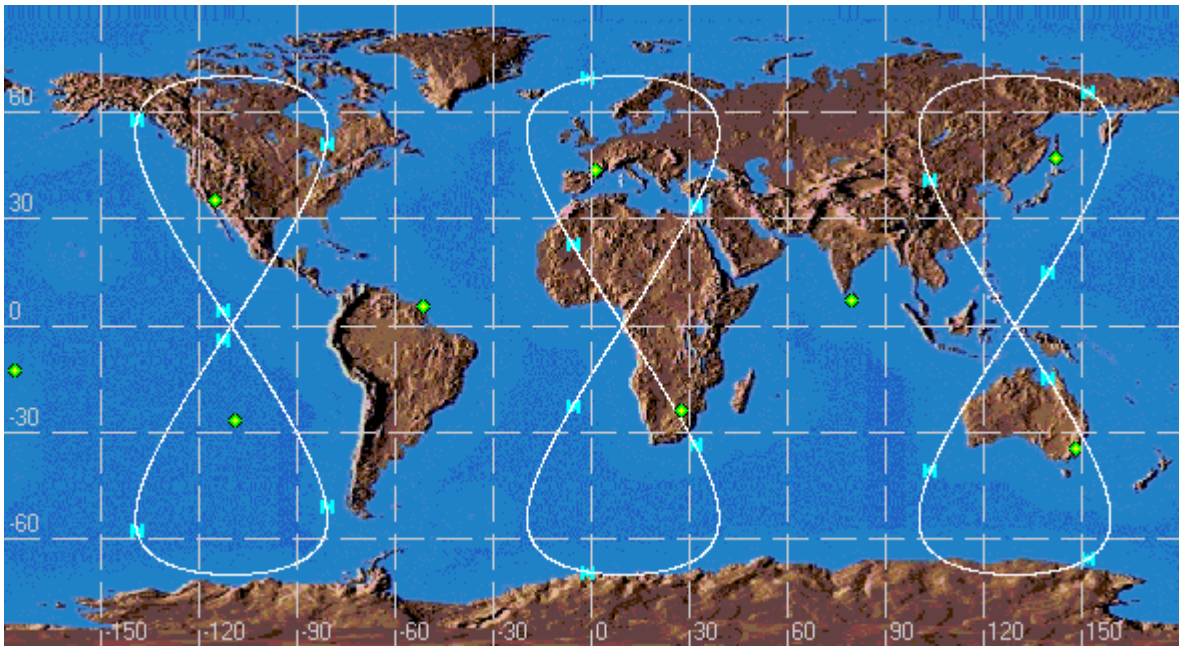

Figure 6-5 Ground Tracks of IGSO Constellation "on three Loops"

This constellation also provides a reasonable coverage, as can be seen in the following picture. A visibility of five or more S/C is ensured globally.

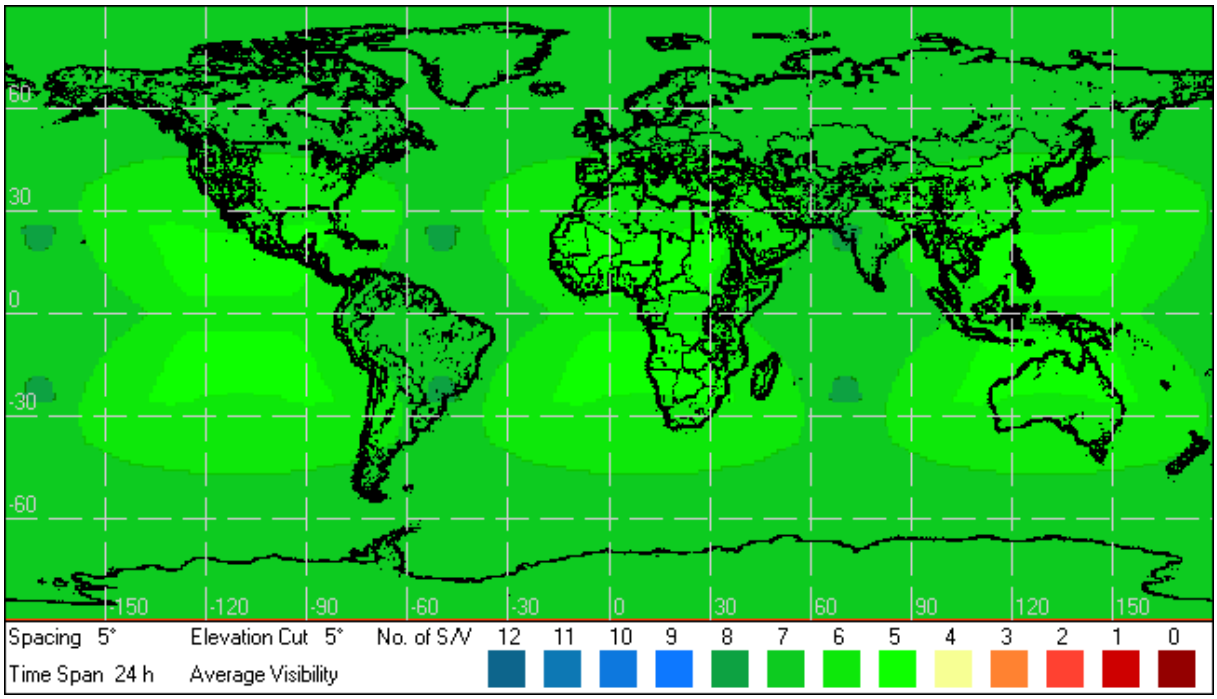

Figure 6-6 Visibility of IGSO Constellation "on three Loops"

6.1.1.4 GEO / IGSO

The next constellation is a mixed one. It consists of

- 9 / 3 / 1 Walker Constellation of IGSO's with Longitude of ascending nodes at 10° E / 130° E / 110°W
- 9 GEO's, longitude of ascending nodes evenly separated by 40° beginning at 30° E.

The following two picture show the ground tracks and the minimum visibility over a period of 24 hours.

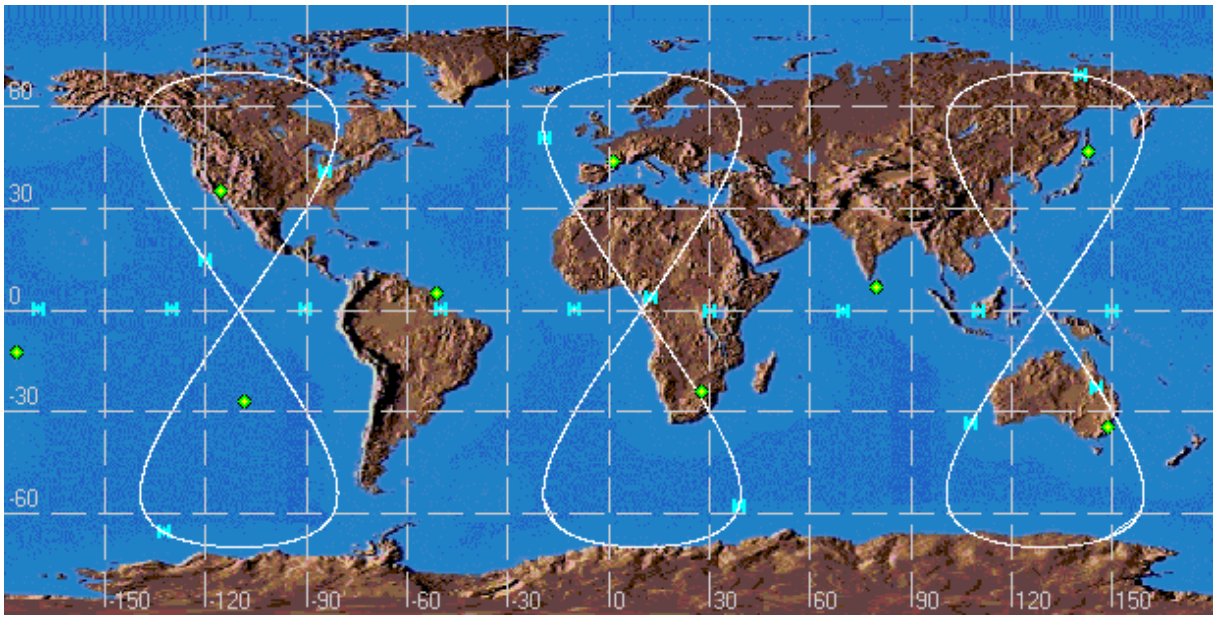

Figure 6-7 Ground Tracks of GEO - IGSO Constellation

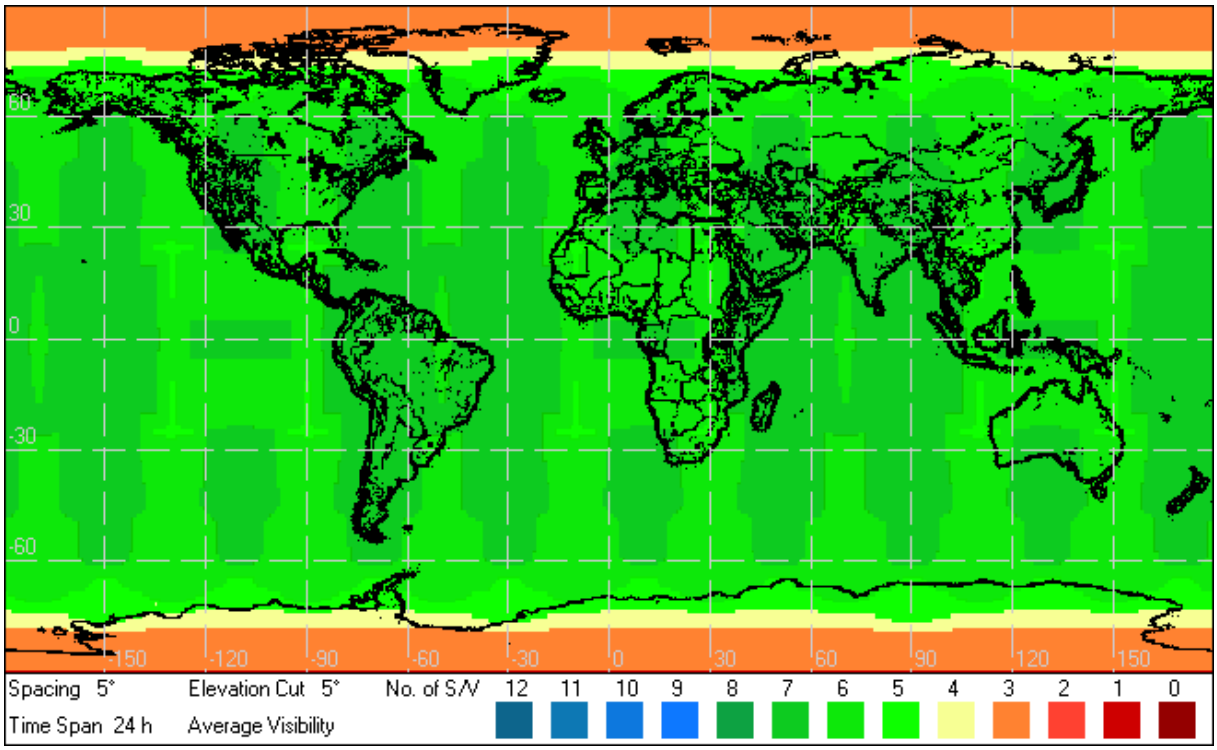

Figure 6-8 Visibility of GEO – IGSO Constellation

The GEO's are not visible ate very high latitude, therefore the coverage at the poles is insufficient for navigation purposes. Besides that fact of latitude restriction, the coverage over the equator and mid latitudes is reasonable.

6.1.1.5 Pure LEO Constellation

The next constellation is a pure 1250 km LEO constellation, with a total of 81 S/V at 9 orbit planes with 1 pattern unit phase difference between adjacent planes. All orbit planes have a 55° inclination. The following picture shows the ground tracks of the satellites, as well as the locations of the DORIS network.

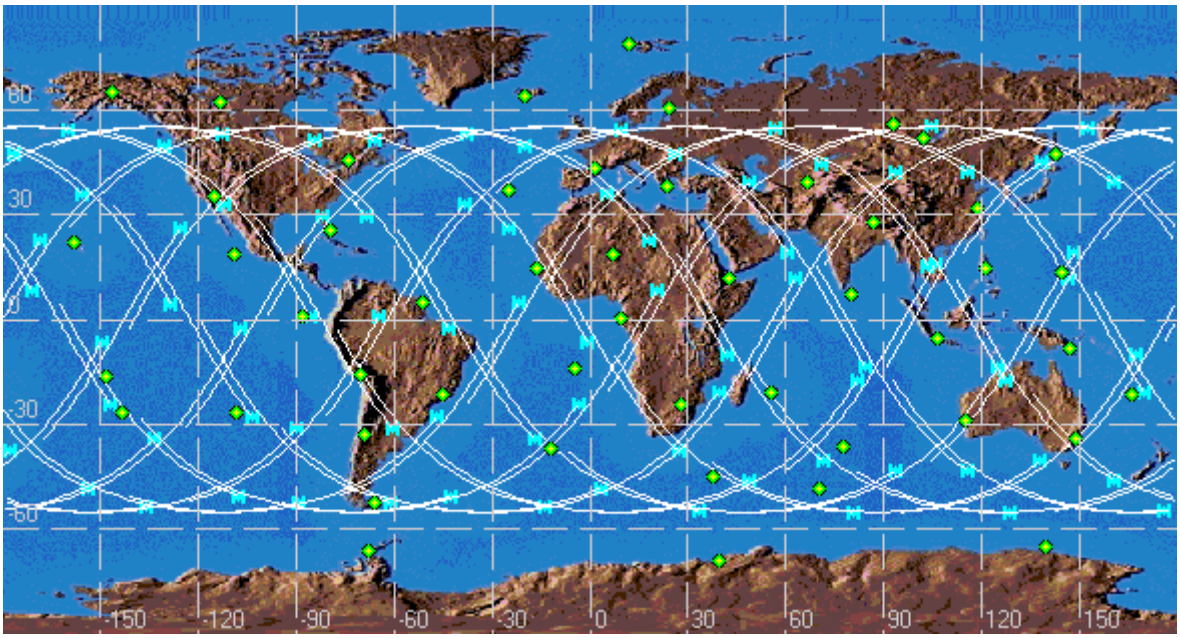

Figure 6-9 Ground Tracks of LEO Constellation

The next picture shows the earth coverage of such a constellation. Due to the low orbit altitude navigation service can be provided only up to ~ 65 ° North / South.

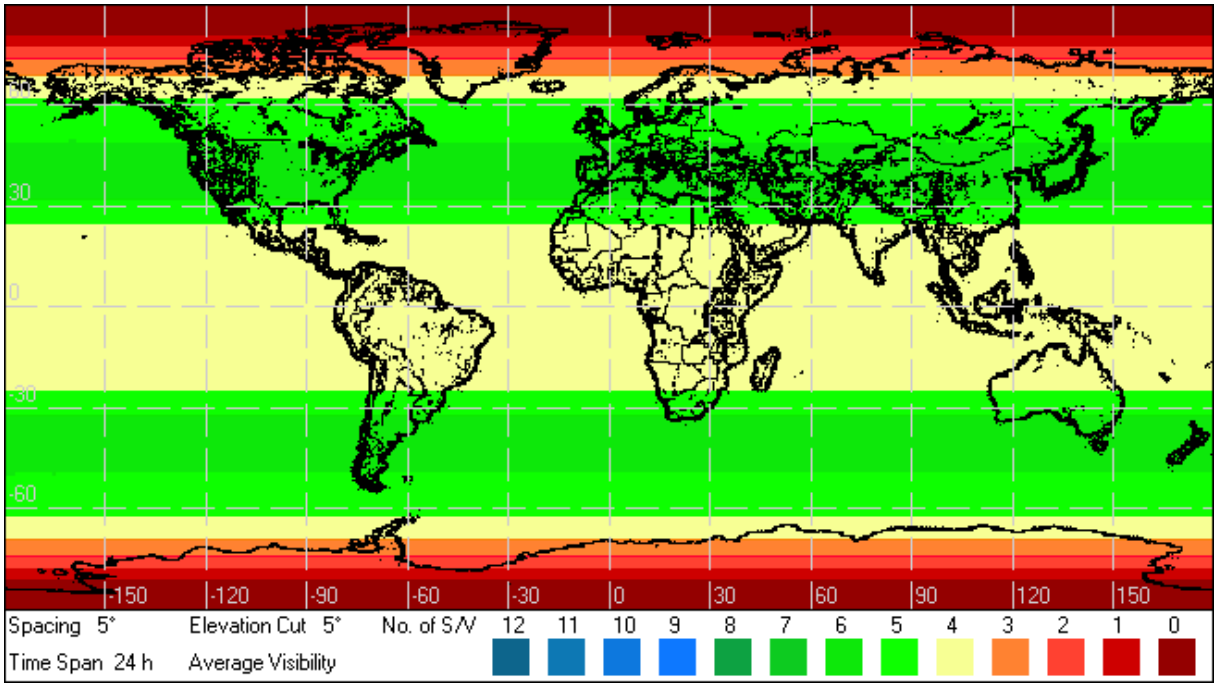

Figure 6-10 Visibility of LEO Constellation

It is clear that building a navigation constellation using satellites at low Earth orbits would require a large number of space crafts. This constellation here with 81 space vehicles can be regarded as the minimum.

6.1.1.6 GEO / LEO

To overcome the bad global coverage of a pure LEO constellation, the next constellation introduces some high altitude satellites in addition to the LEOs. The LEO part is a 72 / 8 / 2 Walker constellation with an orbit altitude of 1250 km and 55° inclination. In addition, there are 9 GEOs, evenly spaced by 40 °, starting at 10°E. The following picture shows ground tracks and S/V positions, as well as the station locations of the DORIS network.

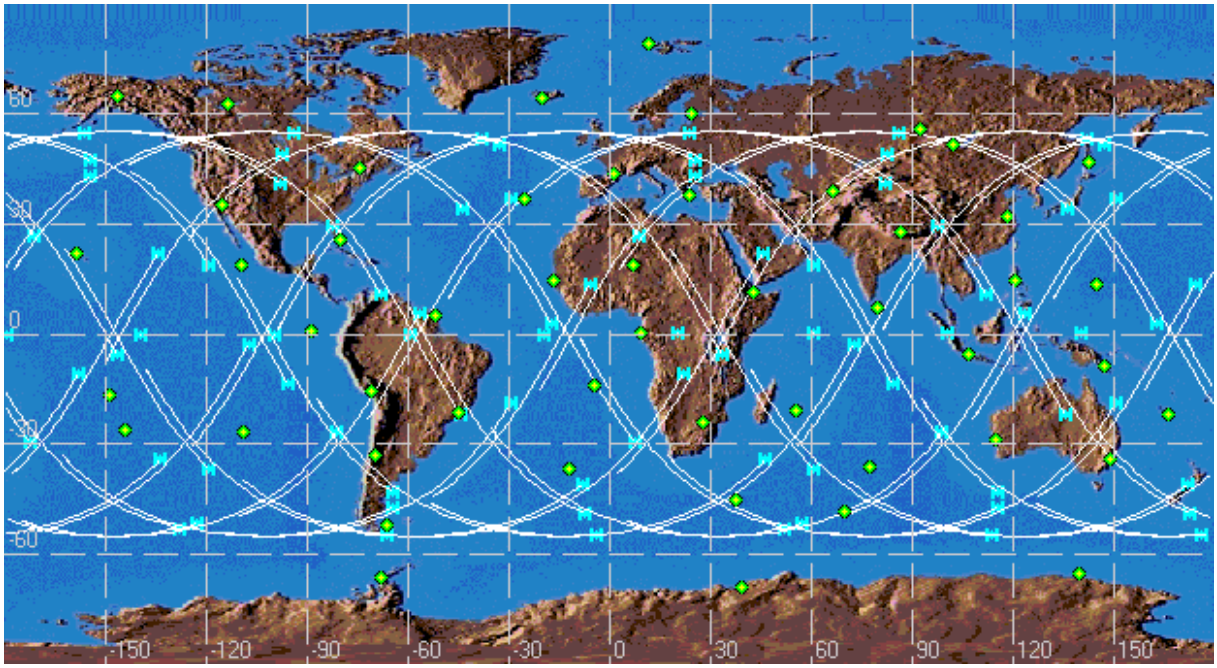

Figure 6-11 Ground Tracks of LEO Constellation

The coverage of such a constellation is much better than that of the pure LEO constellation, due to widely visible GEOs. Nevertheless, the pole regions are also uncovered, because the GEO have a 0° inclination.

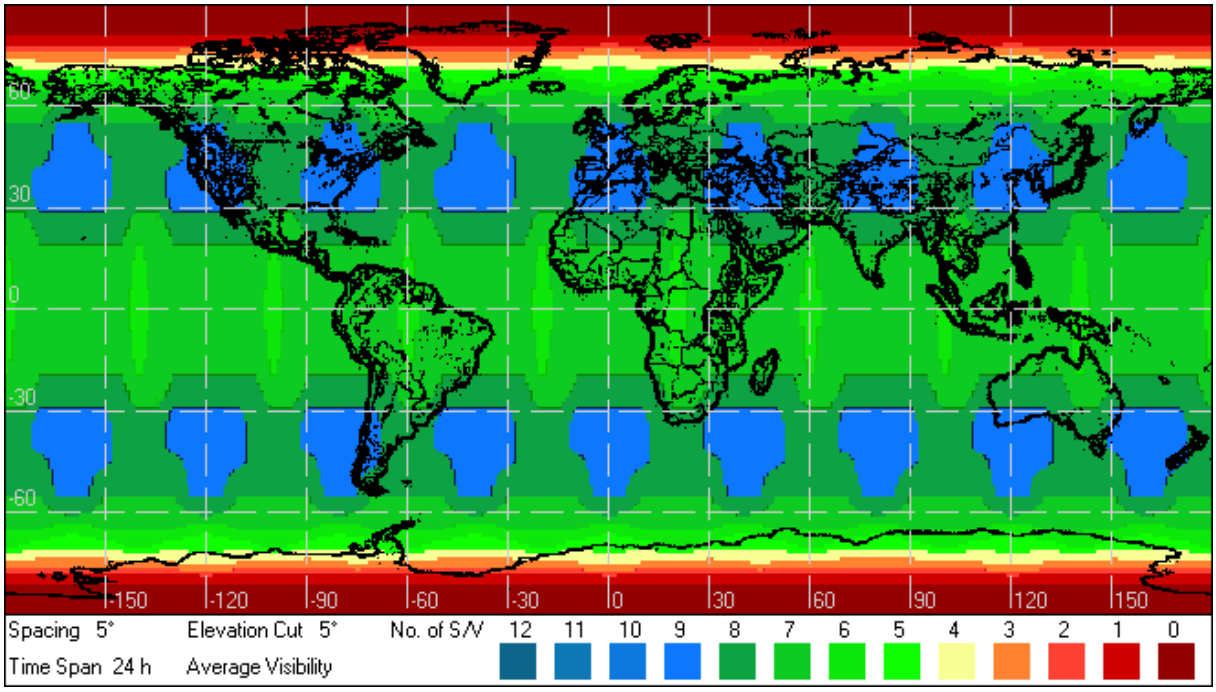

Figure 6-12 Visibility of LEO – GEO Constellation

6.1.1.7 Galileo 1 (Pure MEO)

The future GNSS 2, as planned by ESA, is named Galileo. As far as the orbits are concerned, two options have been chosen, both medium altitude earth orbits (MEO) with a orbit period around 12 hours. This is very similar to both existing satellite navigation systems, GPS and GLONASS.

The first option is a pure MEO 33 / 3 / 1 Walker constellation with an inclination of 50.2° and an orbit altitude of 23983 km. The orbital period is approximately 14 hours. The following picture shows the ground track and S/V positions, as well as the station locations of the proposed ground network.

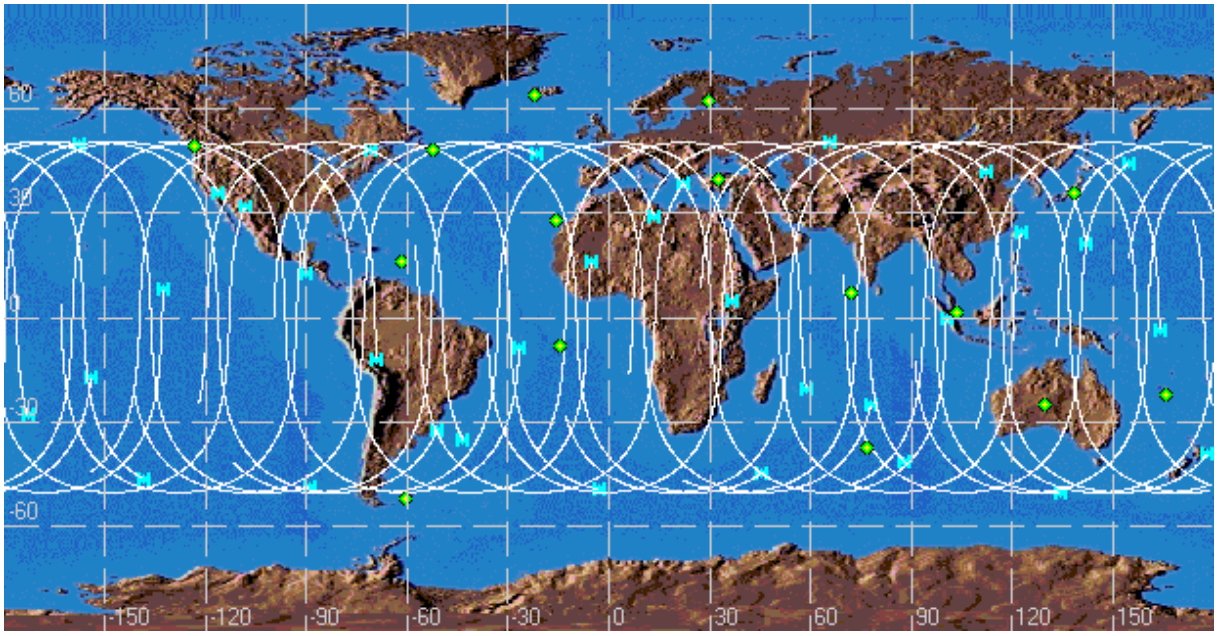

Figure 6-13 Ground Tracks of Galileo Option 1 Constellation

The next picture shows the earth coverage of that constellation, which is very good. Very often more 10S/V or more are visible at the same time. This no surprise, taking into account the relative large number of satellites at high orbit altitude.

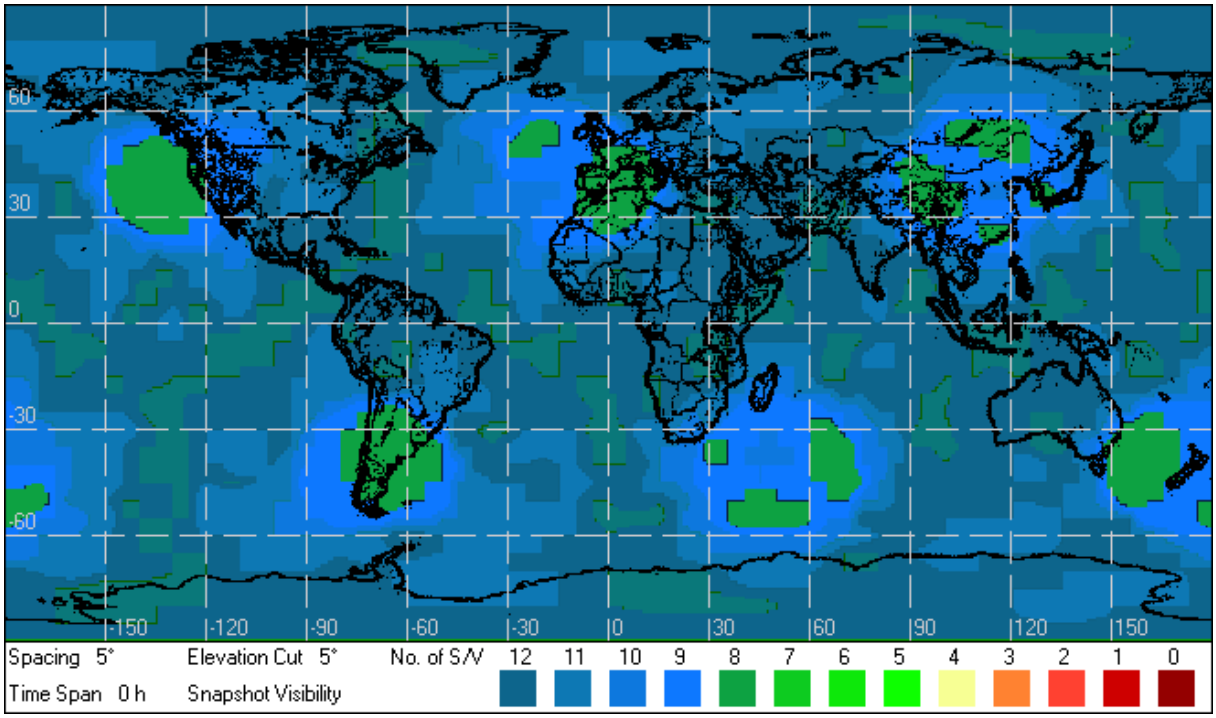

Figure 6-14 Visibility of Galileo Option 1 Constellation

6.1.1.8 Galileo 2 (GEO/MEO)

The second option for Galileo is a mixed constellation, consisting of a MEO 27/3/1 Walker constellation and three GEO. The MEOs have an inclination of 56° and an orbit altitude of 19424 km, the GEOs are located at 10°W, 10°E and 30°E. The following picture shows the ground tracks and S/V positions, as well as the station locations of the proposed ground network.

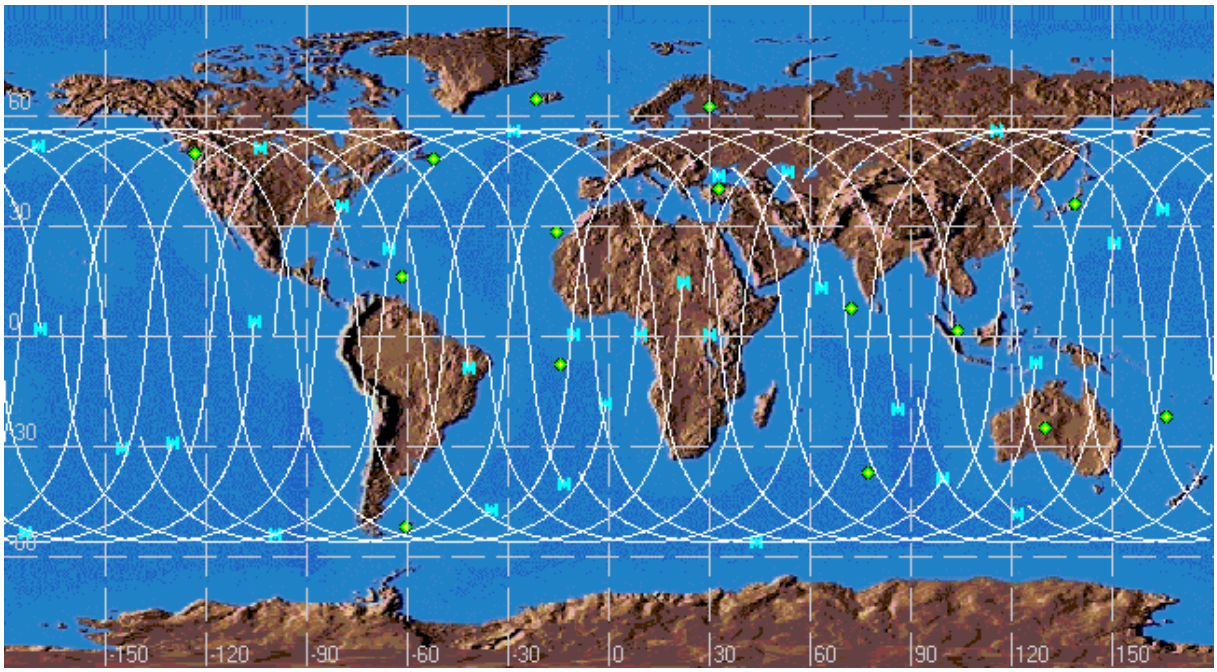

Figure 6-15 Ground Tracks of Galileo Option 2 Constellation

The next picture shows the earth coverage of that constellation. Average coverage is very good with 8 or more S/V visible simultaneously. Especially over Europe and Africa visibility is even enhanced because this area lies within the intersection of the geographical broadcast areas of the three GEO satellites.

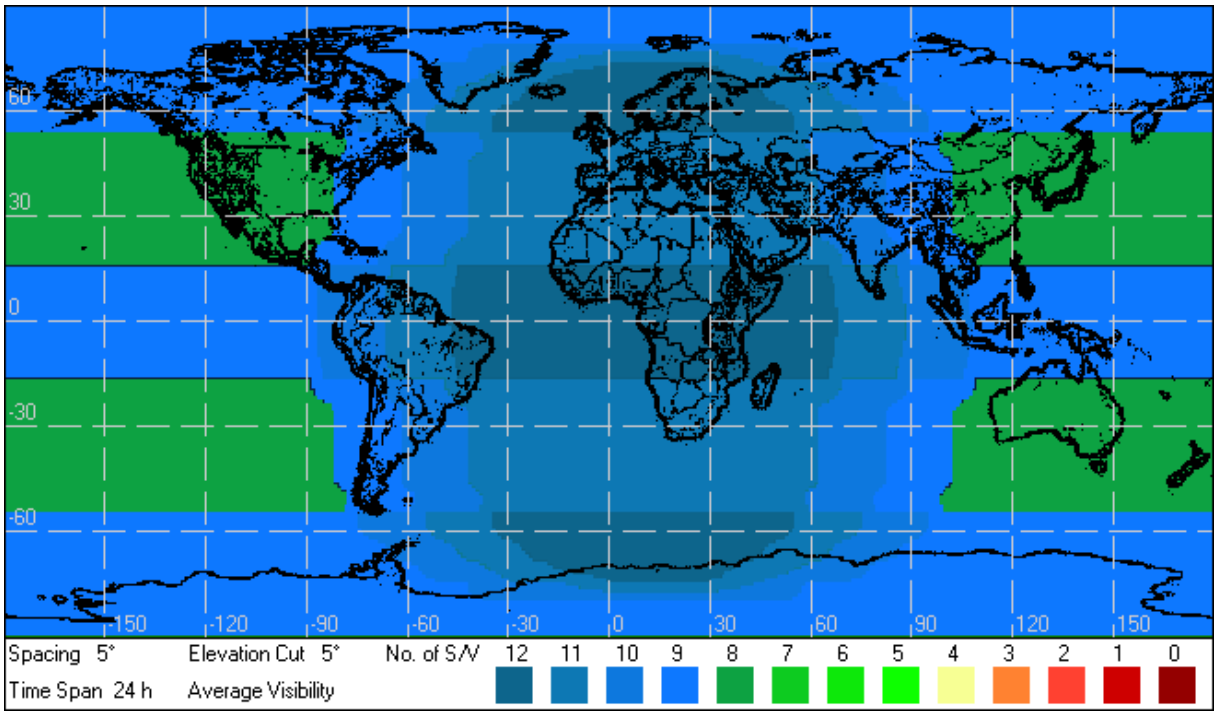

Figure 6-16 Visibility of Galileo Option 2 Constellation

6.1.2 Networks

6.1.2.1 GPS OCS

The following table shows the locations of the five monitoring stations used for orbit determination of the GPS satellites. Their location on a world map is depicted in the chapter "Optimized GPS constellation"

Station	Latitude	Longitude
Ascension Island	7.95° S	14.41° W
Diego Garcia	7.27° S	72.37° E
Kwajalein Atoll	8.72° N	167.73° E
Colorado Springs	38.5° N	104.5° W
Hawaii	21.19° N	157.52° W

6.1.2.2 DORIS Network

The DORIS network is optimised for LEO tracking, and therefore consists of a large number of stations, listed in the following table. The locations are depicted on a world map in the chapters of both LEO constellations.

Station	Latitude	Longitude
Dumont d' Urville	65.33° S	140.0° E
Syowa	69.0° S	39.58° E
Rothera	66.43° S	67.88° W
Rio Grande	52.21° S	66.25° W
Orroral	34.37° S	148.93° E
Yarragadee	28.95° S	115.35° E
Cachoeira Paulista	21.32° S	45.00° W
Ottawa	45.4° N	74.30° W
Yellowknife	62.48° N	113.52° W
Easter Island	26.85° S	108.62° W
Satiago	32.85° S	69.33° W
Purple Mountain	32.06° N	118.82° E
Djibouti	11.53° N	42.85° E
Galpagos	0.9° N	88.38° W

Station	Latitude	Longitude
Metsahovi	60.25° N	24.38° E
Toulouse	43.55° N	1.48° E
Amsterdam	36.20° S	77.57° E
Kourou	5.08° N	51.37° W
Kerguelen	48.65° S	70.27° E
La Reunion	20.78° S	55.57° E
Noumea	21.73° S	166.4° E
Papeete	16.42° S	148.38° W
Rapa	26.38° S	143.67° W
Wallis	12.73° S	176.18° W
Libreville	0.35° N	9.67° E
Dionysos	38.08° N	23.93° E
Reykjavik	64.15° N	20.02° W
Cibinong	5.52° S	106.85° E
Socorro	18.72° N	109.05° W
Everest	27.95° N	86.82° E
Arlit	18.78° N	7.37° E
NY Alesund	78.92° N	11.93° E
Port Moresby	8.57° S	147.18° E
Arequipa	15.53° S	70.50° W
Manila	14.53° N	121.03° E
Santa Maria	36.98° N	24.83° W
Badary	51.77° N	102.23° E
Krsnoyarsk	56.00° N	92.80° E
Yuzhno-Sakhalinsk	47.02° N	142.72° E
Dakar	14.72° N	16.57° W
Hartebeesthoek	24.12° S	27.70° E
Marion Island	45.12° S	37.85° E
Colombo	6.90° N	79.87° E
Goldstone	35.25° N	115.20° W

Station	Latitude	Longitude
Richmond	25.62° N	79.62° W
Fairbanks	64.97° N	146.48° W
Kauai	22.12° N	158.33° W
Guam	13.57° N	144.92° E
Saint Helena	14.05° S	4.33° W
Tristan da Cunha	36.95° S	11.68° W
Kitab	39.13° N	66.87° E

6.1.2.3 Proposed Galileo Network

The following table shows the locations of the proposed ground network for Galileo. Their locations are depicted in the constellation chapters of both Galileo options.

Station	Latitude	Longitude
Pitcairn	25.0° S	130.0° E
Falkland	52.0° S	60.0° W
Point a Pitre	16.2° N	61.3° W
St. Pierre et M.	48.0° N	52.0° W
Reykjavik	64.1° N	21.6° W
Las Palmas	28.1° N	15.3° W
Ascension	7.9° S	14.4° W
Helsinki	62.0° N	30.0° E
Ankara	39.9° N	32.8° E
Indian Ocean British Territory	7.2° N	72.3° E
Amsterdam Island	37.5° S	77.3° E
Singapour	1.2° N	104.0° E
Tokyo	35.6° N	138.8° E
Noumea	22.2° S	166.2° E
Vancouver	49.2° N	123.1° W

6.1.2.4 Custom Global Network

For a global tracking of high altitude satellites, the following network has been chosen. The location are depicted in the chapter "IGSO Walker constellation" and others.

Station	Latitude	Longitude
Orroral	34.37° S	148.93° E
Easter Island	26.85° S	108.62° W
Toulouse	43.55° N	1.48° E
Kourou	5.08° N	51.37° W
Wallis	12.73° S	176.18° W
Yuzhno-Sakhalinsk	47.02° N	142.72° E
Hartebeesthoek	24.12° S	27.70° E
Colombo	6.90° N	79.87° E
Goldstone	35.25° N	115.20° W

6.1.2.5 Custom Regional Network

For a regional tracking of geosynchroneous satellites, i.e. GEO and IGSO, the following network has been chosen. It provides a reasonable tracking geometry for high altitude S/V visible from Europe. The location are not depicted separately but are a sub set of the preceding "global custom network".

Station	Latitude	Longitude
Toulouse	43.55° N	1.48° E
Kourou	5.08° N	51.37° W
Hartebeesthoek	24.12° S	27.70° E
Colombo	6.90° N	79.87° E

6.1.3 Simulation Scenarios

The following scenarios have been evaluated by simulation. Not all possible combination have been investigate, but the chosen ones can be regarded as representative. The following table shows the investigated combinations.

Scenario	Ground Only		With ISL		
	Full Net	Red. Net	Full Net	Red Net	Regional Net
24 Opt. GPS	Galileo	OCS			
IGSO Walker 18/6/2	C. Global		C. Global		C. Regional
18 IGSO on 3 Loops	C. Global		C. Global		
9 IGSO 9 GEO	C. Custom		C. Global		C. Regional
LEO 81 / 9 / 1	DORIS	Galileo		Galileo	
LEO 72 / 9 / 1 + 9 GEO	DORIS	Galileo		Galileo	
Galileo 33	Galileo		Galileo		
Galileo 27 / 3	Galileo		Galileo		

In the case of GPS and Galileo, "Reduced Net" mean the OCS (Operational Control System of GPS), whereas "Full Net" means the proposed Galileo network.

For IGSO and GEO constellations simulation have been made using the custom regional and the custom global network.

For LEO constellations, the DORIS network has been used as a "full coverage " network and the Galileo network as a reduced coverage network.

The investigated constellation / network combinations have been processed with and without using inter satellite links.

6.2 Orbit Determination Accuracy

The following chapter deals with the accuracy of orbit determination. The results have been derived using a numerical simulation of the satellite orbits, tracking geometry and observation errors. The estimator used for orbit determination has been the real time Kalman filter described in detail preceding chapters. The state vector for each satellite has been:

Position errors in X, Y and Z direction (inertial J2000 frame)

Velocity errors in X, Y and Z direction (inertial J2000 frame)

Clock offset.

The unmodelled residual acceleration has been assumed to be

$$\left|a_{\text{residual}}\right| < 10^{-7}\ \frac{\text{m}}{\text{s}^2}$$

and the stability of the satellite clock has been assumed to be

$$10^{-13}\ \frac{\text{s}}{\sqrt{\text{s}}}$$

which correspond to a medium stability rubidium clock. These values have been added as process noise in the Kalman filter process.

The simulation step width has been 30 seconds, for the orbit propagation, i.e. the position has been computed for every 30 seconds. Measurements have been take every 5 minutes.

The figures in this chapter show the real orbit errors on the left, and the standard deviations on the right. The real orbit errors in radial, along track and cross track direction have been derived from the position difference in x, y and z direction by

$$\left(\vec{\varepsilon}_{\text{r,a,c}}\right)^{\text{T}} = \left(\vec{X}_{\text{Estimated}} - \vec{X}_{\text{True}}\right)^{\text{T}} \cdot \left[\vec{e}_{\text{radial}}\ \ \vec{e}_{\text{along}}\ \ \vec{e}_{\text{cross}}\right]$$

where $\vec{e}_{<\text{direction}>}$ denotes the unit vectors in radial, along track and cross track direction.

The standard deviations in radial, along track and cross track directions have been derived from the position error sub matrix of the covariance matrix P, which contains the variances of the position errors in inertial x, y and z direction. The following equation yields the variance in radial direction. It can easily be modified for the other two directions.

$$\sigma^2_{\text{radial}} = \vec{e}_{\text{radial}}{}^{\text{T}} \cdot \begin{bmatrix} \sigma^2_{\text{xx}} & \sigma^2_{\text{xy}} & \sigma^2_{\text{xz}} \\ \sigma^2_{\text{yx}} & \sigma^2_{\text{yy}} & \sigma^2_{\text{yz}} \\ \sigma^2_{\text{zx}} & \sigma^2_{\text{zy}} & \sigma^2_{\text{zz}} \end{bmatrix} \cdot \vec{e}_{\text{radial}}$$

The standard deviation is now obtained by simply computing the square root of the above value.

6.2.1 Optimized GPS Constellation

6.2.1.1 Ground Tracking (OCS)

The orbit determination accuracy for a GPS satellite using the OCS shows large variations in the standard deviations. The space vehicle is tracked by 3 station most of the time. For the periods where it is tracked by only two stations, the covariances increase, although the real orbit errors do not necessarily increase. The real time tracking accuracy is better than 1.2 meter in the radial direction, but up to 3 meters in the along track direction.

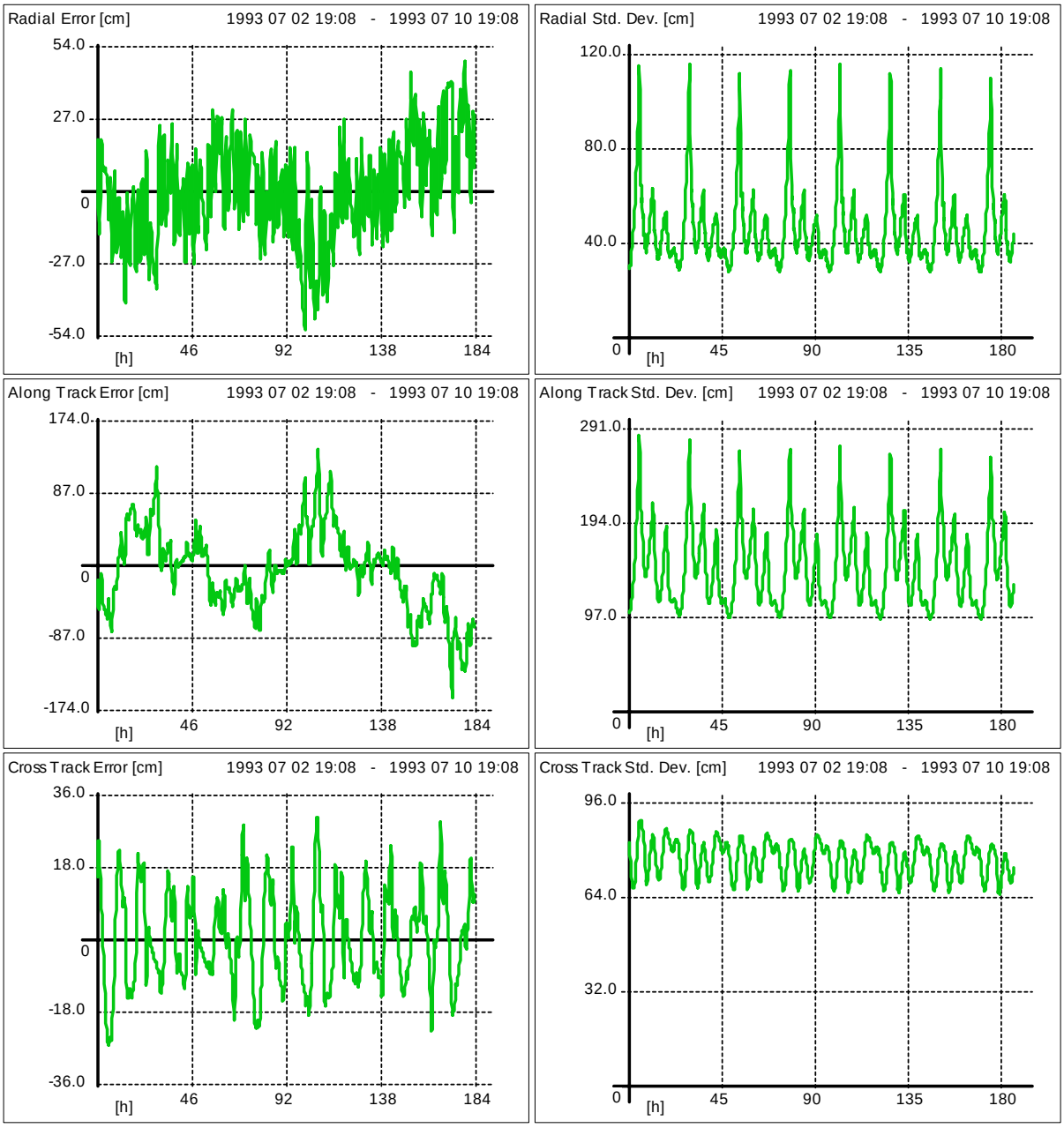

Figure 6-17 Tracking Accuracy with GPS OCS

6.2.1.2 Ground Tracking with Augmented Network

For high precision applications, 1 meter tracking accuracy is not sufficient. One has to keep in mind that the orbit has to be predicted and a high initial position error increases the prediction error. To get a better tracking accuracy, a lager ground network has been chosen. Using the Galileo network, a satellite is tracked by 5 or more ground stations all the time. This leads to a much better tracking geometry reflected in the standard deviations of the orbit errors.

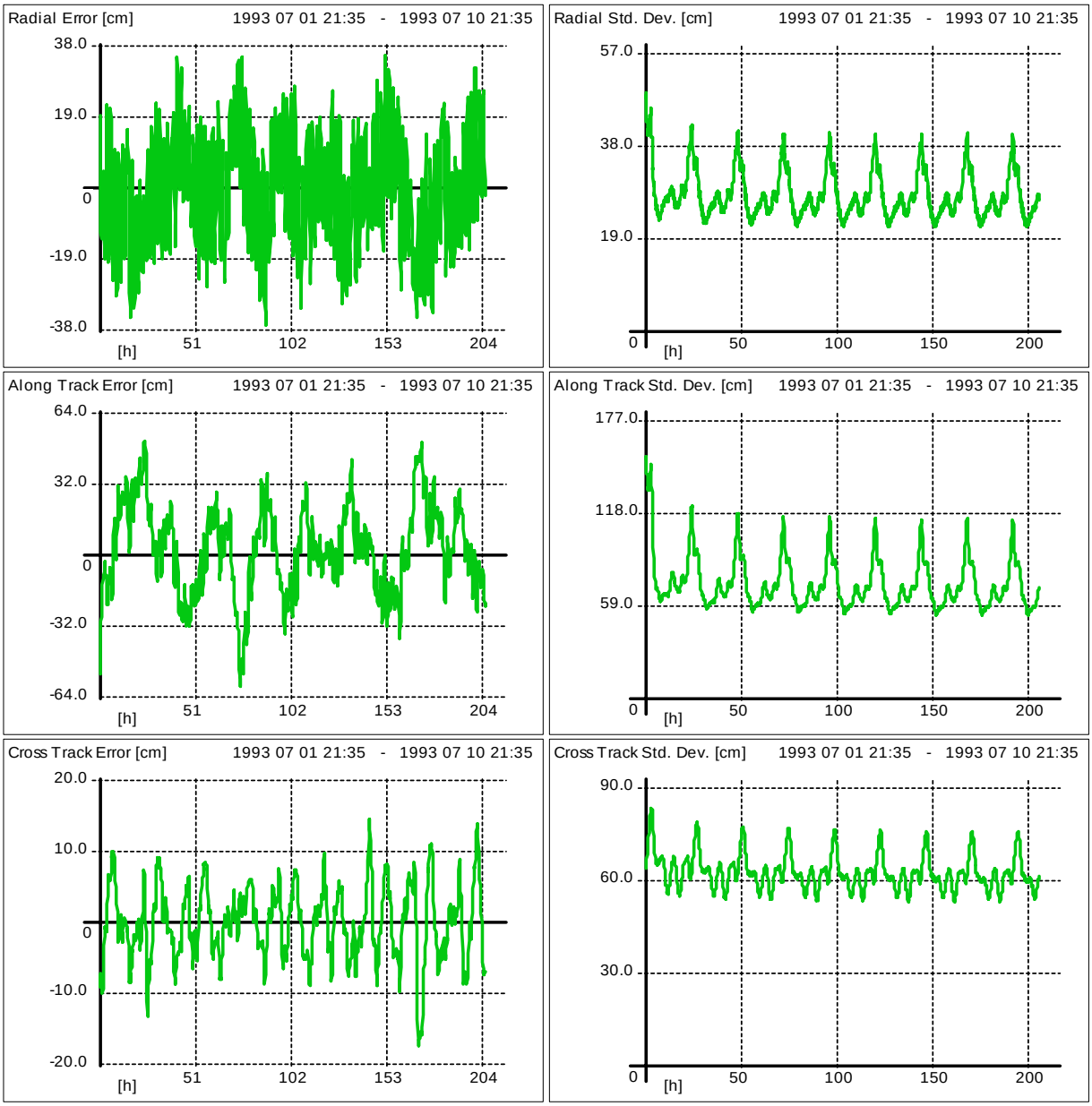

Figure 6-18 Tracking Accuracy with proposed Galileo Ground Network

6.2.2 IGSO Walker Constellation

6.2.2.1 Ground Tracking

The IGSO Walker constellation is reasonably good tracked by custom global network providing 3 – 4 simultaneous ground links. The standard deviation in radial direction is around 35 cm.

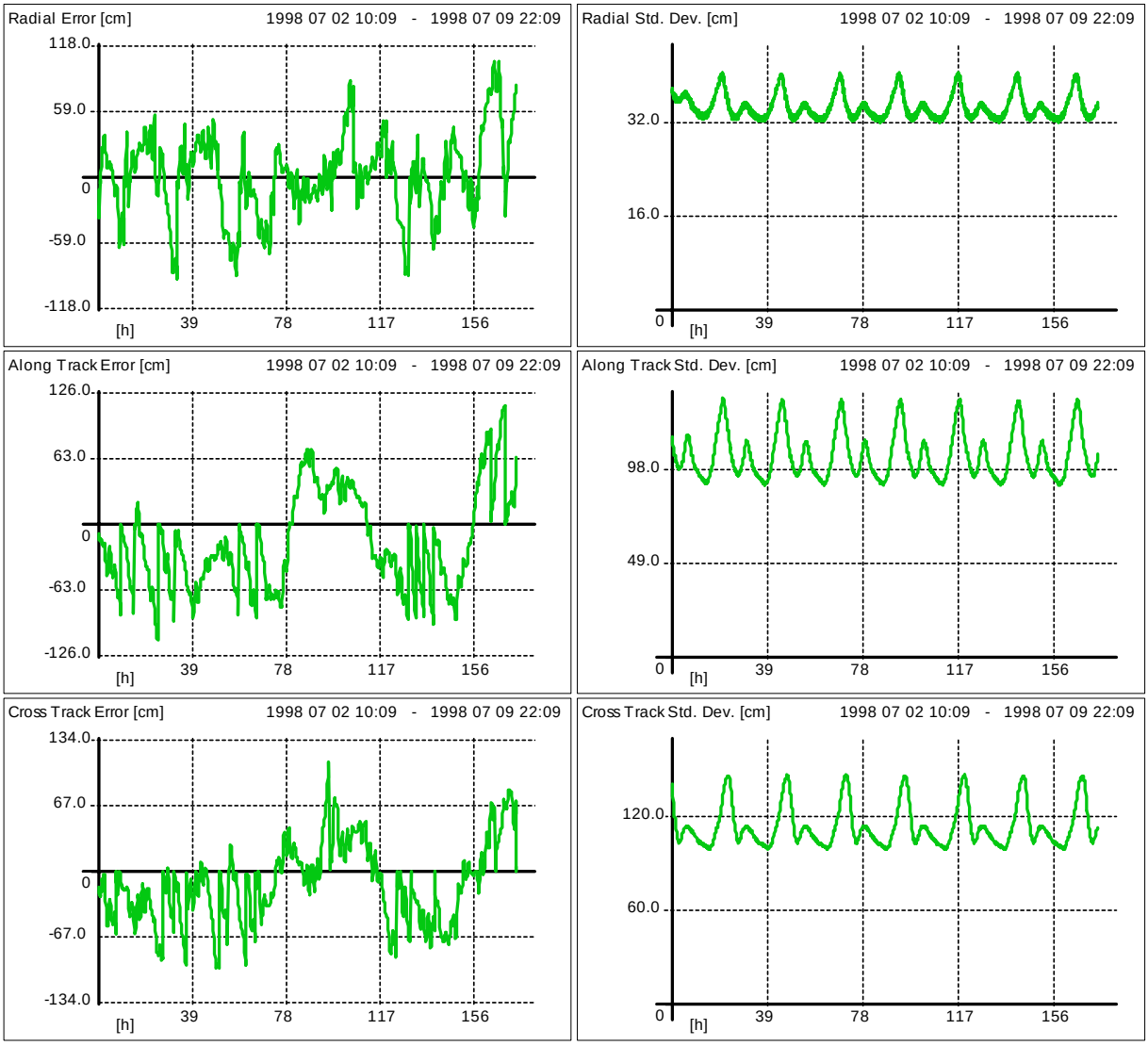

Figure 6-19 Tracking Accuracy with Custom Global Net

6.2.2.2 Ground and Inter Satellite Tracking

The tracking accuracy can be remarkably improved by adding intersatellite links. The radial accuracy increases down to 8 cm and the tangential orbit errors (along track and cross track error) are also decreased down to 20 – 25 cm.

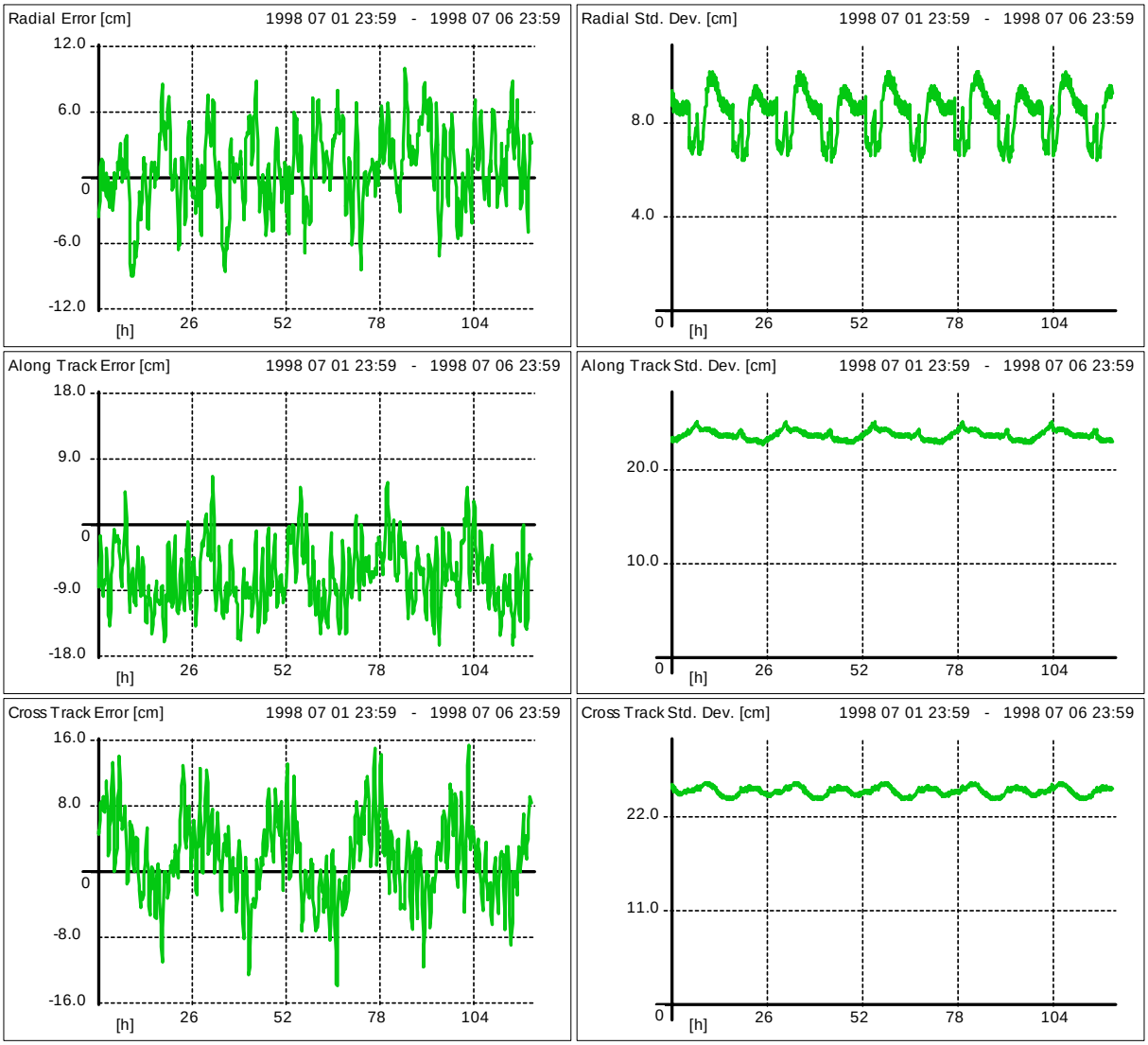

Figure 6-20 Tracking Accuracy with Custom Global Net using additional ISL's

6.2.2.3 Ground and Inter Satellite Tracking with Reduced Network

In the introduction it has already be said that intersatellite links can be used to replace ground likes. This scenario uses the IGSO Walker constellation together with a regional network. The following figure shows the tracking accuracy for a S/C not visible to ground network at all!

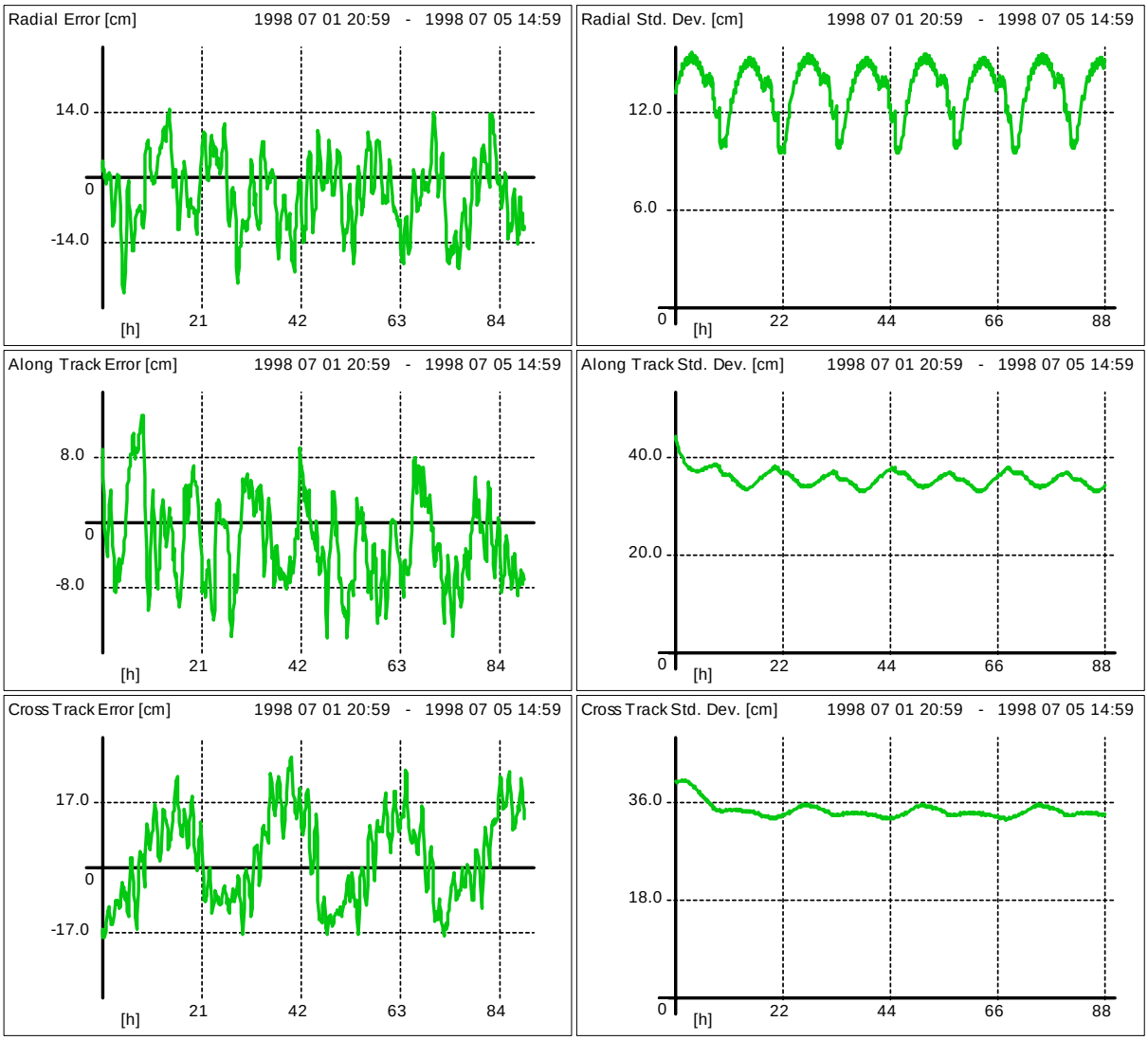

Figure 6-21 Tracking Accuracy of S/C using ISL's, but not visible to Ground Network (Custom Regional Network)

It can be seen that the standard deviations are only twice as high as for the S/C tracked by the ground network. The "non-visible" satellites are only positioned relative to the "visible" satellites. This is an interesting option even for non geosynchroneous orbits, because despite of a regional network, the tracking accuracy is "transferred" to the non-visible satellites via the inter satellite links.

6.2.3 IGSO on three Loops

6.2.3.1 Ground Tracking

This scenario provides nearly as good tracking accuracy as the Walker constellation. The differences result from the higher inclination of the orbits.

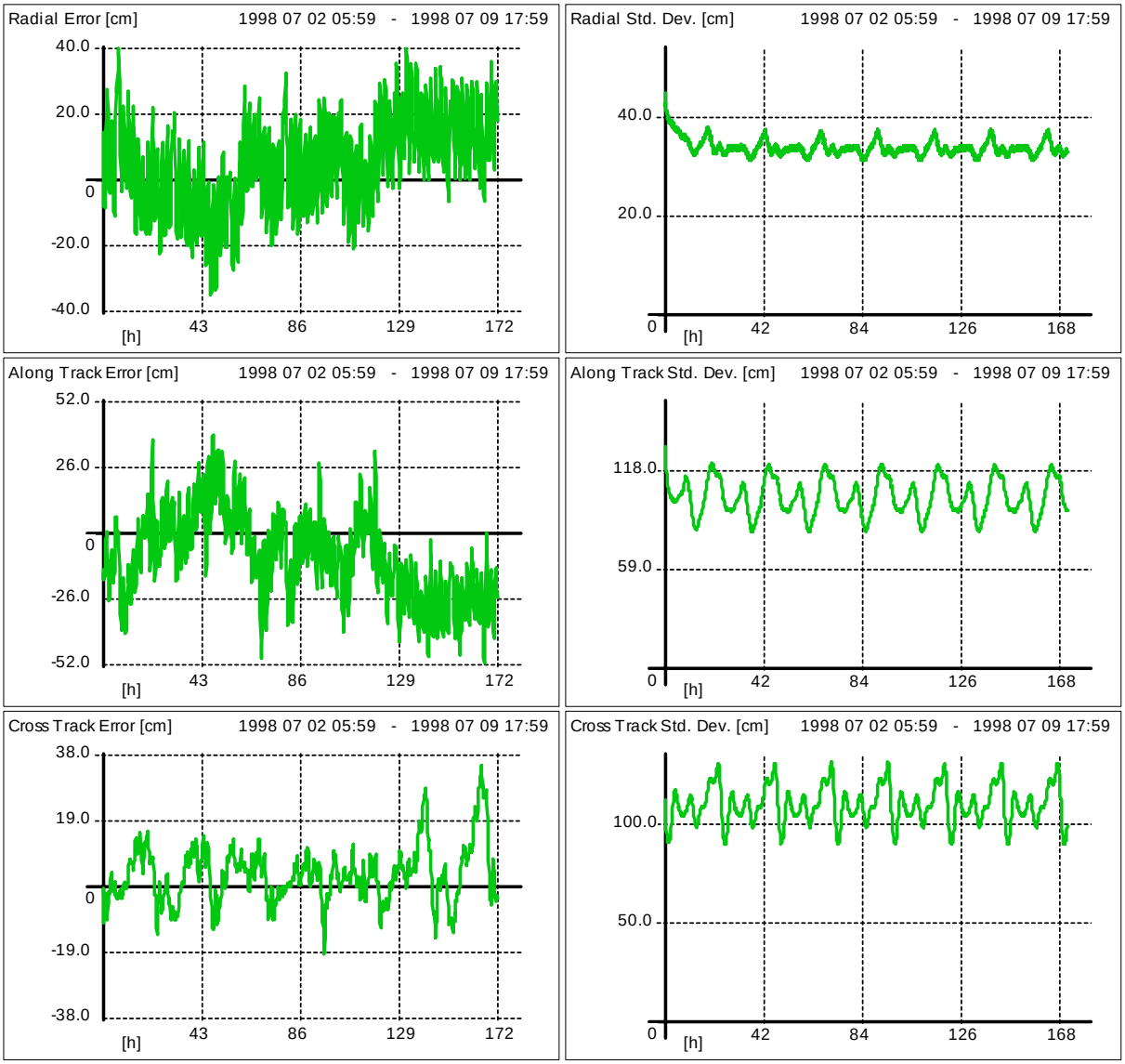

Figure 6-22 Tracking Accuracy of IGSO on a Loop with Custom Global Network

6.2.3.2 Ground and Intersatellite Tracking

In this scenario, intersatellite links provide also an enhancement in accuracy similar to the IGSO Walker constellation.

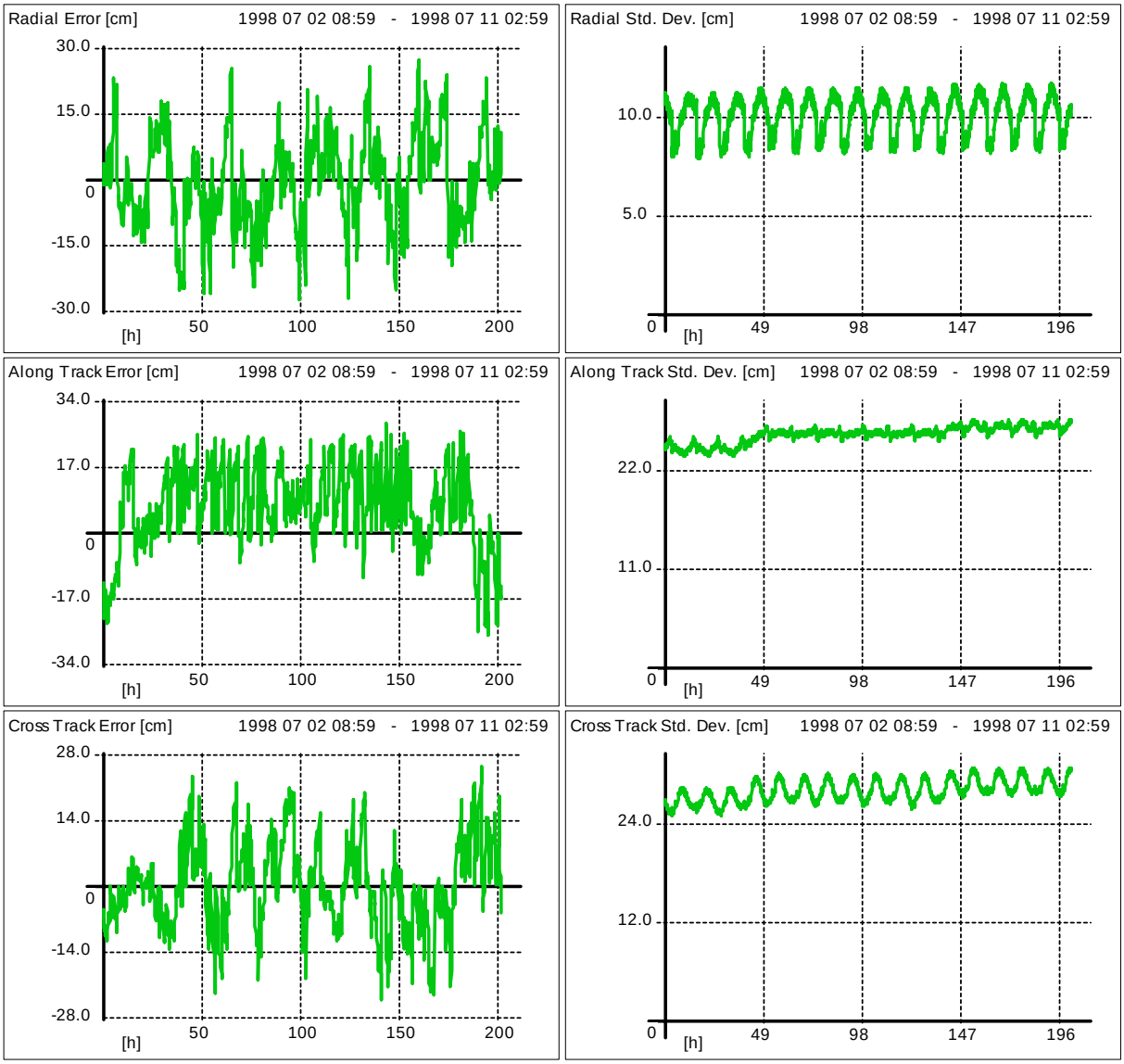

Figure 6-23 Tracking Accuracy of IGSO on a Loop with Custom Global Network using additional ISL's

6.2.4 GEO / IGSO

6.2.4.1 Ground Tracking

In this mixed constellation, the tracking accuracy of IGSO satellites are similar the previous constellations. Only the GEOs have a slightly different tracking geometry. The standard deviations are very stable, and not subject to geometry variations, as can be seen in the figure below.

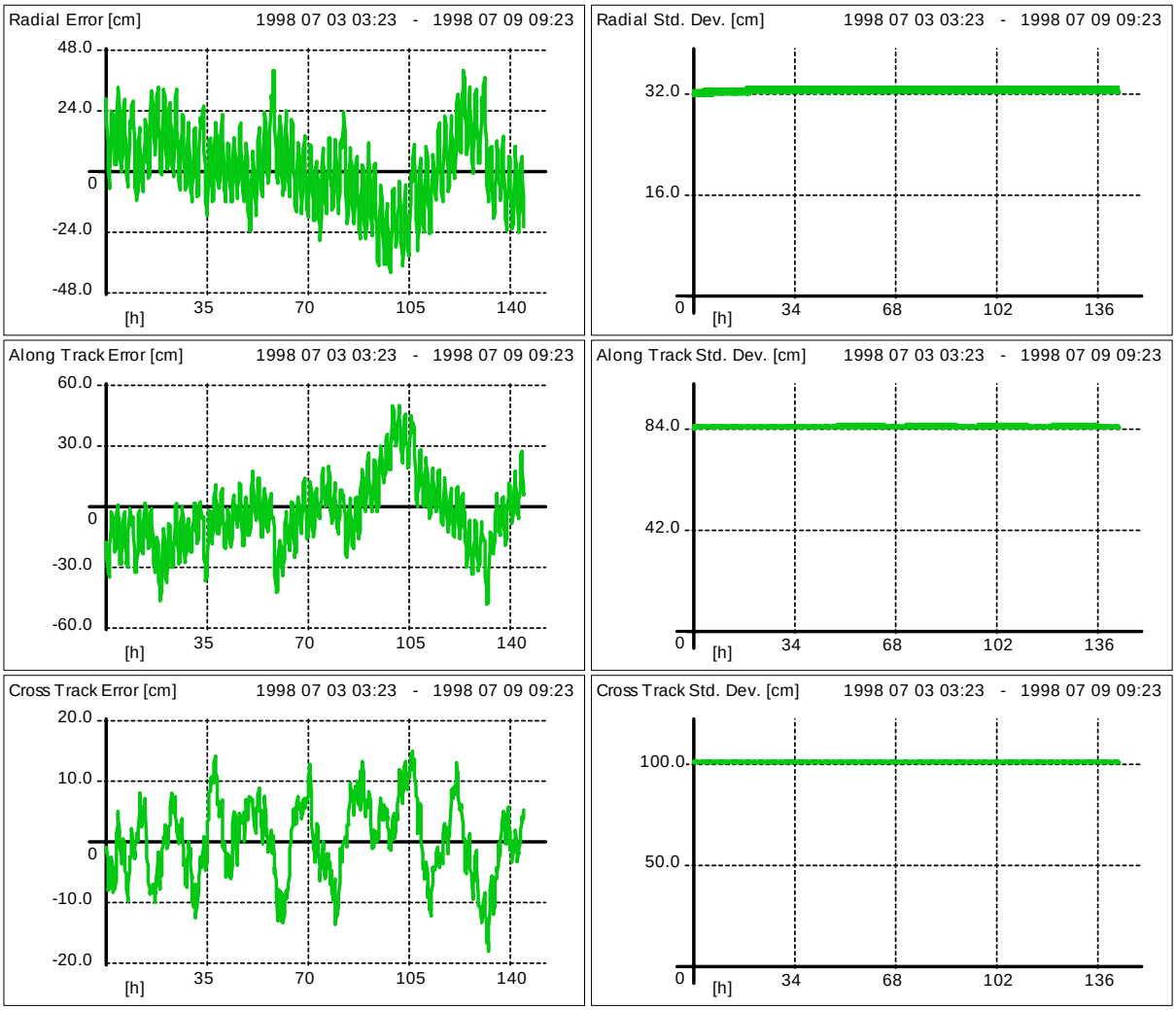

Figure 6-24 Tracking Accuracy of GEO using Ground Links only

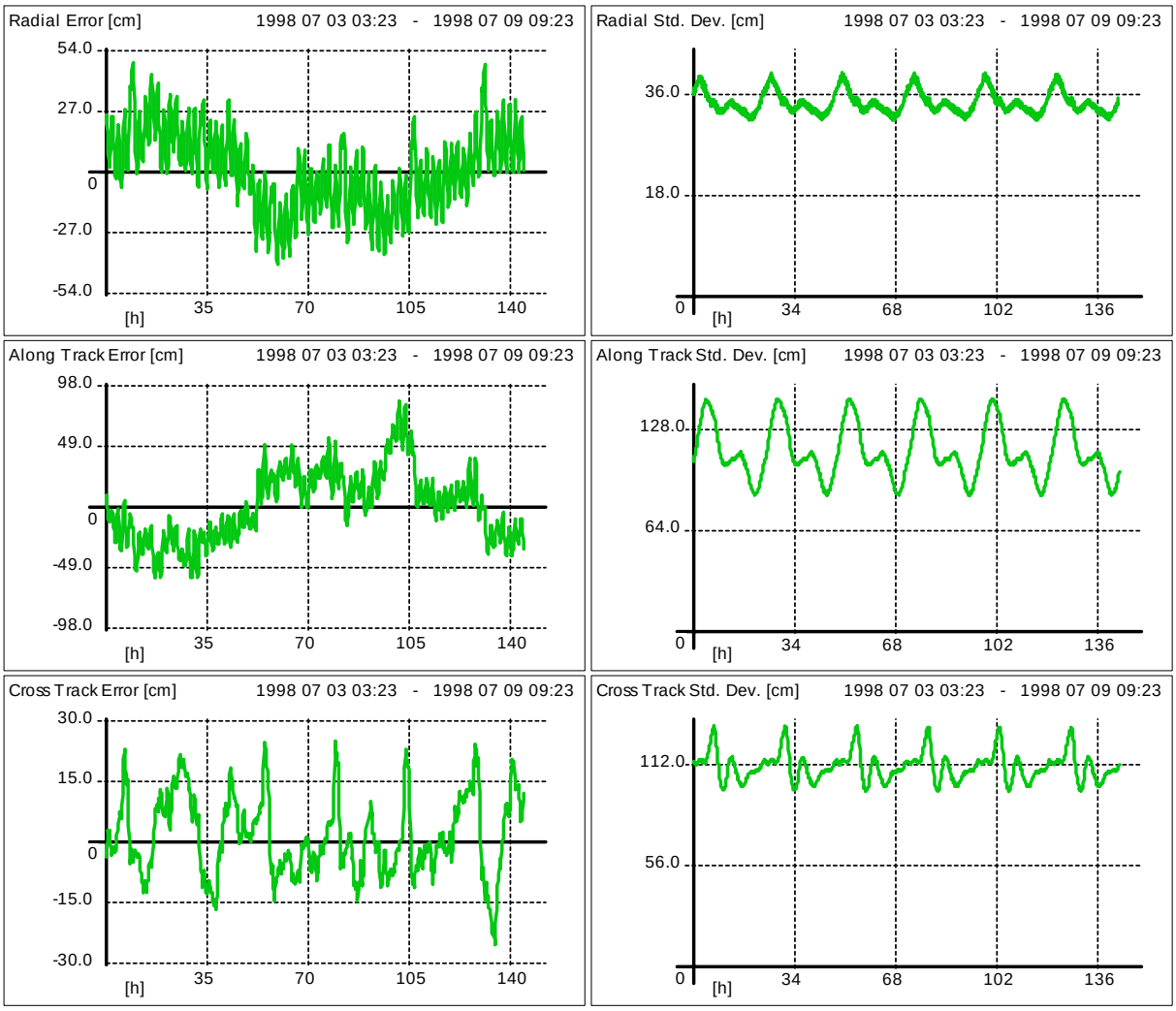

Figure 6-25 Tracking Accuracy of IGSO using Ground Links only

6.2.4.2 Ground and Intersatellite Tracking

This constellation can also be augmented with inter satellite links, leading to a remarkable improvement.

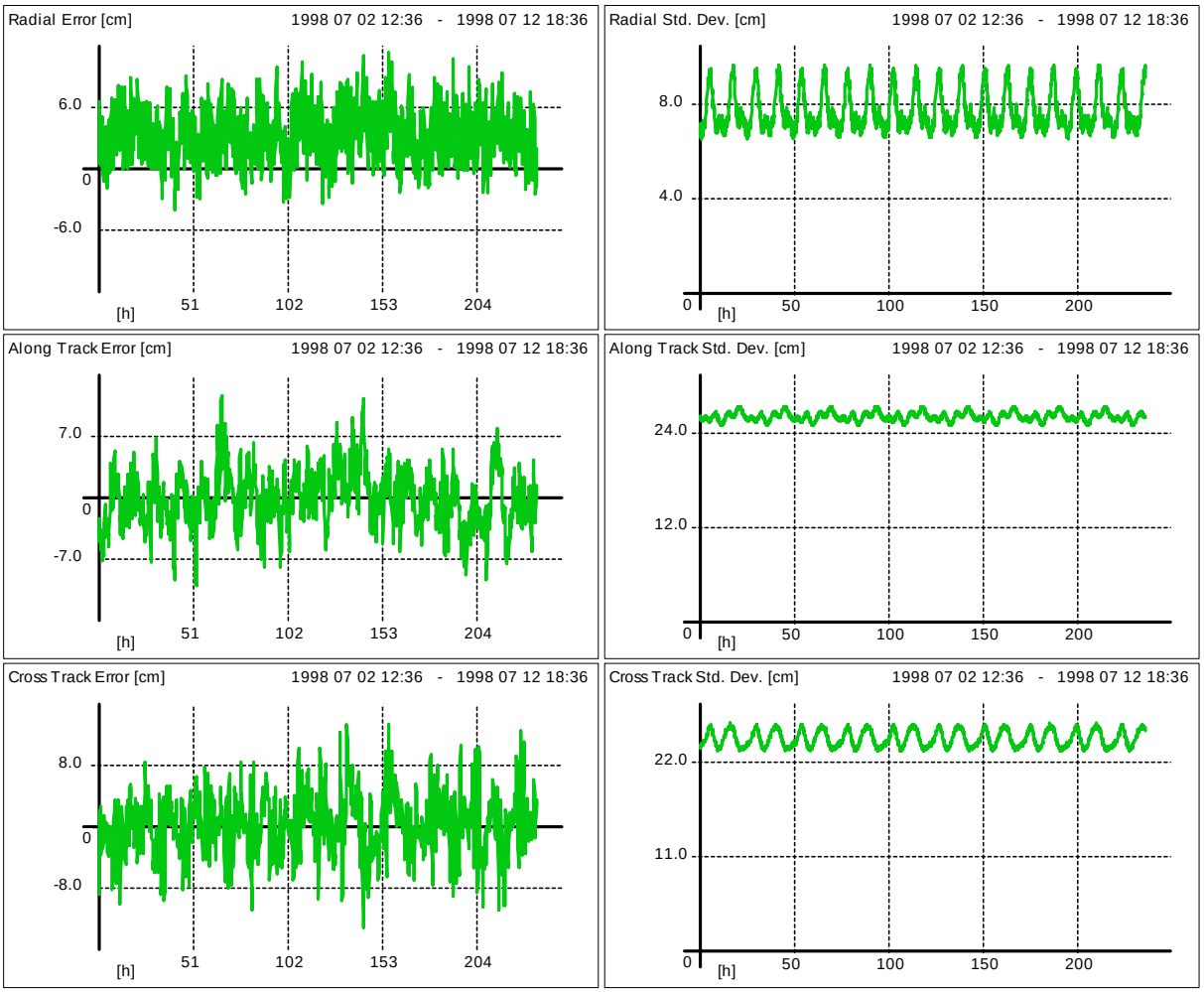

Figure 6-26 Tracking Accuracy of IGSO with ISL's

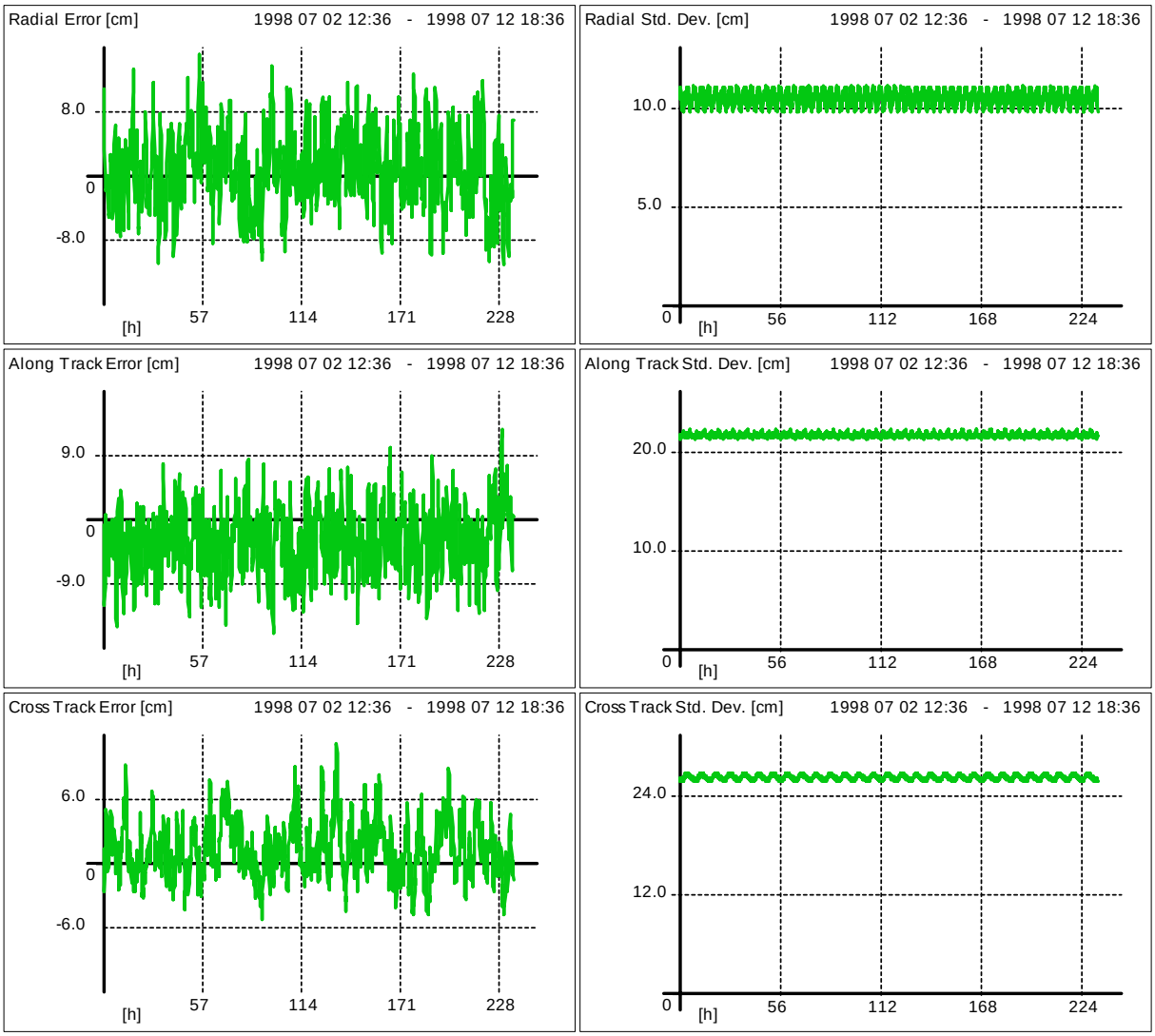

Figure 6-27 Tracking Accuracy of GEO with ISL's

6.2.4.3 Ground and Intersatellite Tracking (Regional Network)

The pure regional tracking is an interesting option (not only) for geosynchroneous satellite constellations. The figures below shows the tracking accuracy for an IGSO with rare ground contact, as well as for a GEO with no ground contact.

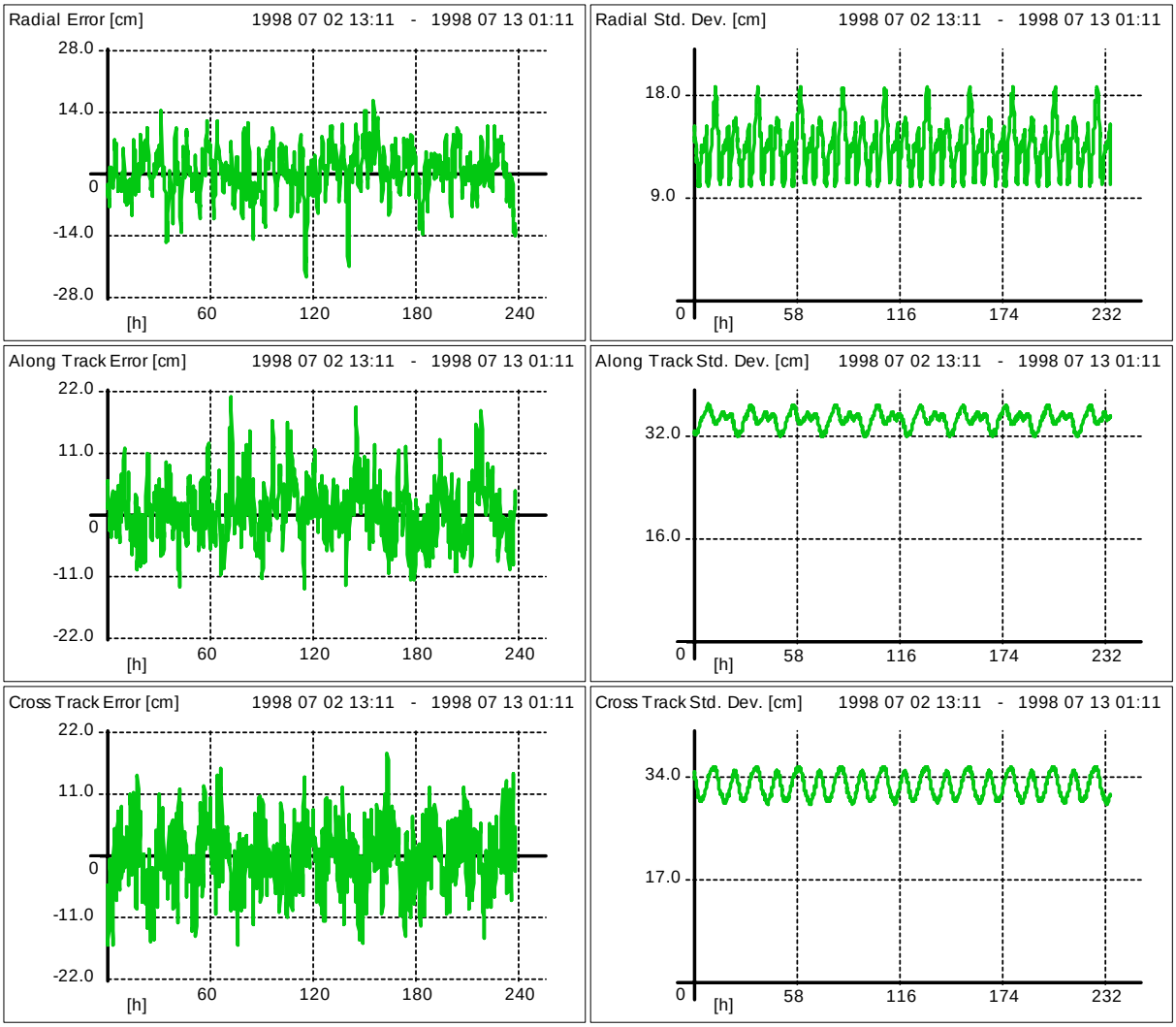

Figure 6-28 Tracking Accuracy of IGSO with rare Ground Contact using ISL's

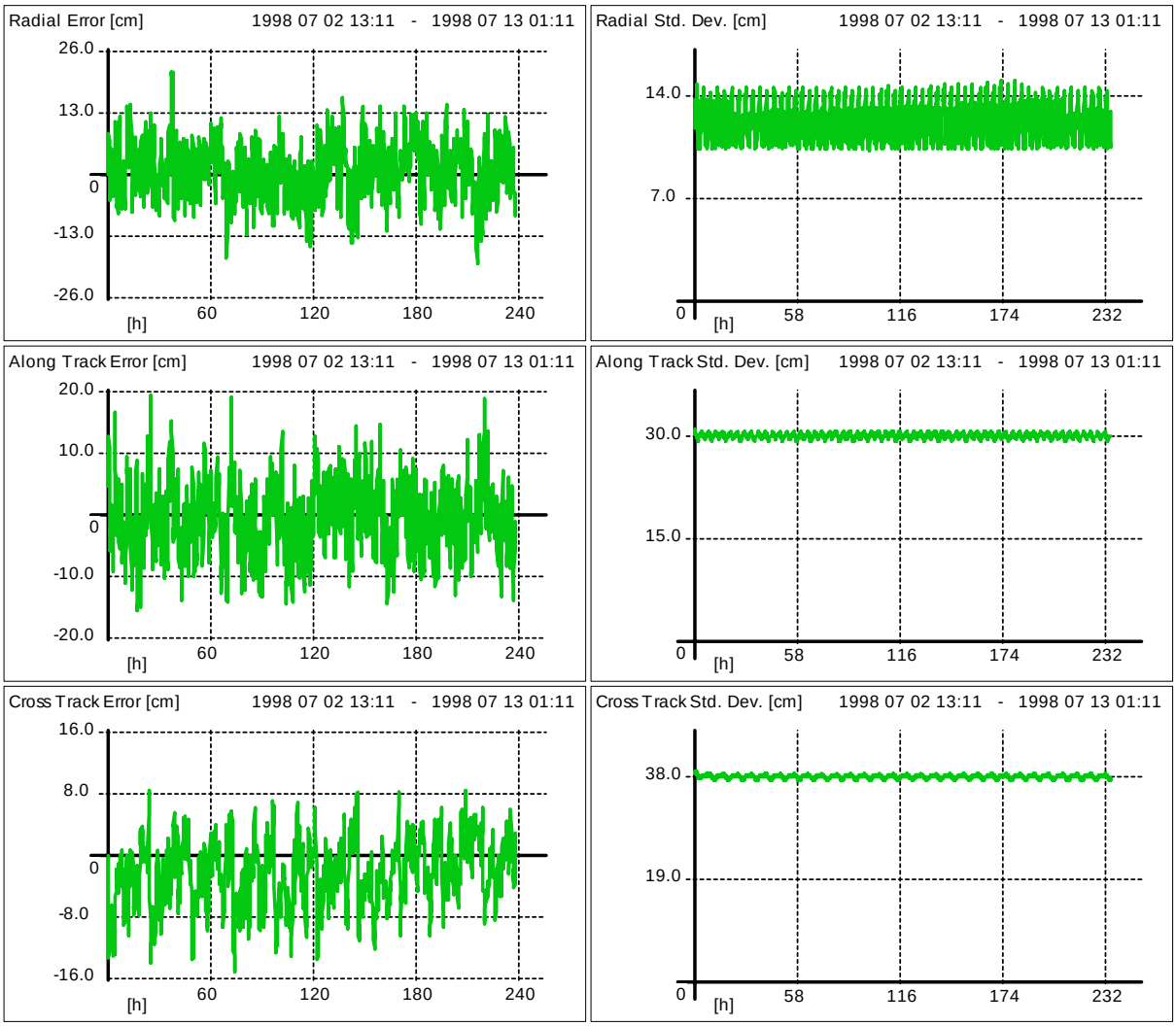

Figure 6-29 Tracking Accuracy of GEO without Ground Contact, only via ISL's

6.2.5 Pure LEO Constellation

6.2.5.1 Ground Tracking with Full Network

In this scenario, orbit determination for the LEO constellation has been done using ground measurements only, but with a large scale network of ground stations. Using the DORIS network provides a good tracking accuracy for LEO satellites. This is due to the large number of tracking stations, distributed over the world. A radial accuracy of better than 30 cm can be reached most of the time. Although LEO satellites have a higher along track error due to the uncertainty in the high altitude air density, a LEO satellite tracked by a large ground network can be seen from more than 5 stations the whole time. Due to the low altitude, the tracking geometry is also good.

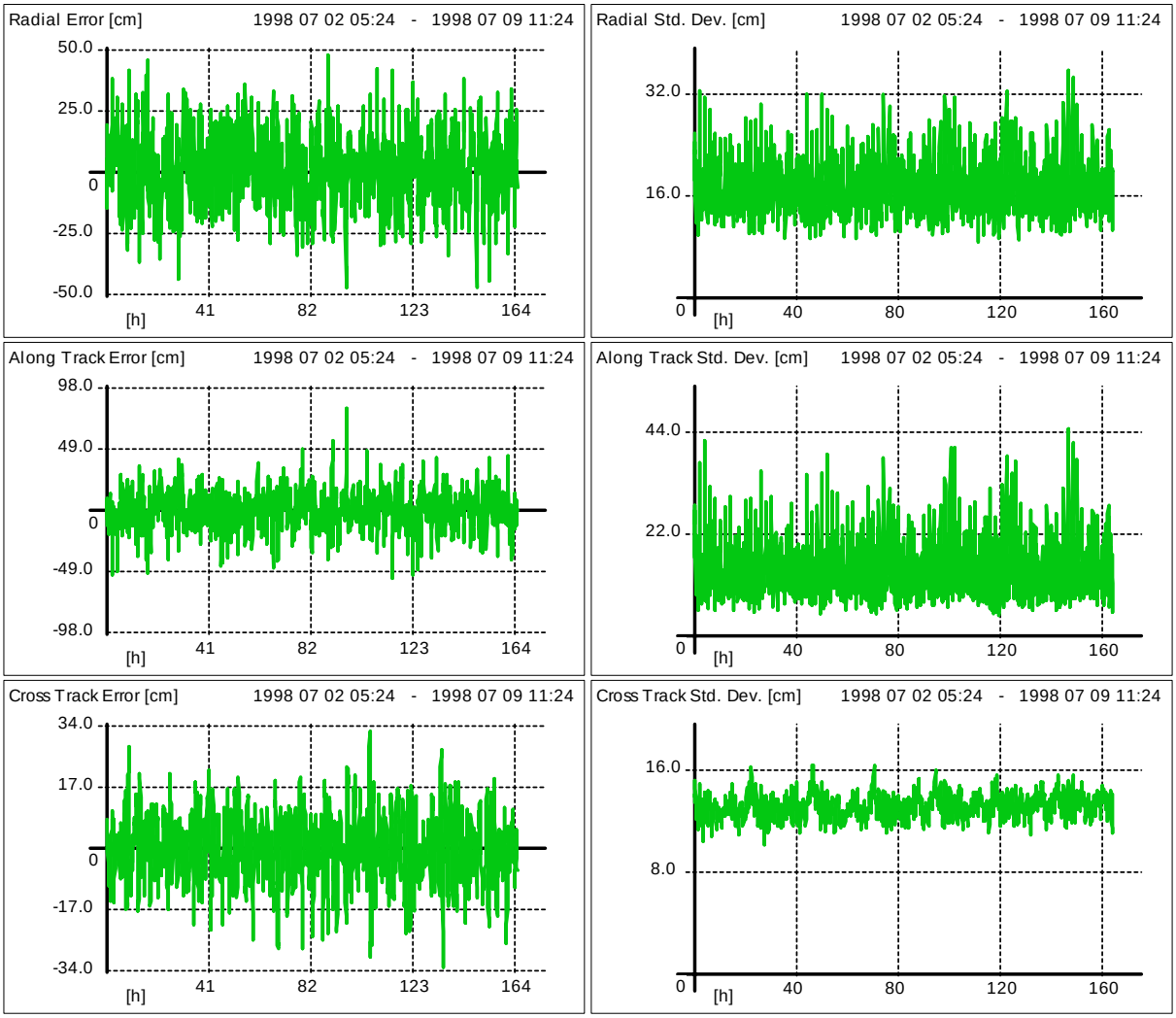

Figure 6-30 Tracking Accuracy of LEO using DORIS Network only

6.2.5.2 Ground Tracking with Reduced Network

If the network is reduced (Galileo network), the accuracy gets degraded. as can be seen from the following figure.

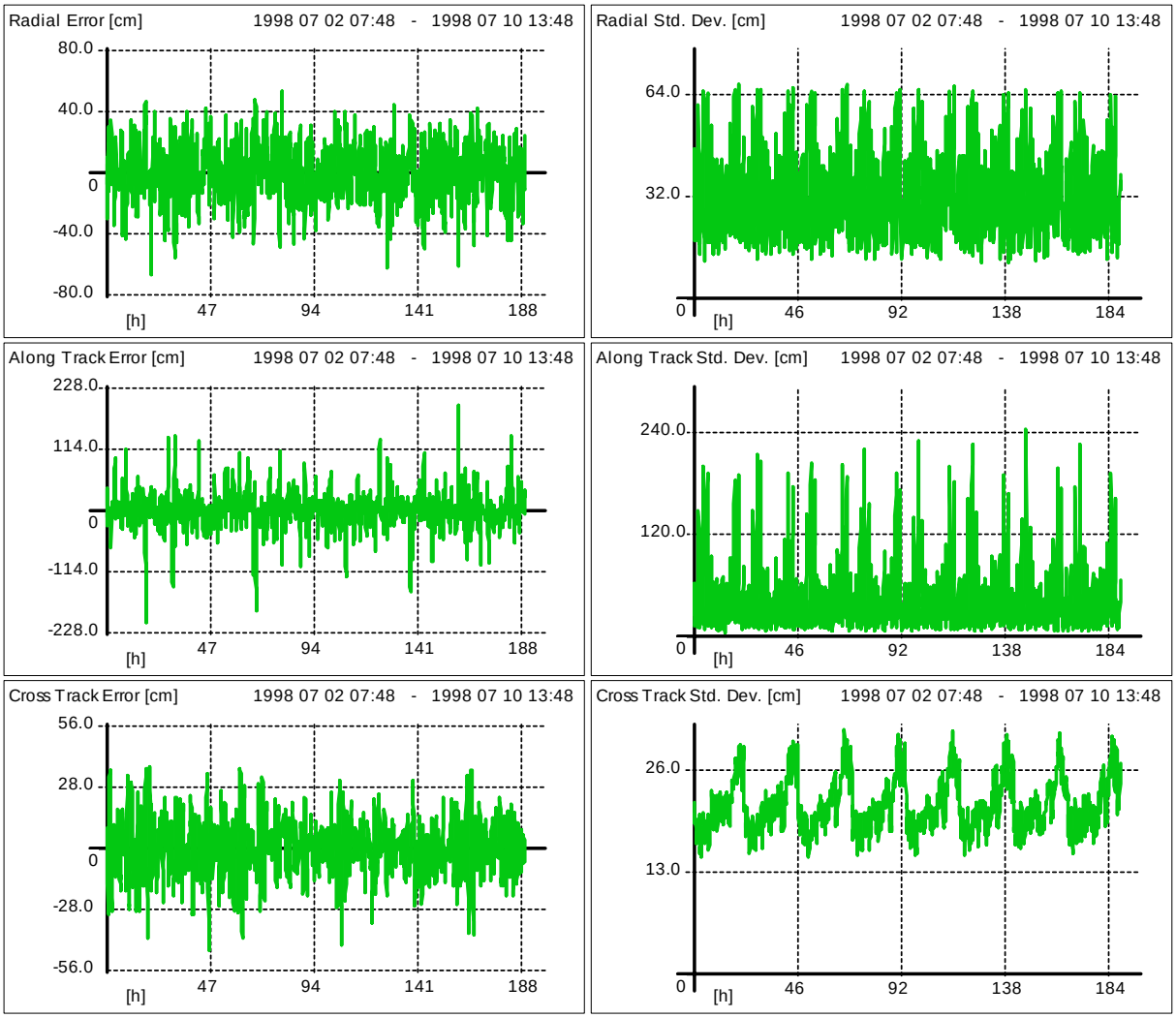

Figure 6-31 Tracking Accuracy of a LEO using Galileo Network

6.2.5.3 Ground and Intersatellite Tracking (Reduced Network)

An accuracy even better as with a large scale ground network can be achieved by introducing inter satellite links. Accuracy is improved by a factor of two in all direction, with respect to the ground tracking.

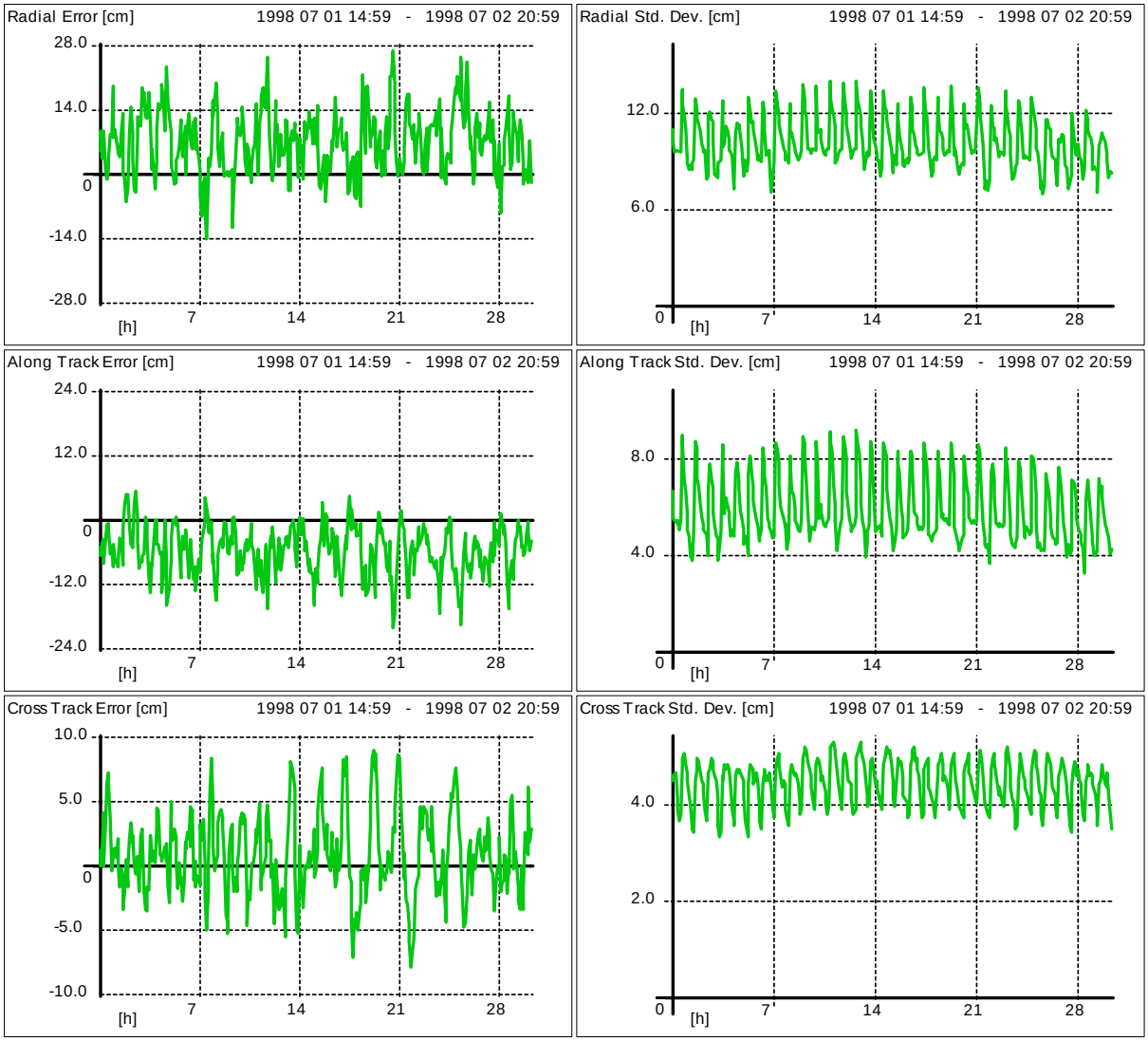

Figure 6-32 Tracking Accuracy of LEO using Ground and Intersatellite Tracking

6.2.6 GEO / LEO

6.2.6.1 Ground Tracking (Full Network)

Ground tracking accuracy for LEO satellites is identically to Pure LEO constellation. The orbit determination accuracy for the GEO is similar to the figures provided with the GEO/IGSO constellation.

6.2.6.2 Ground Tracking (Reduced Network)

Ground tracking accuracy for LEO satellites is identically to Pure LEO constellation. The orbit determination accuracy for the GEO is similar to the figures provided with the GEO/IGSO constellation.

6.2.6.3 Ground and Intersatellite Tracking (Reduced Network)

In this scenario, the following tracking schemes have been applied, as a difference to the inter satellite link scenario of the pure LEO constellation. LEO and GEO satellites have been tracked by the ground stations but not all possible inter satellite links have been used. The following observation have been processed:

Ground – GEO

Ground – LEO

GEO – GEO

LEO – GEO

The results are shown in the following accuracy figure.

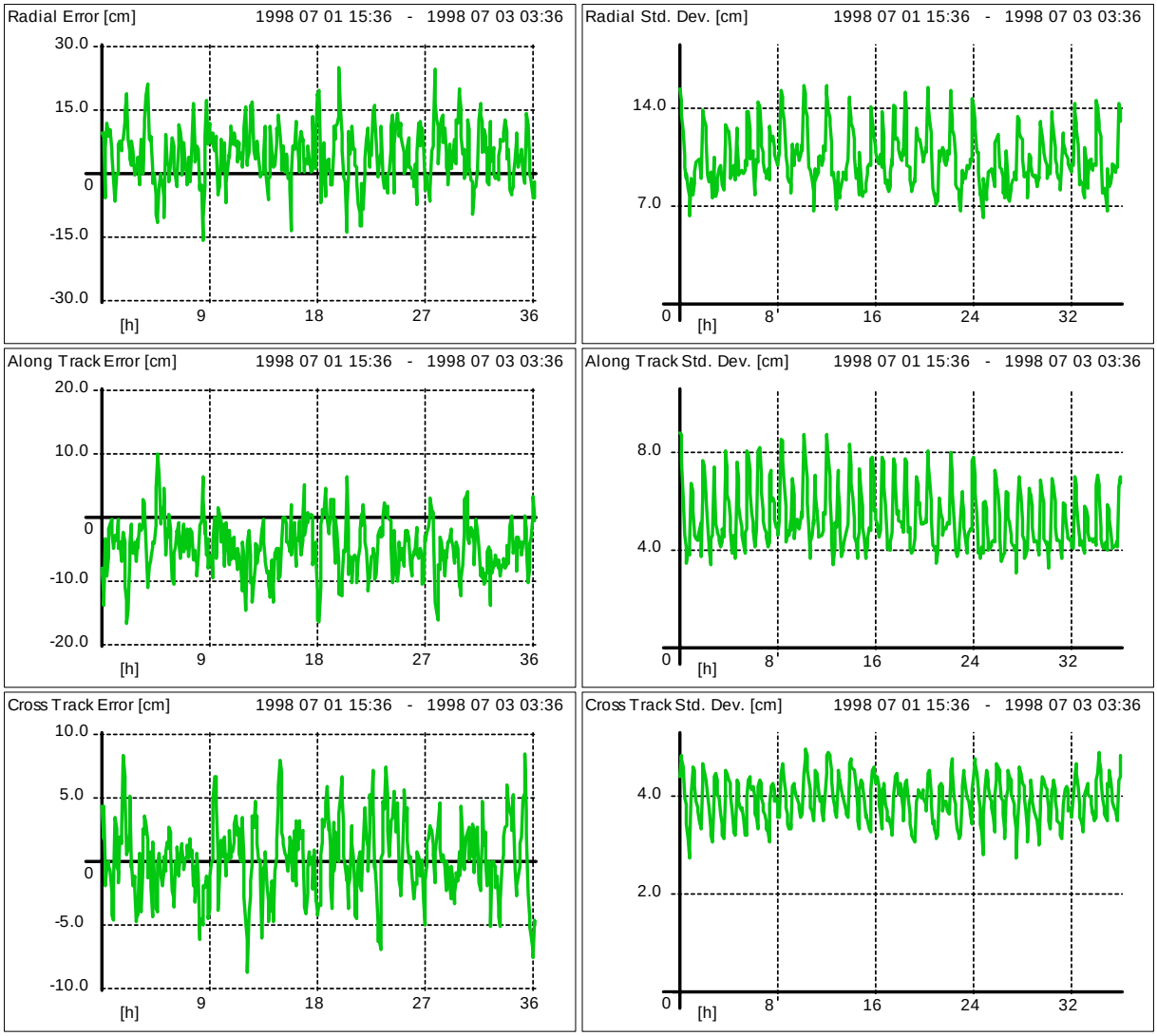

Figure 6-33 Tracking Accuracy of LEO using Ground and LEO-GEO-ISL's

This measuring scheme has the advantage of reducing the number of possible links, but provided a nearly as good performance as if all links would have been established.

6.2.7 Galileo 1 (Pure MEO)

6.2.7.1 Ground Tracking

In this scenario only ground links are processed for orbit determination. The constellation is tracked by the full proposed ground network. The achieved accuracy can be seen in the figure shown below.

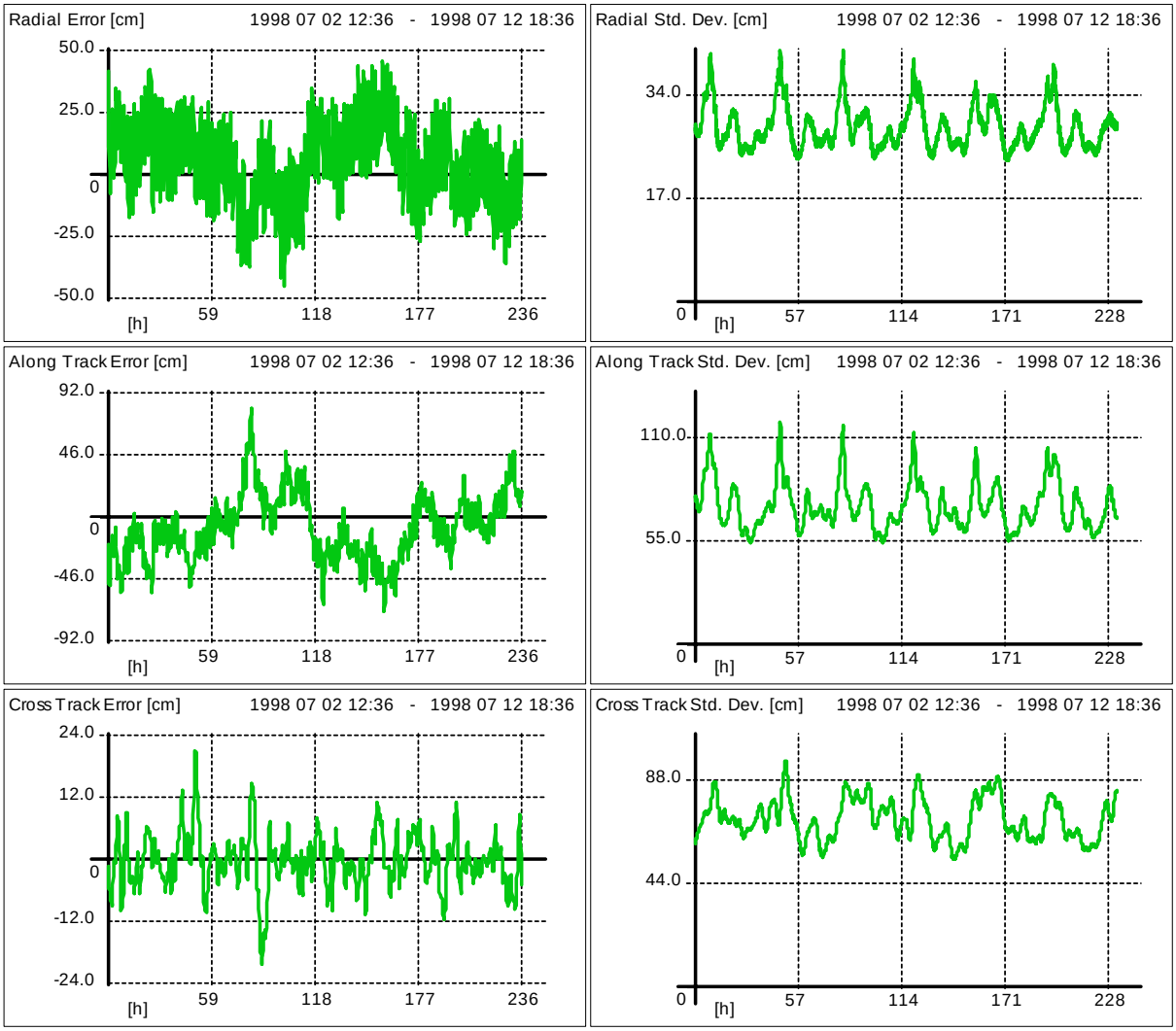

Figure 6-34 Tracking Accuracy of MEO using Galileo Network

6.2.7.2 Ground and Intersatellite Tracking

By adding inter satellite links, tracking accuracy can be improved enormously. Radial accuracy comes down to 2.5 cm, while along track and cross track accuracy are around 10 cm. This is a degree of accuracy which can normally only be reached by post processing. The real time accuracy is that good, further smoothing before prediction becomes (nearly) obsolete.

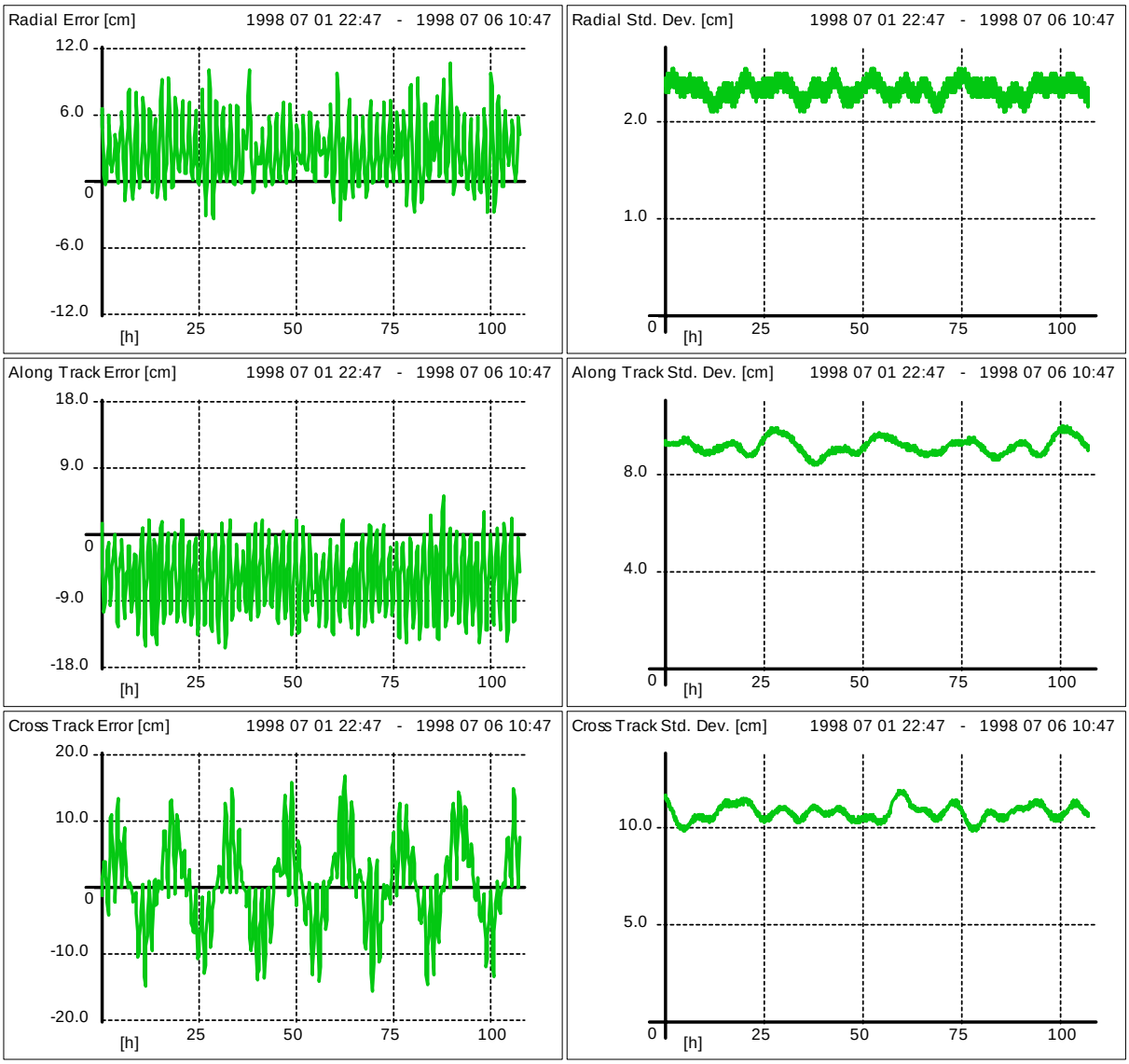

Figure 6-35 Tracking Accuracy of MEO all available ISL's

6.2.8 Galileo 2 (GEO/MEO)

6.2.8.1 Ground Tracking

The second option for Galileo shows a slightly higher real time orbit determination accuracy, although using the same network. This is due to the higher inclination of the orbit planes providing a slightly better observation geometry. Standard deviations and real orbit errors for the MEO satellites can be taken from the following figure.

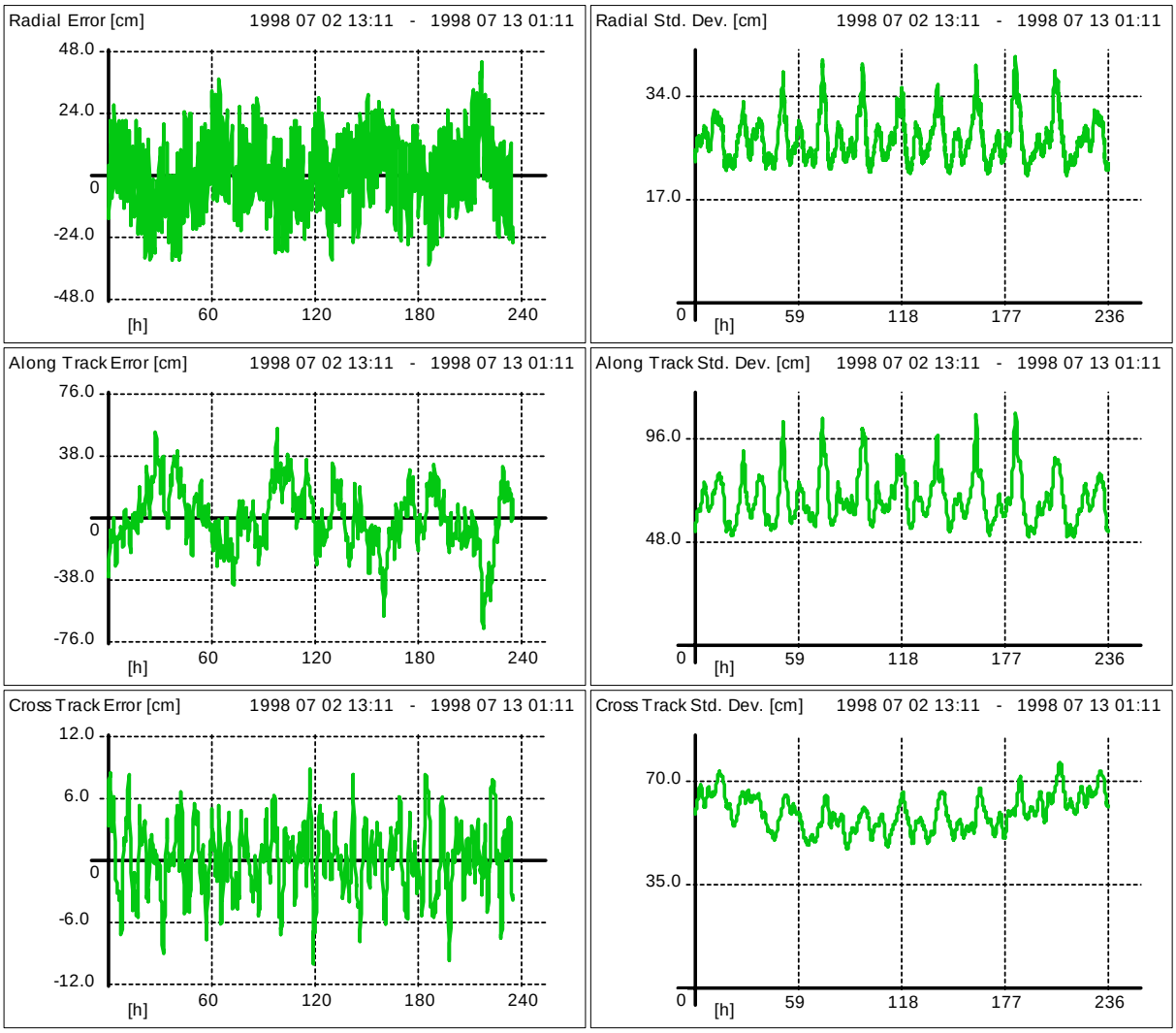

Figure 6-36 Tracking Accuracy of MEO using Galileo Network

The orbit determination accuracy for the GEO is not as good due to a worse observation geometry, but still in a reasonable range. Further post processing of the orbit is definitely necessary.

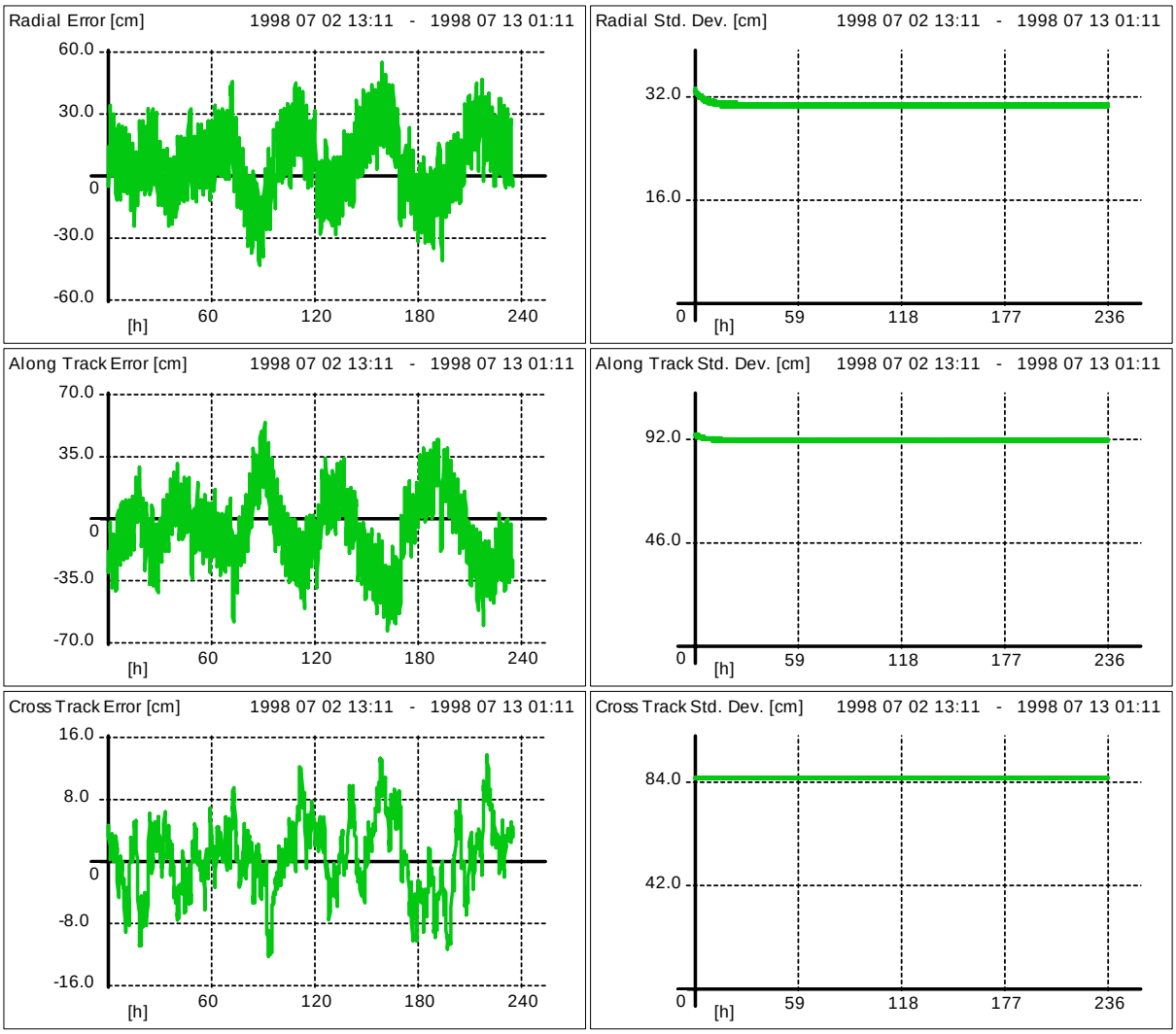

Figure 6-37 Tracking Accuracy of GEO using Galileo Network

6.2.8.2 Ground and Intersatellite Tracking (Full Network)

The following scenario has been processed using all available types of inter satellite links, but limiting the number of simultaneous ISL's to 6. It can be seen that orbit deteremination accuracy is improved well below 10 cm in radial direction for both types of satellites. The following picture show the accuracy figure for the MEO satellites.

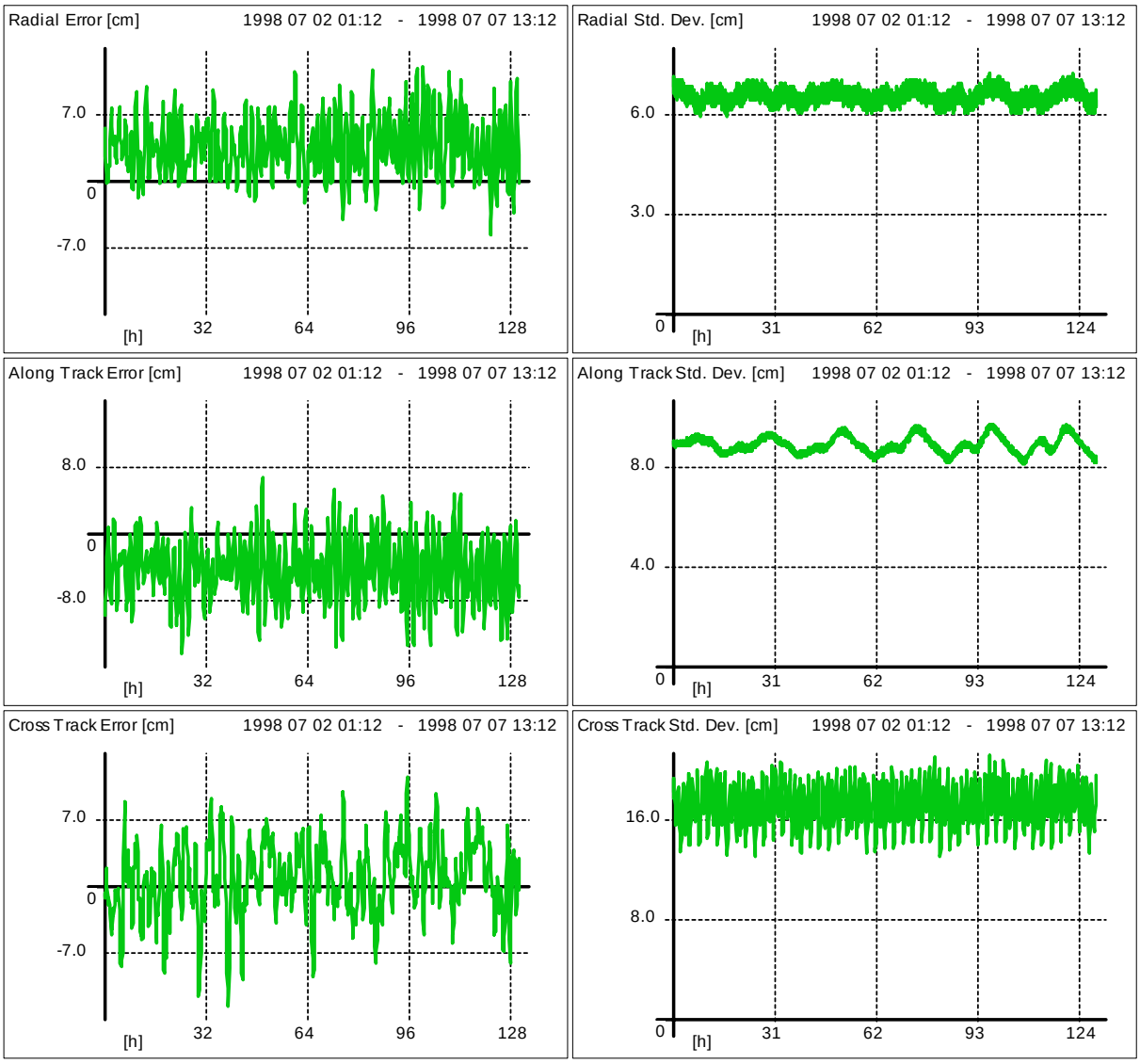

Figure 6-38 Tracking Accuracy of MEO using ISL's

The next picture shows the accuracy figure for the GEO satellites. Radial accuracy is nearly as good as for the MEO, only the tangential accuracy is slightly worse.

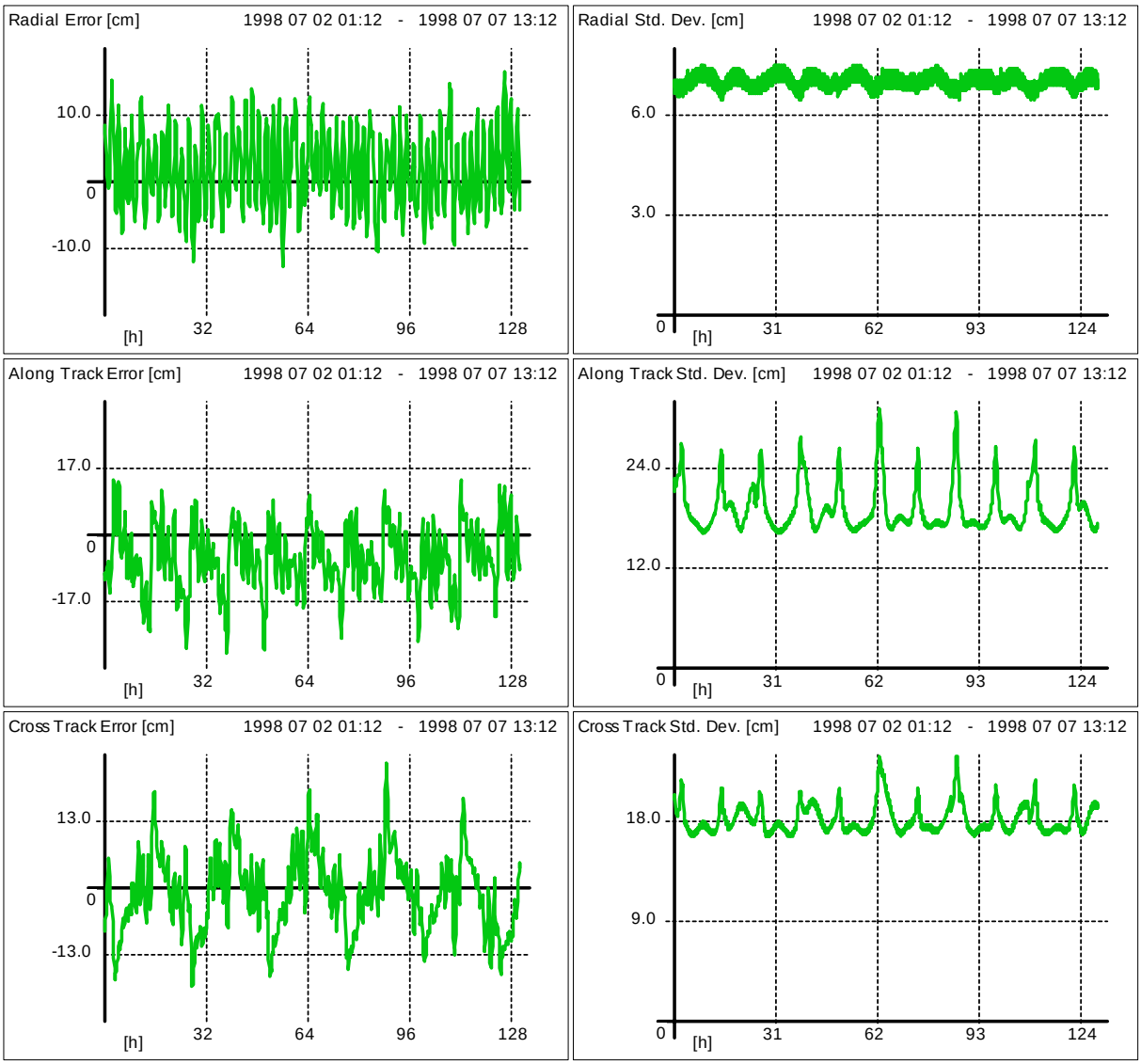

Figure 6-39 Tracking Accuracy of GEO using ISL's

6.3 Accuracy of Broadcast Ephemeris (User Ephemeris)

The ephemeris of a navigation satellite, which is broadcast to the user is derived in several steps:

t0 – t1	**Observation and Processing:** From observation, the error with respect to a reference trajectory is determined. This is done either by real time estimation (Kalman filtering) or in batch process. The result is a time series of satellite positions, as well as some estimated physical model parameters.
t1 - t2	**Propagation and Adjustment:** The satellite trajectory is propagated ahead in time, from t1 up to t2 using the best estimate of the satellites state vector as well as the best available force model. Due to limitations in the accuracy of determining the state vector, as well as the model parameters, the position of the satellite will diverge from the true position with time. A simple orbit propagation model will be adjusted to this propagated trajectory. These are the broadcast or user ephemeris.

Therefore, quality of the broadcast ephemeris is driven by multiple factors:

- Model fitting error: even is the model is fitted on the (in reality unknown) true trajectory, it will have an error due to its simplicity.
- Orbit determination error: even if the satellite trajectory is propagated using a perfect force model, the initial position and velocity will not be perfect, due to limitations in the orbit determination process.
- Orbit propagation error: even if the initial state (position / velocity) of the satellite would have been known perfectly, the imperfection of the force model will cause the propagated trajectory to diverge slowly from the true one.

6.3.1 Model Fitting Error

In the following simulations, several candidates for broadcast ephemeris have been evaluated by fitting them over a specified orbit arc. The orbit class has been varied from about 1250 km orbit altitude (LEO) up to 36000 km (GEO). The error has been derived by comparing the position derived from the broadcast model with that derived from a high order force model integration.

Four different broadcast ephemeris models have been evaluated. All four models are described in chapter 4.

- The GLONASS model using 9 degrees of freedom
- GLONASS type force model integration model using 12 degrees of freedom

- GLONASS type force model integration model using 15 degrees of freedom.
- GPS broadcast ephemeris model using 15 degrees of freedom

To obtain the fitting error only, the models have been adjusted to the true trajectory. The fitting interval has been varied to obtain the sensitivity of the model to this parameter. The error has been given in terms of URE (see chapter 5). The following table indicates the results.

Orbit Class / Fitting Interval	**GLONASS 9 DOF**	**"GLONASS" 12 DOF**	**"GLONASS" 15 DOF**	**GPS 15 DOF**
LEO (1250 km) 1h	150 – 250 m	40 – 110 m	25 - 40 m	23 – 29 m
LEO (1250 km) 30 min	15 - 40 m	5 – 15 m	1.5 – 5 m	2.5 – 6 m
LEO (1250 km) 15 min	1.5 – 8 m	0.5 – 2 m	7 – 25 cm	0.2 – 0.8 m
MEO (26000 km) 30 min	1 – 4 cm	3 – 5 mm	~ 0	-
MEO (26000 km) 1 h	5 - 25 cm	5 – 35 mm	3 – 5 mm	5 – 8 cm
MEO (26000 km) 2 h	0.9 – 1.2 m	0.3 – 0.5 m	4 – 6 cm	8 – 10 cm
MEO (26000 km) 1 Orbit	166 m	55 m	~ 32 m	~ 10 m
GEO / IGSO 1 h	1 – 8 cm	5 mm	~ 0 mm	(2 – 5 cm)
GEO / IGSO 2 h	10 – 50 cm	1 – 5 cm	5 mm	1 – 5 cm
GEO / ISGO 4 h	2 – 4 m	0.2 – 0.5 m	1 – 8 cm	2 – 10 cm

Table 6-2 Fitting error

If we look at the table we see that the fitting error is expressed as a range of URE, not as one constant value. This is due to the broadcast ephemeris model has a different fitting error over different portions of the orbit. Looking at the three GLONASS type models, it can be seen that with growing complexity, or degrees of freedom, the error decreases. The same holds for a decrease in fitting interval. Now if we compare the 15 DOF GLONASS type model with the GPS model which has also 15 degrees of freedom, it can be seen that for short fit intervals the force model integration yields nearly arbitrary small fitting errors. In fact, this model could be fitted to an orbit arc of a few seconds, as long as the arc is represented by more than five position vectors. The GPS model, although offering also 15 degrees of freedom, can for example not be fitted over a MEO orbit arc shorter than one hour. Due to the involved estimation of Kepler elements, the estimation process does not converge for such a short orbit. The representation of an orbit based on keplerian parameters is more suited for longer orbit

arcs. For example, if the broadcast model is fit over a complete MEO orbit, the GPS model yields an errors smaller than the 15 DOF force model integration.

The estimation of Keplerian elements bears some additional problems: if orbits with excentricity of inclination near zero have to be repesented, additional contrains have to be introduced to make the least squares estimation process converge.

6.3.2 Orbit Determination and Propagation Error

To obtain useful broadcast ephemeris, the fit interval has to reside in the future. Therefore, the determined orbit has to be propagated from the last known position using a sophisticated force model. The orbit determination process yields a position, which is accurate only to certain degree. If propagated, it will slowly diverge from the true orbit. In the following example the orbit of a satellite from the Galileo Option 1 constellation has been determined using ground links only. The satellite position and velocity estimated by the real time Kalman filter yields a relatively noisy estimate of the satellite state vector with a 1 σ accuracy of around

- 35 cm in the radial component
- 1 meter in the along track component
- 80 cm in the cross track component

Note, that the real error needs not to be as high as that. The accuracy is taken from the covariance matrix of the filter and represents the internal confidence of the estimation. If this raw estimate is propagated without further smoothing, the orbit errors increase with time relatively fast, as depicted in the following figure.

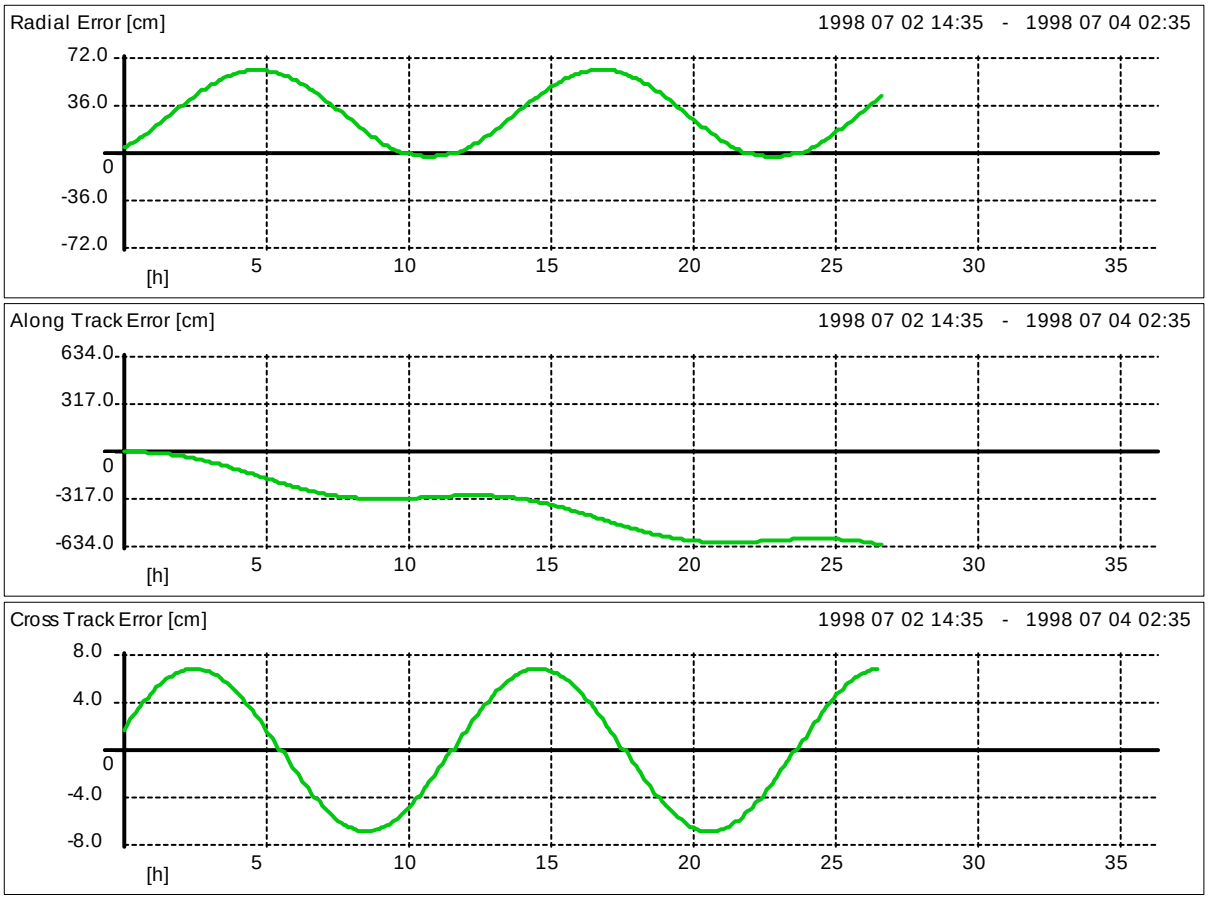

Figure 6-40 Propagation Error MEO raw estimate ground only 12 states 1 hour

The radial and cross track component of the orbit show periodic variations, but the along track error has also a linear error superposed, growing with time. If for example GLONASS type 12 DOF broadcast model is fit over such an orbit, the result is an URE also increasing with time, as can be seen in the following figure.

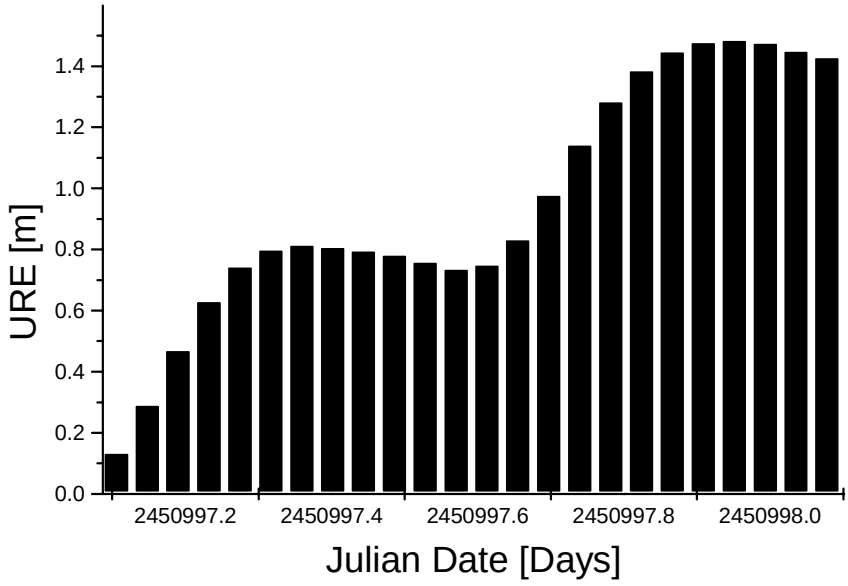

Figure 6-41 Ageing of Ephemeris MEO, raw estimate ground only 12 states 1 hour

Each bar represent the URE of one set of parameters valid for one hour. The satellite ephemeris are degrading fast with time and exceed the 1 meter level after approximately 15 hours.

In the next example, the same determined satellite orbit is used, but now the last 6 hours of position estimates are used to derived a smoothed initial position for the propagation process. This is achieved by feeding a least squares estimator with the positions an estimating the "true" position at the initial epoch. The follwong figure shows the orbit error evolution, if this smoothed position is now propagated.

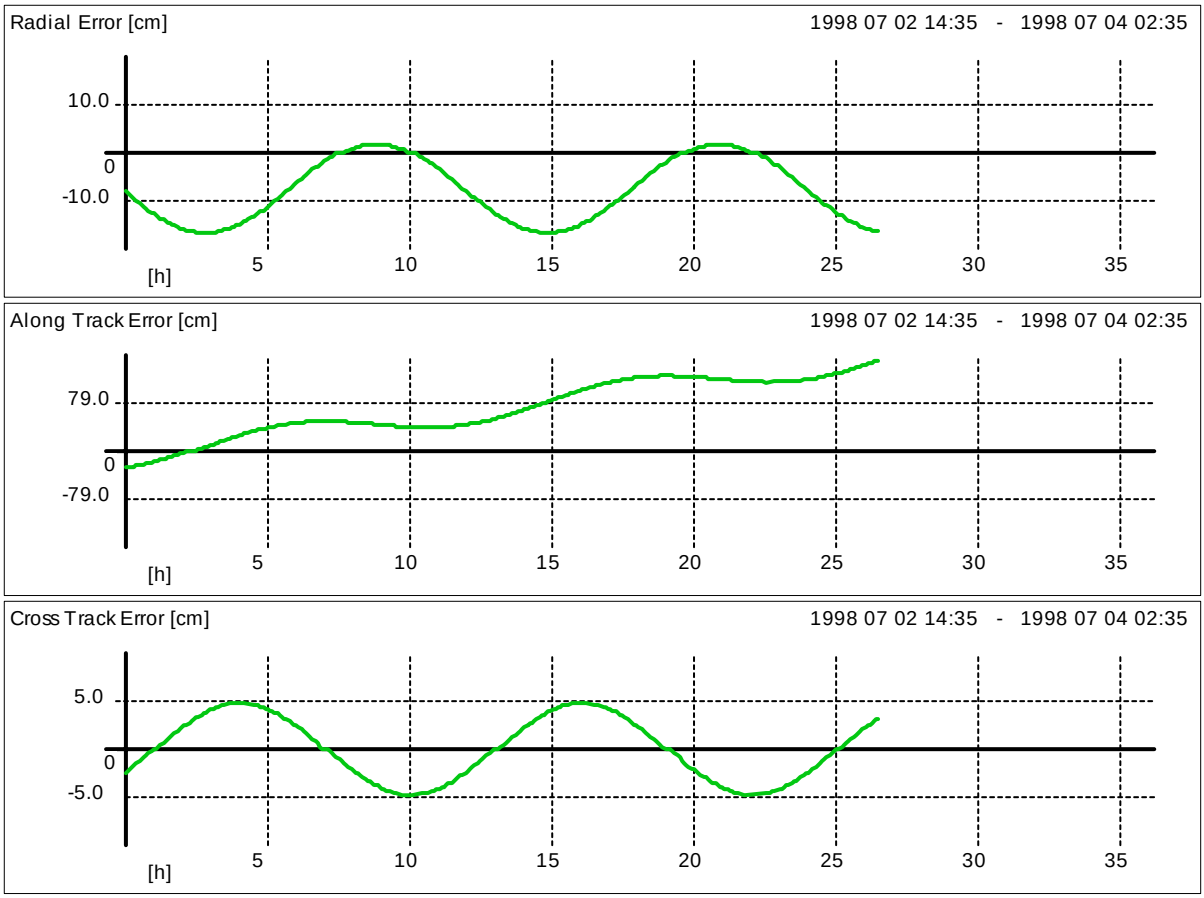

Figure 6-42 MEO propagation error with 6 hour smoothing

The along track error also shows a secular error tendency, but much smaller than that of the propagated raw estimate. If the same broadcast model is fit over this propagated orbit, the URE remain below 30 cm even nearly up to 24 hours, as can be seen in the following picture.

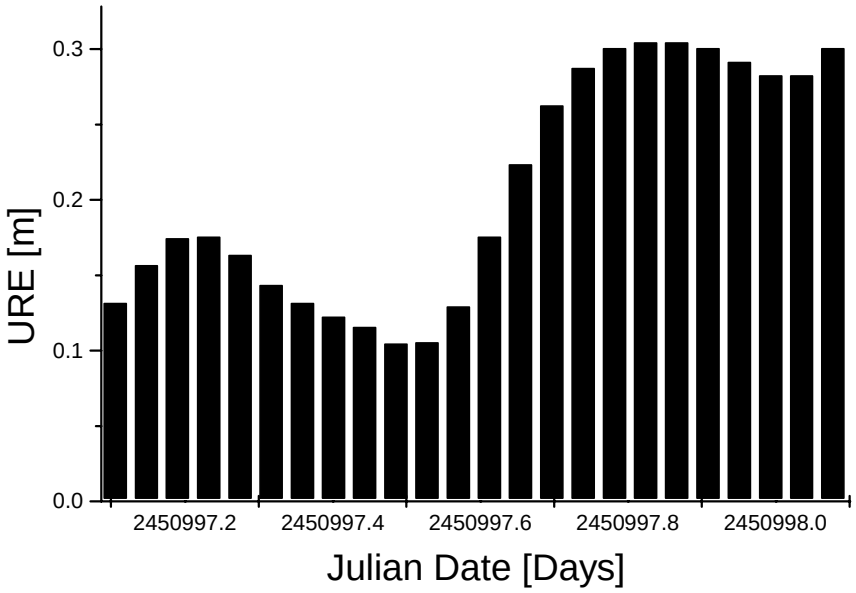

Figure 6-43 Ageing of MEO Ephemeris with 6 hours smoothing

Now let us increase the smoothing interval. The following two figures show the propagation error and the degradation or ageing of the broadcast ephemeris, if the raw estimate of the orbit is smoothed over 12 hours, corresponding to nearly one complete orbit.

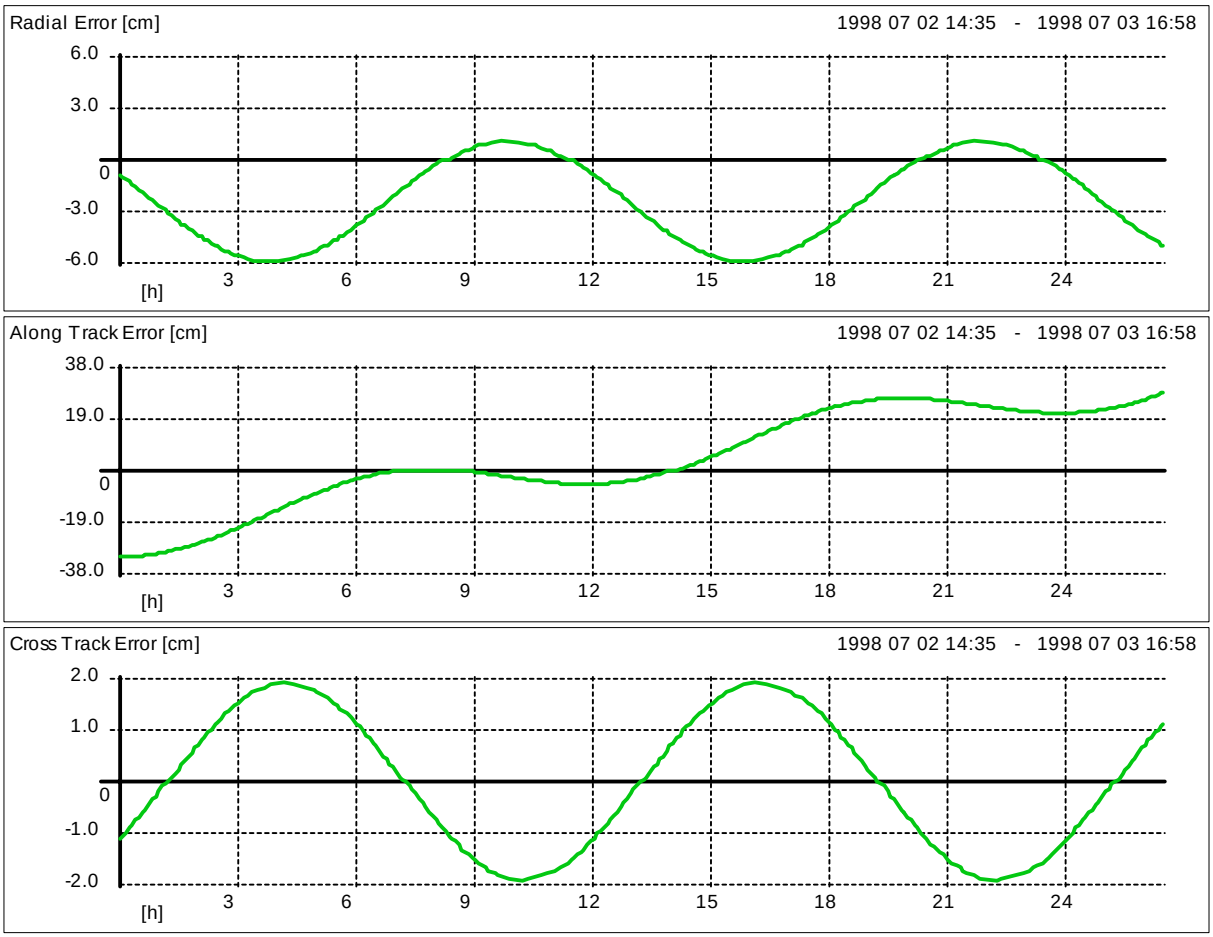

Figure 6-44 MEO Propagation Error with 12 hours of smoothing

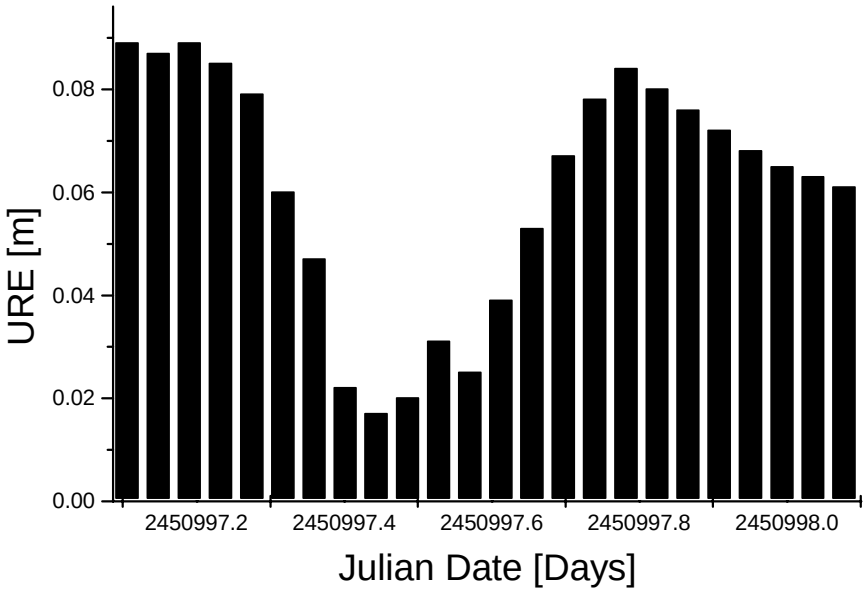

Figure 6-45 URE with 12 hours smoothing

Orbit errors, as well as URE remain below 10 cm up to 24 hours.

In the last example the raw estimate is used again for propagation, but this time it has been derived using inter satellite links. From chapter 6.2.7 it can be seen that the standard deviations, as well as the real orbit errors are much lower compared to ground based only orbit determination.

- around 2.5 cm radial error (1 σ)
- 9 cm along track error (1 σ)
- 11 cm cross track error (1 σ)

The following figure show the orbit propagation error, as well as the URE of the broadcast ephemeris for this tracking scenario.

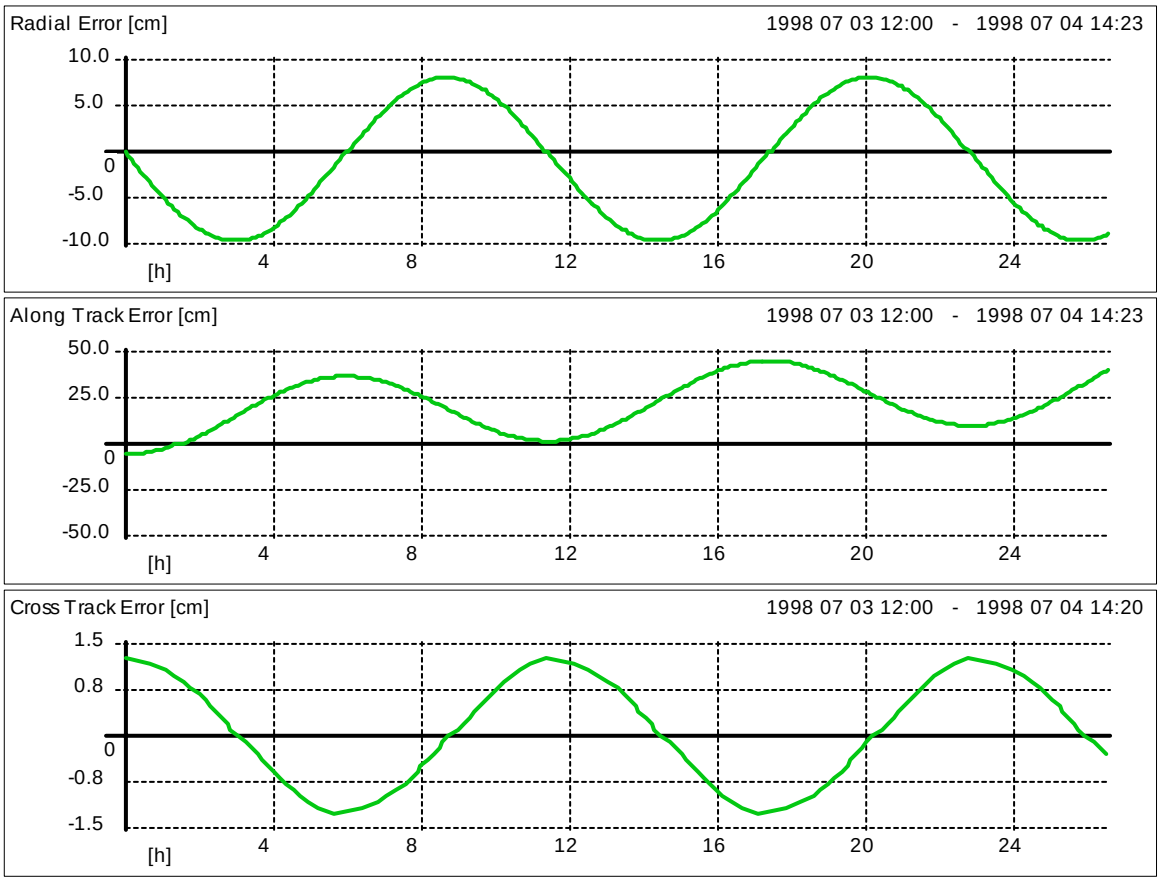

Figure 6-46 MEO Propagation Error without smoothing derived from Raw Estimate using ISL's

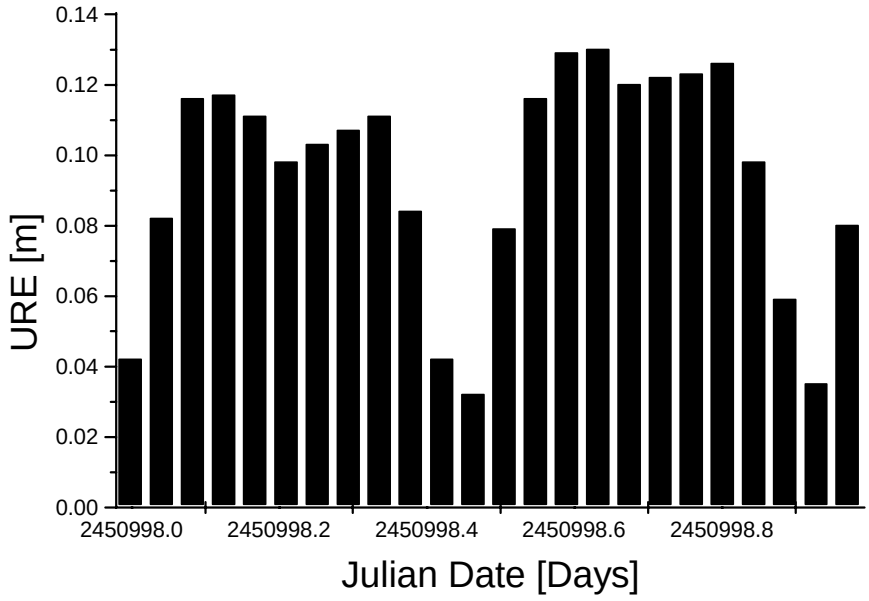

Figure 6-47 URE without smoothing using ISL's

Although the raw estimate has not been smoothed, the orbit prediction error is relativly small if compared to the propagation of the raw estimate derived from ground based only tracking. A better prediction accuracy can only be achieved if the determined orbit is smoothed over a sufficient long period (approximately one orbit revolution).

This fact bears an interesting option if fast generation of broadcast ephemeris together with a reduced computation load is desired, which is especially interesting for board autonomous ephemeris generation.

Of course, if highest precision is desired, the ISL aided orbit determination can be smoothed to. The last two figures show propagation error and broadcast ephemris degradation if the raw estimate is smoothed over 12 hours prior to propagation.

Note that although the values seems to be slightly better than in the example for the ground based only derived orbit with 12 hour smoothing, there is in fact no relevant difference in the orbit accuracy. If the orbit is smoothed a sufficient time prior to propagation, it makes no difference if the raw estimate has been of high or medium accuracy.

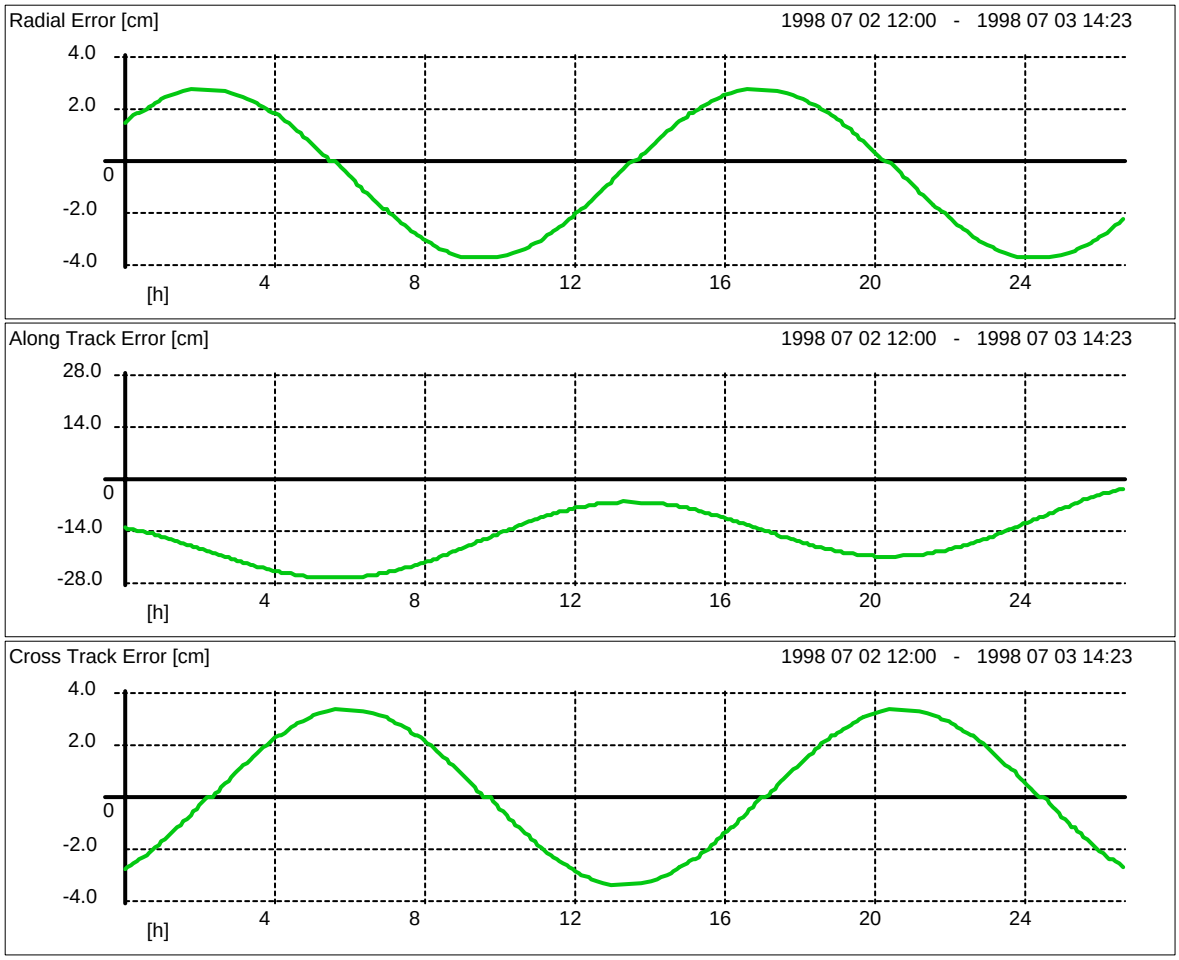

Figure 6-48 MEO Propagation Error with 12 hours smoothing using ISL's

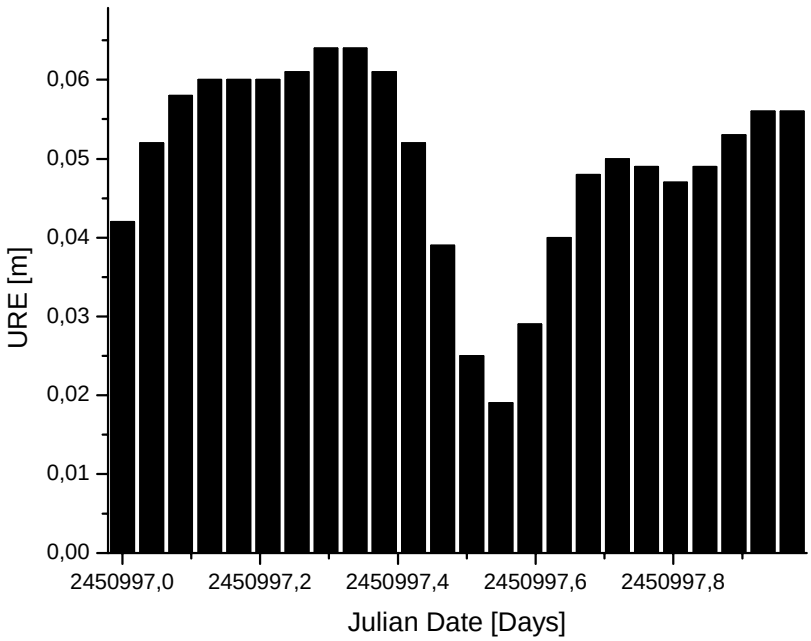

Figure 6-49 URE with 12 hours smoothing using ISL's

6.3.3 Ephemeris Accuracy of Scenarios

In the following section, the achievable accuracy of broadcast ephemeris has been investigated for the different scenarios. To get comparable results, the 15 degree of freedom GLONASS type ephemeris model has been used for all constellations. However, the fit interval has been adopted to the different orbit types to obtain a "useful" accuracy in terms of URE. The following table indicates the fit intervals chosen for the different orbit classes:

Orbit Class	**Fit Interval**
LEO 1250 km	15 Minutes
MEO	2 hours
GEO / IGSO	4 hours

Input to the simulations had been the reference orbits and estimated orbits from section 6.2. One has to keep in mind that the propagation of the raw estimate bears some danger: the position error will not be the same for all "starting position", because the real error is not constant but shows a noise / random walk behaviour within the 3 sigma margin (see section 6.2). Therefore some of the raw estimates had to be replaced by an artificial introduced small offset to obtain the results. However, the numbers derived are representative.

6.3.3.1 Optimized GPS

Tracking Scenario	Mean URE over 24 Hours	Worst URE within 24 Hours
Raw Estimate Reduced Net	56 cm	82 cm
Raw Estimate Full Net	30 cm	42 cm
Smoothed Over 12 Hours	3 cm	5 cm

6.3.3.2 IGSO Walker Constellation

Tracking Scenario	Mean URE over 24 Hours	Worst URE within 24 Hours
Raw Estimate Full Net	103 cm	161 cm
Raw Estimate Full Net with ISL	26 cm	37 cm
Raw Estimate Reduced Net with ISL	26	44
Smoothed Over 12 Hours	16 cm	25 cm

6.3.3.3 IGSO on Three Loops

Tracking Scenario	Mean URE over 24 Hours	Worst URE within 24 Hours
Raw Estimate Full Net	41 cm	52 cm
Raw Estimate Full Net with ISL	20 cm	26 cm
Smoothed Over 12 Hours	18 cm	22 cm

6.3.3.4 GEO / IGSO Constellation

Tracking Scenario	Mean URE over 24 Hours	Worst URE within 24 Hours
Raw Estimate Full Net	52 cm	65 cm
Raw Estimate Full Net with ISL	14 cm	20 cm
Raw Estimate Regional Net with ISL	20 cm	27 cm
Smoothed Over 12 Hours	13 cm	17 cm

6.3.3.5 Pure LEO Walker Constellation

Tracking Scenario	Mean URE over 24 Hours	Worst URE within 24 Hours
Raw Estimate Full Net	175 cm	330 cm
Raw Estimate Reduced Net	192 cm	327 cm
Raw Estimate Reduced Net with ISL	79 cm	173 cm
Smoothed Over 12 Hours	32 cm	61 cm

6.3.3.6 GEO / LEO Constellation

GEO

Tracking Scenario	Mean URE over 24 Hours	Worst URE within 24 Hours
Raw Estimate Full Net	52 cm	65 cm
Raw Estimate Reduced Net with ISL	20 cm	27 cm
Smoothed Over 12 Hours	13 cm	17 cm

LEO

Tracking Scenario	Mean URE over 6 Hours	Worst URE within 6 Hours
Raw Estimate Full Net	175 cm	330 cm
Raw Estimate Reduced Net with ISL	27 cm	35 cm
Smoothed Over 12 Hours	29 cm	52 cm

6.3.3.7 Galileo Option 1 (Pure MEO)

Tracking Scenario	Mean URE over 24 Hours	Worst URE within 24 Hours
Raw Estimate Full Net	32 cm	55 cm
Raw Estimate Full Net with ISL	19 cm	27 cm
Smoothed Over 12 Hours	3 cm	5 cm

6.3.3.8 Galileo Option 2 (GEO / MEO)

GEO

Tracking Scenario	Mean URE over 24 Hours	Worst URE within 24 Hours
Raw Estimate Full Net	52 cm	65 cm
Raw Estimate Full Net with ISL	23 cm	31 cm
Smoothed Over 12 Hours	22 cm	29 cm

MEO

Tracking Scenario	Mean URE over 24 Hours	Worst URE within 24 Hours
Raw Estimate Full Net	32 cm	55 cm
Raw Estimate Full Net with ISL	21 cm	35 cm
Smoothed Over 12 Hours	3 cm	5 cm

7 AUTONOMOUS ONBOARD PROCESSING

7.1 Why Onboard Processing?

In a typical conventional orbit estimation process, ranging signals are transmitted by the satellite whereas measurements are taken by the ground stations. There are two exceptions, the DORIS and the PRARE system: both systems are performing measurements onboard.

- PRARE uses two way the range and range rate measurements in the X-band with phase coherent ground transponders. It has four channels; therefore it is limited to four simultaneous measurements. Moreover, due to the fact that the transponders are phase coherent and X band frequencies require directive antennae, the ground transponders can serve only one satellite at a time. Although PRARE is used for orbit heights between 500 and 2000 km, it is principally not limited to a special orbit class. During the AUNAP project (1996) PRARE has been evaluated as an option for an autonomous navigation processor onboard an IGSO satellite.
- DORIS receives codeless carrier signals on two frequencies (S-band and UHF) from so called ground beacons and performs Doppler[1] measurements. Because range rate measurements are independent of the clock offset, one “Master Beacon” transmits a kind of ranging code, which is needed to perform at least coarse synchronisation of the onboard clocks. Doppler measurements allow precise orbit estimation if the satellite dynamics are high, therefore it is more or less restricted to LEO orbits.

Nevertheless, even in those systems the measurements are downloaded and transmitted via data link to a central facility for further processing. In navigation applications like GPS and GLONASS, the central processing facility performs then orbit determination, orbit prediction and broadcast ephemeris adjustment.

But given the fact that measurements are available, onboard processing has some advantages. The data latency can be reduced to a minimum. Therefore it is best suited for applications were fast reaction is desired. In navigation applications, the following four parameters are a measure for the performance of a system:

- Accuracy
- Availability
- Continuity of Service
- Integrity

The first two parameters are driven by the system’s design. Accuracy is mainly driven by two factors, the radio frequency link (signal-in-space) and the broadcast ephemeris, and can be enhanced e.g. by

[1] Although DORIS performs no ranging but Doppler measurements, the two frequencies are needed to correct for ionospheric effects, which are in fact an issue due to 10 seconds integration time. Because of this long integration time, it would be more appropriate to speak of phase rate instead of Doppler measurements.

- providing two frequencies to allow ionospheric corrections
- increasing chipping rate on the ranging signal
- increasing update rates of broadcast ephemeris
- using accurate broadcast models / short fit intervals
- using accurate clocks

Availability, especially with respect to visibility of enough S/V to perform navigation, is driven by constellation design, and can be enhanced by

- putting enough S/V into service (actives, as well as spares and replenishment)
- choosing benign orbits with respect to visibility

The last two parameters are a bit more critical. They are mainly driven by reliability of the space vehicles and environmental influences degrading the signal-in-space like RF interference, atmospheric effects or jamming. Keeping these parameters high is of utmost interest for civil aviation.

System inherent continuity and integrity of the two existing navigation systems GPS and GLONASS does not meet the requirements of civil aviation and can therefore be not used as a sole means of navigation. To overcome system limitations with respect to integrity, augmentation systems like WAAS, EGNOS and MSAS are under development. Their main output are corrections for

- ionospheric effects
- satellite clock
- satellite ephemeris

emitted by geostationary Inmarsat space crafts. A central processing facility has to recomputed satellite orbits to provide orbit and clock corrections at a high update rate. This has to be done for up to 51 satellites. Fast corrections which are applied directly to the range measurement are provided at an update interval smaller than 6 seconds to meet time-to-alarm requirements for CAT I. So called “long term” corrections provide vector corrections for position and velocity which are updated approximately every 6 minutes. Both, fast and long term corrections have to be applied additionally to the broadcast ephemeris transmitted by the GPS and GLONASS space crafts.

Summarising the measures taken to enhance integrity we find

1. ephemeris correction
2. at a high update rate
3. with minimum data latency
4. and corrections to the ionospheric effects

Future satellite navigation systems like Galileo will provide at least dual or maybe even triple frequency links. Even the existing GPS system is going to be enhanced and the next generation of replenishment satellites (starting with Block II F) will provide a civil available ranging code on two frequencies. What’s left, is the integrity of Satellite orbit and clock.

Now, what this all to do with autonomous onboard processing? The measures 1. / 2. and 3. for one satellite could easily be provided by each satellites onboard processor! Imagine the following: presumed, measurements are taken onboard the satellite. The onboard processor uses these observations to update the error estimates of position, velocity and clock. These errors can directly be used as correction to the ephemeris derived satellite position and therefore be immediately transmitted to the user. Data latency: negligible, especially if compared to a conventional ground based system! This seems should be in fact a sufficient motivation to take the effort with respect to space craft complexity and cost of implementing a onboard processing “facility”.

7.2 Implementation Aspects of Onboard Processing

The software for an autonomous onboard processor has to satisfy some requirement depending on the tasks to be performed. The complete chain from the raw measurements to integer ephemeris information for the navigation user requires the software to provide following functionalities:

- conversion of raw measurements to ranges and range rate observables
- detection and isolation of outlying measurements
- orbit propagation using a precise force model
- estimation of orbit and clock errors from measurements
- a possibility to reset the state estimator if desired or necessary
- coordinate conversion from a terrestrial reference frame to ECI-J2000
- accept upload of celestial body ephemeris, earth rotation parameters ...
- adjusting the broadcast message to a period of predicted position vectors.
- detection and computation of required orbit manoeuvres to maintain desired orbit properties.
- orbit propagation using the broadcast message
- detection and isolation of abnormal clock drift or orbit degradation
- integrity check on the ephemeris and clock parameter message delivered to the user
- accept new upload from ground for reference trajectory data
- consistency check of own computed data

Not all tasks have the same performance requirements. The used CPU should be fast enough to allow at least one duty cycle per second for the integrity processing. Orbit prediction for example can be performed with slower update rates. Integrity checks of ephemeris and clock parameters have to be performed once per second.

The measurements can be ground links, as well as inter satellite links. These are especially valuable to check integrity of the satellite ephemeris.

7.2.1 Complexity of Orbit Prediction and Estimation Algorithms

According to estimations made during the AUNAP project, the computational load for the model using a 4 x 4 earth model requires about 5 – 10 percent of today available space qualified CPU's if performing one duty cycle per second. Also, in the DIODE experiment, a 15 x 15 gravity model has successfully been used in an onboard processor. The following figure shows a block diagram of the precise orbit estimation process.

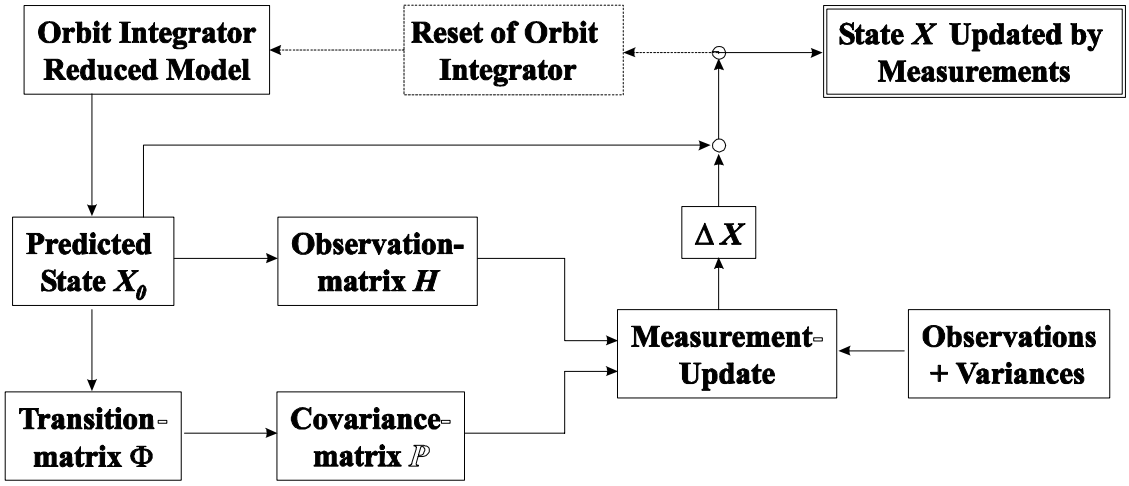

Figure 7-1 Block Diagram of Orbit Determination

The orbit integrator is needed twice, as non linear state predictor in the state estimation process and after determination of an accurate satellite state vector, for orbit propagation. An additional orbit propagator based on the broadcast ephemeris model is also needed.

The following table contains an estimation of the algorithmic complexity of an orbit estimation process (precise estimation). These numbers have been investigated during the German AUNAP project.

All Routines, one Duty Cycle	Add / Subtract	Mul / Div	math. Func.	Loops / Cond. Instructions	Assignments
11 States 8 Obs. GP 4 x 4	15409	19015	826	6216	12614
11 States 8 Obs. GP 15 x 15	33537	27611	10022	7888	25814
11 States 8 Obs. GP 70 x 70	554653	1058323	235878	45288	316874

Table 7-1 Estimated Algorithmic Complexity of Orbit Estimation Process (AUNAP 1996)

From experiences made during this project regarding execution times of different software modules, and under the assumption that the CPU is approximately 20 times slower than a 350 MHz Pentium II, a very rough estimate can be derived for the required computational power onboard a satellite:

~ 100 ms for orbit determination (including non-linear state prediction) per measurement epoch (realtime)

~ 30 ms for orbit propagation per epoch, i.e. 1 s to generate 50 trajectory points ahead, separated 144 s. (offline)

~ 10 s for fitting a 2-hour-valid broadcast ephemeris over approximately 50 trajectory points. (offline)

~ 2 ms for orbit propagation per epoch using broadcast ephemeris force model (for other satellites in constellation); for 20 ISL's requiring 40 ms. (realtime)

~ 50 ms to perform a RAIM-like algorithm using 20 ISL's (realtime)

This results in approximately 200 ms for the tasks which have to be performed in realtime, i.e. once per second, in order to achieve integrity requirements. The remaining 800 ms per one-second-duty-cycle can be used to perform sequentially the (slightly more than) 10 s offline task. The 2-hour-valid broadcast ephemeris could updated, say every 30 minutes and would require less than 6 ms of computing time per one-second-duty-cycle, i.e. 0.6% of the available computing power.

Note that this is a very rough preliminary estimate, but it seems to be feasible to perform all these tasks, required for full autonomous onboard processing with 20% – 25% of the available computing power.

7.2.2 Onboard Processing using ISLs

Inter satellite links are per definition measurements which are taken onboard and therefore seem to perfectly match the requirements for an onboard processor. But ISL's bear some problems for a constellation consisting of autonomous processing satellites.

The optimal approach to process ISL's would be, to process all measurements and all satellites states in one large filter. This is hard to achieve, if each satellite has its own state estimator onboard. The following example shall highlight how satellite state estimates get correlated by the inter satellite links.

Let us assume 3 satellites , represented by their state $X_{1,2,3}$. The measurements are processed together in on Kalman filter some other least squares estimator. The state transition of all three satellites can be written as

$$\begin{bmatrix} x_1 \\ x_2 \\ x_3 \end{bmatrix}_k = \begin{bmatrix} \Phi_1 & 0 & 0 \\ 0 & \Phi_2 & 0 \\ 0 & 0 & \Phi_3 \end{bmatrix}_k \cdot \begin{bmatrix} x_1 \\ x_2 \\ x_3 \end{bmatrix}_{k-1} \qquad \text{Eq. 7.2-1}$$

Up to that point, the covariances of the satellites are assumed to be uncorrelated.

$$P = \begin{bmatrix} p_{11} & 0 & 0 \\ 0 & p_{22} & 0 \\ 0 & 0 & p_{33} \end{bmatrix} \qquad \text{Eq. 7.2-2}$$

Now, satellite number one is transmitting an inter satellite ranging signal which is received by satellites number two and tree. Therefore, the measurement equation system is written as

$$\begin{bmatrix} z_{13} \\ z_{12} \end{bmatrix}_k = \begin{bmatrix} h_{11} & 0 & h_{13} \\ h_{21} & h_{22} & 0 \end{bmatrix}_k \cdot \begin{bmatrix} x_1 \\ x_2 \\ x_3 \end{bmatrix}_{k-1} \quad , \quad R = \begin{bmatrix} r_{13} & 0 \\ 0 & r_{12} \end{bmatrix} \qquad \text{Eq. 7.2-3}$$

with R being the covariance matrix of the (uncorrelated) measurements. The indices for the measurements z and variances r represent the link direction, i.e. z_{13} means "link from satellite one to satellite three". Let us now only look at the equation concerning the Kalman gain matrix,

$$K = PH^T\left(HPH^T + R\right)^{-1} \qquad \text{Eq. 7.2-4}$$

which is a 3 x 2 matrix. The element K_{jk} contains the effect of the k^{th} measurement on the j^{th} state. Performing the equation using our presumptions above leads to a lengthy expression. Here, we only concentrate on a few elements. K_{32} contains the effect of the measurement between sat1 and sat2 (measured by sat2) on the state of sat3. The expression is none-zero and requires all partial matrices to be evaluated.

$$K_{32} = -\left(h_{11}h_{13}h_{21}p_{11}p_{33}\right)\cdot \det(\text{Inv}) \qquad \text{Eq. 7.2-5}$$

with

$$\det(\text{Inv}) = \frac{1}{h_{11}^2h_{22}^2p_{11}p_{22} + h_{13}^2h_{21}^2p_{11}p_{33} + h_{13}^2h_{22}^2p_{22}p_{33} + h_{11}^2p_{11}r_{12} + h_{13}^2p_{33}r_{12} + h_{21}^2p_{11}r_{13} + h_{22}^2p_{22}r_{13} + r_{12}r_{13}} \qquad \text{Eq. 7.2-6}$$

The problem is that the measurement sat1-sat2 is not available at sat3. The Kalman gain on the state of sat2 evaluates to

$$K_{22} = h_{22}^2p_{22}\left(h_{11}^2p_{11} + h_{13}^2p_{33} + r_{13}\right)\cdot \det(\text{Inv}) \qquad \text{Eq. 7.2-7}$$

if all three satellites are processed in one filter.

Let us assume now that we split the filter and process the measurement sat1-sat2 and sat1-sat3 independently in two separate filters.

$$z_{13} = \begin{bmatrix} h_{11} & h_{13} \end{bmatrix} \cdot \begin{bmatrix} x_1 \\ x_3 \end{bmatrix} \quad , \quad P_{filter1} = \begin{bmatrix} p_{11} & 0 \\ 0 & p_{33} \end{bmatrix} \qquad \text{Eq. 7.2-8}$$

$$z_{12} = \begin{bmatrix} h_{21} & h_{22} \end{bmatrix} \cdot \begin{bmatrix} x_1 \\ x_2 \end{bmatrix} \quad , \quad P_{filter2} = \begin{bmatrix} p_{11} & 0 \\ 0 & p_{22} \end{bmatrix}$$

Both filters contain the state of sat1, because sat1 is involved in both measurements . The Kalman gain for the sat2 state is now obtained by

$$K_{22} = \frac{h_{13} p_{33}}{h_{11}^2 p_{11} + h_{13}^2 p_{33} + r_{13}} \qquad \text{Eq. 7.2-9}$$

It can also be shown that both filters yield Kalman gain factors also for sat1, which will not be equal.

All measurements, covariances and satellite states should be available at the same time in the same place to perform an optimal estimation. The easiest way to achieve this would be to download the measurements and process inter satellite links on ground and in post processing. Unfortunately this removes one of the greatest benefits of the inter satellite links with respect to autonomy.

The second approach, to process two satellites pair-wise leads to sub-optimal but maybe also satisfactory results.

A third approach consists in the processing of inter satellite links without estimating the sending satellites state. This would require the smallest amount of communication between the satellites. The partner satellites simply transmit their state vector (or corrections to the state vector) which are frequently updated. In fact, this seems to be the only feasible way.

7.3 Application Example: Availability during Orbit Manoeuvres

Perturbations acting on the satellites orbit make it necessary to correct the space craft trajectory from time to time in order to maintain the desired orbit. These orbit corrections, achieved by activating the spaces craft's propulsion system, lead to a discontinuity in the acceleration acting on the satellite. Although it is no problem to account for thrust forces in the numerical integration during a propulsive flight phase, the accuracy of the broadcast message, which has to be fit over a certain period of validity, will be degraded if engine start or cut off falls within that time span. The amount of degradation depends strongly on the thrust level.

Unintentional thrusters firing on the other hand issues an integrity problem, because the broadcast ephemeris do not apply anymore. This means, the user computes his position relative to a satellite based a wrong S/V position information. However, this topic shall be addressed in the next section.

The conventional approach (GPS for example) is to set the space craft status to unhealthy, short before an orbit manoeuvre and up to the time when the orbit determination provides

nominal accuracy again. A drawback of this strategy is a service interruption during orbit manoeuvres and for a small period afterwards. It leads to an orbit maintenance strategy consisting of infrequent, large orbit corrections. For a highly available system it is desired to keep this service interruption as short as possible.

The amount of fuel which can be store aboard a space craft is, besides battery and solar panel life time, one of the main life time drivers. A satellite consumes propellant to maintain its orbital position. If the complete fuel is burnt, the space craft goes out of services. One of the possibilities to prolong satellite life time is to use high impulsive propulsion, like ion engines. Especially for station keeping of GEO satellites, this is an extreme interesting option. New commercial satellite platforms like the Hughes HS 601 and HS 702 series already offer ion propulsion as an option.

Due to the low mass exhaust and therefore low thrust levels of ion engines, powered flight phases are much longer and have to be performed more frequent, compared to conventional chemical propulsion. Because it would not be acceptable to have that frequent service interruptions, the use of ion propulsion implies the integration of the powered flight phase into normal service, i.e. the broadcast ephemeris have to be adjusted to thrust phases as well as to free flight phases. An ion engine would require too much time for a large (and infrequent) orbit correction manoeuvre, as will be demonstrated by the following example.

	HS 601 HP Thrusters	**HS 702 Thrusters**
Diameter	13 cm	25 cm
Specific Impulse	2568 s	3800 s
Thrust	18 mN	165 mN
Power Consumption	0.5 kW	4.5 kW

Table 7-2 Characteristics of Hughes XIPS Ion Drives

A space craft with a mass of 550 kg (typical End-Of-Life mass) has to be accelerated by 50 m/s using the HS 601 HP ion drive described above. From combining the following equations

$$\Delta v_{ideal} = c_{effective} \cdot \ln\left(\frac{m_{Start}}{m_{Cutoff}}\right) = I_{SP} \cdot g_0 \cdot \ln\left(\frac{m_{Start}}{m_{Cutoff}}\right) \qquad \text{Eq. 7.3-1}$$

$$m_{Cutoff} = m_{Start} - \dot{m} \cdot t_{Burn}$$

$$T = \dot{m} \cdot c_{effective} = \dot{m} \cdot I_{SP} \cdot g_0$$

with

$c_{effective}$ Effective exhaust velocity

T Thrust (2 thrusters are used)

m mass

I_{SP}	Specific Impulse
g_0	nominal gravity force (9.81 m/s²)

we can estimate the required burn time by

$$\frac{m_{Start} - t_{Burn} \cdot \frac{T}{I_{SP} \cdot g_0}}{m_{Start}} = e^{\left(-\frac{\Delta v}{I_{SP} \cdot g_0}\right)} \qquad \text{Eq. 7.3-2}$$

$$t_{Burn} = \frac{I_{SP} \cdot g_0 \cdot m_{Start}}{T} \cdot \left(1 - e^{\left(-\frac{\Delta v}{I_{SP} \cdot g_0}\right)}\right)$$

$$t_{Burn} \approx 7.63 \cdot 10^5 \, s \approx 212 \, h$$

For station keeping of a GEO satellite, Hughes therefore recommends two 5 hour propulsive phases per day. To provide nominal availability of GNSS 2, the satellites will have to be available during these propulsive phases. Although there are further developments like the HS 702 thruster providing 165 mN thrust, there are still 2 x 30 minutes thrust phases per day required for station keeping. Thus, the broadcast message has to be adapted to account for the frequent or nearly permanent presence of propulsive forces. There are several possibilities to do that.

7.3.1 Continued Service during Manoeuvres

If a broadcast message format similar to the GLONASS navigation message is used, where the satellite position is derived from numerically integrating a simple force model, and presumed the thrust phase is sufficiently short, a special navigation message extender could be send. Such a message could look like the following

ENGINE_START_TIME
ENGINE_CUT_OFF_TIME
AVARAGE_THRUST_X
AVARAGE_THRUST_Y
AVARAGE_THRUST _Z

Table 7-3 Thrust Phase Navigation Message Extension

The user receiver would than simply add the thrust forces during the time span covered by the navigation message extender. A geometric ephemeris format based on Keplerian elements,

like the one used by GPS, is much less suited for augmentation. The propulsive forces would have to be modelled as generic “orbit perturbations” which is likely to require more model parameters than in the example above. Although limited to short thrust periods, this method is suited for nearly arbitrary (high) thrust levels.

If thrust levels are low (low thrust chemical or ion propulsion), the thrust can be considered as an additional force in the orbit prediction process. The normal broadcast message is then fit over an interval containing a thrust phase, as would be over a normal free flight phase.

The error introduced by this depends strongly on the acceleration by the propulsion system. If the error introduced remains small, this solution would be favourable, because there is no additional navigation message. In the following, results concerning this method will be shown.

To evaluate the errors introduced by orbit manoeuvres, three different orbit types have been considered: GEO, IGSO and LEO. Thrust and velocity increment have been altered to simulate typical manoeuvres. The following table shows the parameters used in the simulation.

	Chemical Propulsion	**Ion Propulsion**
Specific Impulse	315 s	2568 s
Thrust	4 x 10 N	2 x 18 mN
Burn Time for a 50 m/s Manoeuvre	11.36 min	Not Considered (212 h ~ 9 days)
Burn Time for a 1 m/s Manoeuvre	13.7 s	4.2 h

Table 7-4 Simulation Parameters

The chemical propulsion case is represented by 4 x 10 Newton thrusters using storable propellant like MMH / NO_4 . The ion propulsion consist of two Hughes XIPS thrusters from the HS 601 HP.

Two manoeuvres have been performed for all three satellite types, covering the following cases:

- The 50 m/s manoeuvre represents the case, where orbit manoeuvres are conducted infrequently, with a high velocity increment. This only makes sense using high thrust propulsion, thus the ion propulsion has not been considered for this case.
- The 1 m/s manoeuvre represents the case, where orbit manoeuvres are conducted frequently, but with a low velocity increment. In this case, the ion propulsion has been considered, although the thrust phase is not impulsive, but more like a permanent acting force.

The case where the orbit manoeuvre is performed using the apogee kick motor, has not been considered, because these high thrust engines (> 400 N) are not accurate enough to perform small orbit corrections. Frequently, the apogee-kick is performed using a solid rocket motor, which can't be re-ignited anyway.

The following simulation have been performed considering the orbit manoeuvre in the prediction of the precise ephemeris. The broadcast message, although not intended for propulsive flight phases, has been fit over an interval which contains at least the beginning of the manoeuvre. This is the worst case, because the acceleration changes not smooth, but with a step. The following table represents the simulation results for the three types of orbit manoeuvres.

Manoeuvre	Component	GEO	IGSO	LEO
50 m/s Chemical Propulsion	Radial	1.3 m	72 m	0.4 m
	Along Track	1.4 km	1.2 km	1.5 m
	Cross Track	97 m	891 m	49 m
	URE	221 m	243 m	41 m
1 m/s Chemical Propulsion	Radial	0	1.4 m	0.2 m
	Along Track	51 m	41 m	0.8 m
	Cross Track	11 m	29 m	14.5 m
	URE	8 m	8 m	12.2 m
1 m/s Ion Propulsion	Radial	0 m	0.05 m	0.08 m
	Along Track	0.35 m	0.42 m	0.29 m
	Cross Track	0.35 m	0.31 m	0.17 m
	URE	0.07 m	0.1 m	0.29 m
1 m/s Ion Propulsion 15 Minutes Update Rate	Radial	0.03 m	0.06 m	0.08 m
	Along Track	0.10 m	0.14 m	0.29 m
	Cross Track	0.13 m	0.26 m	0.17 m
	URE	0.05 m	0.07 m	0.29 m

Table 7-5 Ephemeris Error during an Orbit Manoeuvre

The fit error over an interval containing a 50 m/s manoeuvre is intolerable high. In case of a planned orbit correction which requires a high velocity increment, the satellite has to be switched to unhealthy.

A short, but frequently performed orbit correction using chemical propulsion produces also intolerable high fit errors. Due to the fact, that the manoeuvre last only about 14 seconds, the

satellite should be switch to unhealthy. The error introduced by ion propulsion is very low. This is due to the fact that the ephemeris message can easier be fit to a slowly varying force than to a fast changing. The resulting URE is acceptable, when the period of validity is decreased to 15 minutes.

7.3.2 Frequently Updated Ephemeris Corrections

The simulation performed in the preceding section are independent whether the orbit determination is performed onboard or not. Besides the fitting error of the broadcast model, there is another error contributing to the prediction of a power trajectory: the uncertainty introduced by the engine with respect to

- thrust level
- thrust direction
- exact time when nominal thrust level is reached
- engine cut off behaviour.

The significance of these error sources increase with thrust level. During orbit prediction of a powered flight, the Kalman filter process is adapted by increasing process noise.

A major advantage of onboard processing is now that - presumed that measurements are available – orbit corrections can be computed at a high update rate.

7.4 Application Example: Autonomous Onboard Integrity Monitoring

In the following example, an autonomous onboard processing scenario is demonstrated using the Galileo Option 1, consisting of 33 MEO satellites. It is assumed, that the broadcast ephemeris for the next 24 hours have already been determined (onboard or on ground) in post processing, and uploaded. The broadcast ephemeris model used is the 15 parameter extended GLONASS type.

Each satellite has an onboard processor, processing ground and intersatellite links. The onboard processor uses a Kalman filter with the following state vector.

$$\bar{x} = \begin{pmatrix} \Delta x \\ \Delta y \\ \Delta z \\ \Delta T \\ \Delta \dot{x} \\ \Delta \dot{y} \\ \Delta \dot{z} \\ \Delta \dot{T} \end{pmatrix} \qquad \text{Eq. 7.4-1}$$

And the following simplified transition matrix

$$\Phi = \begin{pmatrix} 1 & 0 & 0 & 0 & \Delta t & 0 & 0 & 0 \\ 0 & 1 & 0 & 0 & 0 & \Delta t & 0 & 0 \\ 0 & 0 & 1 & 0 & 0 & 0 & \Delta t & 0 \\ 0 & 0 & 0 & 1 & 0 & 0 & 0 & \Delta t \\ 0 & 0 & 0 & 0 & 1 & 0 & 0 & 0 \\ 0 & 0 & 0 & 0 & 0 & 1 & 0 & 0 \\ 0 & 0 & 0 & 0 & 0 & 0 & 1 & 0 \\ 0 & 0 & 0 & 0 & 0 & 0 & 0 & 1 \end{pmatrix} \quad \text{Eq. 7.4-2}$$

At each epoch, the error state is propagated by

$$\tilde{\bar{x}}_K = \Phi \cdot \hat{\bar{x}}_{k-1} \quad \text{Eq. 7.4-3}$$

And the covariance matrix by

$$\tilde{P}_K = \Phi \cdot \hat{P}_{k-1} \cdot \Phi^T + Q \quad \text{Eq. 7.4-4}$$

The noise matrix Q is a diagonal matrix, adding a small amount of noise on the each state.

To obtain the observations, the nominal ranges to the ground stations and satellites have to be computed.

$$\bar{r}_{LOS} = \bar{r}_{SV} - \bar{r}_{GS} \quad \text{Eq. 7.4-5}$$

$$\bar{r}_{LOS,ISL} = \bar{r}_{SV} - \bar{r}_{SV,ISL} \quad \text{Eq. 7.4-6}$$

The positions of the satellites are derived from the broadcast ephemeris and are therefore referenced in the earth-centred-earth-fixed frame. The range is derived from the magnitude of the line of sight vector

$$R_{GS}^{SV} = \left|\bar{r}_{LOS}\right| \quad \text{Eq. 7.4-7}$$

The measurement vector z is derived from

$$\bar{z} = \begin{pmatrix} z_1 \\ z_2 \\ \\ z_n \end{pmatrix} R_{SV,ISL,measured}^{SV} - R_{SV,ISL}^{SV} \quad \text{Eq. 7.4-8}$$

where the i^{th} row consists of the measured range minus the computed range for one intersatellite link

$$z_i = R_{SV_i,ISL,measured}^{SV} - R_{SV_i,ISL,Computed}^{SV} \quad \text{Eq. 7.4-9}$$

or the same value for one ground link

$$z_j = R^{SV}_{GS_j,measured} - R^{SV}_{GS_j,Computed} \qquad \text{Eq. 7.4-10}$$

The observation matrix H is

$$H = \begin{pmatrix} h_1 \\ h_2 \\ \dots \\ h_n \end{pmatrix} \qquad \text{Eq. 7.4-11}$$

with each row containing the partial derivative for the measurement with respect to the Kalman filter states

$$h_i = \begin{pmatrix} \frac{x^j_{i,LOS}}{R^j_i} & \frac{y^j_{i,LOS}}{R^j_i} & \frac{z^j_{i,LOS}}{R^j_i} & 1 & 0 & 0 & 0 & 0 \end{pmatrix} \qquad \text{Eq. 7.4-12}$$

Before the Kalman filter routines are executed, the covariance matrix of the a priori residuals

$$\mathbf{E} = \bar{e}^T \cdot \bar{e} \qquad \text{Eq. 7.4-13}$$

with

$$\bar{e} = \bar{z} - H \cdot \tilde{\bar{x}} \qquad \text{Eq. 7.4-14}$$

is tested to exclude faulty measurements. The i_{th} measurement, and therefore the i_{th} row of the observation matrix H would be excluded if the following relationship holds

$$T_{i,i} > 9 \Rightarrow \text{Measurement i excluded} \qquad \text{Eq. 7.4-15}$$

with

$T_{i,i}$ diagonal element of matrix T

$$T = E \cdot \left(H \cdot \tilde{P} \cdot H^T + R \right)^{-1} \qquad \text{Eq. 7.4-16}$$

which is the covariance matrix of the a-priori residuals times the inverse of the state covariance matrix P mapped into the residual domain inflated by observation noise. This formulation is close to the equation for the Kalman gain and is therefore proportional to the weight this particular measurement will have. The test is formulated in way that a measurement must not exceed 3 σ, which translates to a 99 % probability if a Gaussian distribution is assumed.

After testing all residuals, it has to be decided if only the measurements where faulty or if the measurements have been excluded due to a satellites own integrity problem. If the more than 50 % of the valid observation had to be removed, the onboard integrity monitor flags the satellite unhealthy.

$$\frac{N_{removed,meas}}{N_{valid,meas}} > 0.5 \Rightarrow \text{SV Health Flag = “unhealthy”} \qquad \text{Eq. 7.4-17}$$

After removal of suspicious observations, the Kalman routines are executed. Note that the Kalman gain matrix has to be recomputed using the reduced Observation matrix H_{red}, if measurements have been removed.

$$K = \tilde{P} \cdot H_{red}^T \left(H_{red} \cdot \tilde{P} \cdot H_{red}^T + R \right)^{-1} \qquad \text{Eq. 7.4-18}$$

The updated estimates of covariance and state are then computed by

$$P = \left(I - K \cdot H_{red} \right) \cdot \tilde{P} \qquad \text{Eq. 7.4-19}$$

and

$$\hat{\bar{x}} = \tilde{\bar{x}} + K\left(\bar{z}_{red} - H_{red} \cdot \tilde{\bar{x}} \right) \qquad \text{Eq. 7.4-20}$$

After the measurement update of the Kalman filter, a Chi-Square test is performed

$$\frac{s^2}{n \cdot \sigma^2} > \varepsilon \Rightarrow \text{SV Health Flag = “unhealthy”} \qquad \text{Eq. 7.4-21}$$

with n being the number of valid observations and

$$s^2 = \sum_i \hat{e}_i^2 \qquad \text{Eq. 7.4-22}$$

is the sample variance of the a-posteriori residuals.

$$\hat{\bar{e}} = \bar{z} - H_{red} \cdot \hat{\bar{x}} \qquad \text{Eq. 7.4-23}$$

The model variance is derived from the a-posteriori covariance matrix

$$\sigma^2 = \text{Trace}(H \cdot \hat{P} \cdot H^T) \qquad \text{Eq. 7.4-24}$$

The sample variance is assumed to be Chi Square distributed, thus ε is derived from a Chi Square distribution with n-1 degrees of freedom.

The estimated state is used as further criterion to estimate the orbit and clock error. It must not exceed a predefined threshold, otherwise the satellite is flagged unhealthy.

$$x_i > e_i \Rightarrow \text{SV Health Flag = “unhealthy”} \qquad \text{Eq. 7.4-25}$$

Because the position as well as the velocity error is estimated, the condition above can be evaluated also to detect a ramp error, i.e. a slow drift in the position and clock error states. In the simulations performed however, a ramp did not result immediately in an unhealthy status.

The following figure summarises the process flow.

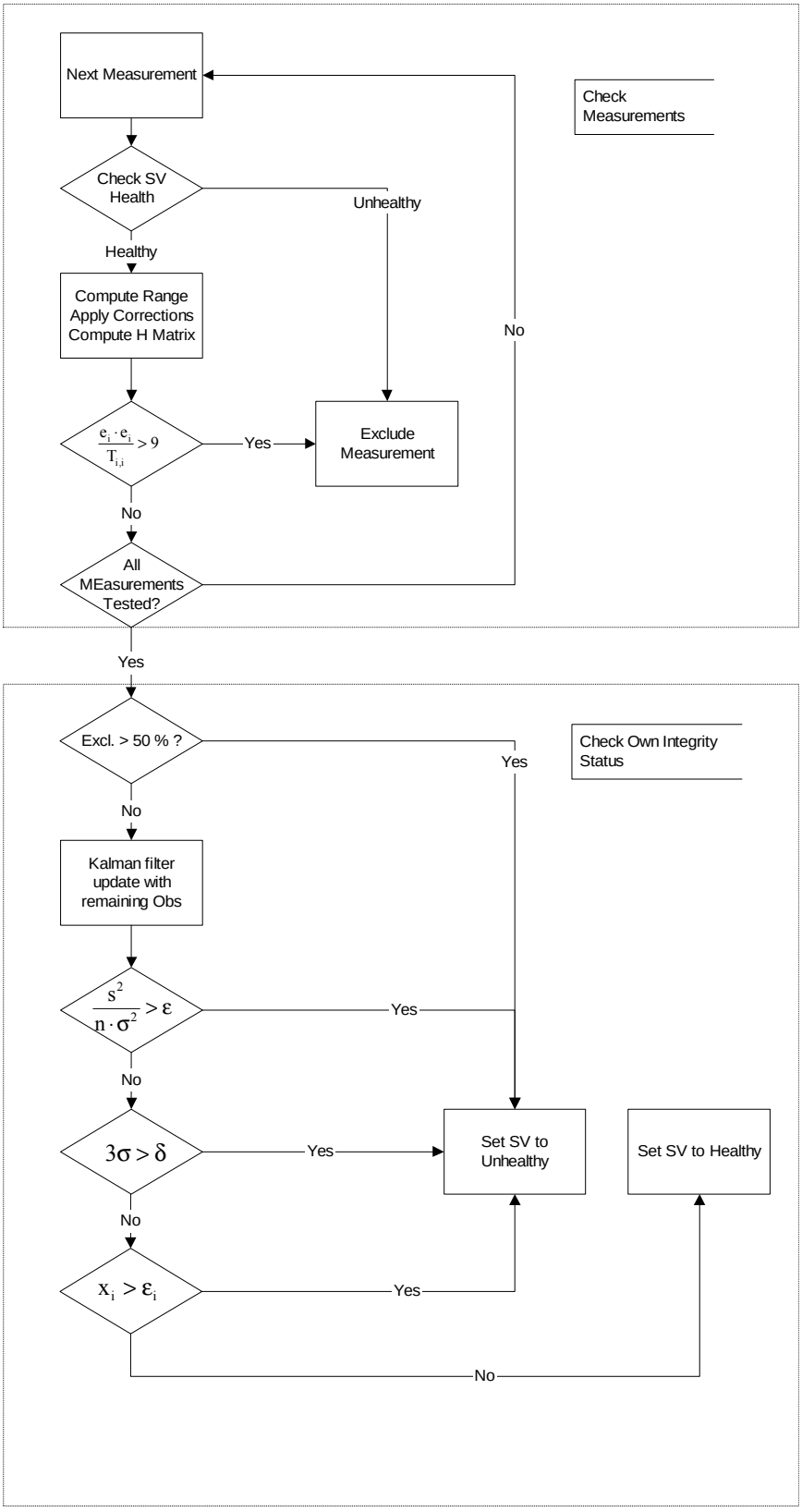

Figure 7-2 Process Flow of the Onboard Integrity Monitor

7.4.1 User Position Error due to Normal Orbit and Clock Degradation

To evaluate the effect of orbit and clock degradation, a user at position

Latitude: 48 °

Longitude: 11 °

(Munich) has been assumed, which computes his position using all satellites in view (approximately 12 SV). The satellites positions are computed using the derived broadcast parameters. The broadcast clock parameters have not been computed, but are assumed to be applied as well. Thus only the residual degradation effect has been modelled by random walk on the frequency and the resulting error has been added to the range.

In the following simulation, no integrity monitoring takes place. The predicted and uploaded broadcast ephemeris, as well as the clock are subject to degradation. The following three figures show examples of the true orbit and clock error due to ageing.

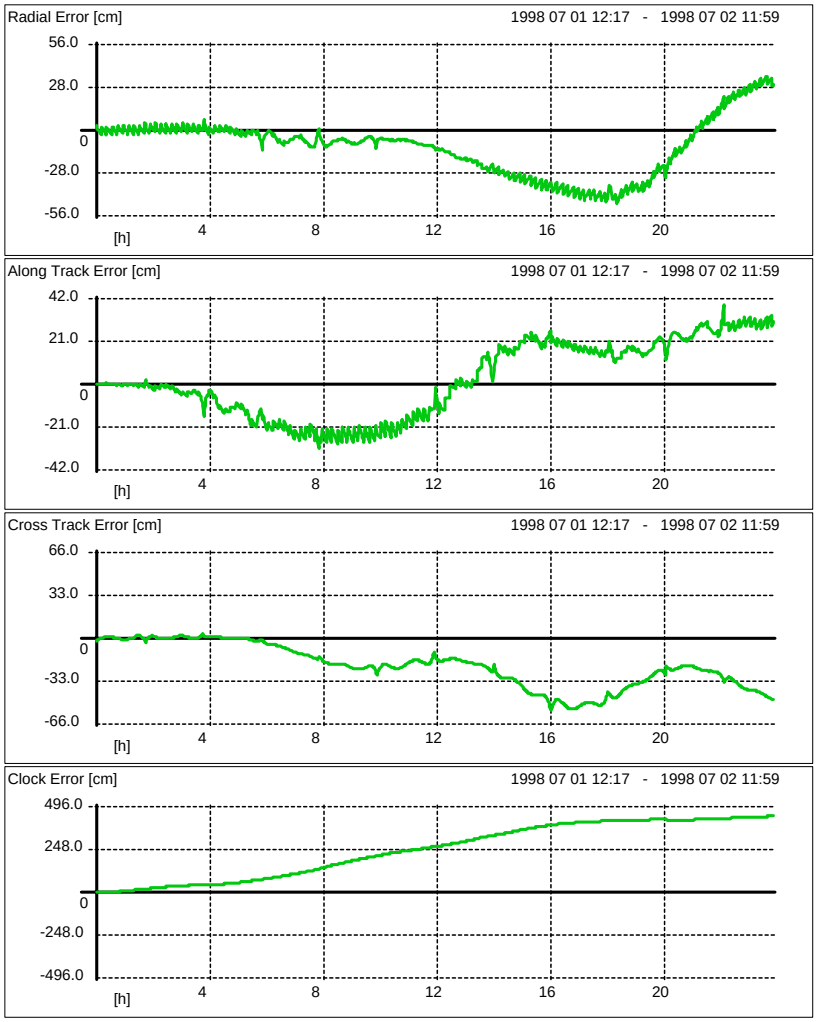

Figure 7-3 Orbit and Clock Degradation of SV 26

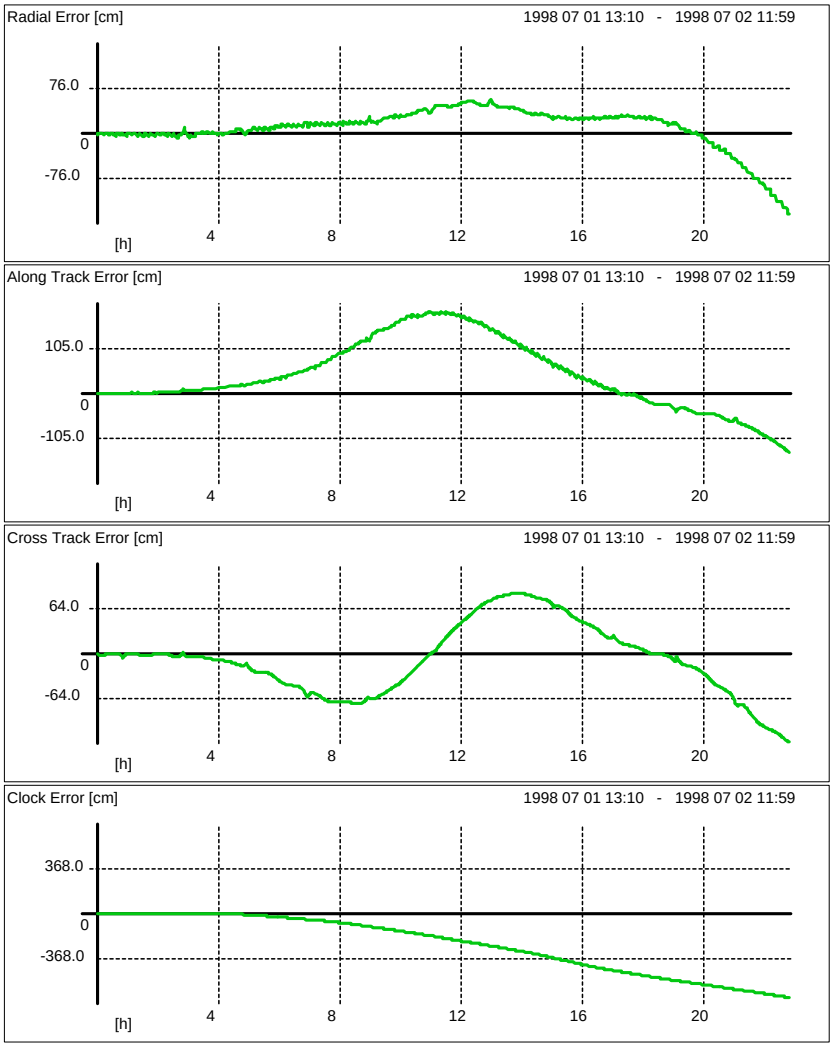

Figure 7-4 Orbit and Clock Degradation of SV 15

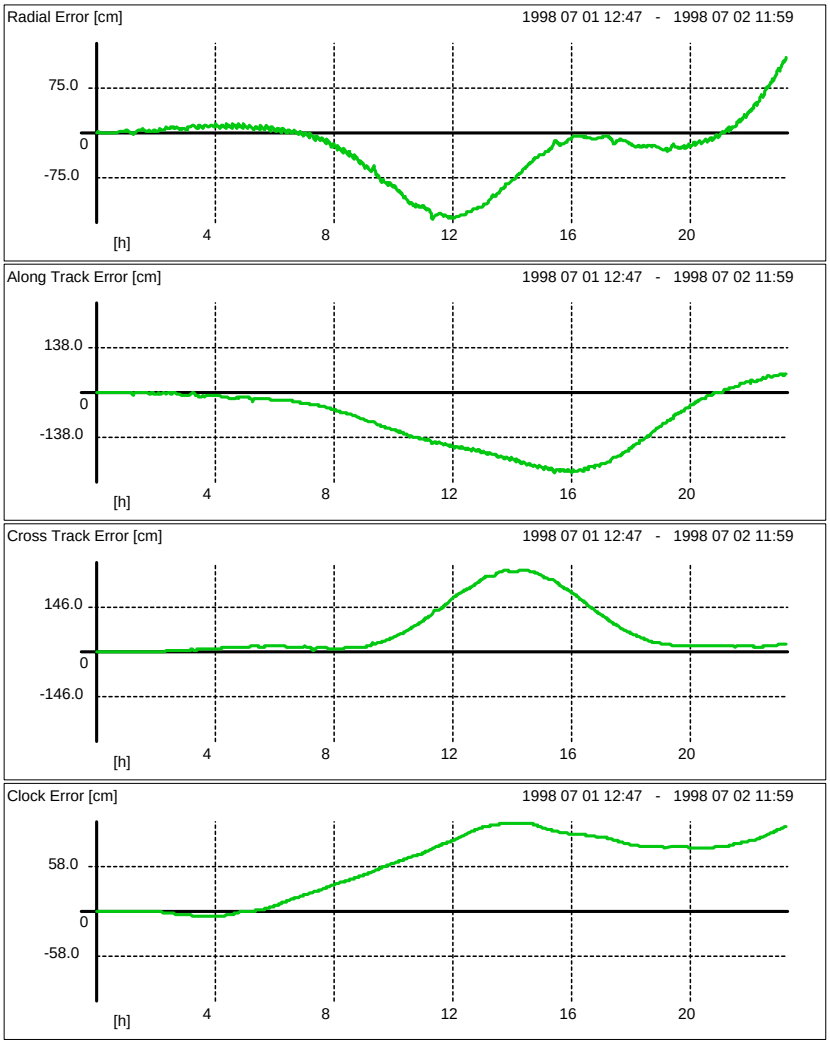

Figure 7-5 Orbit and Clock Degradation of SV 10

If a user computes the satellite positions using the broadcast parameters, his positioning performance will degrade due to the degraded orbit and clock parameters. Remember, the broadcast ephemeris have been derived from a predicted trajectory. In the same way, the clock parameters would have also been derived from prediction. The following figures show the users positioning error over time, and in the horizontal plane.

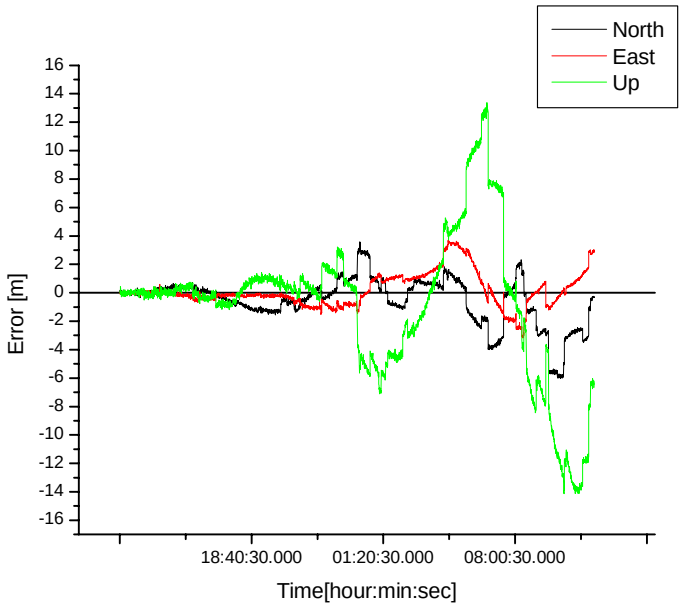

Figure 7-6 User Position Error over Time

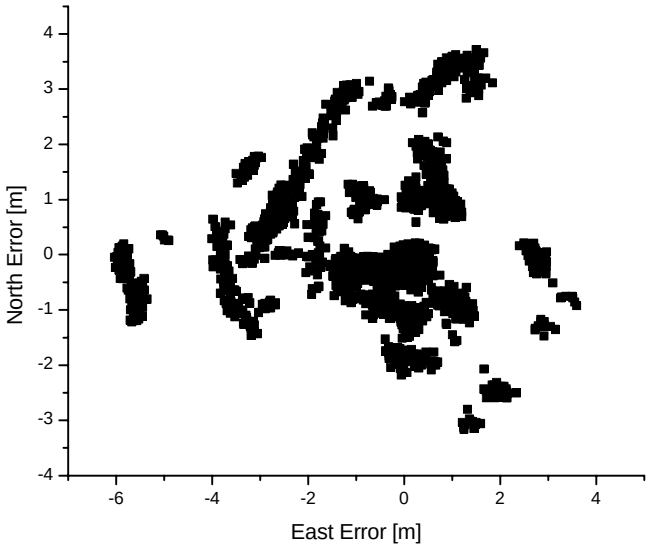

Figure 7-7 User Horizontal Position Error

After nearly 24 hours, the user position error can be up to 15 meters, mostly due to the SV clock error. However, to overcome the problem in normal system operation, the orbit and

clock parameters would be updated at a higher rate than 24 hours, say every 6 hours, to prevent excessive positioning service degradation. This would keep the position error below 2 meters.

7.4.2 User Position Degradation due to Unforeseen Orbit Manoeuvre

But not only the normal orbit degradation impacts the user position. If something happened with the satellite clock, say an excessive increase in frequency (clock drift), this could not be overcome by frequent parameter updates. Especially if the integrity requirement an the satellite position and clock is high, as would be the case in airborne navigation, the user can not rely on predicted orbits only. In the following simulation, one 2 Newton thruster of the orbit control system of SV 26 is fired, resulting in a small 0.1 m/s velocity increment. At the time the event takes place, the satellite is in view of the user position.

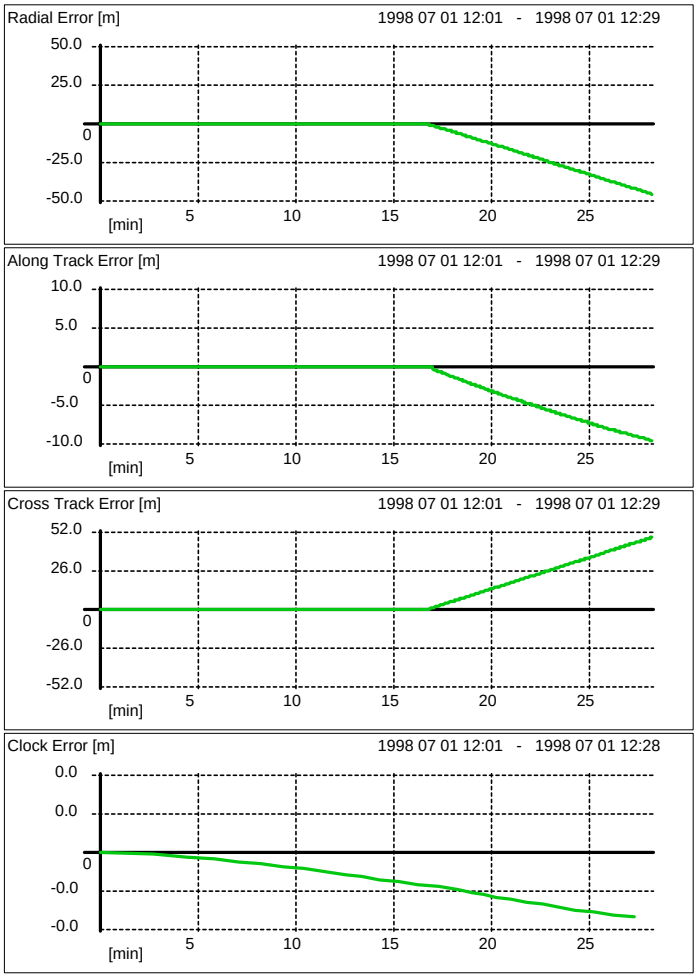

Figure 7-8 SV 26 Orbit Error due to 2N Thrust / 0.1 m/s Delta V

The user computes the satellites position now with orbit information, which is not applicable any more. If the user does not monitor the integrity of his position computation using RAIM, an increasing position error will be the result.

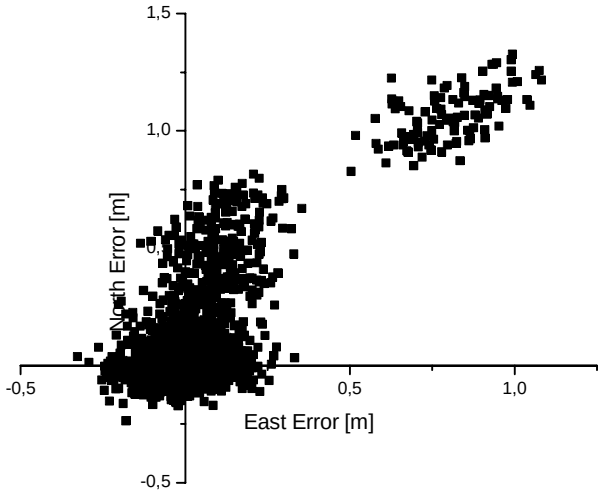

Figure 7-9 User Position Error in Horizontal Plane

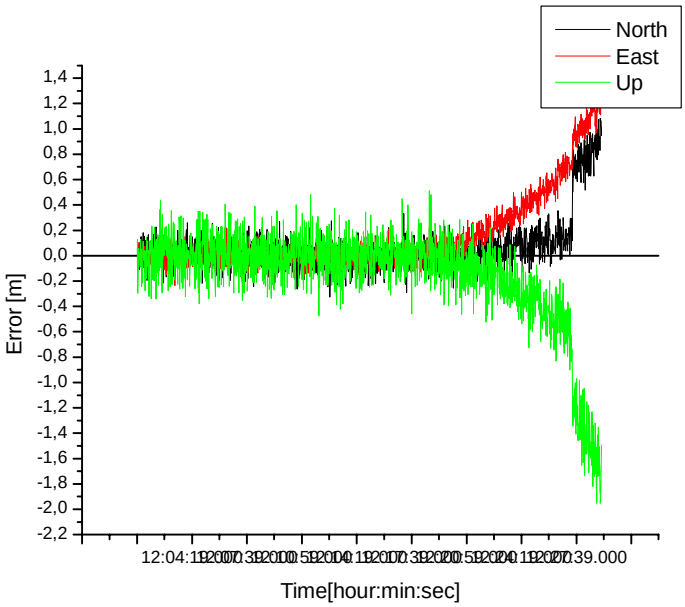

Figure 7-10 User Position Error over Time

7.4.3 User Position Error with Onboard Integrity Monitoring

The next four simulations have been conducted using the onboard integrity monitor described above. This means, there are 33 Kalman filters running in parallel an processing only measurements and information available at the satellite, and at a time when they become available. It is assumed that the satellites broadcasts its integrity status via inter satellite link to the other satellites, which then becomes available at the other satellites in the next epoch, as well as to the user. If a user receives an "Unhealthy" flag from a satellite, this SV is excluded from the position solution. The same applies to the satellites monitoring their own status using ISL's. A received unhealthy flag leads to exclusion of this particular link.

In the simulation, a non integrity case is assumed, if the position error or the clock error exceeds 1 meter in each direction. The trigger values for the state vector alarm are therefore:

State	Trigger Value	Result
X, Y and Z Estimated Position Error	1 Meter	NO GO (Unheathy flag is raised)
Clock Offset	1 Meter	NO GO
VX,VY,VZ Estimated Velocity Error	2 cm/s	Warning Only
Clock Drift	2 cm/s	Warning Only

Figure 7-11 Trigger Values for Fault Detector

7.4.3.1 Strong Orbit Manoeuvre

The first simulated non-integrity case is an orbit manoeuvre with 50 Newtons thrust, producing a velocity increment of 0.5 m/s in the along track direction. The affected satellite is again SV 26, which is visible to the user at a medium elevation. The resulting orbit error over time is depicted in the figure below.

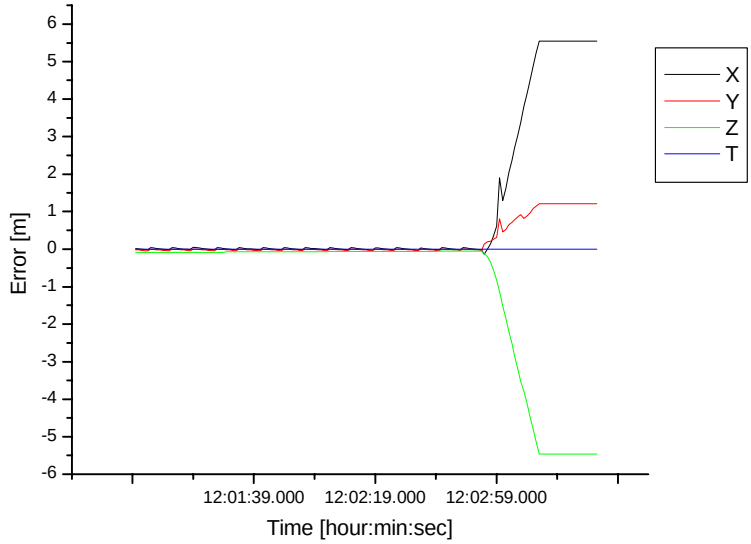

Figure 7-12 Absolute Orbit Error of SV 26

In the Kalman filter, the orbit error is estimated. The following figure shows the relative orbit error of satellite, i.e. estimated versus true error.

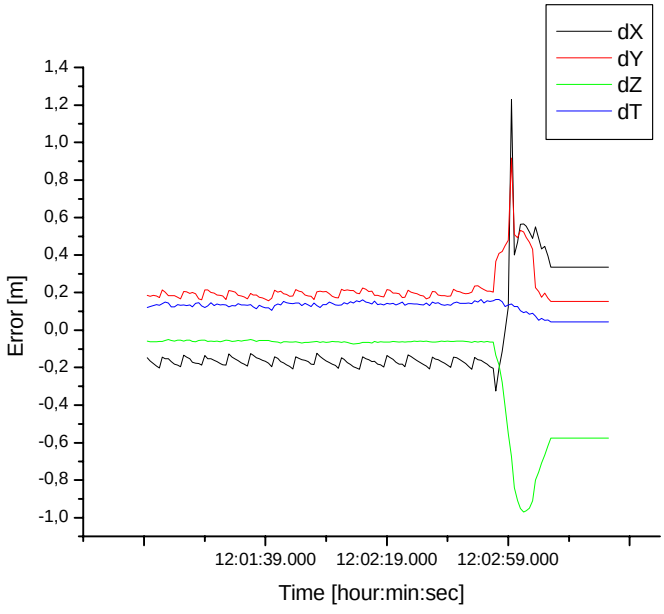

Figure 7-13 Estimated vs. True Error for SV 26

As can be seen from the figure above, the state is not estimated very well, due to the high process noise required to keep the filter adaptable to fast changes. The error estimate of such a Kalman filter is far too noisy to be used as a correction value, but it is sufficient to detect orbit errors. To evaluate the reaction of the onboard processor to the injected fault, the error log of all satellites is shown below. It has the following format

<Year> <Month> < Day> <hour:minute:second> SV <ID> <Error Message>

```
1998 07 01 12:02:59.000 SV 26 Ramp Detected [Position]
1998 07 01 12:03:00.000 SV 26 Ramp Detected [Position]
1998 07 01 12:03:00.000 SV 26 Non Detected Position Error =    0.351 m
1998 07 01 12:03:01.000 SV 26 Ramp Detected [Position]
1998 07 01 12:03:01.000 SV 26 Non Detected Position Error =    0.652 m
1998 07 01 12:03:02.000 SV 26 Ramp Detected [Position]
1998 07 01 12:03:02.000 SV 26 Non Detected Position Error =    0.827 m
1998 07 01 12:03:03.000 SV 26 Ramp Detected [Position]
1998 07 01 12:03:03.000 SV 26 Limit Exceeded [Position]
1998 07 01 12:03:03.000 SV 26 Check Result: NO GO
1998 07 01 12:03:03.000 SV 27 Removed Unhealthy SV ID 26
1998 07 01 12:03:03.000 SV 28 Removed Unhealthy SV ID 26
1998 07 01 12:03:03.000 SV 29 Removed Unhealthy SV ID 26
1998 07 01 12:03:03.000 SV 30 Removed Unhealthy SV ID 26
1998 07 01 12:03:04.000 SV 00 Removed Unhealthy SV ID 26
1998 07 01 12:03:04.000 SV 01 Removed Unhealthy SV ID 26
1998 07 01 12:03:04.000 SV 02 Removed Unhealthy SV ID 26
1998 07 01 12:03:04.000 SV 03 Removed Unhealthy SV ID 26
1998 07 01 12:03:04.000 SV 04 Removed Unhealthy SV ID 26
1998 07 01 12:03:04.000 SV 05 Removed Unhealthy SV ID 26
1998 07 01 12:03:04.000 SV 06 Removed Unhealthy SV ID 26
1998 07 01 12:03:04.000 SV 08 Removed Unhealthy SV ID 26
1998 07 01 12:03:04.000 SV 09 Removed Unhealthy SV ID 26
1998 07 01 12:03:04.000 SV 10 Removed Unhealthy SV ID 26
1998 07 01 12:03:04.000 SV 11 Removed Unhealthy SV ID 26
1998 07 01 12:03:04.000 SV 12 Removed Unhealthy SV ID 26
1998 07 01 12:03:04.000 SV 13 Removed Unhealthy SV ID 26
1998 07 01 12:03:04.000 SV 14 Removed Unhealthy SV ID 26
1998 07 01 12:03:04.000 SV 15 Removed Unhealthy SV ID 26
1998 07 01 12:03:04.000 SV 16 Removed Unhealthy SV ID 26
1998 07 01 12:03:04.000 SV 17 Removed Unhealthy SV ID 26
1998 07 01 12:03:04.000 SV 18 Removed Unhealthy SV ID 26
1998 07 01 12:03:04.000 SV 19 Removed Unhealthy SV ID 26
1998 07 01 12:03:04.000 SV 20 Removed Unhealthy SV ID 26
1998 07 01 12:03:04.000 SV 21 Removed Unhealthy SV ID 26
1998 07 01 12:03:04.000 SV 22 Removed Unhealthy SV ID 26
1998 07 01 12:03:04.000 SV 23 Removed Unhealthy SV ID 26
1998 07 01 12:03:04.000 SV 24 Removed Unhealthy SV ID 26
1998 07 01 12:03:04.000 SV 25 Removed Unhealthy SV ID 26
1998 07 01 12:03:04.000 SV 26 Chi Square Test Failed
1998 07 01 12:03:04.000 SV 26 Ramp Detected [Position]
1998 07 01 12:03:04.000 SV 26 Limit Exceeded [Position]
1998 07 01 12:03:04.000 SV 26 Check Result: NO GO
1998 07 01 12:03:05.000 SV 26 Chi Square Test Failed
1998 07 01 12:03:05.000 SV 26 Ramp Detected [Position]
```

```
1998 07 01 12:03:05.000 SV 26 Limit Exceeded [Position]
1998 07 01 12:03:05.000 SV 26 Check Result: NO GO
1998 07 01 12:03:06.000 SV 26 Chi Square Test Failed
1998 07 01 12:03:06.000 SV 26 Ramp Detected [Position]
1998 07 01 12:03:06.000 SV 26 Limit Exceeded [Position]
1998 07 01 12:03:06.000 SV 26 Check Result: NO GO
1998 07 01 12:03:07.000 SV 26 Chi Square Test Failed
1998 07 01 12:03:07.000 SV 26 Ramp Detected [Position]
1998 07 01 12:03:07.000 SV 26 Limit Exceeded [Position]
1998 07 01 12:03:07.000 SV 26 Check Result: NO GO
1998 07 01 12:03:08.000 SV 26 Chi Square Test Failed
1998 07 01 12:03:08.000 SV 26 Ramp Detected [Position]
1998 07 01 12:03:08.000 SV 26 Limit Exceeded [Position]
1998 07 01 12:03:08.000 SV 26 Check Result: NO GO
1998 07 01 12:03:09.000 SV 26 Chi Square Test Failed
1998 07 01 12:03:09.000 SV 26 Ramp Detected [Position]
1998 07 01 12:03:09.000 SV 26 Limit Exceeded [Position]
1998 07 01 12:03:09.000 SV 26 Check Result: NO GO
1998 07 01 12:03:10.000 SV 26 Chi Square Test Failed
1998 07 01 12:03:10.000 SV 26 Ramp Detected [Position]
1998 07 01 12:03:10.000 SV 26 Limit Exceeded [Position]
1998 07 01 12:03:10.000 SV 26 Check Result: NO GO
1998 07 01 12:03:11.000 SV 26 Chi Square Test Failed
1998 07 01 12:03:11.000 SV 26 Ramp Detected [Position]
1998 07 01 12:03:11.000 SV 26 Limit Exceeded [Position]
1998 07 01 12:03:11.000 SV 26 Check Result: NO GO
1998 07 01 12:03:12.000 SV 26 Chi Square Test Failed
1998 07 01 12:03:12.000 SV 26 Ramp Detected [Position]
1998 07 01 12:03:12.000 SV 26 Limit Exceeded [Position]
1998 07 01 12:03:12.000 SV 26 Check Result: NO GO
1998 07 01 12:03:13.000 SV 26 Chi Square Test Failed
1998 07 01 12:03:13.000 SV 26 Ramp Detected [Position]
1998 07 01 12:03:13.000 SV 26 Limit Exceeded [Position]
1998 07 01 12:03:13.000 SV 26 Check Result: NO GO
1998 07 01 12:03:13.000 SV 26 Switched Off
```

The event takes place at 12:02:55. Four seconds later, a position drift is detected (the ramp detector has a threshold of 2 cm/s). At this time, the satellites position is still within the 1x1x1 meter cube and therefore still considered to be integer. Another second later, the integrity limit of one meter is exceeded by 0.3 meters, but the estimated error is still within the limit. This is the first time a real non-integrity case exists, because the user has a hazardous misleading information. He still used SV 26 although the orbit parameters are not correct anymore. The position error remains undetected for another two seconds and grows to nearly 1 meter, before the estimated position error is large enough to trigger a NO GO. From now on, the user is alarmed and will discontinue to use SV 26.

In the next epoch, all other satellites will exclude SV 26 from their integrity processing. One second after the state limit check has detected the error, the Chi Square test also raises an alarm.

As a result of the simulation, the user has been alarmed 3 seconds after occurrence of the non-integrity situation, which is an acceptable time to alarm event for a CAT I landing (6 seconds

limit). The maximum range error has been 1.8 meter (0.8 meter above the limit), but the error in the user position has been negligible (see figure below).

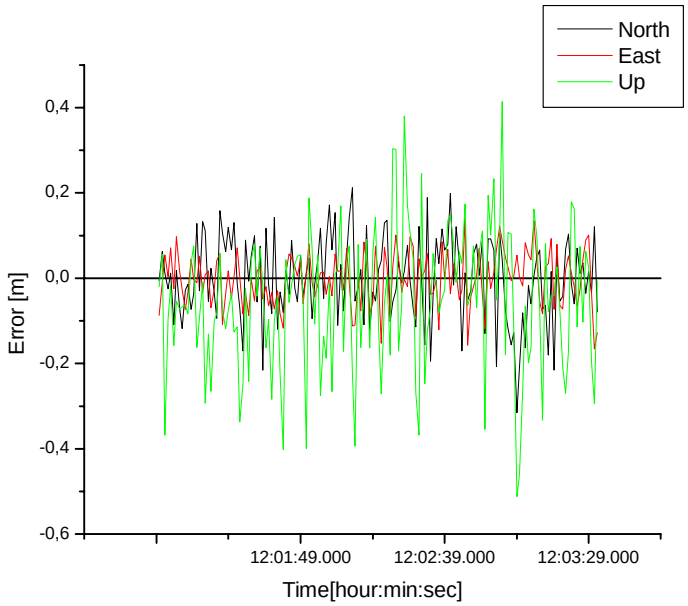

Figure 7-14 User Error during Manoeuvre

7.4.3.2 Weak Orbit Manoeuvre

In the next simulation, a weak thrust of 2N results in a velocity increment of 0.1 m/s in the cross track direction. Affected satellite is again SV 26. The next two figure show again true and estimated versus true error of the satellites onboard processor.

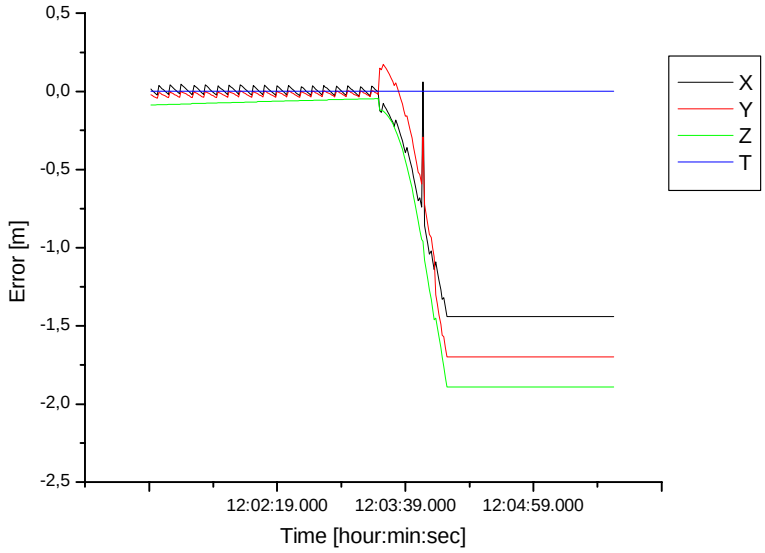

Figure 7-15 Absolute Error SV 26

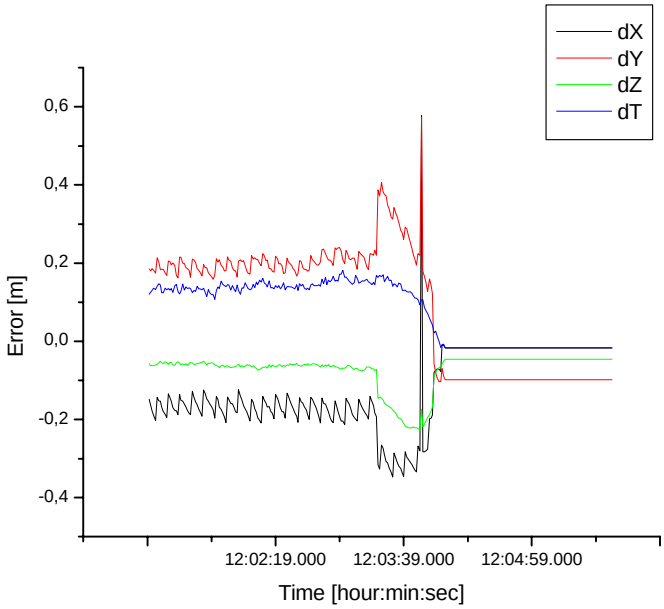

Figure 7-16 Estimated vs True Error SV 26

The error log below indicates the sequence of events and messages.

```
1998 07 01 12:03:42.000 SV 26 Ramp Detected [Position]
1998 07 01 12:03:43.000 SV 26 Ramp Detected [Position]
```

```
1998 07 01 12:03:44.000 SV 26 Ramp Detected [Position]
1998 07 01 12:03:45.000 SV 26 Ramp Detected [Position]
1998 07 01 12:03:46.000 SV 26 Ramp Detected [Position]
1998 07 01 12:03:47.000 SV 26 Ramp Detected [Position]
1998 07 01 12:03:48.000 SV 26 Ramp Detected [Position]
1998 07 01 12:03:49.000 SV 26 Ramp Detected [Position]
1998 07 01 12:03:50.000 SV 26 Ramp Detected [Position]
1998 07 01 12:03:51.000 SV 26 Ramp Detected [Position]
1998 07 01 12:03:52.000 SV 26 Ramp Detected [Position]
1998 07 01 12:03:53.000 SV 26 Ramp Detected [Position]
1998 07 01 12:03:53.000 SV 26 Non Detected Position Error =    0.068 m
1998 07 01 12:03:54.000 SV 26 Ramp Detected [Position]
1998 07 01 12:03:54.000 SV 26 Non Detected Position Error =    0.175 m
1998 07 01 12:03:55.000 SV 26 Ramp Detected [Position]
1998 07 01 12:03:55.000 SV 26 Limit Exceeded [Position]
1998 07 01 12:03:55.000 SV 26 Check Result: NO GO
1998 07 01 12:03:55.000 SV 27 Removed Unhealthy SV ID 26
1998 07 01 12:03:55.000 SV 28 Removed Unhealthy SV ID 26
1998 07 01 12:03:55.000 SV 29 Removed Unhealthy SV ID 26
1998 07 01 12:03:55.000 SV 30 Removed Unhealthy SV ID 26

1998 07 01 12:03:56.000 SV 00 Removed Unhealthy SV ID 26
1998 07 01 12:03:56.000 SV 01 Removed Unhealthy SV ID 26
1998 07 01 12:03:56.000 SV 02 Removed Unhealthy SV ID 26
1998 07 01 12:03:56.000 SV 03 Removed Unhealthy SV ID 26
1998 07 01 12:03:56.000 SV 04 Removed Unhealthy SV ID 26
1998 07 01 12:03:56.000 SV 05 Removed Unhealthy SV ID 26
1998 07 01 12:03:56.000 SV 06 Removed Unhealthy SV ID 26
1998 07 01 12:03:56.000 SV 08 Removed Unhealthy SV ID 26
1998 07 01 12:03:56.000 SV 09 Removed Unhealthy SV ID 26
1998 07 01 12:03:56.000 SV 10 Removed Unhealthy SV ID 26
1998 07 01 12:03:56.000 SV 11 Removed Unhealthy SV ID 26
1998 07 01 12:03:56.000 SV 12 Removed Unhealthy SV ID 26
1998 07 01 12:03:56.000 SV 13 Removed Unhealthy SV ID 26
1998 07 01 12:03:56.000 SV 14 Removed Unhealthy SV ID 26
1998 07 01 12:03:56.000 SV 15 Removed Unhealthy SV ID 26
1998 07 01 12:03:56.000 SV 16 Removed Unhealthy SV ID 26
1998 07 01 12:03:56.000 SV 17 Removed Unhealthy SV ID 26
1998 07 01 12:03:56.000 SV 18 Removed Unhealthy SV ID 26
1998 07 01 12:03:56.000 SV 19 Removed Unhealthy SV ID 26
1998 07 01 12:03:56.000 SV 20 Removed Unhealthy SV ID 26
1998 07 01 12:03:56.000 SV 21 Removed Unhealthy SV ID 26
1998 07 01 12:03:56.000 SV 22 Removed Unhealthy SV ID 26
1998 07 01 12:03:56.000 SV 23 Removed Unhealthy SV ID 26
1998 07 01 12:03:56.000 SV 24 Removed Unhealthy SV ID 26
1998 07 01 12:03:56.000 SV 25 Removed Unhealthy SV ID 26
1998 07 01 12:03:56.000 SV 26 Ramp Detected [Position]
1998 07 01 12:03:56.000 SV 26 Limit Exceeded [Position]
1998 07 01 12:03:56.000 SV 26 Check Result: NO GO
1998 07 01 12:03:57.000 SV 26 Ramp Detected [Position]
1998 07 01 12:03:57.000 SV 26 Limit Exceeded [Position]
1998 07 01 12:03:57.000 SV 26 Check Result: NO GO
1998 07 01 12:03:58.000 SV 26 Ramp Detected [Position]
1998 07 01 12:03:58.000 SV 26 Limit Exceeded [Position]
1998 07 01 12:03:58.000 SV 26 Check Result: NO GO
1998 07 01 12:03:59.000 SV 26 Ramp Detected [Position]
```

```
1998 07 01 12:03:59.000 SV 26 Limit Exceeded [Position]
1998 07 01 12:03:59.000 SV 26 Check Result: NO GO
1998 07 01 12:04:00.000 SV 26 Ramp Detected [Position]
1998 07 01 12:04:00.000 SV 26 Limit Exceeded [Position]
1998 07 01 12:04:00.000 SV 26 Check Result: NO GO
1998 07 01 12:04:01.000 SV 26 Ramp Detected [Position]
1998 07 01 12:04:01.000 SV 26 Limit Exceeded [Position]
1998 07 01 12:04:01.000 SV 26 Check Result: NO GO
1998 07 01 12:04:02.000 SV 26 Ramp Detected [Position]
1998 07 01 12:04:02.000 SV 26 Limit Exceeded [Position]
1998 07 01 12:04:02.000 SV 26 Check Result: NO GO
1998 07 01 12:04:03.000 SV 26 Ramp Detected [Position]
1998 07 01 12:04:03.000 SV 26 Limit Exceeded [Position]
1998 07 01 12:04:03.000 SV 26 Check Result: NO GO
1998 07 01 12:04:04.000 SV 26 Ramp Detected [Position]
1998 07 01 12:04:04.000 SV 26 Limit Exceeded [Position]
1998 07 01 12:04:04.000 SV 26 Check Result: NO GO
1998 07 01 12:04:05.000 SV 26 Ramp Detected [Position]
1998 07 01 12:04:05.000 SV 26 Limit Exceeded [Position]
1998 07 01 12:04:05.000 SV 26 Check Result: NO GO
1998 07 01 12:04:05.000 SV 26 Switched Off
```

The event starts at 12:03:22. Twenty seconds later, the ramp detector is triggered the first time. First occurrence of a non-integrity event is at 12:03:53, the NO GO Flag due to position limit excess is raised at 12:03:55, yielding 2 seconds time to alarm. Impact on the user is negligible, as can be seen in the figure below.

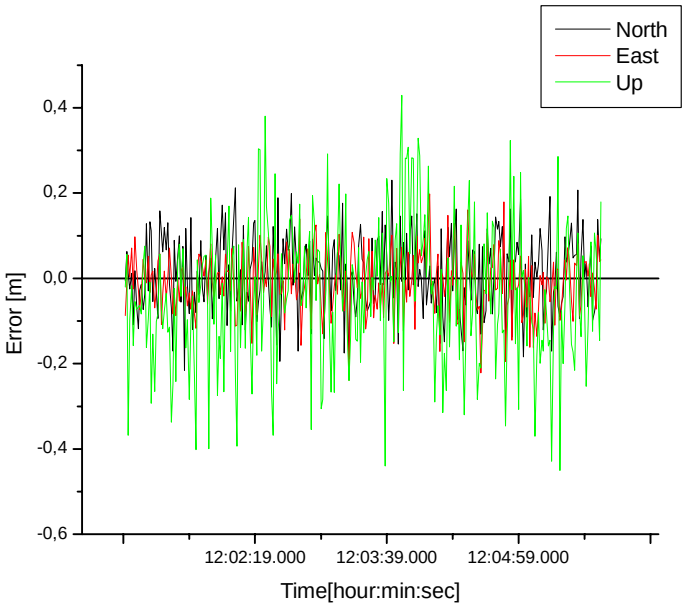

Figure 7-17 User Position Error during Manoeuvre

7.4.3.3 Clock Drift

The third case simulates a sudden excessive drift of 10^{-10} sec/sec in the clock of SV 04, which is visible to the user at a high elevation. The figures below indicate true and estimation error of the onboard processor.

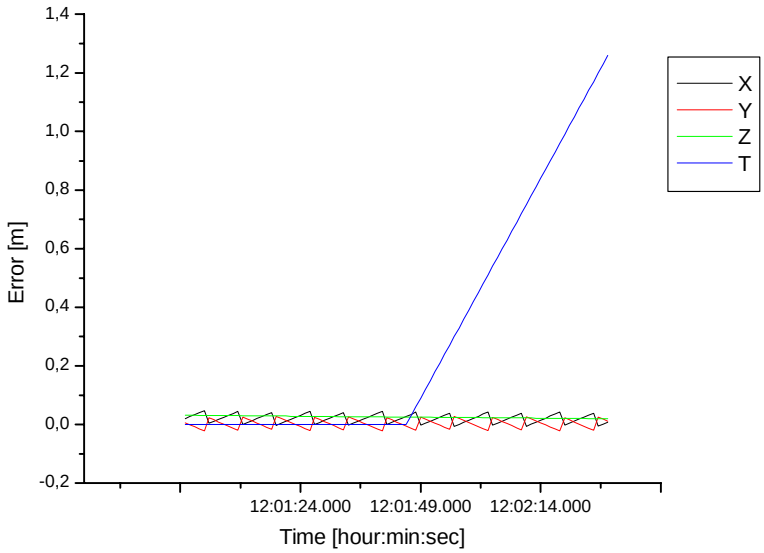

Figure 7-18 Absolute Clock Error SV 04

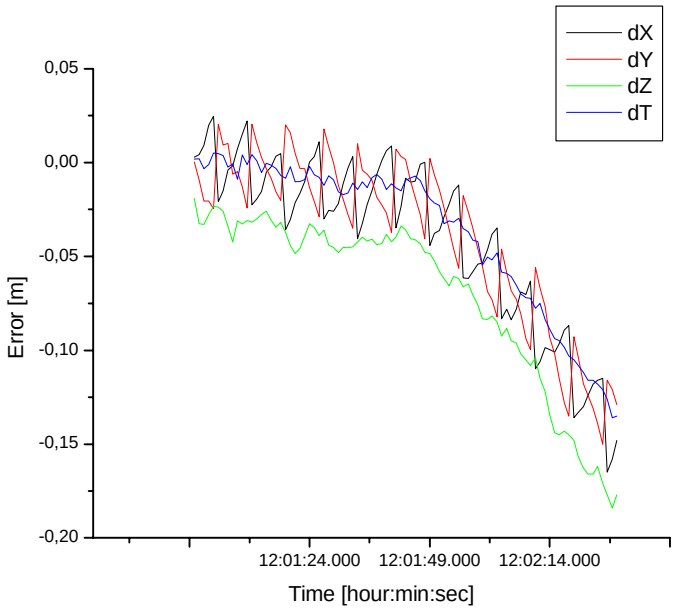

Figure 7-19 Estimated vs True Error SV 04

The error log summarises the sequence of events:

```
1998 07 01 12:01:51.000 SV 04 Chi Square Test Failed
1998 07 01 12:01:51.000 SV 04 Check Result: NO GO [False Alarm]
1998 07 01 12:01:51.000 SV 05 Removed Unhealthy SV ID 04
1998 07 01 12:01:51.000 SV 06 Removed Unhealthy SV ID 04
1998 07 01 12:01:51.000 SV 07 Removed Unhealthy SV ID 04
1998 07 01 12:01:51.000 SV 08 Removed Unhealthy SV ID 04
1998 07 01 12:01:51.000 SV 11 Removed Unhealthy SV ID 04
1998 07 01 12:01:51.000 SV 12 Removed Unhealthy SV ID 04
1998 07 01 12:01:51.000 SV 13 Removed Unhealthy SV ID 04
1998 07 01 12:01:51.000 SV 14 Removed Unhealthy SV ID 04
1998 07 01 12:01:51.000 SV 15 Removed Unhealthy SV ID 04
1998 07 01 12:01:51.000 SV 16 Removed Unhealthy SV ID 04
1998 07 01 12:01:51.000 SV 19 Removed Unhealthy SV ID 04
1998 07 01 12:01:51.000 SV 20 Removed Unhealthy SV ID 04
1998 07 01 12:01:51.000 SV 21 Removed Unhealthy SV ID 04
1998 07 01 12:01:51.000 SV 22 Removed Unhealthy SV ID 04
1998 07 01 12:01:51.000 SV 23 Removed Unhealthy SV ID 04
1998 07 01 12:01:51.000 SV 24 Removed Unhealthy SV ID 04
1998 07 01 12:01:51.000 SV 25 Removed Unhealthy SV ID 04
1998 07 01 12:01:51.000 SV 26 Removed Unhealthy SV ID 04
1998 07 01 12:01:51.000 SV 27 Removed Unhealthy SV ID 04
1998 07 01 12:01:51.000 SV 28 Removed Unhealthy SV ID 04

1998 07 01 12:01:51.000 SV 29 Removed Unhealthy SV ID 04
1998 07 01 12:01:51.000 SV 30 Removed Unhealthy SV ID 04
1998 07 01 12:01:51.000 SV 31 Removed Unhealthy SV ID 04
1998 07 01 12:01:51.000 SV 32 Removed Unhealthy SV ID 04
1998 07 01 12:01:52.000 SV 00 Removed Unhealthy SV ID 04
1998 07 01 12:01:52.000 SV 01 Removed Unhealthy SV ID 04
1998 07 01 12:01:52.000 SV 02 Removed Unhealthy SV ID 04
1998 07 01 12:01:52.000 SV 03 Removed Unhealthy SV ID 04
1998 07 01 12:01:52.000 SV 04 Chi Square Test Failed
1998 07 01 12:01:52.000 SV 04 Check Result: NO GO [False Alarm]
1998 07 01 12:01:53.000 SV 04 Chi Square Test Failed
1998 07 01 12:01:53.000 SV 04 Check Result: NO GO [False Alarm]
1998 07 01 12:01:54.000 SV 04 Chi Square Test Failed
1998 07 01 12:01:54.000 SV 04 Check Result: NO GO [False Alarm]
1998 07 01 12:01:55.000 SV 04 Chi Square Test Failed
1998 07 01 12:01:55.000 SV 04 Check Result: NO GO [False Alarm]
1998 07 01 12:01:56.000 SV 04 Chi Square Test Failed
1998 07 01 12:01:56.000 SV 04 Check Result: NO GO [False Alarm]
1998 07 01 12:01:57.000 SV 04 Chi Square Test Failed
1998 07 01 12:01:57.000 SV 04 Check Result: NO GO [False Alarm]
1998 07 01 12:01:58.000 SV 04 Chi Square Test Failed
1998 07 01 12:01:58.000 SV 04 Check Result: NO GO [False Alarm]
1998 07 01 12:01:59.000 SV 04 Chi Square Test Failed
1998 07 01 12:01:59.000 SV 04 Check Result: NO GO [False Alarm]
1998 07 01 12:02:00.000 SV 04 Chi Square Test Failed
1998 07 01 12:02:00.000 SV 04 Check Result: NO GO [False Alarm]
1998 07 01 12:02:01.000 SV 04 Chi Square Test Failed
1998 07 01 12:02:01.000 SV 04 Check Result: NO GO [False Alarm]
1998 07 01 12:02:01.000 SV 04 Switched Off
```

The event takes place at 12:01:47. Four seconds later, the Chi Square test raises a NO GO, although the true error has not exceeded it's limit yet. The other satellites (as well as the user) immediately exclude the observations to the faulty satellite. In this case, the alarm has to be evaluated not as false alarm, but as a so called early detection. Although the limit has not been exceeded yet at the time the alarm has been raised, this will however be the case only 15 seconds later. Due to the very early alarm, no error in the user position is caused.

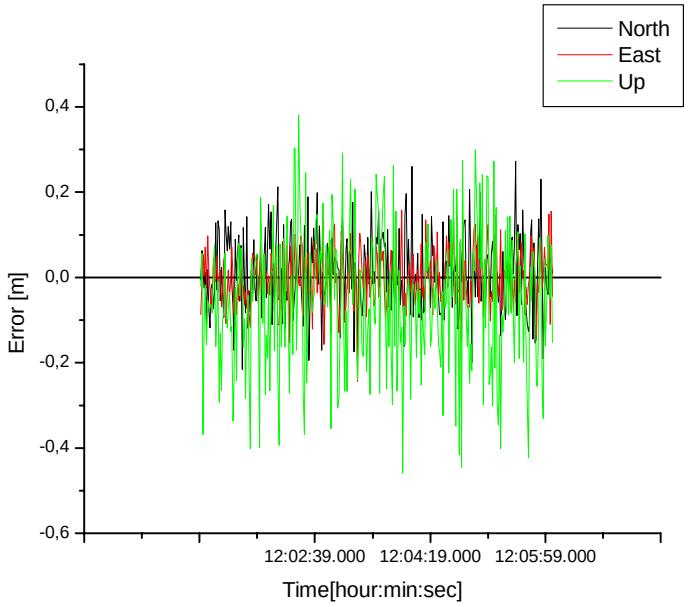

User Error

7.4.3.4 Clock Jump

The last non-integrity case simulated a 1e-8 s clock offset jump on SV 04.

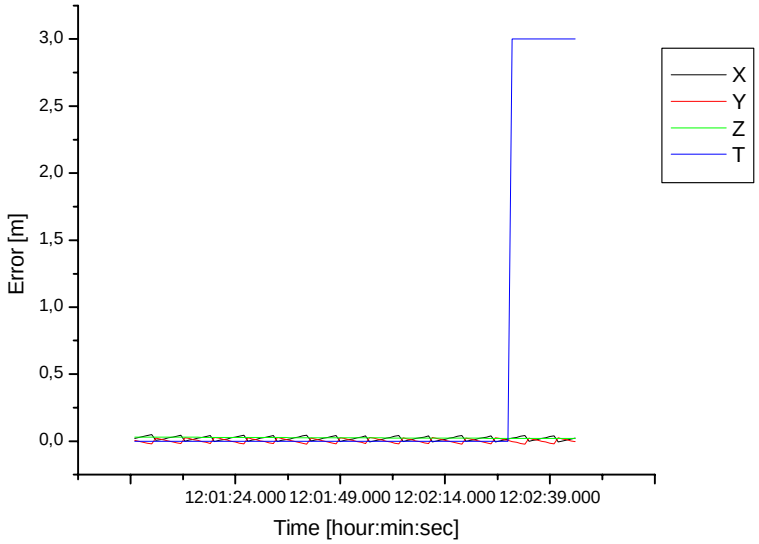

Figure 7-20 Absolute Error SV 04

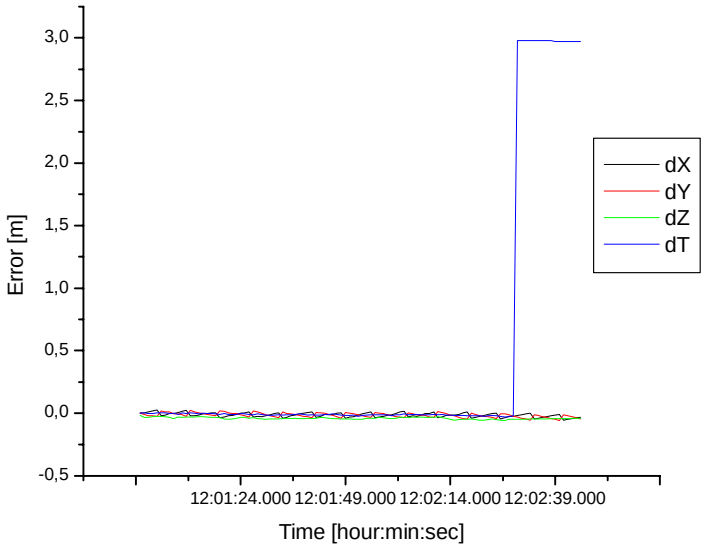

Figure 7-21 Estimated minus True Error

The error log below summarises the sequence of events:

```
1998 07 01 12:02:29.000 SV 11 Removed Suspicious ISL: SV 04
1998 07 01 12:02:29.000 SV 12 Removed Suspicious ISL: SV 04
1998 07 01 12:02:29.000 SV 13 Removed Suspicious ISL: SV 04
1998 07 01 12:02:29.000 SV 14 Removed Suspicious ISL: SV 04
1998 07 01 12:02:29.000 SV 15 Removed Suspicious ISL: SV 04

1998 07 01 12:02:29.000 SV 16 Removed Suspicious ISL: SV 04
1998 07 01 12:02:29.000 SV 19 Removed Suspicious ISL: SV 04
1998 07 01 12:02:29.000 SV 20 Removed Suspicious ISL: SV 04
1998 07 01 12:02:29.000 SV 21 Removed Suspicious ISL: SV 04
1998 07 01 12:02:29.000 SV 22 Removed Suspicious ISL: SV 04
1998 07 01 12:02:29.000 SV 23 Removed Suspicious ISL: SV 04
1998 07 01 12:02:29.000 SV 24 Removed Suspicious ISL: SV 04
1998 07 01 12:02:29.000 SV 25 Removed Suspicious ISL: SV 04
1998 07 01 12:02:29.000 SV 26 Removed Suspicious ISL: SV 04
1998 07 01 12:02:29.000 SV 27 Removed Suspicious ISL: SV 04
1998 07 01 12:02:29.000 SV 28 Removed Suspicious ISL: SV 04
1998 07 01 12:02:29.000 SV 29 Removed Suspicious ISL: SV 04
1998 07 01 12:02:29.000 SV 30 Removed Suspicious ISL: SV 04
1998 07 01 12:02:29.000 SV 31 Removed Suspicious ISL: SV 04
1998 07 01 12:02:29.000 SV 32 Removed Suspicious ISL: SV 04
1998 07 01 12:02:30.000 SV 00 Removed Suspicious ISL: SV 04
1998 07 01 12:02:30.000 SV 01 Removed Suspicious ISL: SV 04
1998 07 01 12:02:30.000 SV 02 Removed Suspicious ISL: SV 04
1998 07 01 12:02:30.000 SV 03 Removed Suspicious ISL: SV 04
1998 07 01 12:02:30.000 SV 04 Removed Suspicious ISL: SV 32
1998 07 01 12:02:30.000 SV 04 Removed Suspicious ISL: SV 31
1998 07 01 12:02:30.000 SV 04 Removed Suspicious ISL: SV 30
1998 07 01 12:02:30.000 SV 04 Removed Suspicious ISL: SV 29
1998 07 01 12:02:30.000 SV 04 Removed Suspicious ISL: SV 28
1998 07 01 12:02:30.000 SV 04 Removed Suspicious ISL: SV 27
1998 07 01 12:02:30.000 SV 04 Removed Suspicious ISL: SV 26
1998 07 01 12:02:30.000 SV 04 Removed Suspicious ISL: SV 25
1998 07 01 12:02:30.000 SV 04 Removed Suspicious ISL: SV 24
1998 07 01 12:02:30.000 SV 04 Removed Suspicious ISL: SV 23
1998 07 01 12:02:30.000 SV 04 Removed Suspicious ISL: SV 22
1998 07 01 12:02:30.000 SV 04 Removed Suspicious ISL: SV 21
1998 07 01 12:02:30.000 SV 04 Removed Suspicious ISL: SV 20
1998 07 01 12:02:30.000 SV 04 Removed Suspicious ISL: SV 19
1998 07 01 12:02:30.000 SV 04 Removed Suspicious ISL: SV 16
1998 07 01 12:02:30.000 SV 04 Removed Suspicious ISL: SV 15
1998 07 01 12:02:30.000 SV 04 Removed Suspicious ISL: SV 14
1998 07 01 12:02:30.000 SV 04 Removed Suspicious ISL: SV 13
1998 07 01 12:02:30.000 SV 04 Removed Suspicious ISL: SV 12
1998 07 01 12:02:30.000 SV 04 Removed Suspicious ISL: SV 11
1998 07 01 12:02:30.000 SV 04 Removed Suspicious ISL: SV 08
1998 07 01 12:02:30.000 SV 04 Removed Suspicious ISL: SV 07
1998 07 01 12:02:30.000 SV 04 Removed Suspicious ISL: SV 06
1998 07 01 12:02:30.000 SV 04 Removed Suspicious ISL: SV 05
1998 07 01 12:02:30.000 SV 04 Removed Suspicious ISL: SV 03
1998 07 01 12:02:30.000 SV 04 Removed Suspicious ISL: SV 02
1998 07 01 12:02:30.000 SV 04 Removed Suspicious ISL: SV 01
1998 07 01 12:02:30.000 SV 04 Removed Suspicious ISL: SV 00
1998 07 01 12:02:30.000 SV 04 Removed Suspicious GL: GS 11
1998 07 01 12:02:30.000 SV 04 Removed Suspicious GL: GS 09
```

```
1998 07 01 12:02:30.000 SV 04 Removed Suspicious GL: GS 08
1998 07 01 12:02:30.000 SV 04 Removed Suspicious GL: GS 07
1998 07 01 12:02:30.000 SV 04 Removed Suspicious GL: GS 06
1998 07 01 12:02:30.000 SV 04 Removed Suspicious GL: GS 05
1998 07 01 12:02:30.000 SV 04 Removed Suspicious GL: GS 04
1998 07 01 12:02:30.000 SV 04 Removed Suspicious GL: GS 03
1998 07 01 12:02:30.000 SV 04 More than 50 % Measurements Excluded
1998 07 01 12:02:30.000 SV 04 Check Result: NO GO
1998 07 01 12:02:30.000 SV 05 Removed Unhealthy SV ID 04
1998 07 01 12:02:30.000 SV 06 Removed Unhealthy SV ID 04
1998 07 01 12:02:30.000 SV 07 Removed Unhealthy SV ID 04
1998 07 01 12:02:30.000 SV 08 Removed Unhealthy SV ID 04
1998 07 01 12:02:30.000 SV 11 Removed Unhealthy SV ID 04
1998 07 01 12:02:30.000 SV 12 Removed Unhealthy SV ID 04
1998 07 01 12:02:30.000 SV 13 Removed Unhealthy SV ID 04
1998 07 01 12:02:30.000 SV 14 Removed Unhealthy SV ID 04
1998 07 01 12:02:30.000 SV 15 Removed Unhealthy SV ID 04
1998 07 01 12:02:30.000 SV 16 Removed Unhealthy SV ID 04
1998 07 01 12:02:30.000 SV 19 Removed Unhealthy SV ID 04
1998 07 01 12:02:30.000 SV 20 Removed Unhealthy SV ID 04
1998 07 01 12:02:30.000 SV 21 Removed Unhealthy SV ID 04
1998 07 01 12:02:30.000 SV 22 Removed Unhealthy SV ID 04
1998 07 01 12:02:30.000 SV 23 Removed Unhealthy SV ID 04
1998 07 01 12:02:30.000 SV 24 Removed Unhealthy SV ID 04
1998 07 01 12:02:30.000 SV 25 Removed Unhealthy SV ID 04
1998 07 01 12:02:30.000 SV 26 Removed Unhealthy SV ID 04
1998 07 01 12:02:30.000 SV 27 Removed Unhealthy SV ID 04
1998 07 01 12:02:30.000 SV 28 Removed Unhealthy SV ID 04
1998 07 01 12:02:30.000 SV 29 Removed Unhealthy SV ID 04
1998 07 01 12:02:30.000 SV 30 Removed Unhealthy SV ID 04
1998 07 01 12:02:30.000 SV 31 Removed Unhealthy SV ID 04
1998 07 01 12:02:30.000 SV 32 Removed Unhealthy SV ID 04
1998 07 01 12:02:31.000 SV 00 Removed Unhealthy SV ID 04
1998 07 01 12:02:31.000 SV 01 Removed Unhealthy SV ID 04
1998 07 01 12:02:31.000 SV 02 Removed Unhealthy SV ID 04
1998 07 01 12:02:31.000 SV 03 Removed Unhealthy SV ID 04
...
1998 07 01 12:02:31.000 SV 04 More than 50 % Measurements Excluded
1998 07 01 12:02:31.000 SV 04 Check Result: NO GO
...
1998 07 01 12:02:32.000 SV 04 More than 50 % Measurements Excluded
1998 07 01 12:02:32.000 SV 04 Check Result: NO GO
...
1998 07 01 12:02:33.000 SV 04 More than 50 % Measurements Excluded
1998 07 01 12:02:33.000 SV 04 Check Result: NO GO
...
1998 07 01 12:02:34.000 SV 04 More than 50 % Measurements Excluded
1998 07 01 12:02:34.000 SV 04 Check Result: NO GO
...
1998 07 01 12:02:35.000 SV 04 More than 50 % Measurements Excluded
1998 07 01 12:02:35.000 SV 04 Check Result: NO GO
...
1998 07 01 12:02:36.000 SV 04 More than 50 % Measurements Excluded
1998 07 01 12:02:36.000 SV 04 Check Result: NO GO
...
1998 07 01 12:02:37.000 SV 04 More than 50 % Measurements Excluded
```

```
1998 07 01 12:02:37.000 SV 04 Check Result: NO GO
...
1998 07 01 12:02:38.000 SV 04 More than 50 % Measurements Excluded
1998 07 01 12:02:38.000 SV 04 Check Result: NO GO
...
1998 07 01 12:02:39.000 SV 04 More than 50 % Measurements Excluded
1998 07 01 12:02:39.000 SV 04 Check Result: NO GO
...
1998 07 01 12:02:40.000 SV 04 More than 50 % Measurements Excluded
1998 07 01 12:02:40.000 SV 04 Check Result: NO GO
1998 07 01 12:02:40.000 SV 04 Switched Off
```

The event takes place at 12:02:29. The other satellites immediately remove the observation to SV 04 from their Kalman filter, due to a failed test of the a-priori residual. The onboard processor of SV 04 also removes the observations to nearly all other satellites as well as the ground links, due to a failed tests of the a-priori residuals. After excluding more than 50 % of all observations, the onboard processor of SV 04 assumes a integrity problem, and raises the NO GO flag. In the next epoch, the other satellites remove SV 04 due to the set NO GO flag, as well as the user. Time to alarm: 1 second.

Note that the Chi Square test has raised no alarm, although the residuals are high. This is due to the fact that by removing nearly all observations, the covariance matrix P has high values values. These are used to normalise the a-posteriori residuals. The Chi Square test is only a good detector, if enough measurements are available.

Due to the high elevation of SV 04, the clock jump of approximately 3 meters leads to a spike in the altitude error of the user. But the overall impact on the user position error is negligible.

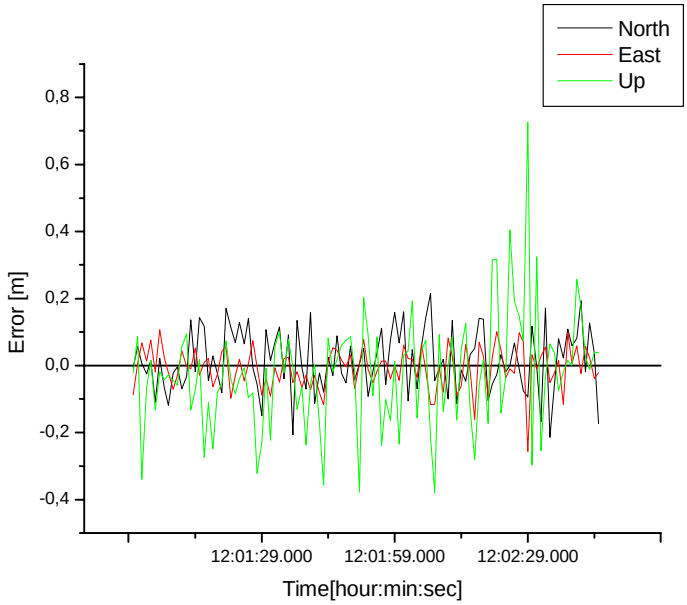

Figure 7-22 User Error over Time (Spike of Altitude Error at T = 12:02:30)

8 CONCLUSION

8.1 Results and further Considerations

In the frame of this Ph.D. thesis, intersatellite links have been investigated as potential observables for orbit determination. Introducing ISL's in an optimal way requires the states of all satellites to be processed in one large filter. This is comparable to a geodetic network adjustment, although the network points are orbiting instead of being fixed. Despite of the fact that in the physical world one satellite is transmitting a ranging signal while another is taking the measurement, they are both equivalent in a mathematical sense. There is no difference between the measuring satellite and the target; both satellites states are improved in the measurement update.

The correlation of the satellite states due to the ISL's provides an inherent capability for bridging tracking gaps. Even if no ground station is in view, a satellite orbit can be observed and determined if it is correlated via ISL with another satellite which is observed from ground. This opens an interesting discussion: How far can the number of ground stations be reduced? In one of the simulations in chapter six a global GEO/IGSO constellation is tracked by a regional ground network of only four stations. This number can indeed be further reduced down to one, however the accuracy of the realtime orbit estimation decreases. Another interesting point is: what happens if the ground links are removed at all? The relative positioning of the satellites would be ensured by the intersatellite links, but there would be a slowly increasing decoupling from the earth's rotation. In the frame of the "Autonav" capability of GPS Block IIR satellites simulations have been conducted concerning exactly this issue. It was found that the position errors would increase up to 10 meters within 180 days.

It has already been mentioned that processing intersatellite links bears some operational and technological problem, i.e. where to place the antennae on the S/V bus? How to get the measurements to a central processing facility? Is it really worth the effort? Looking at the results from chapter six reveals that the real time estimate of the orbit is indeed better, especially in the off-radial components. However, the same accuracy can be achieved with ground links by increasing the smoothing time. This reduces the advantage of ISL's over pure ground links to a shortening of the required orbit arc. Nevertheless, this should not be underestimated; after station keeping maneuvers of a satellite, the time the satellite becomes available again depends exactly on the length of this minimum required orbit arc.

The main advantages of ISLs seem to be their observation accuracy: no troposheric delay, modest ionospheric delay. Besides orbit determination there is another application for ISL, integrity monitoring. Here, instantaneous observation accuracy cannot be so easily replaced by a longer smoothing time. In combination with onboard processing, ISLs are perfectly suited for integrity monitoring. The measurements are taken and processed aboard the spacecraft. The integrity information is immediately available and can be broadcast to the user. The system latency is extremely short, if any. For comparison: in a ground based integrity monitoring system like WAAS or EGNOS data has to be collected by ground stations, transmitted via wide area network to the central processing facility. The obtained

integrity result is then transmitted to an uplink station where it is uploaded to a spacecraft where it can be broadcast to the user. System latency is at minimum four seconds.

Using ISLs for integrity monitoring demands a high technological effort. There is the issue of the access method, for example: a Time Division Multiple Access (TDMA) method like for the GPS Block IIR cross links will not be appropriate because of the time to alarm requirement, which raises the demand for either Code Division Multiple Access (CDMA) or Frequency Division Multiple Access (FDMA). Pure CDMA on one single frequency is not feasible due to the near-far effect, which simply means a spacecraft can not receive on the same frequency it is transmitting. A pure FDMA approach however raises the question of how many frequencies will be needed? One per spacecraft? Frequencies are one of the very rare resources in satellite navigation, thus it is unlikely that 30 frequencies will be allocated to ISLs for Galileo. As a viable option appears the combination CDMA and FDMA. For example, assuming a number of six frequencies and allowing each satellite to send on three and to receive on the remaining three frequencies. For each satellite, the combination of send and receive frequencies is different. Using this approach we would have

$$\binom{6}{3} = \frac{6!}{(6-3)!\cdot 3!} = \frac{720}{36} = 20$$

possible combinations with only 6 frequencies needed, meaning that 20 bi-directional ISLs can be established simultaneously with any combination providing one matching frequency pair.

Even the question of antennae placement is solvable. There is no need to mount 30 antennae on a single S/C bus. Phased array antennae, which use electronic beam steering to manipulate the reception direction appear to be the right technology. Besides solving the antennae placement problem they additionally provide SDMA (Space Division Multiple Access).

8.2 Recommendations for Galileo

While the system design phase for the next generation of satellite navigation systems GNSS 2 is already in progress, the results obtained in this Ph.D. thesis lead to several recommendations for future satellite navigation systems. In the frame of Galileo ISL's have been studied and evaluated with respect to their capability for orbit determination and integrity monitoring. The technological effort has been found very high for orbit determination, but worth further investigation with respect to integrity monitoring. With integrity being the major design driver, ISL is still an option for Galileo today.

Although the use of intersatellite links places a high requirement on the space segment, i.e. the satellites with respect to complexity, the gain could be worth the effort. The ISL provides not only ranging capability, but also offers a communication channel between the satellites which can be exploited to exchange status information as well as broadcast messages which are dedicated to the user. For example, GPS Block IIR spacecraft are capable to use their

"cross-links" to disseminate the broadcast ephemeris of the entire constellation. This overcomes the problem that ephemeris upload can only be done by the master control station, which has rare contact (only twice a day) to each SV. This removes the necessity for the user community to use orbit parameters computed already 24 hours ago, thus improving accuracy. GPS Block IIR has also the capability for autonomous navigation, i.e. observing and improving broadcast ephemeris parameters unaided from ground. The underlying TDMA process with a period of 37 seconds, however, does not support integrity with respect to the time-to-alarm requirement.

The effort of building complex space vehicles may be balanced by the reduction of (number of) ground stations. Even if all monitoring and orbit determination is done on ground, the additional orbit information obtained from the intersatellite ranging can bridge gaps in ground network coverage.

Moreover, the benign geometry especially for higher orbit altitudes like MEO or GEO/IGSO satellites, allows very rapid estimation of the orbits using shorter intervals of observation. This leads to increased availability after manoeuvres, and also allows an increased rate of broadcast ephemeris update rate. The communication capability of ISLs can also be used to keep error due to ageing of broadcast ephemeris low. Keeping the accuracy goal of Galileo in mind: this is an option to achieve it!

Combination of onboard autonomous processing and intersatellite links, although not feasible in an optimal filter, is the most interesting option for autonomous integrity monitoring of the future Galileo system. And last but not least: The two ephemeris models developed in the frame of this work are a perfect match for the need of the Galileo system in terms of flexibility and accuracy.

8.3 Achievements

Software ConAn (Constellation Analyser)

In the frame of this Ph.D. thesis, the theory of orbit determination and orbit computation has been reviewed and a new approach for precise orbit and ephemeris determination using inter satellite links has been developed. To investigate the achievable accuracy, the elaborated models have been coded in a complex software package allowing system level performance analysis as well as detailed evaluation of orbit computation and orbit estimation algorithms. It includes several gravity models, precise planetary ephemeris (JPL DE200, see [STA-90]) and orbit estimation in real time using Kalman filtering as well as conventional batch processing of measurements. The simulations, which are a cornerstone of this Ph.D. thesis have all been conducted using ConAn, as well as the comparison and visualisation of results.

Development of two new ephemeris models

The broadcast ephemeris model of both today's existing satellite navigation systems, GPS and GLONASS have been investigated. It has been shown that superior performance of the GPS model is mainly due to the number of parameters, or simply spoken, due to the degrees of freedom provided by the model. Especially for short periods of validity, i.e. much shorter than

half a revolution, the non-Keplerian GLONASS model has been found superior to the Kepler orbit based GPS model. Based on the GLONASS model, two new user ephemeris models, one with 12, the other with 15 degrees of freedom have been developed and found to be a viable option for MEO satellites, exceeding GPS as well as GLONASS models in terms of model fitting error.

Development of an onboard integrity monitor

A conceptual design for an onboard integrity estimator has been proposed and investigated with respect to the computational load. The necessary algorithms have been developed, implemented and integrated in the ConAn software. The"onboard like" behaviour of the algorithms has been ensured by

1. using only information which is available at a satellite
2. using it only at a time when it becomes available.

By simulating several types of non-integrity cases, it shown that the use of just one fault detection mechanism is likely to be insufficient, because different detectors are triggered by different events. A reasonable combination of fault detection mechanisms, covering different fault cases, has been presented.

9 REFERENCES

[ABR-72] Abramowitz, M. / Stegun, I (Editors): "Handbook of Mathematical Functions", Dover Publication New York, 1972

[BIR-77] Bierman G.J.: "Factorization Methods for Discrete Sequential Estimation", Academic Press, San Diego – New York – Berkley – Boston – London – Sydney – Tokyo – Toronto, 1977

[BLU-96] Parkinson, B. / Spilker, J. / Axelrad, P / Enge, P.: "GPS – Theory and Applications , Volumes I and II", AIAA Washington, 1996

[BOX-76] Box G.E.P., Jenkins G.M.: "Time Series Analysis, Forecasting and Control", Holden-Day, San Francisco – Düsseldorf – Johannesburg – London – Panama – Singapore – Sydney – Toronto, 1976

[BRS-89] Bronstein I.N., Semendjajew K.A: "Taschenbuch der Mathematik", Verlag Harry Deutsch, Thun und Frankfurt / Main, 24.Auflage , 1989

[BRW-92] Brown R.G., Hwang P.Y.C.: "Introduction to Random Signals and Applied Kalman Filtering", John Whiley and Sons, New York – Chichester – Brisbane – Toronto – Singapore, Second Edition, 1992

[COL-81] Colombo O. L., 1981: *Numerical Methods for Harmonic Analysis on the Sphere,* Report No. 310, Department of Geodetic Science, The Ohio State University 1981.

[EHE-86] Eissfeller, B. and G. W. Hein, 1986: *A Contribution to 3D- Operational Geodesy,* Heft 17, Universitärer Studiengang Vermessungswesen der Universität der Bundeswehr München, 1986.

[ESC-65] Escobal, P.R.: "Methods of Orbit determination" John Wiley and Sons, Inc. , New York – London – Sydney, 1965

[GID-95] GLONASS Interface Control Document (Rev. 1995), Coordinational Scientific Information Center of the Russian Space Forces, 1995

[GLB-81] Gelb A.: "Applied Optimal Estimation", The M.I.T. Press, Cambridge – Massachusetts – London, 1974 (Tenth printing, 1988)

[GPS-91] ICD-GPS200, GPS Interface Control Document, Department of Defence, 1991

[GSC-76] "Mathematical Theory of the Goddard Trajectory Determination System", Goddard Space Filght Center, Greenbelt, Maryland, 1976

[GUT-94] Guthmann, A. : "Einführung in die Himmelsmechanik und Ephemeridenrechnung" B.I. Wissenschaftsverlag, Mannheim – Leipzig – Wien – Zürich , 1994

[HKM-67] Heiskanen,A.W. / Moritz, H: "Physical Geodesy" W. H. Freeman and Company, San Francisco and London, 1967

San Francisco and London, 1967

[HUB-68] Huber P.J.: "Robust Statistics", John Whiley and Sons, New York – Chichester – Brisbane – Toronto, 1981

[HWL-94] Hofmann-Wellenhoff B. , Lichtenegger H. , Collins J.: "GPS – Theory and Practice", 3rd revised Edition , Springerverlag, Wien – New York , 1994

[ITN-96] IERS Conventions (1996) , IERS Technical Note 21

[JEN-68] Jenkins G.M. , Watts D.G.: "Spectral Analysis and ist Applications", Holden-Day, San Francisco – Düsseldorf – Johannesburg – London – Panama – Singapore – Sydney – Toronto, 1968

[KOC-80] Koch K.-R.: "Parameterschätzung und Hypothesentests in linearen Modellen", Dümmler, Bonn, 1980

[LEI-90] Leick, Alfred: "GPS Satellite Surveying", John Wiley & Sons, New York 1990

[MAN-98] Mansfeld, Werner: "Satelliten Ortung und Navigation", Friedrich Vieweg & Sohn Verlagsgesellschaft, Braunschweig / Wiesbaden, 1998

[MOPS-98] Minimum Operational Performance Standards for WAAS, RTCA Do 229 A

[NUM-99] Numerical Recipes

[RIZ-79] Rizos C. 1979: *An Efficient Computer Technique for The Evaluation of Geopotential From Spherical Harmonic Models,* Aust. J. Geod. Photo. Surv. No. 31 December 1979.

[RIZ-85] Rizos C. , Stolz A.: "Force Modelling for GPS Satellite Orbits", 1st Int. Symposium Precise Positioning with GPS, Vol. 1 , P. 87 – 98, Rochville , USA 1985

[SOP-94] Soop E. M., 1994: *Handbook of Geostationary Orbits,* European Space Agency and Microcosm Inc., 1994.

[STA-90] Astronomy & Astrophysics, vol. 114, pp. 297-302. Standish, E.M.: 1990, "The Observational Basis for JPL's DE200, the planetary ephemeris of the Astronomical Almanac", Astronomy & Astrophysics, vol. 233, pp. 252-271.

[STRA-97] Strang, G. Borre.K: "Linear Algebra, Geodesy and GPS", Wellesley-Cambridge Press, 1997

[TEU-98] Teunissen, Peter / Kleusberg, Alfred : "GPS for Geodesy" 2nd Edition, Springer Verlag Berlin, Heidelberg, New York, 1998

[WEZ-91] Wertz, J.R. "Space Mission Analysis and Design", Space Technology Library, Kluwer Academic Publishers, Dordrecht – Boston – London, 1991